Instytut Chemii Bioorganicznej

Polskiej Akademii Nauk

Wykorzystanie niekodujących RNA i nanotechnologii w regulacji ekspresji wybranych białek macierzy zewnątrzkomórkowej glejaka i raka piersi

Małgorzata Grabowska

Praca doktorska zrealizowana w Zakładzie Neuroonkologii Molekularnej

Promotor: dr hab. Katarzyna Rolle, prof. ICHB PAN

Poznań 2022

1 WYKAZ PRAC NAUKOWYCH

Lista prac naukowych zawartych w rozprawie doktorskiej:

1. **Grabowska M***, Kuczyński K*, Piwecka M, Rabiasz A, Zemła J, Głodowicz P, Wawrzyniak D, Lekka M, Rolle K.

   miR-218 affects the ECM composition and cell biomechanical properties of glioblastoma cells.

   Journal of Cellular and Molecular Medicine. 2022. 00:1-18.

   $IF_{2022} = 5,31$; pkt MEiN = 100

2. **Grabowska M**, Misiorek JO, Zarębska Ż, Rolle K.

   Applications of noncoding RNAs in brain cancer patients.

   Clinical applications of noncoding RNAs in cancer. Elsevier. 2022. 2:17-64.

   pkt MEiN = 80; liczba cytowań = 1

3. **Grabowska M**, Grześkowiak BF, Rolle K, Mrówczyński R.

   Magnetic Nanoparticles as a Carrier of dsRNA for Gene Therapy.

   Methods in Molecular Biology. Springer. 2021. 2211:69-81.

   pkt MEiN = 80; liczba cytowań = 1

4. Wawrzyniak D, **Grabowska M**, Głodowicz P, Kuczyński K, Kuczyńska B, Fedoruk-Wyszomirska A, Rolle K.

   Down-regulation of tenascin-C inhibits breast cancer cells development by cell growth, migration, and adhesion impairment.

   PLoS One. 2020. 15(8):e0237889.

   $IF_{2020} = 3,24$; pkt MEiN = 100; liczba cytowań = 8

5. **Grabowska M**, Grześkowiak BF, Szutkowski K, Wawrzyniak D, Głodowicz P, Barciszewski J, Jurga S, Rolle K, Mrówczyński R.

   Nano-mediated delivery of double-stranded RNA for gene therapy of glioblastoma multiforme.

   PLoS One. 2019. 14(3):e0213852.

   $IF_{2019} = 2,74$; pkt MEiN = 100; liczba cytowań = 23

Lista publikacji niewchodzących w skład rozprawy doktorskiej:

1. **Grabowska M**, Wawrzyniak D, Rolle K, Chomczyński P, Oziewicz S, Jurga S, Barciszewski J.

   Let food be your medicine: nutraceutical properties of lycopene.

   Food & Function. 2019. 10(6):3090-3102.

   $IF_{2019} = 4,26$; pkt MEiN = 100; liczba cytowań = 59

2   STRESZCZENIE

Nowotwory określane są często zabójcami XXI wieku. Ogólnoświatowa zapadalność i śmiertelność na choroby tego typu stale rośnie. Do problematycznych, biorąc pod uwagę skuteczność leczenia, należą złośliwe nowotwory mózgu i piersi. Glejak IV stopnia (GBM) oraz potrójnie ujemny rak piersi (TNBC) są guzami dającymi częste wznowy. Trudności związane z chirurgicznym usunięciem całości zmienionej chorobowo tkanki GBM, a także brak możliwości zastosowania terapii hormonalnej w przypadku TNBC sprawiają, że wciąż poszukiwane są dla nich nowe podejścia terapeutyczne.

Jedną z najszybciej rozwijanych form terapii jest ta oparta o interferencję RNA (RNAi), umożliwiająca manipulowanie poziomem ekspresji genów. Jej mechanizm został poznany na tyle dobrze, że na rynku dostępne są już leki których substancją czynną jest siRNA. Wyzwaniem na chwilę obecną jest więc wybranie odpowiednich celów terapeutycznych, odróżniających tkanki nowotworowe od właściwych, zarazem kluczowych dla progresji nowotworu, jak również optymalne sposoby dostarczania terapeutyków do miejsca chorobowo zmienionego. Biorąc pod uwagę to, jak niekorzystne dla pacjenta jest rozprzestrzenienie się tkanki nowotworowej, zarówno na przyległe jej tkanki jak i inne organy, obiecującym podejściem wydaje się być celowanie w czynniki związane z migracją komórek nowotworowych.

Głównym celem mojego podejścia badawczego było określenie udziału macierzy zewnątrzkomórkowej (ECM) w procesie nowotworzenia. W pracy przedstawiłam wpływ niekodujących RNA na poziom kluczowych dla ECM białek: tenascyny-C i syndekanu-2. Przeanalizowałam również związane z tym podejściem zmiany zachodzące w komórkach nowotworowych glejaka i raka piersi, ze szczególnym uwzględnieniem procesów migracji, adhezji i tworzenia przerzutów. Zaproponowałam ponadto zastosowanie nowych narzędzi nanotechnologicznych dających możliwość dostarczania regulatorowych RNA do komórek, jak również wstępnie zweryfikowałam wykorzystanie ECM w potencjalnej terapii nowotworów.

3 ABSTRACT

Cancers are often referred to as the fatal diseases of the 21st century. The global incidence and mortality from this type of disorders are continuously increasing. The highly problematic ones, taking into account the effectiveness of the treatment, are malignant tumors of the brain and breast. Grade IV glioma (GBM) and triple negative breast cancer (TNBC) are tumors exhibiting frequent recurrences. Difficulties related to the surgical extraction of the entire affected GBM mass, as well as the inability to use hormone therapy in the case of TNBC, indicate that new therapeutic approaches are still being sought.

One of the most extensively developed therapeutic approach is based on RNA interference (RNAi), which enables the manipulation of gene expression levels. Its mechanism has been studied so broadly that there are already available drugs on the market, containing siRNA as an active ingredient. Therefore, the biggest challenge up to date, is to select the appropriate therapeutic targets that allow for distinguishing neoplastic tissues from the healthy ones, which are also crucial for tumor progression, followed by establishment of optimal methods of therapeutics delivery to the affected area. Taking into account, how disadvantageous for the patient the spreading of tumor mass is, targeting the factors that are related to tumor cell migration appears to be highly auspicious treatment approach.

The main goal of my research approach was to determine the involvement of the extracellular matrix (ECM) in the neoplastic process. In the doctoral dissertation, I presented the impact of non-coding RNAs on the level of key proteins for ECM: tenascin-C and syndecan-2. I also studied the changes associated with application of this approach in glioblastoma and breast cancer cells, with particular emphasis on the processes of migration, adhesion and metastasis. Moreover, I proposed the use of modern nanotechnology tools that enable the delivery of regulatory RNA to cells, as well as I preliminarily characterized and verified the use of ECM in potential cancer therapy.

4 WYKAZ SKRÓTÓW

ATN-RNA – dsRNA o jednej z nici komplementarnej do fragmentu mRNA *TNC* (ang. *anti-tenascin RNA*)

CAF – fibroblasty związane z rakiem (ang. *cancer associated fibroblast*)

CDH1 – kadheryna epitelialna (ang. *cadherin 1*)

circRNA – kolisty RNA (ang. *circular RNA*)

CSC – macierzyste komórki nowotworu (ang. *cancer stem cells*)

CT – tomografia komputerowa (ang. *computed tomography*)

czynników inicjujących translację 4A (ang. *eukaryotic translation initiation factor 4A,* eIF4A

dsRNA – dwuniciowy RNA (ang. *double-stranded RNA*)

ECM – macierz zewnątrzkomórkowa (ang. *extracellular matrix*)

EMT – przejście nabłonkowo-mezenchymalne (ang. *epithelial–mesenchymal transition*)

ER – receptor estrogenowy (ang. *estrogen receptor*)

ET_{50} – połowa maksymalnego efektywnego czasu (ang. *half maximal effective time*)

FDA – Agencja Żywności i Leków (ang. *Food and Drug Administration*)

FN – fibronektyna

GBM – glejak IV stopnia złośliwości, glejak wielopostaciowy (łac. *glioblastoma multiforme*)

HA – kwas hialuronowy (ang. *hyaluronic acid*)

HER2 – receptor ludzkiego nabłonkowego czynnika wzrostu (ang. *human epidermal growth factor receptor 2*)

IC_{50} – połowa maksymalnego stężenia hamującego (ang. *half maximal inhibitory concentration*)

INF-β – interferon β

INFγ – interferon gamma

lncRNA – długi niekodujący RNA (ang. *long noncoding RNA*)

miRNA - mikroRNA

MMP – metaloproteinaza macierzowa (ang. *matrix metalloproteinase*)

MNP – nanocząstka magnetyczna (ang. *magnetic nanoparticle*)

MRE – elementy oddziałujące z miRNA (ang. *miRNA response elements*)

MRI – rezonans magnetycznego (ang. *magnetic resonance imaging*)

ncRNA – niekodujące RNA (ang. *non-coding RNA*)

NGS – sekwencjonowanie nowej generacji (ang. *next generation sequencing*)

OS – wskaźnik ogólnego przeżycia (ang. *overall survival*)

OUN – ośrodkowy układ nerwowy

PDGF – płytkopochodny czynnik wzrostu (ang. *platelet-derived growth factor*)

PEI – polietyleonoiminą

PR – receptor progesteronowy (ang. *progesteron receptor*)

PTT – terapia fototermiczna (ang. *photothermal therapy*)

real-time PCR – reakcja łańcuchowej polimerazy w czasie rzeczywistym (ang. *real-time polymerase chain reaction*)

RIG1 – gen indukowany kwasem retinowym 1 (ang. *retinoic acid-inducible gene 1*)

RISC - kompleks wyciszający indukowany przez RNA (ang. *RNA-induced silencing complex*)

RNAi – interferencja RNA (ang. *RNA interference*)

SDC2 – syndekan-2 (ang. *syndecan-2*)

SDC4 – syndekan-4 (ang. *syndecan-4*)

siRNA – krótki interferujący RNA (ang. *short interfering RNA*)

TGF-β – transformujący czynnik wzrostu beta (ang. *transforming growth factor beta*)

TLR – receptor *toll*-podobnych (ang. *toll-like receptor*)

TMZ – temozolomid

TNBC – potrójnie ujemny rak piersi (ang, *triple-negative breast cancer*)

TNC – tenascyna-C

TNR – tenascyna-R

TTField – pole elektryczne leczenia nowotworów (ang. *tumor treatment field*)

UTR – region niepodlegający translacji (ang. *untranslated region*)

VIM – wimentyna (ang. *vimentin*)

WHO – Światowa Organizacja Zdrowia (ang. *World Health Organization*)

5   CEL PRACY

Głównym celem przedstawionego cyklu prac naukowych było określenie udziału macierzy zewnątrzkomórkowej (ECM) w procesie nowotworzenia, a w szczególności:

- badanie wpływu niekodujących RNA na poziom kluczowych dla ECM białek: tenascyny-C i syndekanu-2 oraz związana z tym podejściem analiza zmian zachodzących w komórkach nowotworowych glejaka i raka piersi, ze szczególnym uwzględnieniem procesów migracji, adhezji i tworzenia przerzutów;
- poszukiwanie i badanie możliwości wykorzystania nowych narzędzi nanotechnologicznych dających możliwość dostarczania regulatorowych RNA do komórek;
- weryfikacja wykorzystania składników ECM w potencjalnej terapii nowotworów.

Cele szczegółowe moich badań pokrywają się z tematyką publikacji eksperymentalnych wchodzących w skład cyklu:

1.   Za cel pracy **Grabowska M, Kuczyński K i wsp. „*MiR-218 affects the ECM composition and cell biomechanical properties of glioblastoma cells*”** przyjęłam określenie wpływu hsa-miR-218-5p na skład macierzy zewnątrzkomórkowej i właściwości biomechaniczne komórek glejaka. Oceniłam poziom ekspresji miR-218 oraz tenascyny-C i syndekanu-2 w tkankach pochodzących od pacjentów z guzami mózgu. Przeprowadziłam następnie analizę właściwości biomechanicznych komórek, takich jak adhezja, sztywność i migracja w wyniku regulacji poziomu ekspresji białek ECM poprzez miR-218.

2.   Praca **Grabowska M i wsp.** „*Nano-mediated delivery of double-stranded RNA for gene therapy of glioblastoma multiforme*” przedstawia zastosowanie nanocząstek magnetycznych w potencjalnym podejściu terapeutycznym glejaka opartym na interferencji RNA skierowanej przeciw tenascynie-C. Celem projektu było wyselekcjonowanie nanocząstek mających potencjał do spełnienia roli nośnika dwuniciowego RNA. Stosowane narzędzie interferencji RNA, zawierające w sobie nić komplementarną do mRNA *TNC*, tzw. ATN-RNA, wykorzystałam do wyciszenia ekspresji tego kluczowego dla budowy i funkcjonowania ECM białka. Badania wzbogaciłam o obserwacje zmian w proliferacji i migracji komórek nowotworowych. Praca ta realizowana była w ramach grantu Narodowego Centrum Nauki Opus 11 „Nowe, wielozadaniowe nanocząstki w skojarzonej geno- i fototerapii” (2016/21/B/ST8/00477)

3.   Praca **Wawrzyniak D i wsp.** *„Down-regulation of tenascin-C inhibits breast cancer cells development by cell growth, migration, and adhesion impairment"* przedstawia wykorzystanie technologii RNAi oraz cząsteczkę ATN-RNA do hamowania procesu nowotworzenia w raku piersi. Podejście to pozwoliło mi na analizę możliwości zastosowania tego narzędzia w innym typie nowotworu niż glejak, wskazując jednocześnie na uniwersalność użytego podejścia terapeutycznego. Zastosowanie ATN-RNA zostało scharakteryzowane pod kątem jego wpływu na następujące procesy: proliferacja, migracja, cykl komórkowy, tworzenie „miniguzów" oraz przebieg przejścia nabłonkowo-mezenchymalnego.

4.   Ponieważ niekodujące RNA stanowią klasę cząsteczek o kluczowym znaczeniu dla rozwoju i progresji nowotworów i jednocześnie jeden z moich głównych obszarów zainteresowań, opracowałam przegląd literaturowy *„Applications of noncoding RNAs in brain cancer patients"* podsumowujący potencjał prognostyczny, diagnostyczny i terapeutyczy miRNA, lncRNA i circRNA.

5.   W pracy *„Nano-mediated delivery of double-stranded RNA for gene therapy of glioblastoma multiforme"* opracowałam protokół umożliwiający powtarzalne przeprowadzenie części z opublikowanych wcześniej eksperymentów dotyczących zastosowania nanocząstek MNP@PEI jako nośników RNA, mogących stanowić ulepszenie potencjalnej terapii glejaka.

6   WPROWADZENIE

6.1   Nowotwory

Nowotworami nazywamy całą grupę chorób sygnowanych kodem 02 w Międzynarodowej Statystycznej Klasyfikacji Chorób i Problemów Zdrowotnych. W schorzeniach tego typu komórki organizmu dzielą się w sposób niekontrolowany, zazwyczaj tworząc tzw. guz nowotworowy. Za niewłaściwe podziały komórkowe odpowiedzialne są kumulujące się mutacje genów kodujących białka związane z przebiegiem cyklu komórkowego, a także onkogenów i genów supresorowych innego typu [1].

W celu usystematyzowania zgromadzonej wiedzy o nowotworach u ludzi Światowa Organizacja Zdrowia (ang. *World Health Organization,* WHO) podjęła uchwałę, na podstawie której miały one zostać sklasyfikowane. W efekcie powstała tzw. Niebieska Księga, publikacja opisująca znane formy chorób nowotworowych. Jej obecna wersja bazuje nie tylko na badaniach histopatologicznych, ale uwzględnia również parametry molekularne. Nowotwory klasyfikowane przy użyciu systemu WHO, który koncentruje się przede wszystkim na cechach patologicznych, dzielimy na przypadki stopnia I i II - zmiany łagodne, oraz stopni III i IV – złośliwe [2]. Według danych Międzynarodowej Agencji Badań nad Rakiem (ang. *International Agency for Research on Cancer*, IARC) w 2020 roku na całym świecie pojawiło się 19,3 mln nowych przypadków nowotworów, jednocześnie odnotowano 10 mln zgonów z ich powodu [3]. Widoczna jest obecnie wyraźna tendencja wzrostowa zapadalności i śmiertelności spowodowanej przez choroby nowotworowe (Rycina 1).

W Polsce od wielu lat nowotwory stanowią drugą, zaraz po chorobach układu krążenia, przyczynę śmierci. Spowodowane jest to starzeniem się polskiego społeczeństwa i ekspozycją na czynniki rakotwórcze związane ze stylem życia [4]. Przewiduje się że do 2025 roku w Polsce zachorowalność na nowotwory złośliwe u mężczyzn będzie charakteryzowała się niewielkim spadkiem względem danych obecnych na ten moment. Współczynnik ten będzie natomiast w dalszym ciągu rósł dla Polek. Różnice w prognozach wynikają z zależnego od płci stopnia zapadalności na nowotwory piersi [5].

Pod względem molekularnym tkanki nowotworowe wyróżniają się na tle ich właściwych, zdrowych odpowiedników. W 2000 roku Hanahan i Weinberg stworzyli listę charakterystycznych cech komórek nowotworowych [1]. Wraz z rozwojem nauki kolejno w 2011 [6] i w 2022 roku [7] zestawienie to ulegało rozszerzeniu i obecnie składa się z następujących właściwości:

 - samodzielne wytwarzanie i reagowanie na czynniki wzrostowe,

- niewrażliwość na sygnały hamujące wzrost,

- unikanie szlaków śmierci komórkowej,

- nieograniczony potencjał replikacyjny,

- tworzenie własnej sieci naczyń krwionośnych,

- inwazyjność i związane z nią tworzenie przerzutów,

- niestabilność genetyczna,

- występowanie stanów zapalnych wokół guza,

- preferencja wobec metabolizmu beztlenowego,

- unikanie odpowiedzi immunologicznej,

- plastyczność fenotypowa związana z różnicowaniem komórek,

- przeprogramowanie epigenetyczne,

- polimorfizm towarzyszącego tkance mikrobiomu,

- wpływ komórek starzejących się [1, 6, 7].
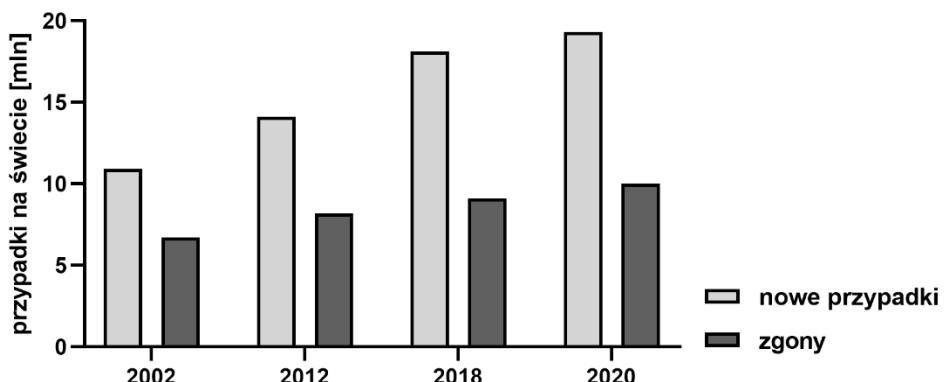
Rycina 1. Ilości nowych przypadków chorób nowotworowych i zgonów nimi wywołanymi w poszczególnych latach. Na podstawie danych z Globalnego Obserwatorium Onkologicznego (ang. *Global Cancer Observatory,* GLOBOCAN) [3, 8-10].

6.1.1 Glejak

Obecnie na świecie guzy mózgu i ośrodkowego układu nerwowego (OUN) stanowią 1,6% wszystkich nowych przypadków nowotworów i odpowiadają za 2,5% zgonów z nimi związanych [3]. Jako że druga z podanych wartości przewyższa pierwszą, ta dysproporcja informuje o wysokiej umieralności. Rozpoznanie choroby następuje w oparciu o obrazy uzyskane z rezonansu magnetycznego (ang. *magnetic resonance imaging,* MRI) i tomografii komputerowej (ang. *computed tomography*, CT). Objawy z którymi zgłaszają się pacjenci zależą w dużej mierze od umiejscowienia guza, do najczęściej występujących zaliczamy

napady padaczkowe, bóle głowy i zaburzenia osobowości [11]. Guzy mózgu mogą rozwijać się *de novo* lub powstawać z przerzutów, wynikających z rozprzestrzenienia się komórek guza pierwotnego w inne miejsca poprzez układ krwionośny [12]. Zakłada się, że 20% zmian pierwotnych zlokalizowanych w innych tkankach da przerzuty do mózgu. Chociaż komórki każdego rodzaju nowotworu mogą przenosić się w te rejony, najczęściej przerzuty do tego organu powodują: rak płuc, rak piersi, czerniak i rak jelita grubego [13]. Najczęściej występującym nowotworem łagodnym mózgu jest oponiak - 37,6% wszystkich nowotworów OUN, podczas gdy najczęstszym nowotworem złośliwym jest glejak IV stopnia złośliwości - 14,6% (Rycina 2) [14].

Rycina 2. Częstotliwość występowania pierwotnych guzów mózgu i OUN. Na podstawie danych CBTRUS [14].

Glejak stopnia IV, wcześniej znany jako glejak wielopostaciowy (łac. *glioblastoma multiforme,* GBM) jest najbardziej śmiertelnym z grupy guzów pierwotnych wywodzących się z OUN. Roczna zapadalność na GBM to 5,26 na 100000 osób [15]. Prawdopodobieństwo rozwinięcia guza wzrasta wraz z wiekiem i osiąga maksimum między 75 a 84 rokiem życia. GBM dają złe rokowania, wskaźnik 5-letniego przeżycia wynosi bowiem mniej niż 5%. Średnia długość życia waha się od 12 do 15 miesięcy w zależności od przeprowadzonej terapii, a w przypadku jej braku osiąga jedyne 3 miesiące od momentu diagnozy [16]. Główną cechą GBM, warunkującą słabą odpowiedź na radioterapię i resekcję, jest jej zdolność naciekania do sąsiednich tkanek [17]. W większości przypadków nawet szybko wykryty i leczony guz powraca w ciągu kilku centymetrów od zmiany pierwotnej [18]. Najgorsze prognozy wystawiane są u około 3% pacjentów, u których nowotwór przechodzi przez ciało modzelowate i obejmuje obie półkule mózgu, tworząc charakterystyczny wzór motyla [19].

Od 2005 roku standardem postępowania u pacjentów z nowo rozpoznanym glejakiem jest chirurgiczna resekcja guza, po której następuje radioterapia (60 Gy w 30 dawkach)

w skojarzeniu z trwającą 6 tygodni chemioterapią temozolomidem (TMZ). Z powodu naciekającego w głąb mózgu charakteru GBM, sama interwencja chirurgiczna nie pozwala na usunięcie z organizmu pacjenta całości masy nowotworu. TMZ to prolek, w warunkach fizjologicznego pH ulegający przemianie do związku aktywnego o właściwościach alkilujących. Wykazuje silne działanie genotoksyczne i teratogenne, ponadto uszkadza szpik kostny [20]. Niestety pomimo podjętej terapii wyniszczającej organizm, przyjęta procedura gwarantuje jedynie 6 miesięcy wolnych od progresji, wszystkie glejaki bowiem ostatecznie postępują [21]. Pacjenci ze wznową miejscową poddawani są drugiej operacji lub powtórnemu napromieniowaniu, jednakowoż nie wykazano, aby któraś z tych interwencji w sposób znaczący przedłużała przeżycie [22]. W przypadku nawrotu choroby stosuje się inny cykl chemioterapii alkilującej, głównie lomustynę [23]. Należy jednak pamiętać, że korzyści z chemioterapii środkami alkilującymi są w dużej mierze ograniczone do pacjentów, których nowotwory wykazują hipermetylację regionu promotora genu metylotransferazy O-metyloguaniny-DNA (ang. *O-methylguanine-DNA methyltransferase,* MGMT) [24].

W przypadku leczenia nowotworów, w tym GBM, rozpatrywane są możliwości ponownego zastosowania leków, które zostały już zatwierdzone do innych wskazań, w oparciu o założenia dotyczące cech biochemicznych lub metabolicznych. Pomimo rozpoczętych badań klinicznych nie uzyskano rozstrzygających dowodów popierających działanie leku przeciwpadaczkowego, czy kwasu walproinowego na zwiększenie przeżywalności pacjentów z guzem mózgu [25]. Brakiem sukcesu zakończyły się również próby zastosowania talampanelu, antagonisty receptora kwasu glutaminowego [26] oraz leku przeciwcukrzycowego – metforminy [27].

Na stan z 2021 roku Agencja Żywności i Leków (ang. *Food and Drug Administration*, FDA) zatwierdziła do leczenia nawracających przypadków GBM sześć terapii. Są to wspomniane już temozolomid i lomustyna a także kormustyna podawana dożylnie i w formie implantów waflowych, bewacyzumab i pole elektryczne leczenia nowotworów (ang. *tumor treatment field*, TTField). Jedynie TMZ, TTField i implanty waflowe kormustyny mogą być stosowane w przypadku guzów pierwotnych [28]. Spośród wymienionych najlepsze skutki wywołuje TTField, wydłużając wskaźnik ogólnego przeżycia (ang. *overall survival,* OS) do 21 miesięcy [29]. Żadna z wymienionych terapii nie gwarantuje remisji nowotworu dłuższej niż dwa lata. Z tego powodu wciąż prowadzone są badania poszukujące alternatywnych metod leczenia, w tym nowych cząsteczek mogących być celem terapii oraz nowoczesnych metod umożliwiających dostarczenie terapeutyków.

6.1.2 Rak piersi

Szacuje się, że rak piersi jest drugim najczęściej występujący nowotworem w ogóle społeczeństwa, a pierwszym pośród kobiet, ze średnią 46,3 przypadków na 100000 ludzi rocznie. Dzięki wprowadzeniu mammografii przesiewowej, zwiększeniu świadomości społeczeństwa oraz ustaleniu procedur terapeutycznych widoczny jest wyraźny spadek śmiertelności tej choroby [30]. Jednakże pomimo stosunkowo korzystnych rokowań zajmuje ona czwarte miejsce jako przyczyna zgonu pośród wszystkich nowotworów [31]. Do czynników ryzyka raka piersi zaliczamy zarówno wczesne miesiączkowanie jak i późną menopauzę. Zachorowalność wśród kobiet rodzących pierwsze dziecko po 30. roku życia jest dwukrotnie wyższa niż u tych decydujących się na wczesne macierzyństwo. Około 10% przypadków raka piersi w krajach zachodnich wynika z predyspozycji genetycznych, a podatność jest na ogół dziedziczona jako autosomalna dominująca [32]. U 52% rodzin z licznymi przypadkami opisywanego nowotworu wykryto występowanie mutacji w genie kodującym białko podatności na raka piersi (ang. *breast cancer susceptibility gene 1, BRCA1*), u 32% *BRCA2* [33].

Jak większość nowotworów, rak piersi jest chorobą niejednorodną, spośród której można wyróżnić podtypy molekularne. Główne podklasy zidentyfikowano na podstawie profilowania genetycznego receptorów estrogenowych (ang. *estrogen receptor*, ER), progesteronowych (ang. *progesteron receptor*, PR) i ludzkiego nabłonkowego czynnika wzrostu 2 (ang. *human epidermal growth factor receptor 2*, HER2). Wyróżniamy typ podstawnokomórkowy, luminalny A, luminalny B oraz typ HER2-dodatni, nazywany również nieluminalnym. Podtypy luminalne, wykazują ekspresję ER i/lub PR bez HER2. Podtyp HER2 charakteryzuje obecność HER2, bez ekspresji ER ani PR. W nowotworze podtypu podstawnokomórkowego brakuje ekspresji wszystkich trzech wspomnianych receptorów, nazywany jest więc potrójnie ujemnym rakiem piersi (ang, *triple-negative breast cancer,* TNBC) [34]. TNBC stanowi około 15% przypadków nowotworów piersi, zazwyczaj występuje u młodszych kobiet i wiąże się z gorszymi prognozami [35]. Charakteryzuje się wczesnym nawrotem choroby i występowaniem przerzutów do wątroby, płuc i mózgu [36], a jego 5-letnia przeżywalność wynosi 77% [37].

Jak wspomniano, guzy TNBC wykazują brak ekspresji ER, PR i HER2. Do ich leczenia nie można więc zastosować, tak jak w przypadku innych podtypów, terapii hormonalnej czy celowanej. Główną formą walki z TNBC jest więc chemioterapia. Międzynarodowe wytyczne onkologiczne zalecają stosowanie terapii skojarzonych opartych na: inhibitorach depolaryzacji mikrotubul podczas podziałów komórkowych – taksoidach [38]; wykazujących działanie alkilujące – cyklofosfamidzie i cisplatynie [39, 40]; antybiotyku - antracyklinie [41]; proleku

hamującego syntezę DNA- fluorouracylu [42]. Obecnie trwają poszukiwania nowych celów molekularnych TNBC pozwalających na poszerzenie możliwości terapeutycznych.

6.2   Macierz zewnątrzkomórkowa

Wszystkie tkanki i narządy zbudowane są z mieszaniny komórek i otaczających je składników niekomórkowych, zwanych macierzą zewnątrzkomórkową (ang. *extracellular matrix*, ECM). ECM nie spełnia jedynie roli wypełnienia czy fizycznego rusztowania dla komórek, ale także inicjuje oraz pośredniczy w przekazywaniu sygnałów biochemicznych i biomechanicznych, potrzebnych do zachowania homeostazy. Odpowiada za integralność komórek, transport czynników wzrostu oraz cytokin, co więcej utrzymuje optymalne pH i nawilżenie mikrośrodowiska. Jako że mechanobiologia odnosi się zarówno do tego, jak systemy biologiczne wyczuwają i reagują na sygnały mechaniczne, a także jak kontrolują mechaniczne właściwości swojego otoczenia, ECM wpływa na zakres aktywności komórek, w tym ich migrację, adhezję, sztywność [43]. Zasadniczo ECM składa się z wody, białek i polisacharydów, jednakże jej szczegółowy skład, właściwości fizyczne i rozmieszczenie komponentów są nie tylko specyficzne tkankowo, ale jest również ulegają przemianom w czasie i różnych stanach fizjologicznych. Poprzez ciągłe reorganizacje ECM generuje biochemiczne i mechaniczne właściwości każdego narządu, takie jak jego wytrzymałość na rozciąganie i ściskanie oraz elastyczność, a także pośredniczy w adhezji komórek do siebie i do podłoża [44].

Przy użyciu skaningowej mikroskopii elektronowej wyróżniono dwie główne formy strukturalne ECM: macierz śródmiąższową, która tworzy sieć otaczającą komórki oraz błonę podstawną, czyli cienką warstwę występującą między nabłonkiem a śródbłonkiem [45]. Macierz śródmiąższowa składa się głównie z kolagenu I i fibronektyny (FN), które zapewniają strukturalne rusztowanie dla tkanek. Natomiast błona podstawna jest bardziej zwarta i składa się głównie z kolagenu IV i laminin [46].

W składzie ECM możemy wyróżnić ponad 30 proteoglikanów, 200 glikoprotein i 300 białek, spośród których dominują te tworzące włókna, takie jak kolageny, lamininy, elastyna i FN [47]. Kolagen jest najobficiej występującym białkiem ECM, stanowiącym do 30% całkowitej masy białka u zwierząt [44]. U człowieka scharakteryzowano 28 typów kolagenu, jednakże w 90% przypadków głównym składnikiem ECM jest ten typu I [48, 49]. Kolageny zapewniają tkance wytrzymałość na rozciąganie, regulują adhezję komórek, wspomagają ich chemotaksję i migrację. W zależności od gęstości i kolejności upakowania włókien kolagenu I mogą konstruować ECM o sztywności sięgającej setek MPa. Jako punkt odniesienia warto

podać FN, osiągającą sztywność do 2 MPa [50]. Proteoglikany, takie jak agrekan, wersykan, czy perlekan, są białkami z przyłączonymi łańcuchami bocznymi glikozaminoglikanu, rozproszonymi między włóknami kolagenu. Wypełniają przestrzeń śródmiąższową i nawadniają tkankę poprzez sekwestrację wody. Glikoproteiny, do których zaliczamy laminiy, fibronektyny i tenascyny, są zaangażowane w interakcje pomiędzy ECM a komórką, działając jako ligandy dla receptorów powierzchniowych komórek np. integryn. Cięcie glikoprotein może generować fragmenty o innych funkcjach niż białka o pełnej długości [46].

Hydroliza składników ECM jest głównym procesem jej przebudowy, wpływającym nie tylko strukturę, ale również uwalnianiającym cząsteczki biologicznie aktywne, między innymi czynniki wzrostu. Składniki ECM mogą być degradowane przez różne rodziny proteaz. Głównymi enzymami biorącymi udział w jej degradacji są zależne od cynku metaloproteinazy macierzowe (ang. *matrix metalloproteinases*, MMP). Zmiany w aktywności MMP zachodzą podczas normalnych procesów biologicznych, m.in. podczas ciąży i gojenia się ran, jak również w chorobach sercowo-naczyniowych, zaburzeniach układu mięśniowo-szkieletowego oraz w różnego typu nowotworach [51]. Innym rodzajem proteaz są rodziny: dezintegryny i metaloproteinazy (ang. *disintegrins and metalloproteinases*, ADAM) oraz ADAM z motywem trombospondyny (ang. *ADAM with a thrombospondin motif,* ADAMTS). ADAM mogą rozszczepiać ektodomeny białek transbłonowych, uwalniając w ten sposób cytokiny, czynniki wzrostu, receptory i cząsteczki adhezyjne [52]. Przykładowo katalizowany przez ADAMTS1 rozszczep syndekanu-4 skutkuje zmianami w ułożeniu włókien aktynowych, wpływając na zmniejszenie zdolności adhezyjnych komórki [53].

W porównaniu do innych tkanek, ECM mózgu jest objętościowo mniejsza, ponadto różni się udziałem poszczególnych komponentów. Włókna kolagenu I występują w niej jedynie w pobliżu naczyń krwionośnych i powierzchni kory mózgowej. Głównymi składnikami, syntetyzowanymi przez neurony oraz komórki glejowe są lektykany (agrekan, wersykan, brewikan i neurokan), tenascyna-R (TNR) i kwas hialuronowy (ang. *hyaluronic acid*, HA) [54] (Rycina 4).

6.2.1   Udział ECM w kancerogenezie

Macierz zewnątrzkomórkowa jest elementem mikrośrodowiska nowotworowego, stanowiąc rusztowanie dla rozwijającego się guza i odpowiadając za promowanie złośliwego fenotypu. ECM w tkankach nowotworowych produkowana jest przede wszystkim przez fibroblasty związane z rakiem (ang. *cancer associated fibroblast,* CAF). Są to komórki mezenchymalne pochodzące z lokalnych fibroblastów, pericytów, makrofagów, komórek

śródbłonka, mezenchymalych komórek macierzystych lub samych komórek nowotworowych [55]. W nowotworze głowy i szyi zaobserwowano istotne różnice w 560 transkryptach CAF, między innymi w mRNA kodujących czynniki wzrostu, cytokiny i chemokiny [56]. Nie istnieje jednak żaden wszechobecny marker CAF, badania RNA-seq prezentują bowiem ich dużą heterogeniczność pomiędzy różnymi rodzajami nowotworów [57]. Wskazuje to na wysokie zróżnicowanie pod względem ilościowym jak i jakościowym produkowanych przez CAF składników ECM.

Zmiany zachodzące w ECM w czasie kancerogenezy dotyczą głownie gęstości jej usieciowania. Zwiększenie sieciowania między białkami zwiększa sztywność macierzy, z drugiej strony przerwanie tego usieciowania skutkuje jej degradacją. Sztywność ECM jest jedyną mechaniczną właściwością nowotworu wykorzystywaną do wstępnych badań przesiewowych w diagnostyce np. raka piersi [58]. Ponadto związana jest ze wzrostem częstości przerzutów i słabą odpowiedzią na leczenie, ponieważ gęsty ECM stanowi przeszkodę mechaniczną przy dostarczaniu leków [59]. Rozpatrywane są metody terapeutyczne opierające się na poluźnieniu ECM celem zwiększenia jej przepuszczalności. Podejście enzymatyczne polega na degradacji poszczególnych komponentów ECM. Dostarczenie kolagenazy w liposomach do gruczolakoraka trzustki u myszy zmniejszyło zawartość pozakomórkowego kolagenu z 12,8% do 5,6%, zwiększając tym samym wnikanie chemioterapeutyku o 17%. Innym sposobem na dotarcie do guza nowotworowego poprzez degradację ECM jest zastosowanie skoncentrowanych ultradźwięków o wysokiej intensywności [60].

Specyficzne dla guzów nowotworowych zjawisko desmoplazji, czyli wzrostu zwłóknień tkanki łącznej, również związane jest z usztywnieniem ECM. Wzrost gęstości macierzy spowodowany jest odkładanymi w guzie kolagenami, FN i tenascyną-C (TNC) [55]. Związane jest to ze zwiększoną produkcją i wydzielaniem zapalnych i rakotwórczych czynników wzrostu takich jak transformujący czynnik wzrostu beta (ang. *transforming growth factor beta,* TGF-β). Guzy desmoplastyczne są uważane za bardziej agresywne i wiążą się z gorszym rokowaniem w kilku typach nowotworów [61, 62].

Nowotwory poprzez siłę nacisku usztywnionej ECM na zdrowe tkanki mogą je rozpychać, zwiększając adhezję komórka-ECM i przerywając połączenia międzykomórkowe, co prowadzi do wzrostu objętości guza. Aby było to możliwe, ECM w guzach musi być co najmniej 1,5 razy sztywniejsza niż w otaczającej normalnej tkance [55]. Poprzez wywoływanie nacisku na naczynia krwionośne, sztywny ECM odpowiada za indukcję niedotlenienia. Ograniczenia w dostarczaniu O_2 oraz składników odżywczych do komórek rakowych stymuluje w nich zależność od glikolizy beztlenowej [63]. Analizy enzymatyczne

pojedynczych komórek dowodzą, że to ten szlak metaboliczny dominuje w CAF [64]. Preferencyjne oddychanie beztlenowe w komórkach nowotworowych, znane jako efekt Warburga [65], częściowo spowodowane jest aktywacją onkogenów, które zmniejszają wykorzystanie fosforylacji oksydacyjnej na korzyść zwiększenia aktywności glikolitycznej i wytwarzania mleczanu. Taki sposób pozyskiwania energii charakteryzuje macierzyste komórki nowotworu (ang. *cancer stem cells*, CSC), preferujące środowisko niszy hipoksyjnej guza [66]. Ze względu na efektywny system naprawczy DNA, CSC są jedną z przyczyn odporności nowotworu na chemio- i radioterapię [67].

Przejście nabłonkowo-mezenchymalne (ang. *epithelial–mesenchymal transition*, EMT) to proces, w którym komórki adherentne nabywają zdolności do migracji. W stanach niepatologicznych odgrywa kluczową rolę podczas embriogenezy. Możliwa jest również jego aktywacja przez komórki nowotworowe, następująca m.in. wskutek odpowiedzi na TGF-β, uwalniany przez komórki CAF [68]. EMT prowadzi do utraty polarności komórek, przerwania połączeń między nimi, uszkodzenia błony podstawnej i reorganizacji macierzy śródmiąższowej. Obniżeniu ulega ekspresja kadheryny epitelialnej (ang. *cadherin 1*, CDH1), β-kateniny, okludyny i kaludyny. Natomiast aktywowana jest ekspresja markerów związanych z fenotypem mezenchymalnym, wśród których wyróżnia się kadherynę neuralną (ang, *cadherin 2*, CDH2), wimentynę (ang. *vimentin*, VIM) oraz FN [69] (Rycina 3). Degradacja ECM ułatwia rozsiew komórek rakowych do odległych tkanek i tworzenie przerzutów [70].
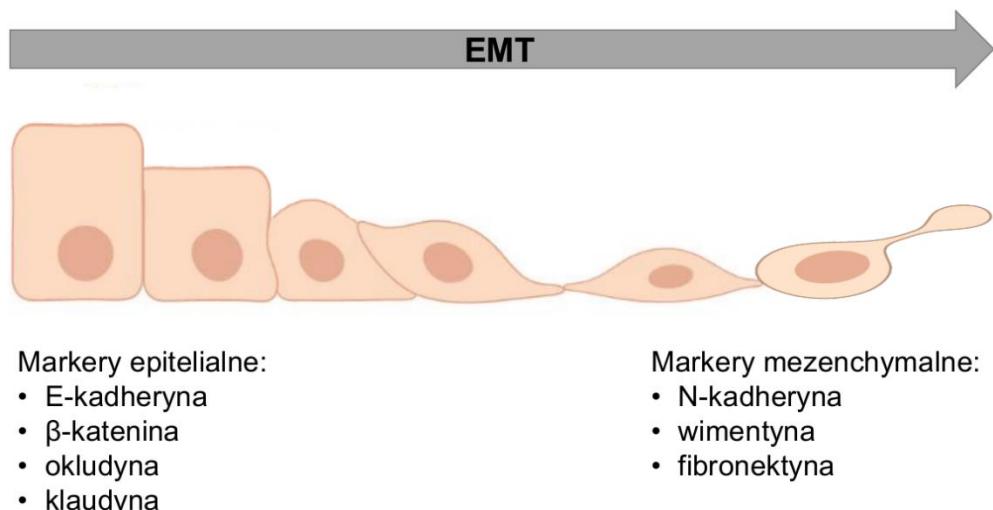
Rycina 3. Schemat przejścia epitelialno-mezenchymalnego wraz z charakterystycznymi dla danego fenotypu markerami. Rysunek wykonano przy pomocy BioRender.com.

Wpływ ECM na przemieszczanie się komórek nie ogranicza się jedynie do pośredniczenia w przebiegu procesu EMT. Kluczowymi atrybutami ECM, regulującymi migrację komórkową są: topologia dwuwymiarowa błony podstawnej a także trójwymiarowa macierzy śródmiąższowej; usieciowanie poszczególnych komponentów; sztywność oraz elastyczność; obecność porów, w tym tych powstałych wskutek proteolizy; gradienty sztywności (durotaksja) lub stężenia ligandów (haptotaksja); skład zarówno jakościowy jak i ilościowy [71]. W odniesieniu do ostatniej z wymienionych cech wysoko inwazyjny GBM charakteryzuje się nadekspresją: kolagenu IV, brewikanu, HA, FN, i TNC, spada w nim natomiast poziom agrekanu i TNR [72, 73] (Rycina 4).
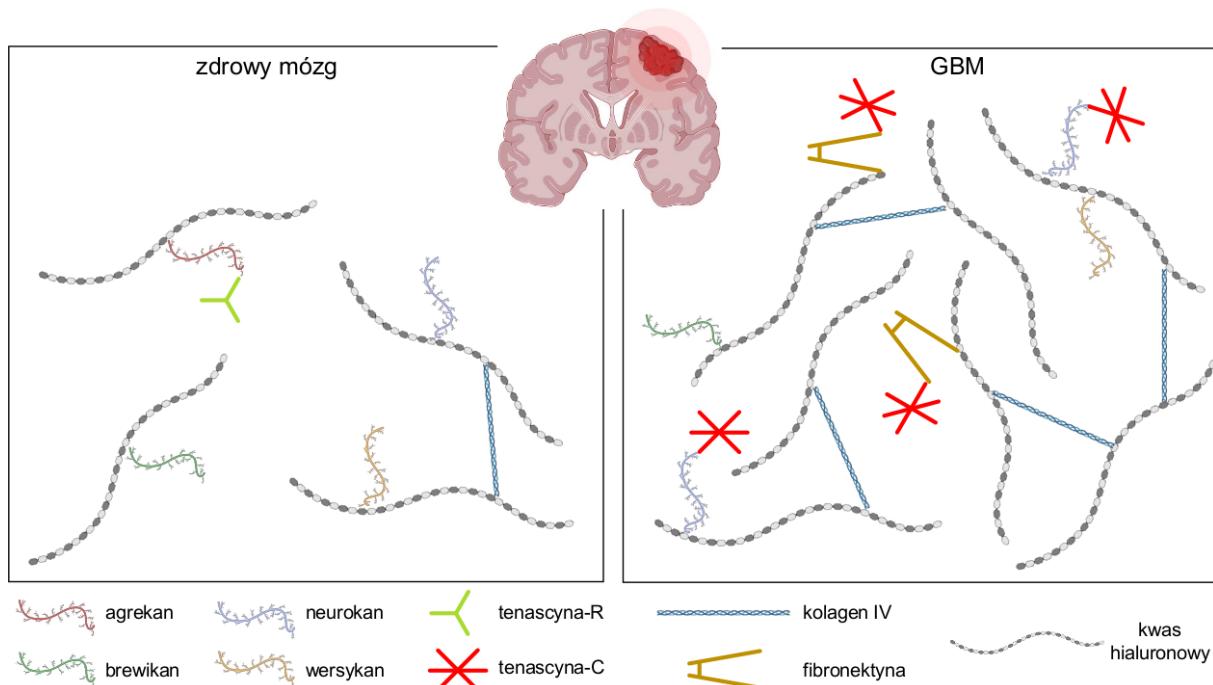
Rycina 4. Macierz zewnątrzkomórkowa zdrowego mózgu i glejaka. Schematyczne przedstawienie względnej ilości poszczególnych komponentów ECM w tkance. Na podstawie [72]. Rysunek wykonano przy pomocy BioRender.com.

6.2.2 Tenascyna-C

Tenascyny to multimeryczne glikoproteiny ECM o masie cząsteczkowej podjednostek pomiędzy 150 a 380 kDa. Jest to rodzina pięciu białek, oznaczonych jako tenascyna-C, -R, -W, -X i -Y (TNC, TNR, TNW, TNX, TNY) [74]. Ich nazwa pochodzi od łacińskich słów *tenere* – trzymać oraz *nasci* - urodzić się, odnoszących się do obecności TNC w ścięgnach i zarodkach [75]. Tenascyny składają się z identycznych podjednostek zbudowanych ze zmiennej liczby powtórzonych domen, w tym powtórzeń heptadowych, powtórzeń podobnych do EGF, domen

fibronektyny typu III (FNIII) i C-końcowej domeny kulistej, podobnej do tej obserwowanej w fibrynogenach (Rycina 5A). Podczas gdy TNR obecna jest głównie podczas rozwoju OUN, a TNX i TNY w tkance łącznej mięśni szkieletowych, TNC i TNW obserwowane są w różnych rozwijających się tkankach [74].
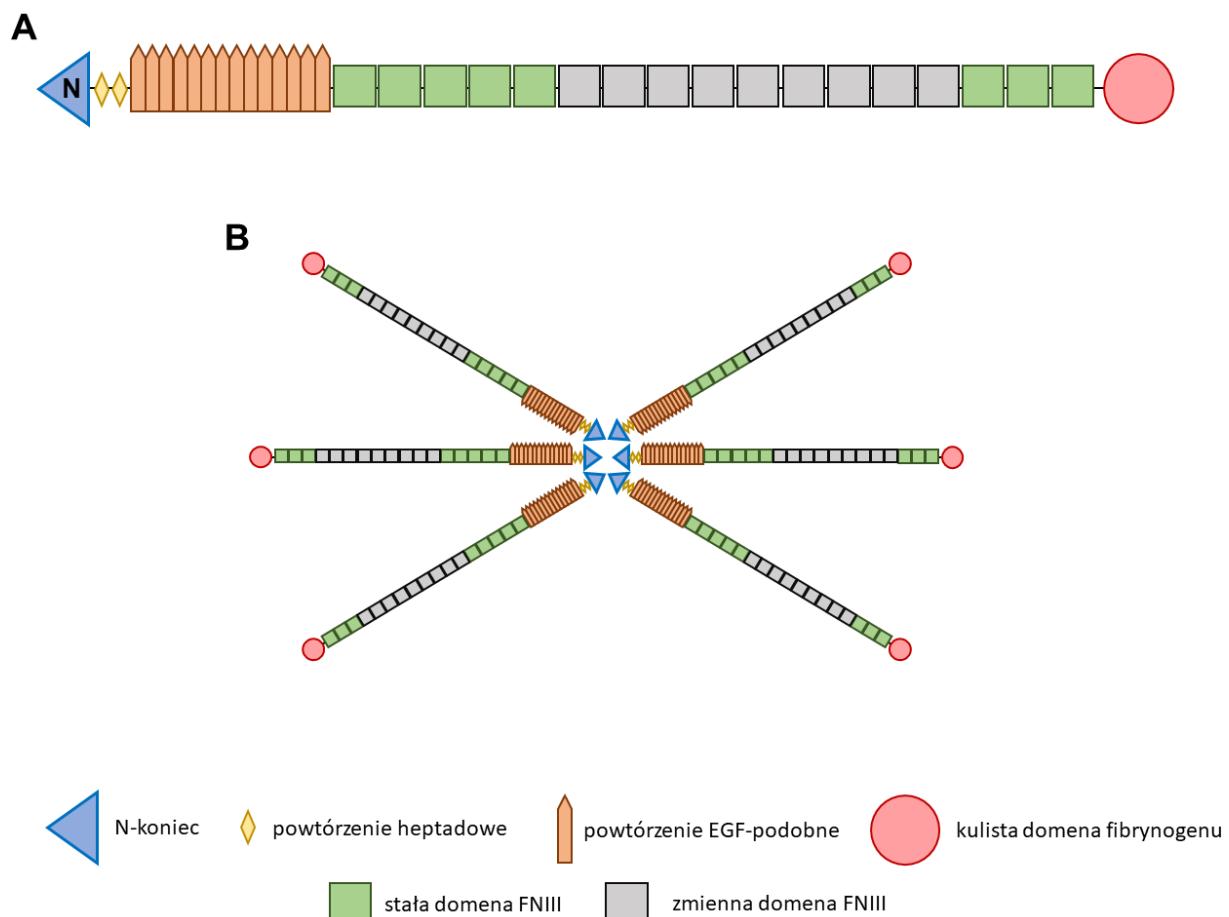
Rycina 5. Budowa tenascyny-C. (A) Pojedynczy monomer zdudowany z domen: N-końcowej, kulistej, FNIII stałych i zmiennych oraz powtórzeń: heptadowych i podobnych do EGF. (B) Połączone N-końcami monomery tworzą *heksabrachion*.

Ludzki gen *TNC* znajdujący się na 9 chromosomie jest stosunkowo długą sekwencją, w skład której wchodzi 29 eksonów [76]. Istnieje wiele różnych izoform TNC powstałych na poziomie transkrypcyjnymi i potranslacyjnymi. W ludzkiej TNC zawsze obecne jest osiem powtórzeń FNIII, a kolejne dziewięć podlega alternatywnemu splicingowi, potencjalnie dając 511 różnych wersji mRNA. Ta teoretyczna wartość przekłada się na nie więcej niż sto rzeczywiście odkrytych wersji splicingowych TNC, jako że poszczególne powtórzenia FNIII są od siebie zależne [77]. Złożoność transkryptu TNC ma znaczący wpływ na jej funkcję, ponieważ powtórzenia FNIII różnią się między sobą miejscami rozszczepienia

proteolitycznego oraz lokalizacją modyfikacji potranslacyjnych, do których zaliczamy glikozylację i cytrulinację. Gotowe białko, zwane również *heksabrachionem* (z greki sześcioramienny) jest kompleksem sześciu identycznych monomerów połączonych ze sobą mostkami dwusiarczkowymi na N-końcu [77] (Rycina 5B). TNC degradowana jest przez MMP oraz proteazy cysteinowe. Większość miejsc cięcia znajduje się w miejscach alternatywnego splicingu [78].

Jak już wspomniano, TNC obecna jest w zarodkach, konkretniej wokół komórek ruchliwych, w miejscach interakcji nabłonkowo-mezenchymalnych, w gęstej tkance łącznej, takiej jak kości, chrząstki i ścięgna, a także w OUN. U dorosłych poziom ekspresji tego białka jest nieporównywalnie niższy. W rozwiniętym organizmie TNC widoczna jest bowiem w jedynie ścięgnach i niszach komórek macierzystych - w mieszkach włosowych, kryptach jelitowych i w szpiku kostnym. Patologicznie pojawia się w okolicach stanów zapalnych i urazów mechanicznych, a także w guzach litych [79]. W stanach nienowotworowych głównym jej źródłem są mezenchymalne komórki macierzyste oraz leukocyty [78].

Jako że obecność TNC jest ograniczona w czasie i przestrzeni, jej ekspresja podlega licznym regulacjom. Region promotorowy *TNC* zawiera kasetę TATA, której aktywność transkrypcyjna zależy od białek regulatorowych [80]. Przykładowo czynnik transkrypcyjny kontrolujący rozwój mózgu i narządów zmysłu (ang. *orthodenticle homeobox 2*, OTX2) wycisza ekspresję genu [76]. Poziom TNC może być ponadto regulowany przez stres mechaniczny. Zauważono, że w fibroblastach poddanych naprężeniom rozciągającym dochodzi do translokacji czynnika transkrypcyjnego związanego z miokardią (ang. *myocardin-like protein 1*, MKL1), aktywującego ekspresję TNC [81]. Produkcję TNC w przypadku uszkodzeń mechanicznych tkanki napędzają TGF-β, płytkopochodny czynnik wzrostu (ang. *platelet-derived growth factor*, PDGF) i glikokortykosteroidy [76].

TNC oddziałuje bezpośrednio z wieloma komponentami ECM. Do najlepiej poznanych interakcji zaliczamy tę z FN powstałą poprzez rozproszone w powtórzeniach FNIII miejsca wiązania dla tego białka. TNC wiąże ponadto kolagen, periostynę, fibrylinę typu drugiego, kontaktynę a także poprzez domenę kulistą lektykany i integryny [78]. Z cząsteczek sygnałowych warto wspomnieć TGF-β, VEGF, PDGF i czynnik wzrostu fibroblastów (ang. *fibroblast growth factor*, FGF), których sekwestracja przez FNIII TNC przedłuża ich okres półtrwania a także przyczynia się do ich lokalnego zatężenia [82].

Za najważniejszy mechanizm działania TNC należy uznać jej wpływ na adhezję komórkową. Przy braku TNC w ECM, fibroblasty przylegają do podłoża wskutek oddziaływania z FN. Odbywa się to za pośrednictwem integryny α5β1 i syndekanu-4 (ang.

syndecan-4, SDC4), dochodzi do aktywacji białka Rho, co stymuluje tworzenie stresowych włókien aktynowych i skutkuje rozpostarciem się komórki. Obecność TNC blokuje oddziaływania między FN a SDC4, ponieważ obecne w niej domeny FNIII maja silne powinowactwo do obu tych białek. Skutkuje to przerwaniem szlaku sygnałowego i destabilizacją struktur aktynowych, co zmniejsza adhezję komórki do podłoża [83]. Dodatkowo TNC poprzez blokowanie aktywacji kinazy ogniskowo-adhezyjnej (ang. *focal adhesion kinase,* FAK) indukuje fenotyp komórek ruchliwych na obrzeżach mechanicznego uszkodzenia tkanki, dzięki czemu ograniczeniu ulegają granice tworzenia zrostów [84]. Procesy ten promują migrację fibroblastów podczas gojenia ran [85].

Wpływ TNC na mechanizmy zwiększające ruchliwość i związaną z nią inwazyjność obserwowane są również w przypadku komórek nowotworowych [86]. TNC ulega silnej nadekspresji także w CAF, komórkach zrębowych guza oraz komórkach CSC [87, 88]. Na podstawie metaanalizy wskazano, że wysoki poziom tego białka koreluje ze stopniem zaawansowania nowotworu i złym rokowaniem dla pacjentów w przypadku 14 typów nowotworu. Wśród nich znalazły się między innymi rak: prostaty, piersi, jelita grubego, trzustki i płuc [89]. Należy jednak pamiętać, że wspomniana metaanaliza nie obejmowała wszystkich typów nowotworów. Na przestrzeni ostatnich dwóch lat opublikowano prace wskazujące na udział TNC w kancerogenezie GBM [90, 91], raka piersi [92, 93], prostaty [94, 95], trzustki [96, 97], okrężnicy [98], żołądka [99], pęcherza [100], jelita grubego [101] i jajnika [102].

6.3 Niekodujące RNA

Podczas gdy wszystkie somatyczne komórki w ludzkim ciele zawierają ten sam materiał DNA, właściwości ich poszczególnych typów różnią się, tak że neuron wygląda i zachowuje się inaczej od leukocytu. Spowodowane jest to występowaniem odmiennych wzorców ekspresji genów, zależnych od stanu i funkcji pełnionej przez komórkę. Regulacja poziomem tejże ekspresji zachodzi zarówno na poziomie tranksrypcyjnym jak i potranskrypcyjnym, zależnym między innymi od interakcji mRNA z białkami lub niekodującymi RNA (ang. *non-coding RNA*, ncRNA) [103]. Różnice występujące w poziomach produkcji określonych produktów genowych są odpowiedzialne również za niektóre stany patologiczne, w tym za kancerogenezę. Badanie tych różnic oraz mechanizmów kryjących się za ich powstawaniem przybliża nas do poznania biologii komórki nowotworowej [104, 105].

Cząsteczki RNA ze względu na ich potencjał translacyjny można podzielić na dwie grupy: kodujące i niekodujące. Ponieważ całkowita długość kodujących eksonów stanowi 1,2% genomu euchromatycznego [106] najwyraźniej ncRNA stanowią większość transkryptów

w komórce. NcRNA mogą być syntetyzowane w sposób ciągły, gdy są związane ze splicingiem - mały jądrowy RNA (ang. *small nuclear RNA*, snRNA), modyfikacjami na etapie transkrypcji - mały jąderkowy RNA (ang. *small nucleolar RNA*, snoRNA) lub translacją - rybosomalny RNA (ang. *ribosomal RNA,* rRNA) i transferowy RNA (ang. *transfer RNA,* tRNA) [106]. Niemniej jednak ekspresja ncRNA może zależeć od stadium poszczególnych komórek, aktywacji szlaków, być odpowiedzią na bodźce z otoczenia lub pojawiać się w stanach patologicznych, pełniąc funkcję regulacyjną. Wśród regulatorowych RNA wyróżniamy: długie niekodujące RNA (ang. *long noncoding RNA*, lncRNA), koliste RNA (ang. *circular RNA*, circRNA) i małe niekodujące RNA, takie jak oddziałujące z białkami Piwi (ang. *Piwi-intaracting RNA,* piRNA), microRNA (miRNA) i krótkie interferujące (ang. *short interfering RNA*, siRNA) [106, 107].

Prace z ostatnich dwudziestu lat zmieniły nasze postrzeganie regulatorowych ncRNA od „śmieciowych" produktów transkrypcyjnych do funkcjonalnych cząsteczek, pośredniczących w licznych procesach komórkowych. Pierwszymi odkrytymi krótkimi ncRNA były dwa fragmenty transkryptu lin-4 pochodzące z *Caenorhabditis elegans,* komplementarne do 3' regionu niepodlegającego translacji (ang. *untranslated region*, UTR) mRNA genu *lin-14* i obniżające poziom ekspresji białka LIN-14 [108]. Opublikowane kilka lat później badania Fire'a i Mello nad nicieniem *C. elegans* dały początek interferencji RNA (ang. *RNA interference*, RNAi). W publikacji z 1998 roku przedstawili wprowadzenie do komórek dwuniciowego RNA (ang. *double-stranded RNA*, dsRNA), wyciszające ekspresję genu, którego transkrypt zawiera komplementarną do niego sekwencję [109].

Badania pojedynczych interakcji ncRNA-mRNA nie pozwalają w pełni dostrzec ich istotności w komórce. Niektóre z ncRNA regulują bowiem ekspresję wielu genów, tworząc złożone sieci regulatorowe. Co więcej, poszczególne ncRNA mogą oddziaływać same ze sobą, wpływając wzajemnie na swoją stabilność i funkcjonalność. Istnienie osi wzajemnych oddziaływań stanowi rdzeń badań nad konkurującymi endogennymi RNA (ang. *competing endogenous RNA*, ceRNA). Wysoce złożona natura niektórych relacji pomiędzy ncRNA wskazuje ich rolę jako kluczowych regulatorów w ważnych szlakach komórkowych. Zaburzenia tych interakcji mają szerokie konsekwencje i są powszechne w przypadku rozwoju tkanki nowotworowej [110].

6.3.1 Powstawanie i mechanizm działania miRNA

MiRNA to krótkie, liczące pomiędzy 19 a 25 nukleotydów, fragmenty kwasu rybonukleinowego. Funkcją miRNA jest potranskrypcyjna regulacja poziomu ekspresji genów. Szacuje się, że kontroli tego typu ulega ponad 30% białek kodujących geny ssaków [111]. MiRNA jest obecne we wszystkich wielokomórkowych eukariontach, przy czym warto wspomnieć, iż istnieją niewielkie różnice w szlakach biogenezy i modelach działania między miRNA u roślin i zwierząt [112]. Analiza z 2019 r., łącząca strategię walidacji *in silico* i podejścia eksperymentalnego, wskazuje na istnienie 2300 ludzkich dojrzałych miRNA [113].

Kanoniczny szlak biogenezy miRNA, (Rycina 6), rozpoczyna się od transkrypcji kilkusetnukleotydowego pierwotnego miRNA (ang. *primary miRNA,* pri-miRNA) o strukturze spinki do włosów. Kompleks mikroprocesorowy, składający się z białka DGCR8 wiążącego RNA i rybonukleazy III Drosha, przetwarza pri-miRNA w prekursorowy RNA (pre-miRNA) o długości 60-70 nt. Ma on nadal strukturę spinki do włosów, tym razem z dwoma niesparowanymi nukleotydami na końcu 3', co jest sygnaturą cięcia za pośrednictwem RNazy III [114, 115]. Pre-miRNA jest eksportowane do cytoplazmy przez mechanizm eksportyny 5 i GTPazy Ran. RNaza III Dicer wraz z białkiem wiążącym RNA (ang. *trans-activation responsive RNA-binding protein*, TRBP) przyłączają się do 3'-końca pre-miRNA, katalizując utworzenie 19-25 nt dwuniciowego miRNA [115]. Dupleks jest następnie włączany do kompleksu z białkiem AGO2, którego domena PAZ wiąże koniec 3' nici wiodącej [116].

Jedna z nici dupleksu jest odrzucana w procesie zwanym selekcją nici. Najczęściej nicią funkcjonalną, wiodącą, zostaje ta o niższej stabilności termodynamicznej lub zawierająca urydynę na 5' końcu. Nić pasażerska, o wyższej stabilności na swoim 5-końcu, ulega na ogół degradacji [117, 118]. Dojrzałe miRNA z ramion 5' i 3' pre-miRNA są oznaczone sufiksami odpowiednio -5p i -3p [119]. MiRNA wraz z AGO2 tworzą efektorowy kompleks wyciszający indukowany przez RNA (ang. *RNA-induced silencing complex*, RISC) [120].

W większości przypadków mechanizm działania miRNA polega na interakcji z 3'UTR docelowych mRNA co skutkuje stłumieniem ich ekspresji. Niemniej jednak jest również możliwe aby miRNA oddziaływały z 5'UTR i sekwencją kodującą [121, 122]. Jeżeli miRNA przyłączy się do 3' UTR mRNA, jego obecność zaindukuje dysocjację eukariotycznych czynników inicjujących translację 4A (ang. *eukaryotic translation initiation factor 4A,* eIF4A), co uniemożliwia rozpoczęcie translacji zależnej od czapeczki na 5' końcu [123].

Jedno miRNA może celować w wiele różnych mRNA, jednocześnie ekspresja jednego transkryptu może być regulowana przez wiele miRNA [124]. Odpowiedni transkrypt rozpoznawany jest w zależności od komplementarności sekwencji elementów odpowiedzi

miRNA (ang. *miRNA response elements,* MRE) z regionem *seed* miRNA zlokalizowanym w pozycji 2-8 nt na końcu 5' miRNA [125, 126]. Idealne parowanie zasad między miRNA i MRE, które jest powszechne u roślin, ale rzadkie u zwierząt, skutkuje endonukleolityczną degradacją docelowego RNA poprzez AGO2. Cięcie następuje w punkcie pomiędzy parowaniem nukleotydów 10 i 11 miRNA. W przypadku braku pełnej komplementarności pomiędzy miRNA a mRNA, powstaje dupleks tychże dwóch cząsteczek. Struktury te tworzą konglomeraty na polisomach lub są przyciągane do komórkowych ciałek P, gdzie następują ich degradacja [127].
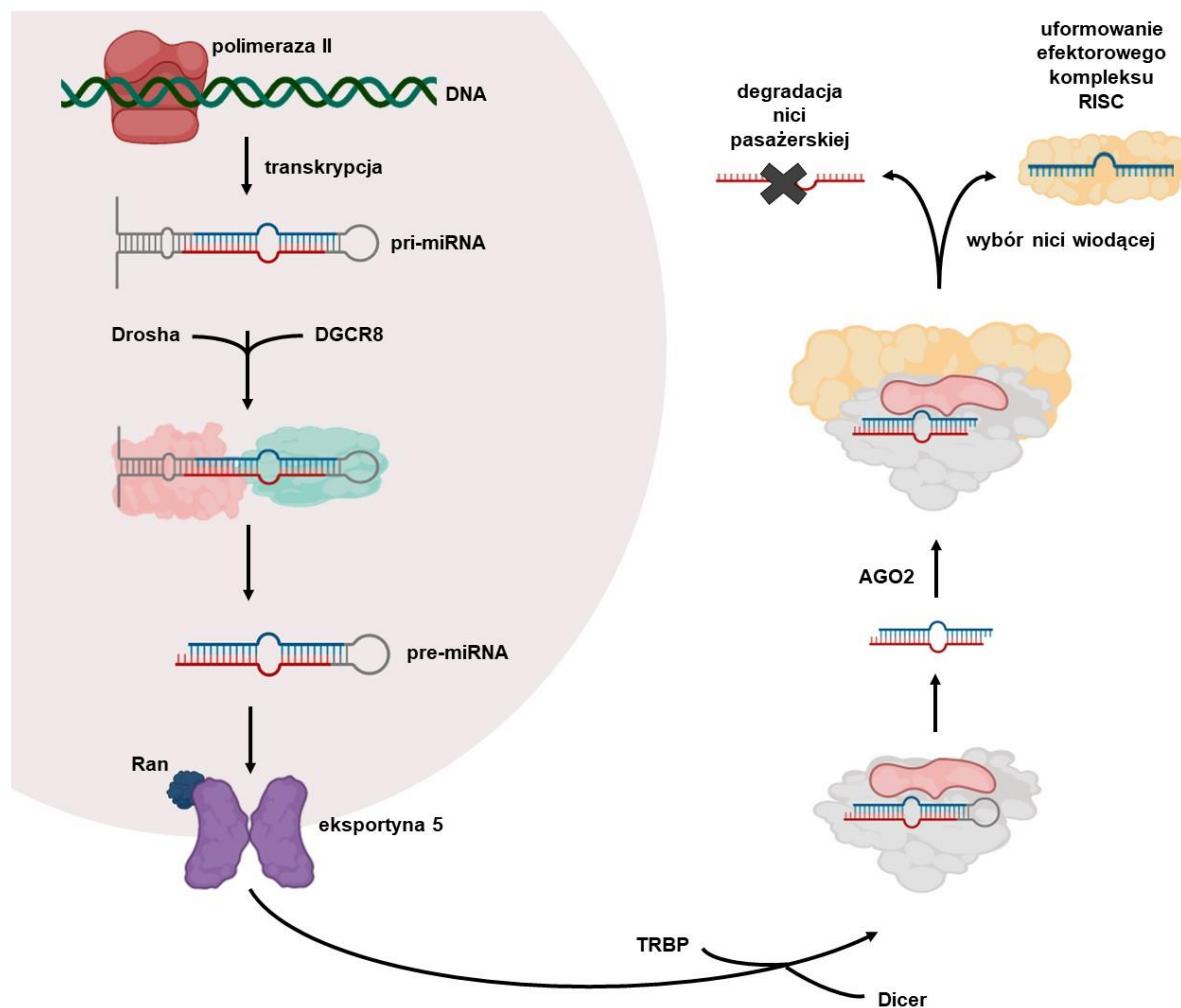
Rycina 6. Biogeneza miRNA. RNA polimeraza II transkrybuje pri-miRNA. Kompleks mikroprocesorowy skraca je do pre-miRNA, które poprzez eksportynę 5 wydostaje się do cytoplazmy. Dicer przecina pre-miRNA tworząc dupleks miRNA. Dicer wraz z TRBP łączy się z AGO2 formując kompleks załadunkowy. Następuje wybór nici wiodącej, która wraz z AGO2 tworzy kompleks RISC. Nić pasażerska ulega degradacji. Rysunek wykonano przy pomocy BioRender.com.

6.3.2 Mechanizm działania siRNA

siRNA to krótkie RNA powstające na drodze mechanizmu RNAi. To proces występujący naturalnie zarówno w roślinach, niższych zwierzętach, jak i u ssaków jako mechanizm obronny np. przed infekcja wirusową [128]. Cząsteczki te są dupleksami RNA, składającymi się z dwóch 21 nukleotydowych nici, powstającymi z dłuższego dsRNA, którego źródłem mogą być np. fragmenty genomów wirusów RNA. dsRNA długości zwykle 30-100 pz hydrolizowane jest przez białko Dicer. W siRNA 19 nukleotydów z 21 tworzy pomiędzy sobą pary zasad, a 2 znajdują się na niesparowanych końcach 3'. Podobnie jak w przypadku miRNA, dupleks zostaje włączony do kompleksu RISC, gdzie dochodzi do selekcji nici wiodącej opartej o stabilność 5' końca [129]. siRNA ma przede wszystkim zapewnić obronę przeciwwirusową i stabilność genomu, podczas gdy miRNA działa jako regulator ekspresji genów endogennych [130]. Różnice pomiędzy tymi dwoma krótkimi ncRNA przedstawiono w Tabeli 1. Mechanizm działania siRNA zakłada pełną komplementarność do docelowego mRNA. Dzięki swojej długości, możliwe jest parowanie siRNA z tylko jednym transkryptem, co czyni tą cząsteczkę bardziej specyficzną niż miRNA. Komplementarne wiązanie aktywuje nukleazę AGO2, która następnie przecina mRNA między zasadami 10 i 11 w stosunku do końca 5' nici wiodącej [131]. Wygenerowane fragmenty mRNA są następnie degradowane przez różnego typu egzonukleazy zawarte w cytoplazmie [130].

Tabela 1. Różnice pomiędzy miRNA a siRNA.

właściwość	miRNA	siRNA
pochodzenie	endogenne	egzogenne: transpozony, wirusy
prekursor	RNA o strukturze spinki do włosów	długie dsRNA
długość	19-25 nt	21 nt
mechanizm	degradacja mRNA lub zahamowanie translacji	degradacja mRNA
funkcja	regulacja ekspresji genów	obrona przeciwwirusowa, odpowiedź na stres
komplementarność	zawężona do regionu *seed*	pełna
wiązanie mRNA	3'UTR	region kodujący
ilość celowanych sekwencji	wiele	jedna

6.3.3 Terapia RNAi

W porównaniu z chemioterapeutycznymi lekami przeciwnowotworowymi, terapie oparte o RNAi mają szereg zalet. Po pierwsze, przy odpowiednim ukierunkowaniu, są bezpieczne dla komórek nienowotworowych. Po drugie, RNAi działa na potranslacyjnym

etapie ekspresji genów, więc nie oddziałuje z DNA, dzięki czemu unika się ryzyka mutacji i teratogenności typowych dla terapii genowej. Po trzecie, RNAi jest wysoce skuteczna, może spowodować radykalne zahamowanie ekspresji genów w pojedynczej komórce przy zaledwie kilku kopiach krótkiego RNA. Po czwarte, w porównaniu z innymi lekami małocząsteczkowymi lub lekami opartymi na przeciwciałach, w przypadku RNAi mamy nieograniczony wybór celów i specyficzność wynikającą z komplementarnego parowania zasad [132].

W przypadku terapii opartej o RNAi należy zidentyfikować transkrypt zaangażowany w rozwój choroby, następnie użyć wybranej sekwencji mRNA do zaprojektowania komplementarnego oligonukleotydu, wprowadzić go do komórek. Leki oparte o RNAi mogą wywoływać niepożądane efekty poprzez kilka mechanizmów [133]. Kwasy nukleinowe mogą m.in. wiązać się z białkami na powierzchni lub wewnątrz komórek, prowadząc do zakłóceń w przekaźnictwie sygnałów, w tym indukcji odpowiedzi interferonowej [134]. RNA może również wykazywać częściową komplementarność z wieloma innymi transkryptami, nawet jeśli są zaprojektowane tak, aby były w pełni komplementarne tylko do jednego.

Istnieje kilka rodzajów cząsteczek, na których można oprzeć terapię RNAi: krótkie RNA tworzące strukturę spinki do włosów (ang. *short hairpin RNA*, shRNA), miRNA i siRNA. shRNA ma bardziej skomplikowaną strukturę niż inne cząsteczki, ponadto wymaga ekspresji z plazmidu lub wektorów wirusowych [135]. miRNA poprzez niekomplementarne wiązanie się z mRNA może wyciszać wiele różnych transkryptów, powodując niespecyficzne efekty (ang. *off-target*) [136]. siRNA dzięki swojej prostocie i efektywności wydaje się być najlepszym narzędziem do terapii RNAi [137].

Jednakże o ile podejście terapeutyczne oparte na siRNA obejmuje jedynie obniżenie ekspresji konkretnego transkryptu, tak w przypadku miRNA możemy wyróżnić dwa mechanizmy. Pierwszy z nich przypomina terapię antysensowną, w której syntetyczne jednoniciowe RNA, komplementarne do nici wiodącej miRNA, działa jako jego antagonista miRNA (antagomiry). Związana w kompleks cząsteczka miRNA jest niefunkcjonalna, poziom ekspresji docelowego mRNA ulega podwyższaniu. W podejściu zastępczym, syntetyczne miRNA (znane również jako miRNA naśladujące, ang. *mimic miRNA*) jest wykorzystywane do imitowania funkcji endogennych miRNA, obniżając tym samym ekspresję docelowego transkryptu [130].

Na chwilę obecną FDA dopuściła do komercyjnej sprzedaży dwie terapie wykorzystujące siRNA: patisiran (Onpattro®, Alnylam Pharms Inc) w leczeniu dziedzicznej amyloidozy transtyretynowej oraz givosiran (Givlaari™, Alnylam Pharms Inc) w leczeniu ostrej

porfirii wątrobowej. Dla dwóch kolejnych leków siRNA zostały złożone wnioski o rejestrację nowego leku: w 2020 roku lumasiran (Oxlumo, Alnylam Pharms Inc) dla pierwotnej hiperoksalurii typu 1 a w 2021 roku inclisiran (Legvio, Novartis) dla pierwotnej hipercholesterolemii [138]. W trzeciej fazie badań klinicznych znajdują się również trzy inne: nedosiran, bevasiranib i tivanisiran (https://clinicaltrials.gov). Patrząc na ilość nowopowstałych zatwierdzonych terapii, zdając sobie sprawę z ilości badań będących jeszcze na etapach przedklinicznych a także mając w pamięci, że mechanizm RNAi odkryty został ledwie 24 lata temu [109], nie sposób pozostać obojętnym wobec potencjału kryjącego się za terapiami wykorzystującymi interferencję RNA.

6.4 Nanonotechnologia

Słowo „*nano*" wywodzące się z greki, gdzie oznacza „karzeł", sugeruje coś bardzo małego. Jako przedrostek, wprowadzony oficjalnie w 1960 roku na Generalnej Konferencji Miar, przedstawia jedną miliardową część danej jednostki (10^{-9}). Nanonauka to badanie struktur i cząsteczek w skali od 1 do 100 nm, a technologia, która wykorzystuje ją w praktycznych zastosowaniach, nazywana jest nanotechnologią [139]. Jedno z najważniejszych zastosowań nanotechnologii w biologii molekularnej dotyczy kwasów nukleinowych. W 2006 r. Rothemund opracował „DNA origami", w którym wytwarzał struktury o dowolnym kształcie, zwiększając złożoność i wielkość samoorganizujących się nanostruktur DNA [140].

W ostatnim czasie zwrócono uwagę na ogromny potencjał, jaki nanotechnologie odgrywają w biomedycynie, zwłaszcza w diagnostyce [141], obrazowaniu na poziomie molekularnym [142] i klinicznym [143], terapiach przeciwnowotworowych [144] oraz w dostarczaniu leków [145]. Obecnie diagnostyka nowotworów opiera się na technikach obrazowania i analizy morfologicznej tkanek (histopatologia) lub komórek (cytologia). Najczęściej stosowane techniki obrazowania, takie MRI, CT, endoskopia i ultrasonografia, umożliwiają wykrycie guza tylko w przypadku widocznej zmiany w tkance. Ponadto nie pozwalają na odróżnienie zmian łagodnych od złośliwych [146].

Nanocząstki pokryte przeciwciałami, peptydami lub aptamerami mogą rozpoznawać krążące we krwi obwodowej komórki uwolnione z guza pierwotnego. W badaniu pacjentek z rakiem piersi w 70% przypadków możliwe było oczyszczenie komórek związanych wcześniej z magnetycznymi nanocząstkami [147]. Wykorzystując złote nanocząstki opłaszczone przeciwciałem anty-CD3 opracowano test immunologiczny do specyficznego wykrywania komórek ostrej białaczki limfoblastycznej T [148]. Do detekcji guza *in vivo* zaprojektowano kropki kwantowe opłaszczone peptydem będącym substratem dla MMP2, fluoroforem oraz

wygaszaczem sygnału. Ponieważ nowotwory takie jak glejak stopnia IV skorelowane są z wysokim poziomem ekspresji MMP2 [149], opisywane nanocząstki zakumulowane wokół GBM uwalniały fluorofor umożliwiając detekcję guza [150]. Skupienie cząstek wokół guza spowodowane było efektem zwiększonej przepuszczalności i retencji nanocząstek wokół tkanki nowotworowej [151].

Ciekawym aspektem nanotechnologii jest zastosowanie jej w terapii fototermicznej (ang. *photothermal therapy,* PTT), będącej alternatywną metodą leczenia nowotworów. PTT polega na aktywacji środków fotouczulających przez pulsacyjne napromienianie laserem w zakresie bliskiej podczerwieni, w celu wytworzenia ciepła niszczącego tkankę, w tym przypadku nowotworową. Podwyższenie temperatury powyżej 42ºC niesie ze sobą skutki letalne takie jak zatrzymanie procesów translacji i transkrypcji, degradację białek i zmiany w przepuszczalności błony komórkowej [152]. W porównaniu z konwencjonalną radioterapią lub chemioterapią, kluczowe zalety PTT obejmują zdolność do głębokiej penetracji tkanek i minimalny wpływ na otaczającą zdrową tkankę, przy założeniu stosowania terapii celowanej lub podania lokalnego [153]. Złote nanocząstki są najczęściej wykorzystywane jako fotosensybilizatory ze względu na ich znakomity potencjał konwersji fototermicznej, efekt powierzchniowego rezonansu plazmonowego [154]. Nanocząstki zbudowane z magnetytu i złota zostały wykorzystane do wywołania PTT w trójwymiarowych modelach GBM *in vitro*. Po 430 sekundach naświetlania laserem zaobserwowano śmierć 90% komórek wewnątrz modelu i jedynie 1% poza nim [155]. Do PTT używane są również inne materiały takie jak węgiel, pallad czy polidopamina [156].

Produkty nanotechnologii pomagają w dostarczaniu leków słabo rozpuszczalnych w wodzie do ich docelowych lokalizacji a także wykazują wyższą biodostępność wykazując typowe mechanizmy endocytozy [157]. Ze względu na swój mały rozmiar, mogą przechodzić przez śródbłonek w miejscach zapalnych, nabłonek przewodu pokarmowego i wątroby lub przenikać do mikrokapilar. Jako że najmniejsze naczynia włosowate w ciele mają średnicę około 5 µm, wielkość cząstek wprowadzanych do krwiobiegu musi być znacznie mniejsza, minimalizując ryzyko zatoru [158].

6.4.1   Nanonośniki

Nanonośniki, czyli nanotechnologiczne moduły transportowe, dzielimy na pięć podtypów: liposomy (struktury dwuwarstwowe lipidów), micele polimerowe (monowarstwy lipidowe), dendrymery (struktury silnie rozgałęzione) oraz nanocząstki (organiczne lub nieorganiczne) [159]. Do nanocząstek organicznych zaliczamy cząstki polimerowe oraz polimerosomy, czyli sztuczne pęcherzyki. W puli nanocząstek nieorganicznych odnajdziemy

przykładowo kropki kwantowe, mezoporowate cząstki krzemowe, złote nanocząstki i nanorurki a także nanocząstki tlenku żelaza [160] (Rycina 7). Ze względu na pełnioną funkcję i wpływ załadunku biologicznego, za nanonośniki uważa się cząstki o średnicy do aż 1 μm, jednak cząstki powyżej 200 nm często nie znajdują zastosowania w nanomedycynie, wykorzystującej urządzenia takie jak mikrokapilary o wspomnianej średnicy [158].
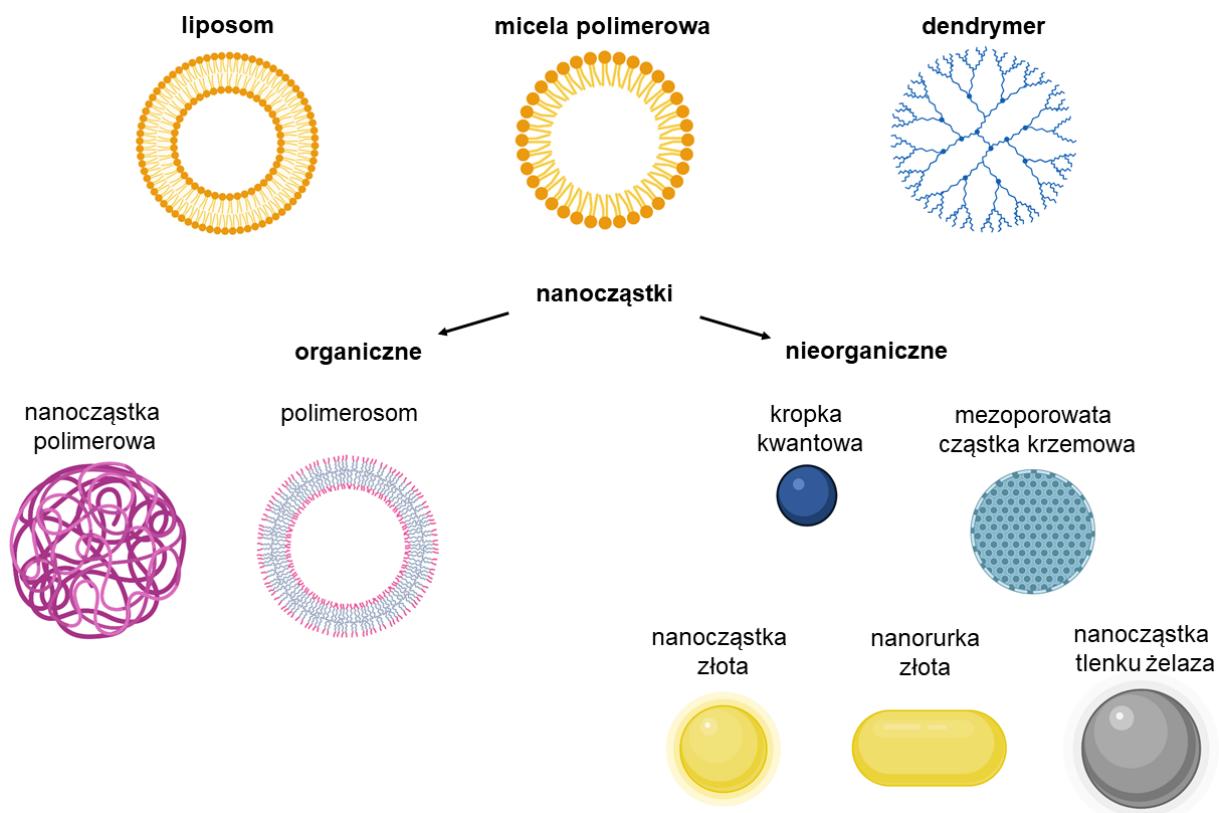
Rycina 7. Rodzaje nanośników. W puli nanocząstek nieorganicznych uwzględniono jedynie najpopularniejsze typy cząstek. Rysunek wykonano przy pomocy BioRender.com.

Nanonośniki można scharakteryzować przy pomocy czterech głównych atrybutów: rdzenia, otoczki, ukierunkowania i załadunku. Rdzeń może być hydrofobowy, anionowy, kationowy lub usieciowujący cząsteczkę, którą należy przenieść we wnętrzu. Otoczka zróżnicowana jest pod względem typu budulca, jego długości, gęstości i ponownie właściwości usieciowujących. Na powierzchni nanonośnika znajdować się mogą również cząsteczki ukierunkowujące, którymi mogą być przeciwciała, białka, witaminy, peptydy lub aptamery. Ponieważ zadaniem nanonośnika jest dostarczanie, wyróżniamy również różne typy załadunków, takie jak chemioterapeutyki, kwasy nukleinowe, białka czy fluorofory [159].

Rozmiar i rozkład wielkości to jedne z najważniejszych cechy nanonośników. Wpływają one bowiem na ich stabilność, toksyczność, efektywność dostarczania i uwalniania

leku [161]. Różne typy komórek są w stanie przyjąć różne wielkości cząstek. I tak komórki płaskonabłonkowego raka głowy i szyi oraz raka pęcherza wykazały zdolność wchłonięcia cząstek 1010 nm, podczas gdy komórki raka wątroby nie przyjmowały cząstek większych niż 93 nm [162]. Dla komórek gruczolakoraka jelita grubego wykazano 2,5-krotnie większą absorpcję cząstek 100 nm w porównaniu do cząstek 1μm [163]. Natomiast badania na komórkach raka szyjki macicy wskazały na wyższy wychwyt cząstek powyżej 375 nm, tłumacząc to niewystarczającą stymulacją fagocytozy przez cząstki mniejsze [164]. Przytoczone przykłady wskazują, że rozkład cząstek można przynajmniej częściowo dostroić, kontrolując ich rozmiar. Warto wspomnieć, iż na wychwyt nanocząstek wpływa również ich kształt, udowodniono bowiem, że cząstki sferyczne wnikają do komórek 5-krotnie efektywniej niż te podłużne, co tłumaczy się dłuższą enkapsulacją tych drugich w procesie endocytozy [165].

Powierzchnia nanonośników jest kolejnym kluczowym elementem decydującym o ich skuteczności. Nośniki mogą być rozpoznawane przez układ odpornościowy gospodarza po podaniu dożylnym i usuwane przez fagocyty [166]. To na pozór negatywne zjawisko wykorzystano niczym konia trojańskiego w terapii na modelu mysim, podczas której za ¼ dostarczonych do guza nanocząstek odpowiadały transportujące je monocyty [167]. Zazwyczaj jednak intencją projektowania nanonośników jest zminimalizowanie opsonizacji i przedłużenie ich obiegu *in vivo*. Można to osiągnąć przez powlekanie ich hydrofilowymi polimerami lub środkami powierzchniowo czynnymi bądź formułowanie ich z biodegradowalnymi polimerami np. glikolem polietylenowym [168]. Inną kwestią związaną z powierzchnią nanonośników jest ich potencjał elektrokinetyczny (zeta potencjał), powszechnie stosowany do charakteryzowania właściwości ładunku powierzchniowego, odnoszący się do potencjału pomiędzy dyspergantem a warstwą płynu przyczepioną do powierzchni cząstki. Wykazano, że nanocząstki o potencjale zeta powyżej 30 mV są stabilne w zawiesinie, gdyż ich ładunek powierzchniowy zapobiega tworzeniu skupisk [158]. Wartości potencjału zeta -14 mV stanowi granicę poniżej której rozpoczyna się agregacja cząstek [169]. Dodatni zeta potencjał umożliwia przyłączenie do nanocząstek negatywnie naładowanych terapeutyków takich jak cząsteczki RNA [170].

Efektywne nanonośniki powinny odznaczać się przede wszystkim wysoką zdolnością wiązania leku. Nasycenie terapeutykiem można osiągnąć dwoma sposobami. Metoda inkorporacji wymaga, aby był on wprowadzany w czasie formułowania nanonośnika. Metody adsorpcji i absorpcji polegają na inkubacji gotowego nanonośnika ze stężonym roztworem leku. Makrocząsteczki takie jak białka wykazują największą wydajność upakowania do nanocząstek, gdy są załadowywane w pobliżu ich punktu izoelektrycznego [171]. W przypadku

mikrocząsteczek skuteczność wiązania zwiększają wiązania jonowe między lekiem a nośnikiem [172].

Podczas opracowywania systemu dostarczania leku należy wziąć pod uwagę również jego późniejsze uwalnianie jak i biodegradację nośnika. W przypadku nanosfer, gdzie lek jest równomiernie rozprowadzony, uwalnianie leku następuje poprzez dyfuzję lub degradację nanocząstki. Jeżeli lek jest ładowany metodą inkorporacji, wówczas układ ma stosunkowo niewielki efekt początkowego wyrzutu i charakterystykę przedłużonego uwalniania. Ponadto na szybkość uwalniania mogą również wpływać interakcje jonowe między lekiem a składnikami pomocniczymi [158]. Uwalnianie załadowanych leków może być regulowane w odpowiedzi na stymulanty wewnętrzne, takie jak czynniki fizjologiczne i patologiczne: pH, potencjał redoks, obecność konkretnych enzymów. Uwalnianie leku może odbywać się również w sposób kontrolowany zewnętrznie, poprzez stymulanty takie jak: pole magnetyczne, światło, ultradźwięki [173]. Aby wykorzystać zewnętrzne pole magnetyczne do celowania w nowotwory, nanonośniki muszą być namagnesowane albo przez wprowadzenie magnetytu (Fe_3O_4) lub maghemitu (γ- Fe_2O_3), lub przez bezpośrednią modyfikację namagnesowanych cząstek metalu biokompatybilnymi polimerami. Nanocząstki tlenków żelaza są szeroko badane w wielu różnych zastosowaniach biomedycznych, w tym w dostarczaniu leków [174], obrazowaniu MRI [175], hipertermii [176] i transfekcji magnetycznej [177].

6.4.2 Dostarczanie RNA przy pomocy nanonośników

Istnieje kilka przeszkód wpływających na dostarczanie terapii opartych o cząsteczki RNA do komórek docelowych. Trudności zależą od umiejscowienia organu, który ma zostać poddany leczeniu oraz powiązanej z tym aspektem drogi administracji leku. Do wyboru jest bowiem podanie leku lokalne, bezpośrednio na tkankę lub do organu, albo podejście systemowe, poprzez naczynia krwionośne. Podanie lokalne można łatwo zaimplementować w przypadku organów typu oczy czy skóry, ale jest to możliwe również w kwestii zbitych guzów nowotworowych, odsłoniętych podczas operacji chirurgicznej [178].

W podaniu systemowym problemem jest między innymi brak stabilności krótkich RNA w warunkach fizjologicznych. Ze względu na małe rozmiary i niską masę (~7 nm, ~13 kDa) mogą one zostać usunięte z organizmu przez nerki podczas filtracji kłębuszkowej. Zwiększanie masy cząsteczkowej RNA poprzez dołączanie do nich różnego rodzaju ligandów może zakończyć się niepożądaną agregacją cząsteczek lub opsonizacją zakończoną rozpoznaniem przez fagocyty [132]. Ponadto zawarte w surowicy nukleazy, głównie 3'egzonukleazy, efektywnie degradują krótkie RNA w przeciągu 5-10 min [179]. Ustalono, że RNA może być

pobierane tylko przez kilka typów komórek w organach o niskiej zawartości nukleaz, np. komórki zwojowe siatkówki w oku [138]. Rozwiązanie stanowią między innymi modyfikacje kwasów nukleinowych, co niestety prowadzić może jednak do spadku ich efektywności [180].

W podaniu lokalnym pierwszą barierą, napotykaną przez cząsteczki RNA w drodze do komórki, jest błona cytoplazmatyczna, ograniczająca przechodzenie hydrofilowych, naładowanych negatywnie cząsteczek [181]. Po ewentualnym przekroczeniu błony, rozpoczyna się wewnątrzkomórkowy transport RNA, zazwyczaj na drodze endocytozy. Wczesne endosomy ulegają fuzji i dojrzewają do późnych endosomów, które następnie przenoszą ich zawartość do lizosomów. Zawarte w nich kwaśne hydrolazy degradują kwasy nukleinowe [132, 182]. Aby uniknąć takiej sytuacji musi dojść do ucieczki endosomalnej podczas której RNA zostaje uwolnione do cytozolu gdzie spełnia swoją molekularną funkcję [183]. W płynie wewnątrzkomórkowym RNA mogą zostać rozpoznane jako obce, zakaźne, potencjalnie patogenne cząsteczki, co aktywuje odpowiedź immunologiczną i produkcję interferonów [184]. W komórkach ssaków odpowiedź tego typu może zostać wywołana przez szlaki zależne lub niezależne od receptorów *toll*-podobnych (ang. *toll-like receptor,* TLR). Krótkie RNA aktywują trzy z trzynastu receptorów: TLR3, TLR7 i TLR8. Pierwszy z nich rozpoznaje dwuniciowe RNA, pozostałe dwa aktywowane zostają pod wpływem specyficznych sekwencji. RNA w szlaku niezależnym od TLR zostaje rozpoznane przez kinazę białkową aktywowaną RNA (ang. *protein kinase RNA-activated*, PKR) oraz produkt genu: indukowanego kwasem retinowym 1 (ang. *retinoic acid-inducible gene 1*, RIG1) [185].

Podsumowując, idealny system dostarczania RNA powinien: ochronić RNA przed nukleazami zawartymi w osoczu; zapobiegać fagocytozie i szybkiemu wydalaniu przez nerki; umożliwiać wniknięcie cząsteczki do wnętrza komórki; unikać degradacji lizosomalnej podczas szlaku przemieszczania wewnątrzkomórkowego; nie zmniejszać efektywności terapeutyku RNA; nie indukować dodatkowej odpowiedzi immunologicznej [186].

6.4.3   Nanonośniki w terapii glejaka

Stosowane w onkologii leki cytotoksyczne uszkadzają komórki szybko dzielące się, jakimi niewątpliwie są komórki nowotworowe, ale również zdrowe komórki naszego organizmu znajdujące się między innymi w szpiku kostnym, przewodzie pokarmowym czy mieszkach włosowych [187]. Dzięki postępowi w genomice i proteomice odkrywane są markery molekularne różnych typów nowotworów, co otwiera nowe ścieżki dla terapii specyficznie zabijających komórki nowotworowe. Projektowanie leków w nanoskali jest zdecydowanie najbardziej zaawansowaną technologią w obszarze zastosowań nanocząstek. Jej

potencjalne zalety to możliwość modyfikowania rozpuszczalności i sposobu uwalniania leków, ich biodostępności czy immunogenności. W konsekwencji rozwijane są dogodne drogi podawania leków, zmniejszające ich toksyczność, co powoduje spadek liczby skutków ubocznych [157].

Interferon β (INF-β) to cytokina naturalnie wytwarzana przez układ odpornościowy w odpowiedzi na bodźce biologiczne i chemiczne. Wywołuje działanie przeciwwirusowe, antyproliferacyjne i immunomodulujące w wielu typach komórek [188]. Zaproponowano terapię GBM polegającą na wprowadzeniu do loży pooperacyjnej plazmidu z wklonowanym genem *INF-β* w kationowym nanonośniku liposomowym. Badania pilotażowe na grupie 5 pacjentów wskazały na ekspresję transgenu u czterech z nich i redukcję masy guza u dwóch osób [189]. W trakcie pierwszej fazy klinicznej wykonano analizy mikromacierzowe skorelowane z ontologią genową na pacjentach pilotażowych. Wskaźnik OS w grupie badanej wyniósł 17 miesięcy. Po zastosowanej terapii zaobserwowano zmiany w ekspresji 29 genów, z czego większość powiązano z procesami apoptozy, odpowiedzi immunologicznej, angiogenezy i migracji komórkowej. W badaniach histologicznych próbek z autopsji wiele komórek nowotworowych wykazywało zmiany martwicze, a immunohistochemia zidentyfikowała obecność limfocytów CD8 i makrofagów infiltrujących guz [190].

Liposomy kationowe zastosowano również do dostarczania zmodyfikowanego, niezdolnego do replikacji, wirusa gorączki lasu Semliki niosącego ludzką interleukinę 12 (IL-12). IL-12 inicjuje różnicowanie limfocytów oraz indukuje produkcję interferonu-γ przez co zahamowane zostają rozrost nowotworu i tworzenie przerzutów [191]. Badania przedkliniczne wykazały brak neurotoksyczności opakowanej w liposom IL-12 u szczurów. W badaniach klinicznych fazy I i II zaplanowano ocenę bezpieczeństwa, maksymalnej tolerowanej dawki i skuteczności przeciwnowotworowej [192].

Na etapie drugiej fazy klinicznej przebadano termoterapię wykorzystującą nanocząstki magnetyczne na puli 59 osób ze wznową GBM. Pacjentom wstrzyknięto biokompatybilne nanocząstki tlenku żelaza bezpośrednio do guza, a następnie ogrzano je w zmiennym polu magnetycznym [144]. Leczenie połączono z radioterapią. Wykonalność i skuteczność tego podejścia wykazano wcześniej w badaniach klinicznych [193, 194] i *post mortem* [195]. Pacjenci z II fazy klinicznej żyli średnio 23,2 miesiąca licząc od momentu wystawienia diagnozy, w porównaniu do 14,6 miesiąca w grupie referencyjnej. W czasie termoterapii około połowa pacjentów odczuwała ciepło w leczonym obszarze, 14% z nich zgłosiła bóle głowy, u 9% temperatura ciała przekroczyła 38ºC. Dodatkowo u co piątej osoby zaobserwowano

drgawki i zaburzenia motoryczne. Skutki uboczne nowego podejścia terapeutycznego oceniono jako umiarkowane, ponadto nie odnotowano poważnych powikłań [144].

W 2021 roku zerową fazę kliniczną przeszły nanocząstki złota sprzężone z siRNA celującymi w transkrypt onkogenu GBM *Bcl2L12* [196]. Bcl2L12 to białko cytoplazmatyczne, ulegające wysokiej ekspresji w złośliwych glejakach, hamujące zależne od p53 szlaki apoptozy zainicjonowanej uszkodzeniami DNA [197]. Wykorzystując wyniki badań na szczurach i małpach oznaczono bezpieczną dla ludzi dawkę terapeutyku, którą następnie zaaplikowano pacjentom z GBM. Wykazano akumulację złota w tkance nowotworowej, obniżenie w niej poziomu ekspresji BclL12 a także zwiększenie ilości białka p55 [196]. Prowadzone badania kliniczne nad nanośnikami wskazują na trwający postęp nanotechnologii medycznej.

.

7 OMÓWIENIE PRAC NAUKOWYCH WCHODZĄCYCH W SKŁAD ROZPRAWY DOKTORSKIEJ

7.1 Applications of noncoding RNAs in brain cancer patients

Grabowska M, Misiorek JO, Zarębska Ż, Rolle K.

Clinical applications of noncoding RNAs in cancer. Elsevier. 2022. 2:17-64.

Niekodujące RNA stanowią klasę cząsteczek o kluczowym znaczeniu dla rozwoju i progresji nowotworów. W powyższym przeglądowym rozdziale podsumowałam dostępną w piśmiennictwie naukowym wiedzę dotyczącą niekodujących RNA w nowotworach mózgu. Zaprezentowane omówienie dotyczy głównie wysokozłośliwego glejaka oraz rdzeniaka zarodkowego, opisując powiązane z nimi miRNA, lncRNA i circRNA.

Początek pracy stanowi opis wymienionych wcześniej jednostek chorobowych pod kątem ich profilu genetycznego i klasyfikacji. Następnie scharakteryzowałam ncRNA zwracając szczególną uwagę na ich biogenezę oraz mechanizm działania. W podrozdziale drugim zestawiłam w formie tabeli dostępne bazy danych i algorytmy umożliwiające deponowanie i przeglądanie informacji dotyczących miRNA, lncRNa i circRNA. Opisane platformy pozwalają między innymi na poznanie profilu ncRNA pochodzącego z sekwencjonowania transkryptomu, wskazują ich lokalizację komórkową i powiązania z chorobami ludzkimi, zezwalają na dokonywanie analiz wzajemnych oddziaływań pomiędzy ncRNA a mRNA i białkami.

Najobszerniejszą część pracy stanowi, zawarty w podrozdziale trzecim, opis poziomu ekspresji ncRNA w nowotworach mózgu. Przedstawiłam w nim zestawienie modeli badawczych wykorzystywanych do określania profili transkryptomicznych. Uwzględniłam w nim zarówno standardowo wykorzystywane materiały biologiczne takie jak adherentne linie komórkowe czy fragmenty tkanek pochodzących od pacjenta, jak i stanowiące *novum* przestrzenne hodowle komórkowe. Opisywane przeze mnie kultury organoidów pozwalają na propagowanie i analizę komórek macierzystych nowotworu. W pracy zebrałam informacje dotyczące profilu ncRNA w CSC zaznaczając jaki wpływ na procesy nowotworzenia mają poszczególne cząsteczki.

W czwartym podrozdziale dokonałam przeglądu metod eksperymentalnych wykorzystywanych do badania ncRNA, ich identyfikacji, wzajemnych oddziaływań

i manipulacji ich poziomem ekspresji. Informacje zebrałam w formie tabeli, eksponującej zarówno wady jak i zalety poszczególnych technik.

Istotną częścią pracy jest zawarte w podrozdziale piątym przedstawienie ncRNA o potencjale prognostycznym jak i diagnostycznym w odniesieniu do nowotworów mózgu. Wyselekcjonowanie najistotniejszych dla rozpoznania choroby cząsteczek, znalazłoby zastosowanie we wciąż rozwijającej się medycynie spersonalizowanej, opartej o indywidualne podejście do konkretnego pacjenta. Również wyznaczenie korelacji pomiędzy poziomem ekspresji ncRNA a czynnikami przeżywalności pacjenta, takimi jak OS lub czas przeżycia bez objawów choroby (ang, *disease-free survival*, DFS), może przyczynić się do dobrania odpowiedniej formy terapii lub do stworzenia całkowicie nowego podejścia terapeutycznego opartego o mechanizm RNAi skierowany przeciw konkretnemu ncRNA. Ponownie, wymienione cząsteczki RNA zostały uporządkowane w formie tabeli.

Rozwinięciem tematyki prognostycznych miRNA, lncRNA i circRNA jest osobny podrozdział, w którym opisałam zależności pomiędzy profilem ncRNA a chemio- oraz radioopornością komórek nowotworowych. W sekcji tej umieściłam listę opisywanych cząsteczek, przedstawiającą sieć zależności lncRNA/circRNA – miRNA – białko – szlak komórkowy. Pracę przeglądową zakończyłam podsumowaniem dostępnych informacji o zastosowaniu ncRNA jako potencjalnych celów terapeutycznych i prowadzonych w tym kierunku badaniach klinicznych.

7.2 MiR-218 affects the ECM composition and cell biomechanical properties of glioblastoma cells.

Grabowska M*, Kuczyński K*, Piwecka M, Rabiasz A, Zemła J, Głodowicz P, Wawrzyniak D, Lekka M, Rolle K.

Journal of Cellular and Molecular Medicine. przyjęte do publikacji.

Punktem wyjścia dla projektu dotyczącego wpływu hsa-miR-218-5p na komórki GBM były wyniki badań wykonanych w Instytucie Chemii Bioorganicznej Polskiej Akademii Nauk, opublikowane w 2015 roku [198]. Piwecka, Rolle i współautorzy na podstawie analiz mikromacierzowych oraz sekwencjonowania nowej generacji (ang. *next generation sequencing,* NGS), wskazali na zmieniony poziom ekspresji miRNA w glajaku w porównaniu ze zdrową tkanką mózgową. Wykazano m.in. że 26 miRNA zidentyfikowanych w glejaku wykazuje znacząco obniżony poziom ekspresji w tkankach GBM pochodzących od pacjentów. Skonfrontowanie tego wyniku z metaanalizą zidentyfikowało miR-218 jako cząsteczkę o silnej, powtarzającej się w wynikach innych zespołów badawczych, deregulacji w tkankach GBM [199-201].

7.2.1 Analiza poziomu ekspresji miR-218 oraz wybranych białek macierzy zewnątrzkomórkowej w tkankach oraz liniach komórkowych GBM

W celu potwierdzenia wyników mikromacierzy i NGS [198] zbadałam poziom ekspresji hsa-miR-218-5p w glejaku WHO IV. Wykorzystując reakcję łańcuchowej polimerazy w czasie rzeczywistym (ang. *real-time polymerase chain reaction,* real-time PCR) przeanalizowałam materiał RNA wyizolowany z tkanek pochodzących od pacjentów cierpiących zarówno na GBM jak i jego wznowę. Do badań wykorzystałam ponadto RNA ze zdrowych mózgów, stanowiące odniesienie do zmian zachodzących w guzach nowotworowych. Poziomy ekspresji miR-218 w tkance GBM i wznowie są odpowiednio o 56% i 69% niższe niż w zdrowym mózgu (Fig. 1A [202]).

Biorąc pod uwagę wyraźny spadek poziomu ekspresji miR-218 w GBM, postanowiłam wytypować transkrypty, z którymi może on oddziaływać. W celu zidentyfikowania miejsc wiązania w 3'UTR mRNA, przeprowadziłam analizę *in silico*, w której zastosowałam dostępne publicznie oprogramowania ENCORI, miRDB, PicTar i TargetScan. Otrzymane listy transkryptów zawęziłam do sekwencji białek macierzy zewnątrzkomórkowej

(Suplement 1 [202]). Spośród wyselekcjonowanych białek ECM, z których transkryptami może oddziaływać potencjalnie miR-218, do dalszych badań wytypowałam syndekan-2 i tenascynę-C, których interakcje z badanym miRNA przewidziały co najmniej trzy z czterech zastosowanych narzędzi.

Wykonane analizy metodą real-time PCR z wykorzystaniem RNA pochodzącego ze zdrowego mózgu oraz materiału wyizolowanego z guzów pierwotnych i wznów nowotworu wskazują na 4-krotny wzrost poziomu ekspresji SDC2 w nowotworze. Poziom TNC był znacząco podwyższony we wszystkich badanych próbkach guza, jest 8-krotnie wyższy w tkance GBM i 21-krotnie wyższy we wznowach. W przypadku TNC widoczny jest wzrost poziomu ekspresji TNC wraz ze stadium rozwoju nowotworu (Fig. 1B [202]). Przeprowadzone przez współautorów pracy analizy wskazały na zgodność otrzymanych przez nas wyników z danymi pochodzącymi z szeregu eksperymentów opartych o sekwencjonowanie RNA, zawartymi w bazach danych TCGA i Rembrandt (Fig. 1C,D [202]).

Dalsze etapy projektu przeprowadzałam wykorzystując hodowle komórkowe *in vitro*. W celu doboru odpowiedniego modelu badawczego oceniłam poziom ekspresji miR-218, TNC i SDC2 w czterech liniach komórkowych glejaka: T98-G, U-118 MG, U-138 MG i U-251 MG (Fig. 2D,E,F,G [202]). Do dalszych badań wybrałam U-118 MG, która charakteryzuje się niskim poziomem ekspresji miR-218 przy jednoczesnym wysokim poziomie SDC2 i TNC, odpowiadając profilom ekspresji tkanek GBM, zgodnie z wcześniej omawianymi wynikami badań.

7.2.2 Określenie sposobu oddziaływania miR-218 na tenascynę-C oraz syndekan-2

Biorąc pod uwagę poprzednią analizę wykazującą odwrotną korelację między ekspresją miR-218 a SDC2 i TNC, zespół badawczy prowadzący projekt zweryfikował eksperymentalnie przewidywane bioinformatycznie interakcje miRNA-mRNA. Wszystkie algorytmy zastosowane do przewidywania oddziaływań miR-218 wykazały jedno miejsce wiązania w obrębie 3'UTR zarówno dla SDC2, jaki i TNC. Przygotowano zestaw konstruktów do reporterowego testu lucyferazy, aby eksperymentalnie zweryfikować przewidywane wiązanie miR-218 z jego miejscami docelowymi (Fig. 2A [202]). Eksperyment potwierdził, iż miR-218 oddziałuje bezpośrednio z analizowanymi transkryptami, obniżając aktywność lucyferazy w próbach z niezmienionym fragmentem 3'UTR analizowanych mRNA (Fig. 2B [202]). Badaniem tym zespół dostarczył dowodów na bezpośrednie wiązanie miR-218 do 3'UTR SDC2 oraz TNC, co wskazuje na funkcjonalność miR-218 jako negatywnego regulatora transkrypcji.

W dalszych etapach pracy starałam się określić rolę miR-218 w regulacji TNC i SDC2 w komórkach GBM. Wykorzystałam tutaj podejście polegające na wprowadzeniu do komórek dodatkowych kopii miRNA (ang. *mimic miRNA*) w podejściu typu „nabycie funkcji" (ang. *gain of function*). Komórki linii U-118 MG transfekowałam syntetycznym miR-218. Analizy wykazały skuteczność transfekcji syntetycznym miRNA, czego efektem było znaczące podniesienie poziomu miRNA linii komórkowej (Fig. 2C [202]).

W celu dalszej weryfikacji funkcji miR-218 przeprowadziliśmy analizę jego wpływu na SDC2 i TNC zarówno na poziomie mRNA, jak i białka za pomocą metod real-time PCR i Western blot. Na poziomie transkryptów suplementacja syntetycznym miR-218 skutkowała obniżeniem poziomu ekspresji zarówno *SDC2* jak i *TNC* (Fig. 2H [202]). Na poziomie białka uzyskałam obniżenie poziomu SDC2 proporcjonalnie do stosowanych stężeń miRNA. W przypadku TNC efekt wyciszenia o uzyskałam jedynie dla wyższego z zastosowanych stężeń (Fig 2I,J [202]).

7.2.3 Ocena wpływu miR-218 na składniki ECM

Biorąc pod uwagę istnienie wzajemnych oddziaływań pomiędzy komponentami macierzy, oceniliśmy także wpływ miR-218 na poziom innych białek ECM oraz tych związanych z migracją komórek. Wykorzystując komercyjne dostępne systemy badania profilu ekspresji genów, przeanalizowano zestawy transkryptów związanych z ruchliwością i adhezją ludzkich komórek, w tym także geny zaangażowane w budowę cytoszkieletu komórkowego. Zidentyfikowano 47 genów wykazujących znacząco różną ekspresję w wyniku podania do komórek syntetycznego miR-218 w stężeniu 50 nM (Fig. 3 w omawianej publikacji). Na liście zidentyfikowanych w ten sposób cząsteczek ulegających zmienionej ekspresji pod wpływem miR-218 znajduje się TNC z ok. 2-krotnym zmniejszeniem ekspresji. Wynik ten jest zgodny z przestawionymi wcześniej badaniami ekspresji metodą real-time PCR, w których również uzyskałam dwukrotną redukcję poziomu ekspresji TNC po transfekcji miR-218.

7.2.4 Analiza wpływu nadekspresji miR-218 na właściwości biomechaniczne komórek GBM

Na podstawie przedstawionych w poprzednich podrozdziałach wyników postawiliśmy hipotezę badawczą, zakładającą, że zmiany w składzie ECM spowodowane regulacją miR-218 wpływają również na właściwości biomechaniczne komórek nowotworowych. Przebadałam więc następnie takie atrybuty komórkowe, jak zdolność do migracji i adhezji oraz ich sztywność.

Do przeanalizowania wpływu miR-218 na migrację komórek, wykorzystałam dwa funkcjonalne testy komórkowe. W pierwszym z nich, stosując system xCELLigence do

monitorowania położenia komórek, rejestrowałam przebieg migracji komórkowej w czasie rzeczywistym. W eksperymencie trwającym 48 godzin porównałam tempo migracji komórek U-118 MG transfekowanych miR-218 z kontrolnymi, traktowanymi niespecyficznym siRNA (Fig. 4A [202]). Wykazałam, iż miR-218 wpływa na wydłużenie czasu migracji komórek (ang. *half maximal effective time*, ET$_{50}$) o średnio 4 godziny w odniesieniu do kontroli (Fig. 4B [202]). Jako drugi niezależny eksperyment, przeprowadziłam test gojenia się rany (Fig. 4C [202]). Oba wykonane testy *in vitro* wskazują na opóźnienie w szybkości migracji komórek GBM , a co za tym idzie na regulacyjną rolę miR-218.

Zgodnie z hipotezą *„go-or-grow"*, migracja i proliferacja komórek nowotworowych nie zachodzą jednocześnie w tym samym miejscu i czasie [203]. Mając na uwadze wyniki tempa migracji w komórkach GBM, zadałam sobie pytanie, czy uda mi się także zaobserwować zmiany w tempie podziałów komórkowych. W tym celu wykonałam dwa testy *in vitro*. Trwająca 48 godzin obserwacja proliferacji komórek w czasie rzeczywistym systemem xCELLigence wskazała na jej wzrost w komórkach traktowanych miR-218 (Fig. 4E [202]). Również test inkorporacji znakowanej tymidyny, pozwalający na śledzenie przyrostu ilości DNA, potwierdził, że miR-218 pozytywnie wpływa na proliferację komórkową (Fig. 4F [202]).

Kolejną ze zbadanych w pracy biomechanicznych cech komórek jest ich adhezja do podłoża. W analizach ponownie wykorzystałam system xCELLigence. Pomiary adhezji w czasie rzeczywistym wykazały na statystycznie istotne zmiany przyczepności komórek do powierzchni płytki w czasie trwania eksperymentu tj. 4 godziny. Doszło do około 2-krotnego wzrostu analizowanej wartości (Fig. 5E [202]).

Do szeregu omówionych powyżej testów biologicznych, wdrożyliśmy wraz z zespołem, badania biofizyczne, takie jak: pomiar adhezji i sztywności komórkowej przy pomocy mikroskopii sił atomowych (ang. *atomic force microscopy*, AFM) w trybie spektroskopii sił pojedynczej komórki (ang. *single cell force spectroscopy*, SCFS). W tym podejściu eksperymentalnym każda pojedyncza komórka została użyta jako sonda siłowa. Dane pomiarowe wskazują na 1,6-krotny dla stężenia 50 nM i 1,8-krotny dla stężenie 10 nM statystycznie istotny wzrost pracy adhezji komórek traktowanych syntetycznym miR-218 (Fig. 5D [202]). Podsumowując, niezależnie od techniki zastosowanej do badania adhezji, wykazaliśmy wzrost adhezji komórek GBM z nadekspresją miR-218. Zawarte w publikacji wyniki pomiarów sztywności komórki wskazały na jej statystycznie istotny wzrost o około 30% (Fig. 6D [202]). Ponieważ sztywność powiązana jest z organizacją cytoszkieletu, dokonaliśmy także wizualizacji włókien aktynowych, które wyraźnie wskazują na udział miR-218 w jego przebudowie (Fig. 6E [202]).

7.2.5   Podsumowanie

W opisanej pracy eksperymentalnej przedstawiłam miR-218 jako potencjalny supresor nowotworzenia w komórkach glejaka. Zaprezentowałam bezpośredni wpływ miR-218 na poziom ekspresji dwóch białek ECM: SDC2 i TNC. Przedstawiłam dane świadczące o obniżonym poziomie ekspresji miR-218 w tkankach GBM przy jednoczesnej nadekspresji transkryptów tychże białek. Ponadto w publikacji przedstawiono panel genów ulegających w sposób pośredni deregulacji pod wpływem badanego miRNA. Projekt poszerzony został o szereg testów funkcjonalnych, wskazujących iż zmiany wywołane nadekspresją miR-218 w komórkach GBM wpłynęły na ich właściwości biomechaniczne, tj.: adhezję, migrację i sztywność. Zwiększenie przyczepności do podłoża a zarazem zmniejszenie ruchliwości nadaje komórkom fenotyp nienowotworowy, co wpływa negatywnie na potencjał inwazyjny nowotworu. Przebieg zmian na poziomie komórki wywołanych miR-218 przedstawiłam schematycznie na Rycinie 8.
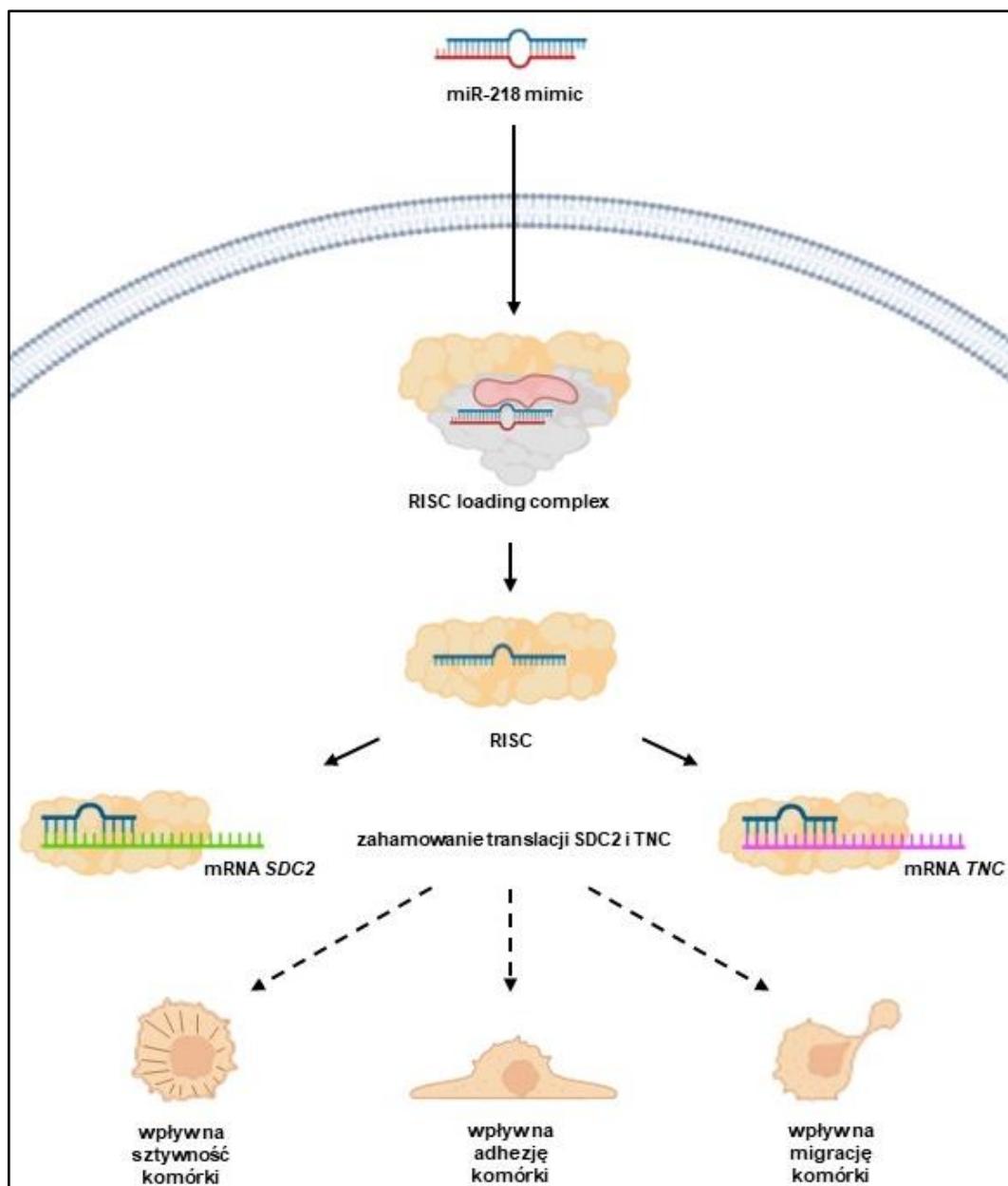
Rycina 8. Schemat regulacji poziomu docelowych transkryptów przez miR-218 oraz jej wpływ na właściwości biologiczne i biomechaniczne komórek nowotworowych.

7.3 Nano-mediated delivery of double-stranded RNA for gene therapy of glioblastoma multiforme.

Grabowska M, Grześkowiak BF, Szutkowski K, Wawrzyniak D, Głodowicz P, Barciszewski J, Jurga S, Rolle K, Mrówczyński R.

PLoS One. 2019. 14(3):e0213852.

Projekt, w którym przeanalizowałam nanocząstki magnetyczne pod kątem zastosowania ich jako nośniki kwasów nukleinowych, jest kontynuacją badań nad terapią GBM opartą o interferencję RNA skierowaną przeciw białku TNC [204, 205]. Prace badawcze wykonane w Instytucie Chemii Bioorganicznej PAN w Poznaniu w kooperacji z Katedrą i Kliniką Neurochirurgii i Neurotraumatologii Uniwersytetu Medycznego w Poznaniu, przedstawiają wpływ obniżenia poziomu ekspresji TNC na przeżywalność pacjentów. Wykorzystano unikalne podejście terapeutyczne, nazwane interwencją z RNAi (iRNAi), oparte na zaaplikowaniu narzędzia molekularnego interferencji RNA bezpośrednio do niszy pooperacyjnej powstałej w wyniku resekcji guza. Terapię skierowano na nieoperacyjne nowotworowe nacieki w głąb mózgu. Wykorzystaną cząsteczką było dwuniciowe RNA długości 163 bp komplementarne do fragmentu mRNA *TNC* (ang. *anti-tenascin RNA*, ATN-RNA). Żukiel i wsp. [204] oraz Rolle i wsp. [205] wykazali znaczne obniżenie poziomu TNC w wyniku zastosowania ATN-RNA oraz wydłużenie wskaźnika przeżywalności pacjentów. Celem niżej opisywanego projektu było znalezienie nowego bezpiecznego, efektywnego nośnika, wprowadzającego ATN-RNA do komórek przy ewentualnej możliwości zastosowania jednoczesnej terapii uzupełniającej - fototermii.

7.3.1 Charakterystyka nanocząstek

Przedstawiona praca eksperymentalna powstała w ramach projektu Narodowego Centrum Nauki, Opus 11 „Nowe, wielozadaniowe nanocząstki w skojarzonej geno- i fototerapii" (2016/21/B/ST8/00477), w konsorcjum z Centrum NanoBioMedycznym (CNBM) Uniwersytetu im. Adama Mickiewicza w Poznaniu.

W wyniku realizacji projektu zespół CNBM przeprowadził syntezę, funkcjonalizację oraz wstępną charakterystykę nanocząstek magnetycznych (ang. *magnetic nanoparticle,* MNP) składają się z Fe_3O_4 funkcjonalizowanego polietyleonoiminą (PEI) (MNP@PEI). Rdzeń magnetyczny może zostać wykorzystany do dystrybucji cząstek [206] oraz dodatkowo, jako czynnik kontrastujący w obrazowaniu rezonansem magnetycznym [207]. PEI odpowiada

natomiast za nadanie cząstkom ładunku pozwalającego na przyłączenie się ujemnie naładowanego kwasu nukleinowego [208, 209].

Morfologię otrzymanych nanokompozytów oceniano za pomocą transmisyjnego mikroskopu elektronowego (ang. *transmission electron microscope*, TEM). Wykazano że MNP@PEI mają kulisty kształt, o średnicy 3-12 nm, zaobserwowano również częściową agregację cząstek (Fig. 2A [210]). Z wykorzystaniem spektroskopii fourierowskiej w podczerwieni (ang. *Fourier-transform infrared spectroscopy,* FTIR) potwierdzono obecność PEI na powierzchni nanocząstek magnetycznych (Fig. 2B [210]).

W celu zbadania wielkości zsyntetyzowanych nanocząstek, a także ich ładunku powierzchniowego, przeprowadzono pomiary dynamicznego rozpraszania światła (ang. *dynamic light scattering,* DLS). MNP@PEI charakteryzowały się średnicą hydrodynamiczną ~ 150 nm (Fig. 3D [210]), ich potencjał zeta wynosił + 40,6 mV (Fig. 2C [210]). Potencjał zeta o wartości powyżej 30 mV wskazuje na stabilność cząstek w zawiesinie [158] a także umożliwia przyłączenie do nich negatywnie naładowanego dsRNA. Pomiary interferometrem kwantowym nadprzewodnikowym (ang. *superconducting quantum interference device,* SQUID) wykazały, iż MNP@PEI zachowują się jak cząstki superparamagnetyczne (Fig. 2C [210]). Wyniki obrazowania metodą echa spinowego wskazują na wysoką wartość relaksacyjności nanokompozytu (225 mM^{-1}s^{-1}) (Fig. 3 [210]) przewyższającą wartości komercyjnych środków kontrastowych opartych na nanocząstkach magnetycznych [211], co wskazuje na możliwość zastosowania MNP@PEI w obrazowaniu MRI.

Pod względem biologicznym wykazano, że MNP@PEI efektywnie wiąże dsRNA w stosunku wagowym 3:1 (Fig. 4A,B [210]). W dalszych badaniach zawartych w pracy to właśnie ten stosunek wiązania obowiązywał podczas tworzenia kompleksów nanocząstek z ATN-RNA. Obrazy mikroskopowe wykonane komórkom traktowanym wybarwionymi kompleksami wskazują, że zarówno nanocząstki jak i dsRNA wnikają do cytoplazmy (Fig. 5 [210]).

7.3.2 Cytotoksyczność nanocząstek i ich kompleksów z dsRNA, immunogenność ATN-RNA

Współautorzy projektu przebadali również cytotoksyczność samych nanocząstek MNP@PEI, jak i kompleksów niosących ATN-RNA. Pomiary wykonano z wykorzystaniem linii komórkowej glejaka U-118 MG. Dla MNP@PEI przeprowadzono test oparty o wybarwianie białek sulforodaminą B (SRB). Nie wykazano znaczącego efektu cytotoksycznego w przedziale stężeń 0-1300 ng/ml MNP@PEI (Fig. C, Suplement [210]). Toksyczność kompleksów oceniano dwoma niezależnymi pomiarami przeżywalności, tj.

testem kolorymetryczny oparty o WST-1 oraz barwieniem typu „*live/dead*". Badania prowadzono w zakresie stężeń 0-100 nM ATN-RNA w kompleksie, czyli ilości dsRNA używanych w dalszych eksperymentach transfekcyjnych. Oba testy cytotoksyczności wykazały wysoką żywotność komórek (Fig. 7 [210]), wskazującą na brak efektów cytotoksycznych ze strony nanocząstek.

Biorąc pod uwagę możliwość wykorzystania kompleksów MNP@PEI wraz z ATN-RNA jako narzędzia terapeutycznego w leczeniu GBM, zespół badawczy, przeprowadził analizę poziomu ekspresji genów zaangażowanych w nieswoistą odpowiedź immunologiczną. Wprowadzenie dsRNA do komórki może wywołać odpowiedź interferonową poprzez interakcję z RIG1 [212], czy TLR3 [213]. W komórkach U-118 MG poddanych transfekcji kompleksem MNP@PEI z ATN-RNA zmierzono więc poziom ekspresji genów odpowiedzi immunologicznej: syntetazy 2'5'-oligoadenylowej 1 i 3 (ang. *2'5'-oligoadenylate synthetase 1/3*, OAS 1/3), RIG1, TLR3 i interferonu gamma (INFγ). Wyniki real-time PCR wskazują brak aktywacji OAS1, OAS3 i RIG1. ATN-RNA w stężeniu 50 i 100 nM powodowało słabą, mniej niż półtorakrotną, aktywację TLR3 i INFγ. Wyższy poziom ekspresji wspomnianych genów zaobserwowano w przypadku wprowadzania ATN-RNA do komórek na drodze transfekcji komercyjnym czynnikiem Lipofectamine^{TM} 2000 (Fig. 8 [210]).

7.3.3 Porównanie skuteczności terapii RNAi w komórkach GBM po zastosowaniu dsRNA na różnych nośnikach

Znane jest zastosowanie ATN-RNA w obniżaniu poziomu ekspresji TNC [205]. Do tej pory do dostarczania cząsteczki ATN-RNA *in vitro* wykorzystywano Lipofectamine^{TM} 2000. Dane literaturowe wskazują na znamienną a zarazem zmienną cytotoksyczność Lipofectamine^{TM} 2000. W linii komórek nienowotworowych, HEK-293, zaobserwowano spadek przeżywalności o 50% przy stężeniu 20 µg/ml tego czynnika transfekcyjnego [214]. W przypadku linii nowotworowej płucnej A549, w zależności od źródła, wartości połowicznego maksymalnego stężenia hamującego (ang. *half maximal inhibitory concentration,* IC$_{50}$) dla Lipofectamine^{TM} 2000 wyniosła w przybliżeniu 6 µg/ml [215] lub 30 µg/ml [216]. Jest to przyczyną dla której w moich badaniach poszukiwałam innego, bezpiecznego a zarazem efektywnego nośnika dla ATN-RNA.

Jako model badawczy zastosowałam linię komórkową U-118 MG, charakteryzującą się wysokim poziomem ekspresji TNC, co wykazałam w pracy **„*MiR-218 affects the ECM composition and cell biomechanical properties of glioblastoma cells*"**. Przeprowadzając transfekcję ATN-RNA przy użyciu testowanych w projekcie nanocząstek, jednocześnie

wykonywałam analogiczny eksperyment z wykorzystaniem Lipofectamine[TM] 2000. Ponieważ profil ekspresji genów może ulec zmianie wraz z rosnącą liczbą wykonanych pasaży komórkowych [217, 218], lipofekcja w moich badaniach stanowi punkt odniesienia, do którego przyrównywałam wyniki uzyskane w dalszej części pracy. W tym i kolejnych etapach projektu jako kontrolę transfekcji przyjęłam komórki traktowane nośnikami w ilości potrzebnej do wprowadzenia ATN-RNA w stężeniu 25 nM, osobno dla Lipofectamine[TM] 2000 i MNP@PEI.

24 godziny po transfekcji oceniłam poziom ekspresji *TNC* za pomocą metody real-time PCR. W przypadku wykorzystania nanocząstek MNP@PEI jako nośnika dsRNA zaobserwowałam statystycznie istotne różnice w poziomie ekspresji transkryptu, w odniesieniu do prób traktowanych tym samym stężeniem ATN-RNA wprowadzanych przy użyciu Lipofectamine[TM] 2000. MNP@PEI wykazały większą efektywność w dostarczaniu ATN-RNA niż nośnik lipidowy (Fig. 9A [210]). Analizą poziomu białka TNC metodą Western blot dostarczyłam informacji, że do uzyskania tego samego, 40% wyciszenia należało użyć kompleksu MNP@PEI z 10 nM ATN-RNA i aż 50 nM dsRNA dostarczanego za pośrednictwem Lipofectamine[TM] 2000 (Fig. 9B [210]). Uzyskane wyniki wskazują na wyższą wydajność dostarczania dsRNA na nośniku nanocząstkowym w porównaniu do komercyjnego nośnika lipidowego. Ponadto potwierdziłam skuteczność ATN-RNA w wyciszaniu TNC w komórkach GBM.

7.3.4 Analiza proliferacji i migracji komórek GBM po obniżeniu poziomu ekspresji TNC różnymi czynnikami transfekcyjnymi

Rezultatem terapii opartej na obniżeniu poziomu TNC poprzez zastosowanie ATN-RNA było wydłużenie życia i poprawa jego jakości u pacjentów z GBM poprzez ograniczenie i spowolnienie wznowy miejscowej guza nowotworowego [205]. Nie dowiedziono jednakże na jakie konkretne cechy komórek nowotworowych wpłynęła terapia. Jako że rozrost masy nowotworowej związany jest z nadmiernymi podziałami komórek oraz ich przemieszczaniem się, a literatura dostarcza dowodów na zaangażowanie TNC w te dwa mechanizmy [219, 220], jak wskazano także w przypadku poprzedniej omawianej pracy, w dalszej części projektu zbadałam efekt wywołany przez ATN-RNA na proliferację i migrację komórek GBM.

Cząsteczkę ATN-RNA wprowadzałam do linii komórkowej U-118 MG ponownie przy pomocy MNP@PEI i Lipofectamine[TM] 2000. Następnie, wykorzystując system xCELLigence, przez 72 godziny obserwowałam proliferację komórek w czasie rzeczywistym. Próby traktowane ATN-RNA wprowadzanym przez Lipofectamine[TM] 2000 w każdym punkcie pomiarowym i dla wszystkich stosowanych stężeń charakteryzował niższy przyrost ilości

komórek niż w kontroli. Badana wartość spadała wraz ze wzrostem stężenia ATN-RNA (Fig 10 B [210]). Wprowadzając dsRNA na nośniku MNP@PEI po 24 godzinach zaobserwowałam przyrost ilości komórek. W punkach czasowych 48 i 72 godziny odnotowałam spadek proliferacji traktowanych komórek (Fig 10 A [210]). Uznałam, że wyniki dla obu testowanych czynników transfekcyjnych, wskazujące na spadek przeżywalności komórkowej po 48 i 72 godzinach tego eksperymentu, wynikają z samoistnego obumarcia komórek spowodowanego zbyt długim trwaniem pomiarów.

Wpływ obniżenia poziomu TNC przez ATN-RNA na migrację komórek GBM zbadałam wykorzystując dwa testy funkcjonalne. Pierwszy z nich opierał się o rejestrowanie położenia komórek w czasie rzeczywistym poprzez system xCELLigence. Do danych uzyskanych z eksperymentu dopasowałam czteroparametrowe równania sigmoidalne i wyznaczyłam w ten sposób ET_{50}. Zaprezentowane w publikacji w formie Figury 11 dane odnoszą się jedynie do komórek traktowanych MNP@PEI (Fig. 11A [210]). Prezentowane przeze mnie w niniejszym opracowaniu na Rycinie 9 analizy wskazują na statystycznie istotne różnice w opóźnieniu migracji pomiędzy komórkami transfekowanymi tym samym stężeniem dsRNA w kompleksie z Lipofectamine^{TM} 2000 a MNP@PEI. Dla komórek poddanych działaniu czynnika lipidowego opóźnienie migracji spadało wraz ze wzrostem stężenia ATN-RNA o wartości z zakresu 18,3-0,4 godziny. Dla komórek traktowanych MNP@PEI migracja spowolniła o 5,8-31,5 godzin przy stosowanych stężeniach ATN-RNA.

Wpływ wprowadzenia ATN-RNA różnymi czynnikami transfekcyjnymi na migrację komórek zbadałam również testem zabliźniania ran. Po zastosowaniu Lipofectamine^{TM} 2000 nie zaobserwowałam oczekiwanego w eksperymencie tego typu zmniejszenia powierzchni szramy (Fig. D Suplement [210]). Wraz ze wzrostem stosowanego stężenia ATN-RNA rana ulegała poszerzeniu. Do całkowitego zarośnięcia szramy nie doszło nawet w próbie kontrolnej, traktowanej samym nośnikiem, skąd wniosek iż to efekt toksyczności Lipofectamine^{TM} 2000. Wyniki uzyskane w tym eksperymencie dla komórek traktowanych kompleksami MNP@PEI z ATN-RNA wskazują na spowolnienie migracji komórkowej w odniesieniu do kontroli. Po 48 godzinach transfekcja ATN-RNA o stężeniu 10-100 nM zwiększyła stopień otwarcia rany w statystycznie istotny sposób o 53-95% (Fig 11B [210]).
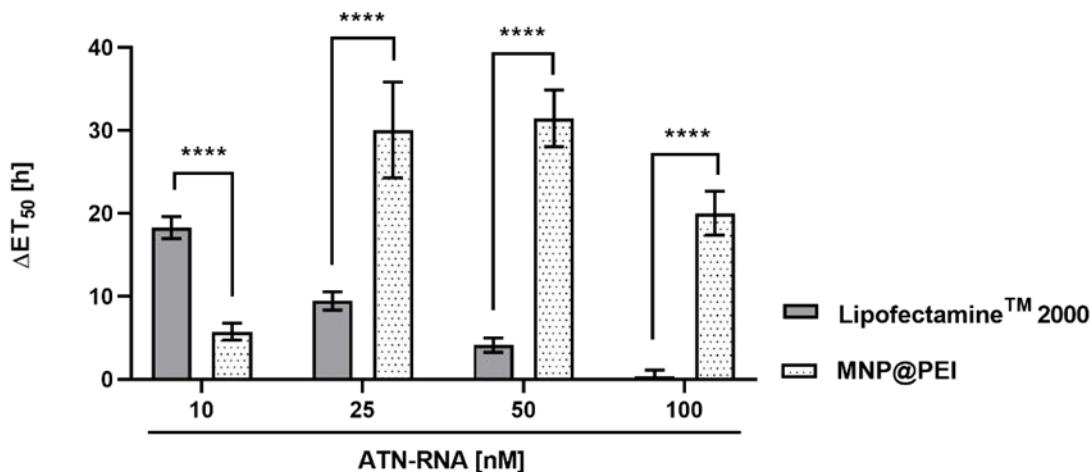
Rycina 9. Aktywność migracyjna komórek po dostarczeniu ATN-RNA za pośrednictwem Lipofectamine[TM] 2000 i nanocząstek MNP@PEI. Eksperyment przeprowadzono na linii komórkowej U-118 MG. Migrację w czasie rzeczywistym rejestrowano za pomocą systemu xCELLigence. Na podstawie uzyskanych wartości impedancji wykreślano wykres funkcji czasu, dopasowano go do czteroparametrowej równania sigmoidalnego i wyznaczano połowę maksymalnego czasu efektywnego, ET_{50}. Od wartości ET_{50} dla komórek traktowanych ATN-RNA odejmowano wartość ET_{50} dla komórek traktowanych samym nośnikiem otrzymując ΔET_{50}. Wynik przedstawiono jako wartości średnie ± SEM. Istotność statystyczną określono analizą two-way ANOVA, rozszerzoną testem Bonferroniego; **** dla $p < 0{,}0001$.

7.3.5 Podsumowanie

W ramach prezentowanego podejścia przedstawiłam nowy system dostarczania ATN-RNA do komórek glejaka. Opracowane przez zespół nanocząstki MNP@PEI okazały się efektywnie wiązać dsRNA i wprowadzać go do wnętrza komórki. Ponadto w pracy wskazano na możliwość wykorzystanie MNP@PEI w obrazowaniu MRI. Zarówno same nanocząstki, jak i ich kompleksy z dsRNA nie wykazały toksyczności i nie wywołały niepożądanej odpowiedzi immunologicznych w linii komórkowej U-118 MG. Analizując poziom ekspresji TNC wykazałam, że MNP@PEI jest efektywniejszym i bezpieczniejszym czynnikiem transfekcyjny niż standardowo stosowany czynnik transfekcyjny. Wykazałam także znaczący spadek tempa migracji komórek pod wpływem MNP@PEI z ATN-RNA, co sugeruje potencjał terapeutyczny zastosowanego nanokompozytu (Rycina 10).
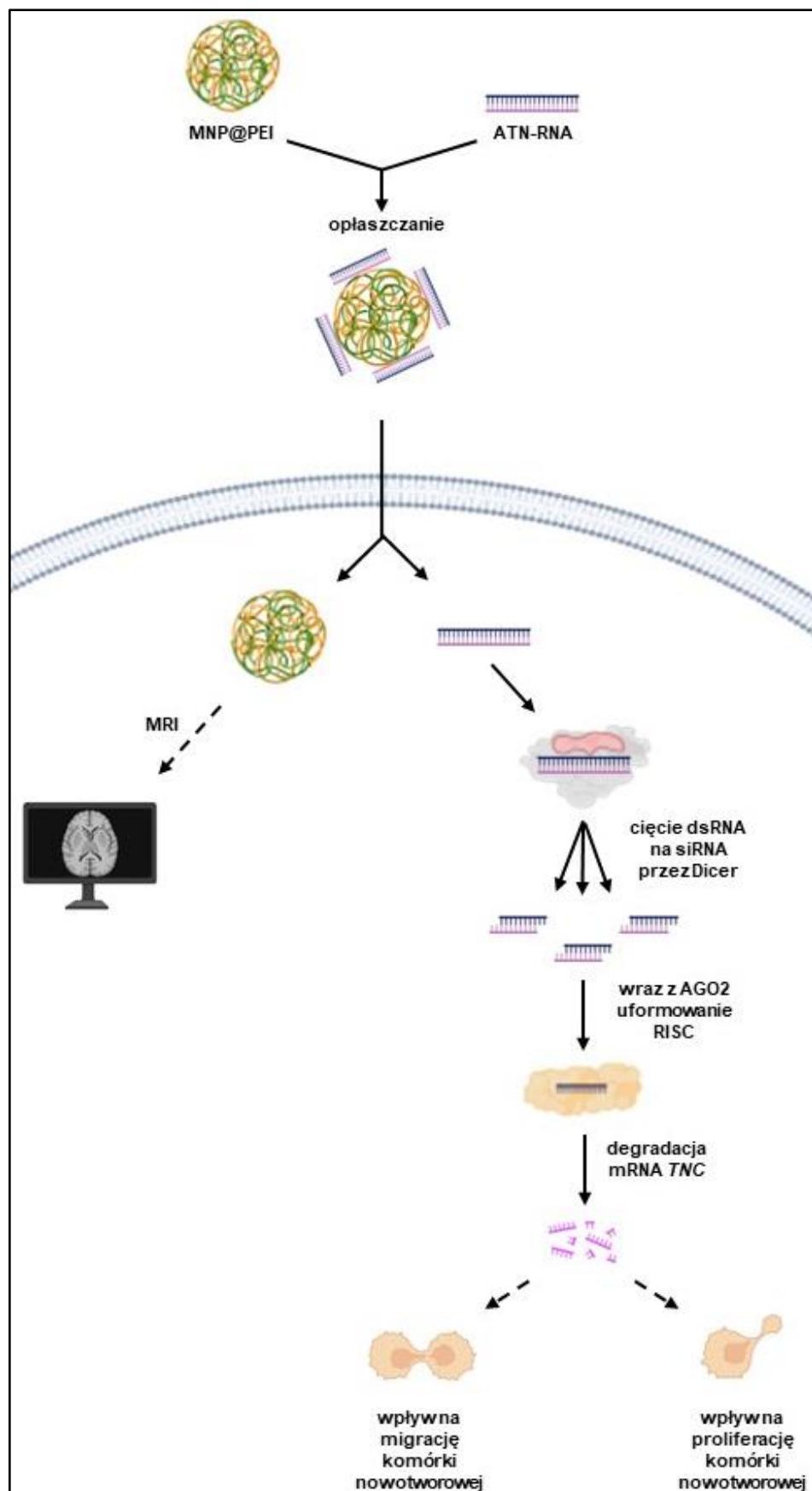
Rycina 10. Schemat działania nanocząstek MNP@PEI połączonych z dsRNA w linii komórkowej glejaka.

7.4   Magnetic Nanoparticles as a Carrier of dsRNA for Gene Therapy.

Grabowska M, Grześkowiak BF, Rolle K, Mrówczyński R.

Methods in Molecular Biology. Springer. 2021. 2211:69-81.

Przedstawiony rozdział cyklu wydawniczego *Methods in Molecular Biology* stanowi opis metodyki badań będących podstawą opisywanej wyżej publikacji „*Nano-mediated delivery of double-stranded RNA for gene therapy of glioblastoma multiforme*". We wstępie przedstawiłam krótki opis glejaka, jak również zastosowaną uprzednio terapię eksperymentalną opartą na interferencji RNA, skierowanej przeciw tenascynie-C [205]. Wskazałam również na możliwość wykorzystania nanocząstek MNP@PEI jako nośników RNA, mogących stanowić ulepszenie wspomnianej terapii.

Praca jest protokołem umożliwiającym powtarzalne przeprowadzenie części z opublikowanych wcześniej eksperymentów. Całość podzielona została na sekcje: materiały, metody oraz ułatwiające pracę laboratoryjną notatki. W rozdziale opisałam metodologię dotyczącą: syntezy i funkcjonalizacji nanocząstek magnetycznych; transkrypcji *in vitro* oraz hybrydyzacji cząsteczki ATN-RNA; przygotowania kompleksów MNP@PEI+ATN-RNA w uwzględnieniem oceny efektywności wiązania dsRNA przez nanocząstki magnetyczne; sposobu hodowli komórkowej i przeprowadzania na niej transfekcji otrzymanymi kompleksami; mikroskopowego obrazowania wnikania kompleksów do komórki jak i kolokalizacji w niej ich komponentów; oceny ich cytotoksyczności kompleksów testami opartymi o WST-1 oraz barwienie żywe/martwe; wszystkich etapów analizy poziomu ekspresji transkryptu *TNC* oraz migracji komórkowej po transfekcji kompleksami MNP@PEI+ATN-RNA.

7.5 Down-regulation of tenascin-C inhibits breast cancer cells development by cell growth, migration, and adhesion impairment.

Wawrzyniak D, Grabowska M, Głodowicz P, Kuczyński K, Kuczyńska B, Fedoruk-Wyszomirska A, Rolle K.

PLoS One. 2020. 15(8):e0237889.

Na bazie zaprezentowanych wcześniej i opublikowanych badań *in vitro* [210], a także terapii eksperymentalnej przeprowadzonej na grupie pacjentów cierpiących na GBM [204, 205] potwierdzono skuteczność cząsteczki ATN-RNA w wyciszaniu poziomu ekspresji tenascyny-C w komórkach nowotworu mózgu. Celem niniejszego projektu było sprawdzenie czy TNC może być rozpatrywana również jako cel terapeutyczny nowotworów innych niż guzy mózgu, a także czy cząsteczka ATN-RNA wpłynie na poziom ekspresji wspomnianego białka oraz cechy nowotworowe komórek innego typu niż GBM.

7.5.1 Porównanie poziomu ekspresji TNC w różnych typach nowotworów

Wykorzystując analizy sekwencjonowania RNA dostępnych w publicznej bazie danych TCGA określiłam profile ekspresji *TNC* w różnych rodzajach nowotworów. Wykorzystane w tym celu oprogramowanie z serweru GEPIA pozwoliło na ocenę poziomu transkryptów dla 33 typów nowotworów. Wyselekcjonowałam spośród nich te, w których *TNC* ulega podniesionej ekspresji w odniesieniu do właściwych, niepatologicznych tkanek (Rycina 11). Spośród nich najwyraźniejsza różnica pomiędzy tkanką nowotworową a właściwą występuje w przypadku GBM. Pomimo rozwoju terapii przeciwnowotworowych, potrójnie negatywny rak piersi pozostaje w dalszym ciągu w kategorii nowotworów trudno poddającym się leczeniu [35]. Dlatego też to właśnie na nim skupiłam się w prezentowanym projekcie.
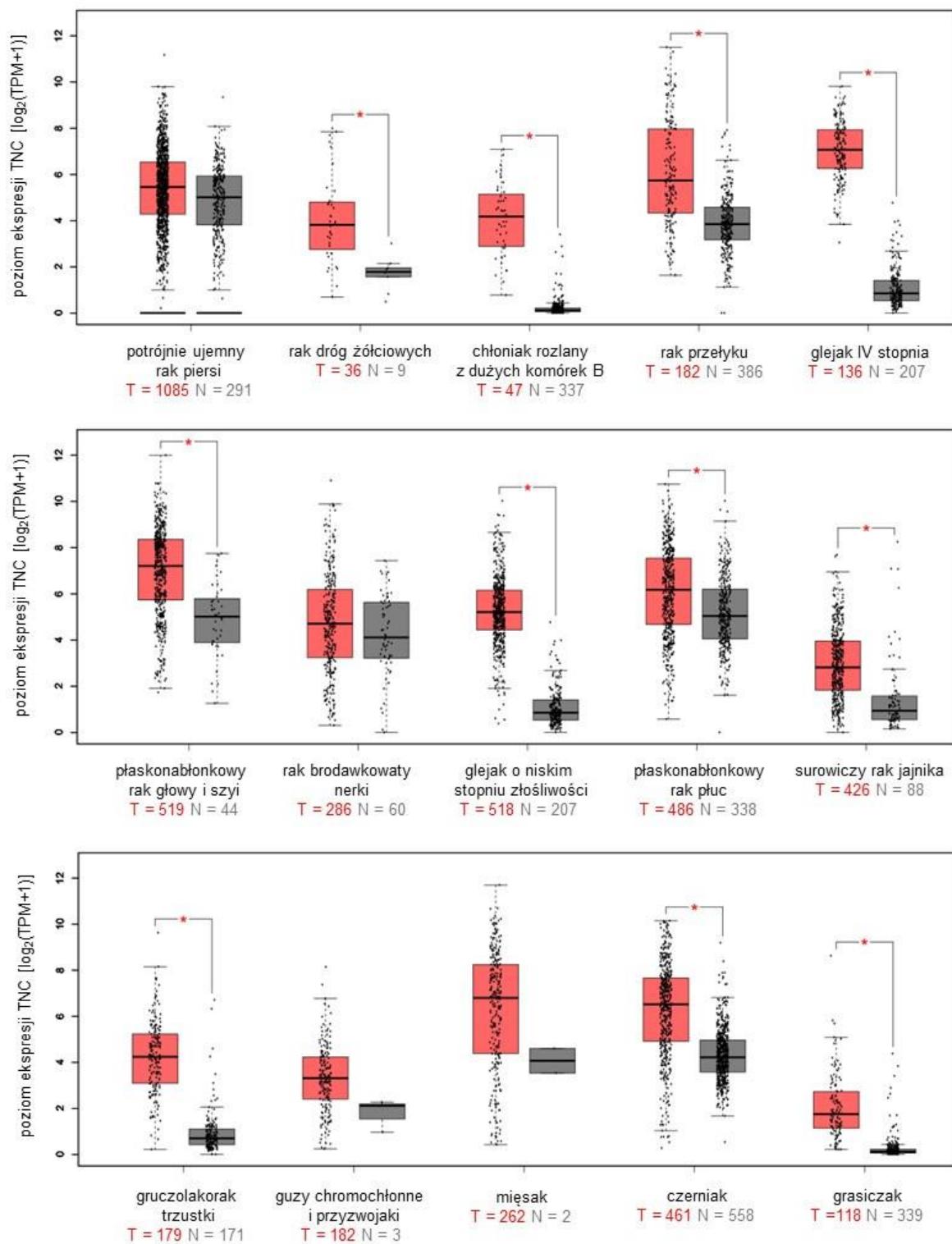
Rycina 11. Poziom ekspresji tenascyny-C w różnych typach nowotworów. Analizę wykonano z wykorzystaniem danych zdeponowanych w TCGA, wykorzystując oprogramowanie serweru GEPIA. TPM – metoda normalizacji, ang. transcripts per milion. Czerwone wykresy dotyczą tkanek nowotworowych, szare tkanek nienowotworowych. W podpisach podano liczbę zsekwencjonowanych tkanek: T – nowotwór, N – tkanka nienowotworowa. Wynik przedstawiono w formie wykresów pudełkowych uwzględniających medianę, pierwszy i trzeci kwartyl oraz ekstrema, a także wartości dla pojedynczych prób. Wartość statystyczna wyników * dla p < 0,05.

7.5.2 Wyznaczenie korelacji *in silico* pomiędzy TNC a progresją raka piersi

W ramach realizacji projektu przeanalizowaliśmy dane dotyczące całego genomu raka piersi za pomocą dostępnych portali onkogenomicznych takich jak: GEPIA, Human Protein Atlas, cBioPortal i PPISURV. Porównanie poziomu ekspresji *TNC* w czterech podtypach raka piersi wskazało, że jest on wyższy w tym potrójnie ujemnym (Suplement [221]). Dlatego też do dalszych badań *in vitro* wybrano, reprezentujące ten typ nowotworu, komórki linii MDA-MB-231. Interpretując poziomy ekspresji białek rodziny tenascyn wykazano, że zarówno na poziomie transkryptu jak i białka, TNC ulega nadekspresji w tkankach TNBC w porównaniu do materiału nienowotworowego (Fig. 1 [221]). Analiza oparta na statystyce Kaplana-Meiera wykazała bardzo wyraźnie silną korelację pomiędzy ekspresją TNC a przeżywalnością pacjentów (Fig. 2B [221]). Wysoki poziom TNC wpływa na krótsze przeżycie pacjentów, co sugeruje, że TNC można również uznać za czynnik prognostyczny dla raka piersi.

7.5.3 Zastosowanie ATN-RNA do obniżenia poziomu ekspresji TNC w komórkach raka piersi

W celu weryfikacji skuteczności narzędzia interferencji RNA na modelu innym niż dotychczas pokazano, lipofekcji ATN-RNA w zakresie stężeń 10-100 nM poddałam komórki linii raka piersi, MDA-MB-231. W przypadku tego projektu prezentowane wyniki pochodzą z materiału zebranego 48 godzin po dodaniu ATN-RNA, a kontrolę stanowią komórki traktowane niespecyficznym siRNA. Stopień zmian ekspresji TNC zbadano na zarówno na poziomie transkryptu jak i białka. Dla mRNA spadek ekspresji *TNC* jest tym większy im wyższe zastosowane stężenie ATN-RNA. Przy 100 nM ilość transkryptu spadła do 46% względem kontroli (Fig. 3A [221]). W przypadku poziomu białka statystycznie istotne różnice względem kontroli uzyskałam dla prób traktowanych ATN-RNA w stężeniu 50 nM i 100 nM. Ilość TNC spadła w nich kolejno do 55% i 10%. W przypadku niższych stężeń nie zaobserwowałam znaczących zmian (Fig. 3B,C [221]).

Chcąc ustalić stopień aktywacji odpowiedzi immunologicznej komórek po wprowadzeniu do nich ATN-RNA, przeanalizowałam poziom ekspresji genów z nią zwianych, tj.: OAS1, OAS3, RIG1 i białka indukowanego interferonem gamma (ang. *interferon gamma inducible protein 16,* IFI16). Równolegle jako kontrolę pozytywną eksperymentu zastosowałam syntetyczną postać dsRNA, kwas poliinozynowy-policytydylowy (poli I:C), który stosowany jest do indukowania odpowiedzi przeciwwirusowej [222]. Wykazałam brak

zmiany poziomu ekspresji badanych genów po transfekcji ATN-RNA w zakresie stężeń 10–100 nM (Fig 3A [221]).

7.5.4 Wpływ obniżenia poziomu TNC na biologię komórek raka piersi

Po ustaleniu, że ATN-RNA obniża poziom ekspresji TNC w komórkach raka piersi, postanowiłam odpowiedzieć na pytanie, w jaki sposób ta zmiana na nie wpływa. W tym celu wykorzystując pomiary położenia komórek w czasie rzeczywistym, przeanalizowałam proliferację, migrację i adhezję komórek. Zaobserwowałam spadek tempa podziałów komórkowych zależny od czasu i stężenia. Traktując jako kontrolę komórki traktowanymi niespecyficznym siRNA, ATN-RNA 100 nM spowodował obniżenie proliferacji o 45% po 72 godzinach (Fig. 4A [221]). Wykorzystując zebrane dane wyznaczyłam IC_{50} dla ATN-RNA. Traktując jako kontrolę komórki nietransfekowane po 24, 72 i 96 godzinach trwania testu uzyskałam wartości kolejno 97,6, 92,1 i 88,4 nM (Fig. 4B [221]).

Kontynuując temat podziałów komórkowych, zbadaliśmy także wpływ ATN-RNA na przebieg cyklu komórkowego. Analizy wykorzystujące cytometrię przepływową wskazały, że w populacji transfekowanej ATN-RNA spada liczba komórek w fazie G0/G1, natomiast zwiększa się ilość tych w fazie S (Fig. 5 [221]). Analiza cyklu komórkowego wykazała, że ATN-RNA zmniejsza proliferację komórek głównie poprzez zatrzymanie cyklu komórkowego w fazie S.

Następnie eksperymentalnie wykazałam, że obniżenie ekspresji TNC przez ATN-RNA znacząco osłabiło migrację komórek raka piersi (Fig. 4C [221]). Wyniki z trwającego 72 godziny pomiaru pokazują, że ATN-RNA opóźnia migrację komórek MDA-MB-231 o 22,45-12,40 godziny. Opóźnienie zmniejsza się wraz ze wzrostem stosowanego stężenia ATN-RNA. Ponieważ TNC bierze udział również w adhezji komórkowej [83], przyjrzałam się jej przebiegowi w komórkach traktowanych ATN-RNA. Obniżenie poziomu TNC w niewielkim, jednakże istotnie statystycznie stopniu wpłynęło na zwiększenie adhezji komórek średnio o 15% (Fig. 4D [221]).

Z progresją nowotworu związane jest zjawisko przejścia nabłonkowo-mezenchymalnego [223]. W celu sprawdzenia, czy zmiany poziomu TNC mogą odwrócić jego przebieg i zmienić fenotyp z komórki nowotworowej do prawidłowej, przeanalizowałam poziom ekspresji białek zaangażowanych w EMT. Wzięłam pod uwagę dwa główne markery tego procesu: charakteryzującą fenotyp epitelialny E-kadherynę i podwyższoną w fenotypie mezenchymalnym wimentynę. Analizą Western blot wykazałam znaczny wzrost poziomu

ekspresji CDH1, przy jednoczesnym spadku dla VIM. Wskazuje to na odwrócenie zjawiska EMT (Fig. 8 [221]).

7.5.5 Obserwacja formacji komórkowych struktur 3D po zastosowaniu ATN-RNA

Ponieważ TNC jest składnikiem ECM, czyli trójwymiarowego rusztowania spajającego komórki, w dalszej części pracy zaprezentowano wpływ ATN-RNA na proces formowania się przestrzennej struktury guza. Wykorzystano do tego celu model hodowli 3D, sferoidy linii MDA-MB-231. Zaobserwowano, że zwiększające się stężenia dsRNA miało negatywny wpływ na formowanie struktur komórkowych (Fig 7A [221]). Obrazy mikroskopowe komórek poddanych barwieniu wskazały na koncentrację martwych komórek wewnątrz sferoidów powstałych z komórek transfekowanych ATN-RNA. ATN-RNA 100 nM deformował sferoid do stopnia uniemożliwiającego zobrazowanie struktury 3D w mikroskopie konfokalnym (Fig 7B [221]).

7.5.6 Podsumowanie

Na podstawie zaprezentowanych wyników wskazuję TNC jako obiecujący cel terapeutyczny dla raka piersi. Decydują o tym nie tylko dane onkogenomiczne, korelujące poziom ekspresji tego białka z przeżywalnością pacjentów, ale również badania przeprowadzone w wykorzystaniem linii komórkowej TNBC traktowanej ATN-RNA. Obniżenie poziomu TNC wpłynęło na zmniejszenie ruchliwości komórek nowotworowych, co wykazałam na badając ich migrację, adhezję i a także poziom markerów EMT. Co najistotniejsze wykazaliśmy użyteczność narzędzia RNAi stosowanego do tej pory wyłącznie na komórkach GBM w innym typie nowotworu (Rycina 12), wskazując na możliwość zastosowania opracowanego wcześniej narzędzia terapeutycznego w przypadku innych nowotworów wykazujących podniesiony poziom TNC.
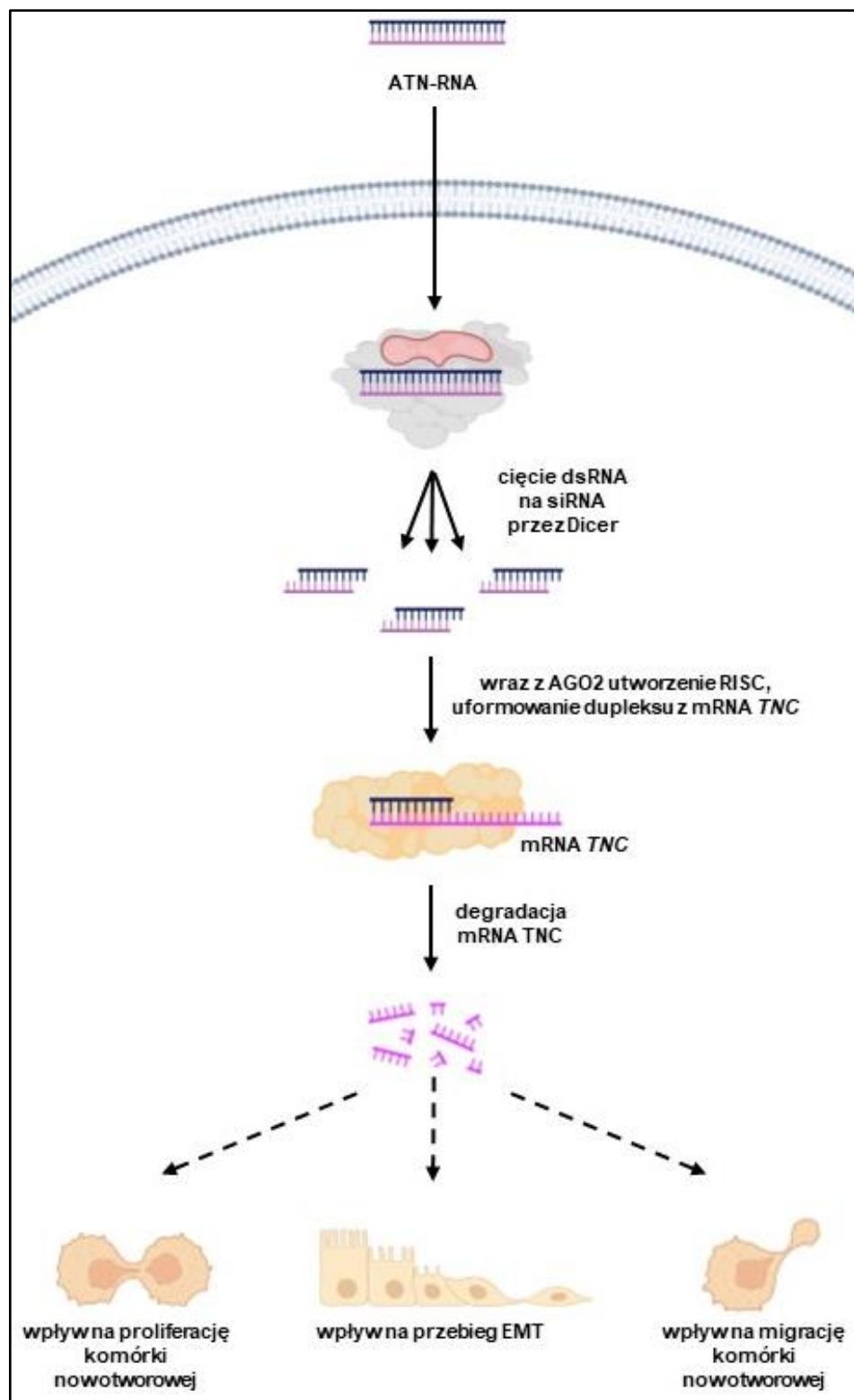
Rycina 12. Schemat wpływu ATN- RNA na właściwości komórek nowotworowych potrójnie negatywnego raka piersi.

8   WNIOSKI

Celem niniejszej pracy doktorskiej było wykorzystanie niekodujących RNA oraz nanonośników do regulacji poziomu ekspresji wybranych białek macierzy zewnątrzkomórkowej. Zastosowanym przeze mnie modelem badawczym były linie komórkowe nowotworów mózgu i piersi. Przedstawiam ponadto wyniki analiz ekspresji RNA w oparciu o materiał biologiczny pochodzącego z tkanek pacjentów cierpiących na GBM. W pracy skoncentrowałam się na analizie funkcji dwóch rodzajach cząsteczek regulatorowych: występującego naturalnie w komórce ludzkiej miRNA-218 oraz syntetycznego dsRNA zawierającego sekwencję komplementarną do mRNA *TNC*, tzw. ATN-RNA, o potencjale regulacji ekspresji genu docelowego.

Najważniejsze wnioski wynikające z realizacji pracy doktorskiej to:

- miR-218 jest bezpośrednio zaangażowany w regulację ekspresji białek macierzy zewnątrzkomórkowej TNC i SDC2, wpływając tym samym na proliferację, migrację, adhezję oraz właściwości biomechaniczne komórek linii komórkowej glejaka;

- nanocząstki MNP@PEI są efektywnym i bezpiecznym nośnikiem wiążącym i wprowadzającym dsRNA do wnętrza komórek glejaka, skutecznie obniżając poziom ekspresji docelowego białka TNC i wpływając na obniżenie potencjału migracyjnego komórek;

- dsRNA – ATN-RNA skutecznie obniża poziom ekspresji TNC w komórkach raka piersi, wpływając na ekspresję markerów przejścia nabłonkowo-mezenchymalnego, obniżając proliferację i migrację komórek raka piersi oraz tworzenie „miniguzów" w warunkach *in vitro*. Wskazuje na potencjalną uniwersalność zastosowanego podejścia w odniesieniu do nowotworów, w których obserwuje się znacząco podniesiony poziom ekspresji TNC.

Podsumowując, wyniki wskazują, że TNC jest istotnym białkiem macierzy zewnątrzkomórkowej GBM i raka piersi. Obniżenie poziomu jej ekspresji wpływa na ruchliwość komórek, co ma istotny potencjalny wpływ na inwazyjność komórek nowotworowych. Obserwacja ta, a także zaprezentowane efekty zastosowania RNAi oraz wskazanie efektywnej metody dostarczania cząsteczki efektorowej do komórek dają podwaliny pod rozwój nowych terapii przeciwnowotworowych.

9 BIBLIOGRAFIA

1. Hanahan, D. & Weinberg, R. A. (2000) The hallmarks of cancer, *Cell.* 100, 57-70.

2. Louis, D. N., Perry, A., Reifenberger, G., von Deimling, A., Figarella-Branger, D., Cavenee, W. K., Ohgaki, H., Wiestler, O. D., Kleihues, P. & Ellison, D. W. (2016) The 2016 World Health Organization Classification of Tumors of the Central Nervous System: a summary, *Acta Neuropathol.* 131, 803-20.

3. Sung, H., Ferlay, J., Siegel, R. L., Laversanne, M., Soerjomataram, I., Jemal, A. & Bray, F. (2021) Global Cancer Statistics 2020: GLOBOCAN Estimates of Incidence and Mortality Worldwide for 36 Cancers in 185 Countries, *CA Cancer J Clin.* 71, 209-249.

4. Jassem, J. (2014) Zwalczanie nowotworów w Polsce: potrzeba nowej strategii in *Zachorowalność i umieralność na nowotwory a sytuacja demograficzna Polski* (Alicja Potrykowska, Z. S., Janusz Szymborski, Janusz Witkowski, ed) pp. 86-102, Rządowa Rada Ludnościowa, Warszawa.

5. Urszula Wojciechowska, K. C., Agata Ciuba, Paweł Olasek, Joanna Didkowska (2018) Nowotwory złośliwe w Polsce w 2016 roku in, Ministerstwo Zdrowia, Warszawa.

6. Hanahan, D. & Weinberg, R. A. (2011) Hallmarks of cancer: the next generation, *Cell.* 144, 646-74.

7. Hanahan, D. (2022) Hallmarks of Cancer: New Dimensions, *Cancer Discov.* 12, 31-46.

8. Parkin, D. M., Bray, F., Ferlay, J. & Pisani, P. (2005) Global cancer statistics, 2002, *CA Cancer J Clin.* 55, 74-108.

9. Torre, L. A., Bray, F., Siegel, R. L., Ferlay, J., Lortet-Tieulent, J. & Jemal, A. (2015) Global cancer statistics, 2012, *CA Cancer J Clin.* 65, 87-108.

10. Bray, F., Ferlay, J., Soerjomataram, I., Siegel, R. L., Torre, L. A. & Jemal, A. (2018) Global cancer statistics 2018: GLOBOCAN estimates of incidence and mortality worldwide for 36 cancers in 185 countries, *CA Cancer J Clin.* 68, 394-424.

11. Gerrard, G. E., Prestwich, R. J., Franks, K. N. & Levy, D. (2003) Neuro-oncology practice in the UK, *Clin Oncol (R Coll Radiol).* 15, 478-84.

12. Achrol, A. S., Rennert, R. C., Anders, C., Soffietti, R., Ahluwalia, M. S., Nayak, L., Peters, S., Arvold, N. D., Harsh, G. R., Steeg, P. S. & Chang, S. D. (2019) Brain metastases, *Nat Rev Dis Primers.* 5, 5.

13. Berghoff, A. S., Schur, S., Fureder, L. M., Gatterbauer, B., Dieckmann, K., Widhalm, G., Hainfellner, J., Zielinski, C. C., Birner, P., Bartsch, R. & Preusser, M. (2016) Descriptive statistical analysis of a real life cohort of 2419 patients with brain metastases of solid cancers, *ESMO Open.* 1, e000024.

14. Ostrom, Q. T., Cioffi, G., Gittleman, H., Patil, N., Waite, K., Kruchko, C. & Barnholtz-Sloan, J. S. (2019) CBTRUS Statistical Report: Primary Brain and Other Central Nervous System Tumors Diagnosed in the United States in 2012-2016, *Neuro Oncol.* 21, v1-v100.

15. Omuro, A. & DeAngelis, L. M. (2013) Glioblastoma and other malignant gliomas: a clinical review, *JAMA.* 310, 1842-50.

16. Gately, L., McLachlan, S. A., Dowling, A. & Philip, J. (2017) Life beyond a diagnosis of glioblastoma: a systematic review of the literature, *J Cancer Surviv.* 11, 447-452.

17. Louis, D. N., Ohgaki, H., Wiestler, O. D., Cavenee, W. K., Burger, P. C., Jouvet, A., Scheithauer, B. W. & Kleihues, P. (2007) The 2007 WHO classification of tumours of the central nervous system, *Acta Neuropathol.* 114, 97-109.

18. Autier, L., Clavreul, A., Cacicedo, M. L., Franconi, F., Sindji, L., Rousseau, A., Perrot, R., Montero-Menei, C. N., Castro, G. R. & Menei, P. (2019) A new glioblastoma cell trap for implantation after surgical resection, *Acta Biomater.* 84, 268-279.

19. Finneran, M., Marotta, D. A., Altenburger, D. & Nardone, E. (2020) Long-term Survival in a Patient with Butterfly Glioblastoma: A Case Report, *Cureus.* 12, e6914.

20. Stupp, R., Mason, W. P., van den Bent, M. J., Weller, M., Fisher, B., Taphoorn, M. J., Belanger, K., Brandes, A. A., Marosi, C., Bogdahn, U., Curschmann, J., Janzer, R. C., Ludwin, S. K., Gorlia, T., Allgeier, A., Lacombe, D., Cairncross, J. G., Eisenhauer, E., Mirimanoff, R. O., European Organisation for, R., Treatment of Cancer Brain, T., Radiotherapy, G. & National Cancer Institute of Canada Clinical Trials, G. (2005) Radiotherapy plus concomitant and adjuvant temozolomide for glioblastoma, *N Engl J Med.* 352, 987-96.

21. Davis, M. E. (2016) Glioblastoma: Overview of Disease and Treatment, *Clin J Oncol Nurs.* 20, S2-8.

22. Le Rhun, E., Preusser, M., Roth, P., Reardon, D. A., van den Bent, M., Wen, P., Reifenberger, G. & Weller, M. (2019) Molecular targeted therapy of glioblastoma, *Cancer Treat Rev.* 80, 101896.

23. Wick, W., Gorlia, T., Bendszus, M., Taphoorn, M., Sahm, F., Harting, I., Brandes, A. A., Taal, W., Domont, J., Idbaih, A., Campone, M., Clement, P. M., Stupp, R., Fabbro, M., Le Rhun, E., Dubois, F., Weller, M., von Deimling, A., Golfinopoulos, V., Bromberg, J. C., Platten, M., Klein, M. & van den Bent, M. J. (2017) Lomustine and Bevacizumab in Progressive Glioblastoma, *N Engl J Med.* 377, 1954-1963.

24. Binabaj, M. M., Bahrami, A., ShahidSales, S., Joodi, M., Joudi Mashhad, M., Hassanian, S. M., Anvari, K. & Avan, A. (2018) The prognostic value of MGMT promoter methylation in glioblastoma: A meta-analysis of clinical trials, *J Cell Physiol.* 233, 378-386.

25. Happold, C., Gorlia, T., Chinot, O., Gilbert, M. R., Nabors, L. B., Wick, W., Pugh, S. L., Hegi, M., Cloughesy, T., Roth, P., Reardon, D. A., Perry, J. R., Mehta, M. P., Stupp, R. & Weller, M. (2016) Does Valproic Acid or Levetiracetam Improve Survival in Glioblastoma? A Pooled Analysis of Prospective Clinical Trials in Newly Diagnosed Glioblastoma, *J Clin Oncol.* 34, 731-9.

26. Grossman, S. A., Ye, X., Chamberlain, M., Mikkelsen, T., Batchelor, T., Desideri, S., Piantadosi, S., Fisher, J. & Fine, H. A. (2009) Talampanel with standard radiation and temozolomide in patients with newly diagnosed glioblastoma: a multicenter phase II trial, *J Clin Oncol.* 27, 4155-61.

27. Seliger, C., Genbrugge, E., Gorlia, T., Chinot, O., Stupp, R., Nabors, B., Weller, M., Hau, P. & Group, E. B. T. (2020) Use of metformin and outcome of patients with newly diagnosed glioblastoma: Pooled analysis, *Int J Cancer.* 146, 803-809.

28. Fisher, J. P. & Adamson, D. C. (2021) Current FDA-Approved Therapies for High-Grade Malignant Gliomas, *Biomedicines.* 9.

29. Stupp, R., Taillibert, S., Kanner, A. A., Kesari, S., Steinberg, D. M., Toms, S. A., Taylor, L. P., Lieberman, F., Silvani, A., Fink, K. L., Barnett, G. H., Zhu, J. J., Henson, J. W., Engelhard, H. H., Chen, T. C., Tran, D. D., Sroubek, J., Tran, N. D., Hottinger, A. F., Landolfi, J., Desai,

R., Caroli, M., Kew, Y., Honnorat, J., Idbaih, A., Kirson, E. D., Weinberg, U., Palti, Y., Hegi, M. E. & Ram, Z. (2015) Maintenance Therapy With Tumor-Treating Fields Plus Temozolomide vs Temozolomide Alone for Glioblastoma: A Randomized Clinical Trial, *JAMA.* 314, 2535-43.

30. Ahmad, A. (2019) Breast Cancer Statistics: Recent Trends, *Adv Exp Med Biol.* 1152, 1-7.

31. Mattiuzzi, C. & Lippi, G. (2019) Current Cancer Epidemiology, *J Epidemiol Glob Health.* 9, 217-222.

32. Fahad Ullah, M. (2019) Breast Cancer: Current Perspectives on the Disease Status, *Adv Exp Med Biol.* 1152, 51-64.

33. Jin, T. Y., Park, K. S., Nam, S. E., Yoo, Y. B., Park, W. S. & Yun, I. J. (2022) BRCA1/2 Serves as a Biomarker for Poor Prognosis in Breast Carcinoma, *Int J Mol Sci.* 23.

34. Fisusi, F. A. & Akala, E. O. (2019) Drug Combinations in Breast Cancer Therapy, *Pharm Nanotechnol.* 7, 3-23.

35. Bergin, A. R. T. & Loi, S. (2019) Triple-negative breast cancer: recent treatment advances, *F1000Res.* 8.

36. Haffty, B. G., Yang, Q., Reiss, M., Kearney, T., Higgins, S. A., Weidhaas, J., Harris, L., Hait, W. & Toppmeyer, D. (2006) Locoregional relapse and distant metastasis in conservatively managed triple negative early-stage breast cancer, *J Clin Oncol.* 24, 5652-7.

37. Wu, Q., Siddharth, S. & Sharma, D. (2021) Triple Negative Breast Cancer: A Mountain Yet to Be Scaled Despite the Triumphs, *Cancers (Basel).* 13.

38. Abu Samaan, T. M., Samec, M., Liskova, A., Kubatka, P. & Busselberg, D. (2019) Paclitaxel's Mechanistic and Clinical Effects on Breast Cancer, *Biomolecules.* 9.

39. Helsby, N., Yong, M., Burns, K., Findlay, M. & Porter, D. (2021) Cyclophosphamide bioactivation pharmacogenetics in breast cancer patients, *Cancer Chemother Pharmacol.* 88, 533-542.

40. Wang, H., Guo, S., Kim, S. J., Shao, F., Ho, J. W. K., Wong, K. U., Miao, Z., Hao, D., Zhao, M., Xu, J., Zeng, J., Wong, K. H., Di, L., Wong, A. H., Xu, X. & Deng, C. X. (2021) Cisplatin prevents breast cancer metastasis through blocking early EMT and retards cancer growth together with paclitaxel, *Theranostics.* 11, 2442-2459.

41. Nicolazzi, M. A., Carnicelli, A., Fuorlo, M., Scaldaferri, A., Masetti, R., Landolfi, R. & Favuzzi, A. M. R. (2018) Anthracycline and trastuzumab-induced cardiotoxicity in breast cancer, *Eur Rev Med Pharmacol Sci.* 22, 2175-2185.

42. Zheng, M., Mei, Z., Junaid, M., Tania, M., Fu, J., Chen, H. C. & Khan, M. A. (2022) Synergistic Role of Thymoquinone on Anticancer Activity of 5-Fluorouracil in Triple Negative Breast Cancer Cells, *Anticancer Agents Med Chem.* 22, 1111-1118.

43. Humphrey, J. D., Dufresne, E. R. & Schwartz, M. A. (2014) Mechanotransduction and extracellular matrix homeostasis, *Nat Rev Mol Cell Biol.* 15, 802-12.

44. Frantz, C., Stewart, K. M. & Weaver, V. M. (2010) The extracellular matrix at a glance, *J Cell Sci.* 123, 4195-200.

45. Singh, P., Carraher, C. & Schwarzbauer, J. E. (2010) Assembly of fibronectin extracellular matrix, *Annu Rev Cell Dev Biol.* 26, 397-419.

46. Bonnans, C., Chou, J. & Werb, Z. (2014) Remodelling the extracellular matrix in development and disease, *Nat Rev Mol Cell Biol.* 15, 786-801.

47. Hynes, R. O. & Naba, A. (2012) Overview of the matrisome--an inventory of extracellular matrix constituents and functions, *Cold Spring Harb Perspect Biol.* 4, a004903.

48. Ricard-Blum, S. (2011) The collagen family, *Cold Spring Harb Perspect Biol.* 3, a004978.

49. Theocharis, A. D., Skandalis, S. S., Gialeli, C. & Karamanos, N. K. (2016) Extracellular matrix structure, *Adv Drug Deliv Rev.* 97, 4-27.

50. Tang, V. W. (2020) Collagen, stiffness, and adhesion: the evolutionary basis of vertebrate mechanobiology, *Mol Biol Cell.* 31, 1823-1834.

51. Cui, N., Hu, M. & Khalil, R. A. (2017) Biochemical and Biological Attributes of Matrix Metalloproteinases, *Prog Mol Biol Transl Sci.* 147, 1-73.

52. Malemud, C. J. (2019) Inhibition of MMPs and ADAM/ADAMTS, *Biochem Pharmacol.* 165, 33-40.

53. Rodriguez-Manzaneque, J. C., Carpizo, D., Plaza-Calonge Mdel, C., Torres-Collado, A. X., Thai, S. N., Simons, M., Horowitz, A. & Iruela-Arispe, M. L. (2009) Cleavage of syndecan-4 by ADAMTS1 provokes defects in adhesion, *Int J Biochem Cell Biol.* 41, 800-10.

54. Song, I. & Dityatev, A. (2018) Crosstalk between glia, extracellular matrix and neurons, *Brain Res Bull.* 136, 101-108.

55. Najafi, M., Farhood, B. & Mortezaee, K. (2019) Extracellular matrix (ECM) stiffness and degradation as cancer drivers, *J Cell Biochem.* 120, 2782-2790.

56. Strnad, H., Lacina, L., Kolar, M., Cada, Z., Vlcek, C., Dvorankova, B., Betka, J., Plzak, J., Chovanec, M., Sachova, J., Valach, J., Urbanova, M. & Smetana, K., Jr. (2010) Head and neck squamous cancer stromal fibroblasts produce growth factors influencing phenotype of normal human keratinocytes, *Histochem Cell Biol.* 133, 201-11.

57. Biffi, G. & Tuveson, D. A. (2021) Diversity and Biology of Cancer-Associated Fibroblasts, *Physiol Rev.* 101, 147-176.

58. Nazari, S. S. & Mukherjee, P. (2018) An overview of mammographic density and its association with breast cancer, *Breast Cancer.* 25, 259-267.

59. Grasset, E. M., Bertero, T., Bozec, A., Friard, J., Bourget, I., Pisano, S., Lecacheur, M., Maiel, M., Bailleux, C., Emelyanov, A., Ilie, M., Hofman, P., Meneguzzi, G., Duranton, C., Bulavin, D. V. & Gaggioli, C. (2018) Matrix Stiffening and EGFR Cooperate to Promote the Collective Invasion of Cancer Cells, *Cancer Res.* 78, 5229-5242.

60. Lee, S., Han, H., Koo, H., Na, J. H., Yoon, H. Y., Lee, K. E., Lee, H., Kim, H., Kwon, I. C. & Kim, K. (2017) Extracellular matrix remodeling in vivo for enhancing tumor-targeting efficiency of nanoparticle drug carriers using the pulsed high intensity focused ultrasound, *J Control Release.* 263, 68-78.

61. Ueno, H., Shinto, E., Hashiguchi, Y., Shimazaki, H., Kajiwara, Y., Sueyama, T., Yamamoto, J. & Hase, K. (2015) In rectal cancer, the type of desmoplastic response after preoperative chemoradiotherapy is associated with prognosis, *Virchows Arch.* 466, 655-63.

62. Chargari, C., Clemenson, C., Martins, I., Perfettini, J. L. & Deutsch, E. (2013) Understanding the functions of tumor stroma in resistance to ionizing radiation: emerging targets for pharmacological modulation, *Drug Resist Updat.* 16, 10-21.

63. Gouirand, V., Guillaumond, F. & Vasseur, S. (2018) Influence of the Tumor Microenvironment on Cancer Cells Metabolic Reprogramming, *Front Oncol.* 8, 117.

64. Miller, A., Nagy, C., Knapp, B., Laengle, J., Ponweiser, E., Groeger, M., Starkl, P., Bergmann, M., Wagner, O. & Haschemi, A. (2017) Exploring Metabolic Configurations of Single Cells within Complex Tissue Microenvironments, *Cell Metab.* 26, 788-800 e6.

65. Warburg, O., Wind, F. & Negelein, E. (1927) The Metabolism of Tumors in the Body, *J Gen Physiol.* 8, 519-30.

66. Colwell, N., Larion, M., Giles, A. J., Seldomridge, A. N., Sizdahkhani, S., Gilbert, M. R. & Park, D. M. (2017) Hypoxia in the glioblastoma microenvironment: shaping the phenotype of cancer stem-like cells, *Neuro Oncol.* 19, 887-896.

67. Alves, A. L. V., Gomes, I. N. F., Carloni, A. C., Rosa, M. N., da Silva, L. S., Evangelista, A. F., Reis, R. M. & Silva, V. A. O. (2021) Role of glioblastoma stem cells in cancer therapeutic resistance: a perspective on antineoplastic agents from natural sources and chemical derivatives, *Stem Cell Res Ther.* 12, 206.

68. Hao, Y., Baker, D. & Ten Dijke, P. (2019) TGF-beta-Mediated Epithelial-Mesenchymal Transition and Cancer Metastasis, *Int J Mol Sci.* 20.

69. Lamouille, S., Xu, J. & Derynck, R. (2014) Molecular mechanisms of epithelial-mesenchymal transition, *Nat Rev Mol Cell Biol.* 15, 178-96.

70. Dongre, A. & Weinberg, R. A. (2019) New insights into the mechanisms of epithelial-mesenchymal transition and implications for cancer, *Nat Rev Mol Cell Biol.* 20, 69-84.

71. Yamada, K. M. & Sixt, M. (2019) Mechanisms of 3D cell migration, *Nat Rev Mol Cell Biol.* 20, 738-752.

72. Mohiuddin, E. & Wakimoto, H. (2021) Extracellular matrix in glioblastoma: opportunities for emerging therapeutic approaches, *Am J Cancer Res.* 11, 3742-3754.

73. Fabian, C., Han, M., Bjerkvig, R. & Niclou, S. P. (2021) Novel facets of glioma invasion, *Int Rev Cell Mol Biol.* 360, 33-64.

74. Halper, J. & Kjaer, M. (2014) Basic components of connective tissues and extracellular matrix: elastin, fibrillin, fibulins, fibrinogen, fibronectin, laminin, tenascins and thrombospondins, *Adv Exp Med Biol.* 802, 31-47.

75. Chiquet-Ehrismann, R., Mackie, E. J., Pearson, C. A. & Sakakura, T. (1986) Tenascin: an extracellular matrix protein involved in tissue interactions during fetal development and oncogenesis, *Cell.* 47, 131-9.

76. Chiovaro, F., Chiquet-Ehrismann, R. & Chiquet, M. (2015) Transcriptional regulation of tenascin genes, *Cell Adh Migr.* 9, 34-47.

77. Giblin, S. P. & Midwood, K. S. (2015) Tenascin-C: Form versus function, *Cell Adh Migr.* 9, 48-82.

78. Midwood, K. S., Chiquet, M., Tucker, R. P. & Orend, G. (2016) Tenascin-C at a glance, *J Cell Sci.* 129, 4321-4327.

79. Hasegawa, M., Yoshida, T. & Sudo, A. (2020) Tenascin-C in Osteoarthritis and Rheumatoid Arthritis, *Front Immunol.* 11, 577015.

80. Pugh, B. F. (2000) Control of gene expression through regulation of the TATA-binding protein, *Gene.* 255, 1-14.

81. Lutz, R., Sakai, T. & Chiquet, M. (2010) Pericellular fibronectin is required for RhoA-dependent responses to cyclic strain in fibroblasts, *J Cell Sci.* 123, 1511-21.

82. De Laporte, L., Rice, J. J., Tortelli, F. & Hubbell, J. A. (2013) Tenascin C promiscuously binds growth factors via its fifth fibronectin type III-like domain, *PLoS One.* 8, e62076.

83. Chiquet-Ehrismann, R. & Chiquet, M. (2003) Tenascins: regulation and putative functions during pathological stress, *J Pathol.* 200, 488-99.

84. Midwood, K. S. & Schwarzbauer, J. E. (2002) Tenascin-C modulates matrix contraction via focal adhesion kinase- and Rho-mediated signaling pathways, *Mol Biol Cell.* 13, 3601-13.

85. Trebaul, A., Chan, E. K. & Midwood, K. S. (2007) Regulation of fibroblast migration by tenascin-C, *Biochem Soc Trans.* 35, 695-7.

86. Cai, J., Du, S., Wang, H., Xin, B., Wang, J., Shen, W., Wei, W., Guo, Z. & Shen, X. (2017) Tenascin-C induces migration and invasion through JNK/c-Jun signalling in pancreatic cancer, *Oncotarget.* 8, 74406-74422.

87. Popova, N. V. & Jucker, M. (2022) The Functional Role of Extracellular Matrix Proteins in Cancer, *Cancers (Basel).* 14.

88. Nie, S., Gurrea, M., Zhu, J., Thakolwiboon, S., Heth, J. A., Muraszko, K. M., Fan, X. & Lubman, D. M. (2015) Tenascin-C: a novel candidate marker for cancer stem cells in glioblastoma identified by tissue microarrays, *J Proteome Res.* 14, 814-22.

89. Ming, X., Qiu, S., Liu, X., Li, S., Wang, Y., Zhu, M., Li, N., Luo, P., Liang, C. & Tu, J. (2019) Prognostic Role of Tenascin-C for Cancer Outcome: A Meta-Analysis, *Technol Cancer Res Treat.* 18, 1533033818821106.

90. Angel, I., Pilo Kerman, O., Rousso-Noori, L. & Friedmann-Morvinski, D. (2020) Tenascin C promotes cancer cell plasticity in mesenchymal glioblastoma, *Oncogene.* 39, 6990-7004.

91. Zhang, Q., Xu, B., Hu, F., Chen, X., Liu, X., Zhang, Q. & Zuo, Y. (2021) Tenascin C Promotes Glioma Cell Malignant Behavior and Inhibits Chemosensitivity to Paclitaxel via Activation of the PI3K/AKT Signaling Pathway, *J Mol Neurosci.* 71, 1636-1647.

92. Murdamoothoo, D., Sun, Z., Yilmaz, A., Riegel, G., Abou-Faycal, C., Deligne, C., Velazquez-Quesada, I., Erne, W., Nascimento, M., Morgelin, M., Cremel, G., Paul, N., Carapito, R., Veber, R., Dumortier, H., Yuan, J., Midwood, K. S., Loustau, T. & Orend, G. (2021) Tenascin-C immobilizes infiltrating T lymphocytes through CXCL12 promoting breast cancer progression, *EMBO Mol Med.* 13, e13270.

93. Katoh, D., Kozuka, Y., Noro, A., Ogawa, T., Imanaka-Yoshida, K. & Yoshida, T. (2020) Tenascin-C Induces Phenotypic Changes in Fibroblasts to Myofibroblasts with High Contractility through the Integrin alphavbeta1/Transforming Growth Factor beta/SMAD Signaling Axis in Human Breast Cancer, *Am J Pathol.* 190, 2123-2135.

94. Lee, Y. C., Lin, S. C., Yu, G., Zhu, M., Song, J. H., Rivera, K., Pappin, D. J., Logothetis, C. J., Panaretakis, T., Wang, G., Yu-Lee, L. Y. & Lin, S. H. (2022) Prostate tumor-induced stromal reprogramming generates Tenascin C that promotes prostate cancer metastasis through YAP/TAZ inhibition, *Oncogene.* 41, 757-769.

95. Kiebish, M. A., Cullen, J., Mishra, P., Ali, A., Milliman, E., Rodrigues, L. O., Chen, E. Y., Tolstikov, V., Zhang, L., Panagopoulos, K., Shah, P., Chen, Y., Petrovics, G., Rosner, I. L., Sesterhenn, I. A., McLeod, D. G., Granger, E., Sarangarajan, R., Akmaev, V., Srinivasan, A., Srivastava, S., Narain, N. R. & Dobi, A. (2020) Multi-omic serum biomarkers for prognosis of disease progression in prostate cancer, *J Transl Med.* 18, 10.

96. Modica, C., Olivero, M., Zuppini, F., Milan, M., Basilico, C. & Vigna, E. (2021) HGF/MET Axis Induces Tumor Secretion of Tenascin-C and Promotes Stromal Rewiring in Pancreatic Cancer, *Cancers (Basel).* 13.

97.   Hagiwara, K., Harimoto, N. & Shirabe, K. (2020) ASO Author Reflections: Clinical Significance of Large Tenascin C Splice Variants and Annexin A2 for Pancreatic Cancer, *Ann Surg Oncol.* 27, 931-932.

98.   Fujita, M., Suzuki, H. & Fukai, F. (2021) Involvement of integrin-activating peptides derived from tenascin-C in colon cancer progression, *World J Gastrointest Oncol.* 13, 980-994.

99.   Kang, X., Xu, E., Wang, X., Qian, L., Yang, Z., Yu, H., Wang, C., Ren, C., Wang, Y., Lu, X., Xia, X., Guan, W. & Qiao, T. (2021) Tenascin-c knockdown suppresses vasculogenic mimicry of gastric cancer by inhibiting ERK- triggered EMT, *Cell Death Dis.* 12, 890.

100. Silvers, C. R., Messing, E. M., Miyamoto, H. & Lee, Y. F. (2021) Tenascin-C expression in the lymph node pre-metastatic niche in muscle-invasive bladder cancer, *Br J Cancer.* 125, 1399-1407.

101. Yang, Z., Zhang, C., Feng, Y., Quan, M., Cui, Y. & Xuan, Y. (2020) Tenascin-C predicts poor outcomes for patients with colorectal cancer and drives cancer stemness via Hedgehog signaling pathway, *Cancer Cell Int.* 20, 122.

102. Steitz, A. M., Steffes, A., Finkernagel, F., Unger, A., Sommerfeld, L., Jansen, J. M., Wagner, U., Graumann, J., Muller, R. & Reinartz, S. (2020) Tumor-associated macrophages promote ovarian cancer cell migration by secreting transforming growth factor beta induced (TGFBI) and tenascin C, *Cell Death Dis.* 11, 249.

103. Blencowe, B., Brenner, S., Hughes, T. & Morris, Q. (2009) Post-transcriptional gene regulation: RNA-protein interactions, RNA processing, mRNA stability and localization, *Pac Symp Biocomput*, 545-8.

104. Anastasiadou, E., Jacob, L. S. & Slack, F. J. (2018) Non-coding RNA networks in cancer, *Nat Rev Cancer.* 18, 5-18.

105. Ali Syeda, Z., Langden, S. S. S., Munkhzul, C., Lee, M. & Song, S. J. (2020) Regulatory Mechanism of MicroRNA Expression in Cancer, *Int J Mol Sci.* 21.

106. International Human Genome Sequencing, C. (2004) Finishing the euchromatic sequence of the human genome, *Nature.* 431, 931-45.

107. Latowska, J., Grabowska, A., Zarebska, Z., Kuczynski, K., Kuczynska, B. & Rolle, K. (2020) Non-coding RNAs in Brain Tumors, the Contribution of lncRNAs, circRNAs, and snoRNAs to Cancer Development-Their Diagnostic and Therapeutic Potential, *Int J Mol Sci.* 21.

108. Lee, R. C., Feinbaum, R. L. & Ambros, V. (1993) The C. elegans heterochronic gene lin-4 encodes small RNAs with antisense complementarity to lin-14, *Cell.* 75, 843-54.

109. Fire, A., Xu, S., Montgomery, M. K., Kostas, S. A., Driver, S. E. & Mello, C. C. (1998) Potent and specific genetic interference by double-stranded RNA in Caenorhabditis elegans, *Nature.* 391, 806-11.

110. Cen, L., Liu, R., Liu, W., Li, Q. & Cui, H. (2021) Competing Endogenous RNA Networks in Glioma, *Front Genet.* 12, 675498.

111. Lewis, B. P., Burge, C. B. & Bartel, D. P. (2005) Conserved seed pairing, often flanked by adenosines, indicates that thousands of human genes are microRNA targets, *Cell.* 120, 15-20.

112. Zhang, Y., Yun, Z., Gong, L., Qu, H., Duan, X., Jiang, Y. & Zhu, H. (2018) Comparison of miRNA Evolution and Function in Plants and Animals, *Microrna.* 7, 4-10.

113. Alles, J., Fehlmann, T., Fischer, U., Backes, C., Galata, V., Minet, M., Hart, M., Abu-Halima, M., Grasser, F. A., Lenhof, H. P., Keller, A. & Meese, E. (2019) An estimate of the total number of true human miRNAs, *Nucleic Acids Res.* 47, 3353-3364.

114. Denli, A. M., Tops, B. B., Plasterk, R. H., Ketting, R. F. & Hannon, G. J. (2004) Processing of primary microRNAs by the Microprocessor complex, *Nature.* 432, 231-5.

115. Han, J., Lee, Y., Yeom, K. H., Kim, Y. K., Jin, H. & Kim, V. N. (2004) The Drosha-DGCR8 complex in primary microRNA processing, *Genes Dev.* 18, 3016-27.

116. Kobayashi, H. & Tomari, Y. (2016) RISC assembly: Coordination between small RNAs and Argonaute proteins, *Biochim Biophys Acta.* 1859, 71-81.

117. Meijer, H. A., Smith, E. M. & Bushell, M. (2014) Regulation of miRNA strand selection: follow the leader?, *Biochem Soc Trans.* 42, 1135-40.

118. Schwarz, D. S., Hutvagner, G., Du, T., Xu, Z., Aronin, N. & Zamore, P. D. (2003) Asymmetry in the assembly of the RNAi enzyme complex, *Cell.* 115, 199-208.

119. Matsuyama, H. & Suzuki, H. I. (2019) Systems and Synthetic microRNA Biology: From Biogenesis to Disease Pathogenesis, *Int J Mol Sci.* 21.

120. Hammond, S. M., Bernstein, E., Beach, D. & Hannon, G. J. (2000) An RNA-directed nuclease mediates post-transcriptional gene silencing in Drosophila cells, *Nature.* 404, 293-6.

121. Spengler, R. M., Zhang, X., Cheng, C., McLendon, J. M., Skeie, J. M., Johnson, F. L., Davidson, B. L. & Boudreau, R. L. (2016) Elucidation of transcriptome-wide microRNA binding sites in human cardiac tissues by Ago2 HITS-CLIP, *Nucleic Acids Res.* 44, 7120-31.

122. Wongfieng, W., Jumnainsong, A., Chamgramol, Y., Sripa, B. & Leelayuwat, C. (2017) 5'-UTR and 3'-UTR Regulation of MICB Expression in Human Cancer Cells by Novel microRNAs, *Genes (Basel).* 8.

123. Fukao, A., Mishima, Y., Takizawa, N., Oka, S., Imataka, H., Pelletier, J., Sonenberg, N., Thoma, C. & Fujiwara, T. (2014) MicroRNAs trigger dissociation of eIF4AI and eIF4AII from target mRNAs in humans, *Mol Cell.* 56, 79-89.

124. Balachandran, A. A., Larcher, L. M., Chen, S. & Veedu, R. N. (2020) Therapeutically Significant MicroRNAs in Primary and Metastatic Brain Malignancies, *Cancers (Basel).* 12.

125. Wang, B., Love, T. M., Call, M. E., Doench, J. G. & Novina, C. D. (2006) Recapitulation of short RNA-directed translational gene silencing in vitro, *Mol Cell.* 22, 553-60.

126. Kiriakidou, M., Nelson, P. T., Kouranov, A., Fitziev, P., Bouyioukos, C., Mourelatos, Z. & Hatzigeorgiou, A. (2004) A combined computational-experimental approach predicts human microRNA targets, *Genes Dev.* 18, 1165-78.

127. Liu, J., Valencia-Sanchez, M. A., Hannon, G. J. & Parker, R. (2005) MicroRNA-dependent localization of targeted mRNAs to mammalian P-bodies, *Nat Cell Biol.* 7, 719-23.

128. Berkhout, B. (2018) RNAi-mediated antiviral immunity in mammals, *Curr Opin Virol.* 32, 9-14.

129. de Fougerolles, A., Manoharan, M., Meyers, R. & Vornlocher, H. P. (2005) RNA interference in vivo: toward synthetic small inhibitory RNA-based therapeutics, *Methods Enzymol.* 392, 278-96.

130. Lam, J. K., Chow, M. Y., Zhang, Y. & Leung, S. W. (2015) siRNA Versus miRNA as Therapeutics for Gene Silencing, *Mol Ther Nucleic Acids.* 4, e252.

131. Elbashir, S. M., Lendeckel, W. & Tuschl, T. (2001) RNA interference is mediated by 21- and 22-nucleotide RNAs, *Genes Dev.* 15, 188-200.

132. Subhan, M. A. & Torchilin, V. P. (2019) Efficient nanocarriers of siRNA therapeutics for cancer treatment, *Transl Res.* 214, 62-91.

133. Matsui, M. & Corey, D. R. (2017) Non-coding RNAs as drug targets, *Nat Rev Drug Discov.* 16, 167-179.

134. Schweinoch, D., Bachmann, P., Clausznitzer, D., Binder, M. & Kaderali, L. (2020) Mechanistic modeling explains the dsRNA length-dependent activation of the RIG-I mediated immune response, *J Theor Biol.* 500, 110336.

135. McAnuff, M. A., Rettig, G. R. & Rice, K. G. (2007) Potency of siRNA versus shRNA mediated knockdown in vivo, *J Pharm Sci.* 96, 2922-30.

136. Esau, C. C. & Monia, B. P. (2007) Therapeutic potential for microRNAs, *Adv Drug Deliv Rev.* 59, 101-14.

137. Sajid, M. I., Moazzam, M., Kato, S., Yeseom Cho, K. & Tiwari, R. K. (2020) Overcoming Barriers for siRNA Therapeutics: From Bench to Bedside, *Pharmaceuticals (Basel).* 13.

138. Hu, B., Zhong, L., Weng, Y., Peng, L., Huang, Y., Zhao, Y. & Liang, X. J. (2020) Therapeutic siRNA: state of the art, *Signal Transduct Target Ther.* 5, 101.

139. Bayda, S., Adeel, M., Tuccinardi, T., Cordani, M. & Rizzolio, F. (2019) The History of Nanoscience and Nanotechnology: From Chemical-Physical Applications to Nanomedicine, *Molecules.* 25.

140. Rothemund, P. W. (2006) Folding DNA to create nanoscale shapes and patterns, *Nature.* 440, 297-302.

141. Chaturvedi, V. K., Singh, A., Singh, V. K. & Singh, M. P. (2019) Cancer Nanotechnology: A New Revolution for Cancer Diagnosis and Therapy, *Curr Drug Metab.* 20, 416-429.

142. Colombo, I., Overchuk, M., Chen, J., Reilly, R. M., Zheng, G. & Lheureux, S. (2017) Molecular imaging in drug development: Update and challenges for radiolabeled antibodies and nanotechnology, *Methods.* 130, 23-35.

143. Calle, D., Ballesteros, P. & Cerdan, S. (2018) Advanced Contrast Agents for Multimodal Biomedical Imaging Based on Nanotechnology, *Methods Mol Biol.* 1718, 441-457.

144. Maier-Hauff, K., Ulrich, F., Nestler, D., Niehoff, H., Wust, P., Thiesen, B., Orawa, H., Budach, V. & Jordan, A. (2011) Efficacy and safety of intratumoral thermotherapy using magnetic iron-oxide nanoparticles combined with external beam radiotherapy on patients with recurrent glioblastoma multiforme, *J Neurooncol.* 103, 317-24.

145. Unsoy, G. & Gunduz, U. (2018) Smart Drug Delivery Systems in Cancer Therapy, *Curr Drug Targets.* 19, 202-212.

146. Zhang, Y., Li, M., Gao, X., Chen, Y. & Liu, T. (2019) Nanotechnology in cancer diagnosis: progress, challenges and opportunities, *J Hematol Oncol.* 12, 137.

147. Talasaz, A. H., Powell, A. A., Huber, D. E., Berbee, J. G., Roh, K. H., Yu, W., Xiao, W., Davis, M. M., Pease, R. F., Mindrinos, M. N., Jeffrey, S. S. & Davis, R. W. (2009) Isolating highly enriched populations of circulating epithelial cells and other rare cells from blood using a magnetic sweeper device, *Proc Natl Acad Sci U S A.* 106, 3970-5.

148. Zhang, Y., Chen, B., He, M., Yang, B., Zhang, J. & Hu, B. (2014) Immunomagnetic separation combined with inductively coupled plasma mass spectrometry for the detection of tumor cells using gold nanoparticle labeling, *Anal Chem.* 86, 8082-9.

149. Sinceviciute, R., Vaitkiene, P., Urbanaviciute, R., Steponaitis, G., Tamasauskas, A. & Skiriute, D. (2018) MMP2 is associated with glioma malignancy and patient outcome, *Int J Clin Exp Pathol.* 11, 3010-3018.

150. Wang, Y., Lin, T., Zhang, W., Jiang, Y., Jin, H., He, H., Yang, V. C., Chen, Y. & Huang, Y. (2015) A Prodrug-type, MMP-2-targeting Nanoprobe for Tumor Detection and Imaging, *Theranostics.* 5, 787-95.

151. Shi, Y., van der Meel, R., Chen, X. & Lammers, T. (2020) The EPR effect and beyond: Strategies to improve tumor targeting and cancer nanomedicine treatment efficacy, *Theranostics.* 10, 7921-7924.

152. Mantso, T., Vasileiadis, S., Anestopoulos, I., Voulgaridou, G. P., Lampri, E., Botaitis, S., Kontomanolis, E. N., Simopoulos, C., Goussetis, G., Franco, R., Chlichlia, K., Pappa, A. & Panayiotidis, M. I. (2018) Hyperthermia induces therapeutic effectiveness and potentiates adjuvant therapy with non-targeted and targeted drugs in an in vitro model of human malignant melanoma, *Sci Rep.* 8, 10724.

153. Li, X., Lovell, J. F., Yoon, J. & Chen, X. (2020) Clinical development and potential of photothermal and photodynamic therapies for cancer, *Nat Rev Clin Oncol.* 17, 657-674.

154. Kim, H. S. & Lee, D. Y. (2018) Near-Infrared-Responsive Cancer Photothermal and Photodynamic Therapy Using Gold Nanoparticles, *Polymers (Basel).* 10.

155. Caro, C., Gamez, F., Quaresma, P., Paez-Munoz, J. M., Dominguez, A., Pearson, J. R., Pernia Leal, M., Beltran, A. M., Fernandez-Afonso, Y., De la Fuente, J. M., Franco, R., Pereira, E. & Garcia-Martin, M. L. (2021) Fe3O4-Au Core-Shell Nanoparticles as a Multimodal Platform for In Vivo Imaging and Focused Photothermal Therapy, *Pharmaceutics.* 13.

156. Farokhi, M., Mottaghitalab, F., Saeb, M. R. & Thomas, S. (2019) Functionalized theranostic nanocarriers with bio-inspired polydopamine for tumor imaging and chemo-photothermal therapy, *J Control Release.* 309, 203-219.

157. Patra, J. K., Das, G., Fraceto, L. F., Campos, E. V. R., Rodriguez-Torres, M. D. P., Acosta-Torres, L. S., Diaz-Torres, L. A., Grillo, R., Swamy, M. K., Sharma, S., Habtemariam, S. & Shin, H. S. (2018) Nano based drug delivery systems: recent developments and future prospects, *J Nanobiotechnology.* 16, 71.

158. Singh, R. & Lillard, J. W., Jr. (2009) Nanoparticle-based targeted drug delivery, *Exp Mol Pathol.* 86, 215-23.

159. Glaser, T., Han, I., Wu, L. & Zeng, X. (2017) Targeted Nanotechnology in Glioblastoma Multiforme, *Front Pharmacol.* 8, 166.

160. Tang, W., Fan, W., Lau, J., Deng, L., Shen, Z. & Chen, X. (2019) Emerging blood-brain-barrier-crossing nanotechnology for brain cancer theranostics, *Chem Soc Rev.* 48, 2967-3014.

161. Hoshyar, N., Gray, S., Han, H. & Bao, G. (2016) The effect of nanoparticle size on in vivo pharmacokinetics and cellular interaction, *Nanomedicine (Lond).* 11, 673-92.

162. Zauner, W., Farrow, N. A. & Haines, A. M. (2001) In vitro uptake of polystyrene microspheres: effect of particle size, cell line and cell density, *J Control Release.* 71, 39-51.

163. Desai, M. P., Labhasetwar, V., Walter, E., Levy, R. J. & Amidon, G. L. (1997) The mechanism of uptake of biodegradable microparticles in Caco-2 cells is size dependent, *Pharm Res.* 14, 1568-73.

164. Dawson, G. F. & Halbert, G. W. (2000) The in vitro cell association of invasin coated polylactide-co-glycolide nanoparticles, *Pharm Res.* 17, 1420-5.

165. Rybak-Smith, M. J., Tripisciano, C., Borowiak-Palen, E., Lamprecht, C. & Sim, R. B. (2011) Effect of functionalization of carbon nanotubes with psychosine on complement activation and protein adsorption, *J Biomed Nanotechnol.* 7, 830-9.

166. Muller, R. H., Maassen, S., Weyhers, H. & Mehnert, W. (1996) Phagocytic uptake and cytotoxicity of solid lipid nanoparticles (SLN) sterically stabilized with poloxamine 908 and poloxamer 407, *J Drug Target.* 4, 161-70.

167. Smith, B. R., Ghosn, E. E., Rallapalli, H., Prescher, J. A., Larson, T., Herzenberg, L. A. & Gambhir, S. S. (2014) Selective uptake of single-walled carbon nanotubes by circulating monocytes for enhanced tumour delivery, *Nat Nanotechnol.* 9, 481-7.

168. Bhadra, D., Bhadra, S., Jain, P. & Jain, N. K. (2002) Pegnology: a review of PEG-ylated systems, *Pharmazie.* 57, 5-29.

169. Tavakol, S., Hoveizi, E., Kharrazi, S., Tavakol, B., Karimi, S. & Rezayat Sorkhabadi, S. M. (2017) Organelles and chromatin fragmentation of human umbilical vein endothelial cell influence by the effects of zeta potential and size of silver nanoparticles in different manners, *Artif Cells Nanomed Biotechnol.* 45, 817-823.

170. Morsi, N. G., Ali, S. M., Elsonbaty, S. S., Afifi, A. A., Hamad, M. A., Gao, H. & Elsabahy, M. (2018) Poly(glycerol methacrylate)-based degradable nanoparticles for delivery of small interfering RNA, *Pharm Dev Technol.* 23, 387-399.

171. Gonzalez Solveyra, E., Thompson, D. H. & Szleifer, I. (2022) Proteins Adsorbing onto Surface-Modified Nanoparticles: Effect of Surface Curvature, pH, and the Interplay of Polymers and Proteins Acid-Base Equilibrium, *Polymers (Basel).* 14.

172. Thomas, T. J., Tajmir-Riahi, H. A. & Thomas, T. (2016) Polyamine-DNA interactions and development of gene delivery vehicles, *Amino Acids.* 48, 2423-31.

173. Fleige, E., Quadir, M. A. & Haag, R. (2012) Stimuli-responsive polymeric nanocarriers for the controlled transport of active compounds: concepts and applications, *Adv Drug Deliv Rev.* 64, 866-84.

174. Mohammadi, M. & Pourseyed Aghaei, F. (2021) Magnetite Fe3O4 surface as an effective drug delivery system for cancer treatment drugs: density functional theory study, *J Biomol Struct Dyn.* 39, 2798-2805.

175. Shokrollahi, H. (2013) Contrast agents for MRI, *Mater Sci Eng C Mater Biol Appl.* 33, 4485-97.

176. Tomitaka, A. & Takemura, Y. (2019) Magnetic Relaxation of Intracellular Magnetic Nanoparticles for Hyperthermia, *Crit Rev Biomed Eng.* 47, 489-494.

177. Kami, D., Takeda, S., Itakura, Y., Gojo, S., Watanabe, M. & Toyoda, M. (2011) Application of magnetic nanoparticles to gene delivery, *Int J Mol Sci.* 12, 3705-22.

178. Vicentini, F. T., Borgheti-Cardoso, L. N., Depieri, L. V., de Macedo Mano, D., Abelha, T. F., Petrilli, R. & Bentley, M. V. (2013) Delivery systems and local administration routes for therapeutic siRNA, *Pharm Res.* 30, 915-31.

179. Soutschek, J., Akinc, A., Bramlage, B., Charisse, K., Constien, R., Donoghue, M., Elbashir, S., Geick, A., Hadwiger, P., Harborth, J., John, M., Kesavan, V., Lavine, G., Pandey, R. K., Racie, T., Rajeev, K. G., Rohl, I., Toudjarska, I., Wang, G., Wuschko, S., Bumcrot, D., Koteliansky, V., Limmer, S., Manoharan, M. & Vornlocher, H. P. (2004) Therapeutic silencing of an endogenous gene by systemic administration of modified siRNAs, *Nature.* 432, 173-8.

180. Lee, S. J., Son, S., Yhee, J. Y., Choi, K., Kwon, I. C., Kim, S. H. & Kim, K. (2013) Structural modification of siRNA for efficient gene silencing, *Biotechnol Adv.* 31, 491-503.

181. Wagstaff, K. M. & Jans, D. A. (2006) Protein transduction: cell penetrating peptides and their therapeutic applications, *Curr Med Chem.* 13, 1371-87.

182. Huotari, J. & Helenius, A. (2011) Endosome maturation, *EMBO J.* 30, 3481-500.

183. Smith, S. A., Selby, L. I., Johnston, A. P. R. & Such, G. K. (2019) The Endosomal Escape of Nanoparticles: Toward More Efficient Cellular Delivery, *Bioconjug Chem.* 30, 263-272.

184. Judge, A. D., Sood, V., Shaw, J. R., Fang, D., McClintock, K. & MacLachlan, I. (2005) Sequence-dependent stimulation of the mammalian innate immune response by synthetic siRNA, *Nat Biotechnol.* 23, 457-62.

185. Meng, Z. & Lu, M. (2017) RNA Interference-Induced Innate Immunity, Off-Target Effect, or Immune Adjuvant?, *Front Immunol.* 8, 331.

186. Yan, Y., Liu, X. Y., Lu, A., Wang, X. Y., Jiang, L. X. & Wang, J. C. (2022) Non-viral vectors for RNA delivery, *J Control Release.* 342, 241-279.

187. Kim, J. Y., Ohn, J., Yoon, J. S., Kang, B. M., Park, M., Kim, S., Lee, W., Hwang, S., Kim, J. I., Kim, K. H. & Kwon, O. (2019) Priming mobilization of hair follicle stem cells triggers permanent loss of regeneration after alkylating chemotherapy, *Nat Commun.* 10, 3694.

188. Haji Abdolvahab, M., Mofrad, M. R. & Schellekens, H. (2016) Interferon Beta: From Molecular Level to Therapeutic Effects, *Int Rev Cell Mol Biol.* 326, 343-72.

189. Yoshida, J., Mizuno, M., Fujii, M., Kajita, Y., Nakahara, N., Hatano, M., Saito, R., Nobayashi, M. & Wakabayashi, T. (2004) Human gene therapy for malignant gliomas (glioblastoma multiforme and anaplastic astrocytoma) by in vivo transduction with human interferon beta gene using cationic liposomes, *Hum Gene Ther.* 15, 77-86.

190. Wakabayashi, T., Natsume, A., Hashizume, Y., Fujii, M., Mizuno, M. & Yoshida, J. (2008) A phase I clinical trial of interferon-beta gene therapy for high-grade glioma: novel findings from gene expression profiling and autopsy, *J Gene Med.* 10, 329-39.

191. Yan, J., Smyth, M. J. & Teng, M. W. L. (2018) Interleukin (IL)-12 and IL-23 and Their Conflicting Roles in Cancer, *Cold Spring Harb Perspect Biol.* 10.

192. Ren, H., Boulikas, T., Lundstrom, K., Soling, A., Warnke, P. C. & Rainov, N. G. (2003) Immunogene therapy of recurrent glioblastoma multiforme with a liposomally encapsulated replication-incompetent Semliki forest virus vector carrying the human interleukin-12 gene--a phase I/II clinical protocol, *J Neurooncol.* 64, 147-54.

193. Johannsen, M., Gneveckow, U., Taymoorian, K., Thiesen, B., Waldofner, N., Scholz, R., Jung, K., Jordan, A., Wust, P. & Loening, S. A. (2007) Morbidity and quality of life during thermotherapy using magnetic nanoparticles in locally recurrent prostate cancer: results of a prospective phase I trial, *Int J Hyperthermia.* 23, 315-23.

194. Maier-Hauff, K., Rothe, R., Scholz, R., Gneveckow, U., Wust, P., Thiesen, B., Feussner, A., von Deimling, A., Waldoefner, N., Felix, R. & Jordan, A. (2007) Intracranial thermotherapy using magnetic nanoparticles combined with external beam radiotherapy: results of a feasibility study on patients with glioblastoma multiforme, *J Neurooncol.* 81, 53-60.

195. van Landeghem, F. K., Maier-Hauff, K., Jordan, A., Hoffmann, K. T., Gneveckow, U., Scholz, R., Thiesen, B., Bruck, W. & von Deimling, A. (2009) Post-mortem studies in glioblastoma patients treated with thermotherapy using magnetic nanoparticles, *Biomaterials.* 30, 52-7.

196. Kumthekar, P., Ko, C. H., Paunesku, T., Dixit, K., Sonabend, A. M., Bloch, O., Tate, M., Schwartz, M., Zuckerman, L., Lezon, R., Lukas, R. V., Jovanovic, B., McCortney, K., Colman, H., Chen, S., Lai, B., Antipova, O., Deng, J., Li, L., Tommasini-Ghelfi, S., Hurley, L. A., Unruh, D., Sharma, N. V., Kandpal, M., Kouri, F. M., Davuluri, R. V., Brat, D. J., Muzzio, M., Glass, M., Vijayakumar, V., Heidel, J., Giles, F. J., Adams, A. K., James, C. D., Woloschak, G. E., Horbinski, C. & Stegh, A. H. (2021) A first-in-human phase 0 clinical study of RNA interference-based spherical nucleic acids in patients with recurrent glioblastoma, *Sci Transl Med.* 13.

197. Stegh, A. H., Brennan, C., Mahoney, J. A., Forloney, K. L., Jenq, H. T., Luciano, J. P., Protopopov, A., Chin, L. & Depinho, R. A. (2010) Glioma oncoprotein Bcl2L12 inhibits the p53 tumor suppressor, *Genes Dev.* 24, 2194-204.

198. Piwecka, M., Rolle, K., Belter, A., Barciszewska, A. M., Zywicki, M., Michalak, M., Nowak, S., Naskret-Barciszewska, M. Z. & Barciszewski, J. (2015) Comprehensive analysis of microRNA expression profile in malignant glioma tissues, *Mol Oncol.* 9, 1324-40.

199. Li, Z., Qian, R., Zhang, J. & Shi, X. (2019) MiR-218-5p targets LHFPL3 to regulate proliferation, migration, and epithelial-mesenchymal transitions of human glioma cells, *Biosci Rep.* 39.

200. Mathew, L. K., Skuli, N., Mucaj, V., Lee, S. S., Zinn, P. O., Sathyan, P., Imtiyaz, H. Z., Zhang, Z., Davuluri, R. V., Rao, S., Venneti, S., Lal, P., Lathia, J. D., Rich, J. N., Keith, B., Minn, A. J. & Simon, M. C. (2014) miR-218 opposes a critical RTK-HIF pathway in mesenchymal glioblastoma, *Proc Natl Acad Sci U S A.* 111, 291-6.

201. Liu, Y., Yan, W., Zhang, W., Chen, L., You, G., Bao, Z., Wang, Y., Wang, H., Kang, C. & Jiang, T. (2012) MiR-218 reverses high invasiveness of glioblastoma cells by targeting the oncogenic transcription factor LEF1, *Oncol Rep.* 28, 1013-21.

202. Grabowska, M., Kuczynski, K., Piwecka, M., Rabiasz, A., Zamla, J., Glodowicz, P., Wawrzyniak, D., Lekka, M. & Rolle, K. (2022) miR-218 affects the ECM composition and cell biomechanical properties of glioblastoma cells, *J Cell Mol Med.* 00, 1-18.

203. Oliveira, A. I., Anjo, S. I., Vieira de Castro, J., Serra, S. C., Salgado, A. J., Manadas, B. & Costa, B. M. (2017) Crosstalk between glial and glioblastoma cells triggers the "go-or-grow" phenotype of tumor cells, *Cell Commun Signal.* 15, 37.

204. Zukiel, R., Nowak, S., Wyszko, E., Rolle, K., Gawronska, I., Barciszewska, M. Z. & Barciszewski, J. (2006) Suppression of human brain tumor with interference RNA specific for tenascin-C, *Cancer Biol Ther.* 5, 1002-7.

205. Rolle, K., Nowak, S., Wyszko, E., Nowak, M., Zukiel, R., Piestrzeniewicz, R., Gawronska, I., Barciszewska, M. Z. & Barciszewski, J. (2010) Promising human brain tumors therapy with interference RNA intervention (iRNAi), *Cancer Biol Ther.* 9, 396-406.

206. Karvelas, E. G., Lampropoulos, N. K., Benos, L. T., Karakasidis, T. & Sarris, I. E. (2021) On the magnetic aggregation of Fe3O4 nanoparticles, *Comput Methods Programs Biomed.* 198, 105778.

207. Avasthi, A., Caro, C., Pozo-Torres, E., Leal, M. P. & Garcia-Martin, M. L. (2020) Magnetic Nanoparticles as MRI Contrast Agents, *Top Curr Chem (Cham).* 378, 40.

208. Hussein, W. M., Cheong, Y. S., Liu, C., Liu, G., Begum, A. A., Attallah, M. A., Moyle, P. M., Torchilin, V. P., Smith, R. & Toth, I. (2019) Peptide-based targeted polymeric nanoparticles for siRNA delivery, *Nanotechnology.* 30, 415604.

209. Radmanesh, F., Sadeghi Abandansari, H., Ghanian, M. H., Pahlavan, S., Varzideh, F., Yakhkeshi, S., Alikhani, M., Moradi, S., Braun, T. & Baharvand, H. (2021) Hydrogel-mediated delivery of microRNA-92a inhibitor polyplex nanoparticles induces localized angiogenesis, *Angiogenesis.* 24, 657-676.

210. Grabowska, M., Grzeskowiak, B. F., Szutkowski, K., Wawrzyniak, D., Glodowicz, P., Barciszewski, J., Jurga, S., Rolle, K. & Mrowczynski, R. (2019) Nano-mediated delivery of double-stranded RNA for gene therapy of glioblastoma multiforme, *PLoS One.* 14, e0213852.

211. Cho, E. C., Glaus, C., Chen, J., Welch, M. J. & Xia, Y. (2010) Inorganic nanoparticle-based contrast agents for molecular imaging, *Trends Mol Med.* 16, 561-73.

212. Sui, H., Zhou, M., Chen, Q., Lane, H. C. & Imamichi, T. (2014) siRNA enhances DNA-mediated interferon lambda-1 response through crosstalk between RIG-I and IFI16 signalling pathway, *Nucleic Acids Res.* 42, 583-98.

213. Mainini, F. & Eccles, M. R. (2020) Lipid and Polymer-Based Nanoparticle siRNA Delivery Systems for Cancer Therapy, *Molecules.* 25.

214. Shi, B., Zhang, H., Shen, Z., Bi, J. & Dai, S. (2013) Developing a chitosan supported imidazole Schiff-base for high-efficiency gene delivery, *Polymer Chemistry.* 4, 840-850.

215. Hu, F. Q., Zhao, M. D., Yuan, H., You, J., Du, Y. Z. & Zeng, S. (2006) A novel chitosan oligosaccharide-stearic acid micelles for gene delivery: properties and in vitro transfection studies, *Int J Pharm.* 315, 158-66.

216. Chen, H., Liu, X., Dou, Y., He, B., Liu, L., Wei, Z., Li, J., Wang, C., Mao, C., Zhang, J. & Wang, G. (2013) A pH-responsive cyclodextrin-based hybrid nanosystem as a nonviral vector for gene delivery, *Biomaterials.* 34, 4159-4172.

217. Sambuy, Y., De Angelis, I., Ranaldi, G., Scarino, M. L., Stammati, A. & Zucco, F. (2005) The Caco-2 cell line as a model of the intestinal barrier: influence of cell and culture-related factors on Caco-2 cell functional characteristics, *Cell Biol Toxicol.* 21, 1-26.

218. O'Driscoll, L., Gammell, P., McKiernan, E., Ryan, E., Jeppesen, P. B., Rani, S. & Clynes, M. (2006) Phenotypic and global gene expression profile changes between low passage and high passage MIN-6 cells, *J Endocrinol.* 191, 665-76.

219. Nishio, T., Kawaguchi, S., Yamamoto, M., Iseda, T., Kawasaki, T. & Hase, T. (2005) Tenascin-C regulates proliferation and migration of cultured astrocytes in a scratch wound assay, *Neuroscience.* 132, 87-102.

220. Yalcin, F., Dzaye, O. & Xia, S. (2020) Tenascin-C Function in Glioma: Immunomodulation and Beyond, *Adv Exp Med Biol.* 1272, 149-172.

221. Wawrzyniak, D., Grabowska, M., Glodowicz, P., Kuczynski, K., Kuczynska, B., Fedoruk-Wyszomirska, A. & Rolle, K. (2020) Down-regulation of tenascin-C inhibits breast cancer cells development by cell growth, migration, and adhesion impairment, *PLoS One.* 15, e0237889.

222. Zhao, L., Zhong, Z., Zhuang, D., Jiang, Y., Zou, P., Wang, Y. & Zhang, Z. (2020) Evidence of virus-responsive pathways in response to poly I: C challenge in a muscle cell line derived from large yellow croaker Larimichthys crocea, *Fish Shellfish Immunol.* 100, 179-185.

223. Derynck, R. & Weinberg, R. A. (2019) EMT and Cancer: More Than Meets the Eye, *Dev Cell.* 49, 313-316.

10. ZAŁĄCZNIKI

1. Oświadczenia o wkładzie kandydata w prace naukowe wchodzące w skład rozprawy doktorskiej

2. Publikacje:

   a) Grabowska M*, Kuczyński K*, Piwecka M, Rabiasz A, Zemła J, Głodowicz P, Wawrzyniak D, Lekka M, Rolle K. miR-218 affects the ECM composition and cell biomechanical properties of glioblastoma cells. Journal of Cellular and Molecular Medicine. 00:1-18.

   b) Grabowska M, Misiorek JO, Zarębska Ż, Rolle K. Applications of noncoding RNAs in brain cancer patients. Clinical applications of noncoding RNAs in cancer. Elsevier. 2022. 2:17-64.

   c) Grabowska M, Grześkowiak BF, Rolle K, Mrówczyński R. Magnetic Nanoparticles as a Carrier of dsRNA for Gene Therapy. Methods in Molecular Biology. Springer. 2021. 2211:69-81.

   d) Wawrzyniak D, Grabowska M, Głodowicz P, Kuczyński K, Kuczyńska B, Fedoruk-Wyszomirska A, Rolle K. Down-regulation of tenascin-C inhibits breast cancer cells development by cell growth, migration, and adhesion impairment. PLoS One. 2020. 15(8):e0237889.

   e) Grabowska M, Grześkowiak BF, Szutkowski K, Wawrzyniak D, Głodowicz P, Barciszewski J, Jurga S, Rolle K, Mrówczyński R. Nano-mediated delivery of double-stranded RNA for gene therapy of glioblastoma multiforme. PLoS One. 2019. 14(3):e0213852.

Oświadczenia o wkładzie
kandydata w prace naukowe
wchodzące w skład
rozprawy doktorskiej

Mgr Małgorzata Grabowska   21.05.2022

Zakład Neuroonkologii Molekularnej

Instytut Chemii Bioorganicznej PAN

OŚWIADCZENIE KANDYDATA O WKŁADZIE WŁASNYM W PRACE NAUKOWE WCHODZĄCE W SKŁAD ROZPRAWY DOKTORSKIEJ

Tytuł artykułu naukowego: MiR-218 affects the ECM composition and cell biomechanical properties of glioblastoma cells

Autorzy: Małgorzata Grabowska*, Konrad Kuczyński*, Monika Piwecka, Alicja Rabiasz, Joanna Zemła, Paweł Głodowicz, Dariusz Wawrzyniak, Małgorzata Lekka, Katarzyna Rolle

Czasopismo: Journal of Cellular and Molecular Medicine

Data opublikowania: czerwiec 2022

Oświadczam, że mój wkład w powstanie wyżej wymienionej pracy naukowej obejmuje:

- zgromadzenie i analizę stosownej literatury,
- znaczny udział w pisaniu manuskryptu, opisanie: wstępu teoretycznego, metodyki, wyników i części ich dyskusji,
- przygotowanie części figur,
- analizę statystyczną danych eksperymentalnych,
- prowadzenie hodowli komórkowej oraz wprowadzanie do komórek badanej cząsteczki na drodze transfekcji,
- wykonanie analiz poziomu ekspresji białek metodą Western blot w liniach komórkowych glejaka nietraktowanych jak i traktowanych syntetycznym miRNA-218,
- wykonanie analiz poziomu ekspresji genów metodą real-time PCR w tkankach GBM pochodzących od pacjentów,
- wykonanie testów *in vitro* migracji, proliferacji oraz adhezji w czasie rzeczywistym z zastosowaniem systemu xCELLigence,
- wykonanie analizy migracji komórkowej testem zabliźniania rany,
- wykonanie analizy proliferacji komórek glejaka metodą inkorporacji znakowanej radioaktywnie tymidyny.

Tytuł rozdziału: Applications of noncoding RNAs in brain cancer patients

Autorzy: Małgorzata Grabowska, Julia O. Misiorek, Żaneta Zarębska, Katarzyna Rolle

Seria wydawnicza: Clinical Applications of Noncoding RNAs in Cancer

Data opublikowania: styczeń 2022

Oświadczam, że mój wkład w powstanie wyżej wymienionej pracy naukowej obejmuje:

- zgromadzenie i analizę stosownej literatury,
- znaczny udział w pisaniu manuskryptu, opisanie: nowotworów mózgu i ich modeli badawczych, eksperymentalnych metod badania interakcji pomiędzy ncRNA a mRNA i białkami, zawartych we wszystkich podrozdziałach informacji dotyczących miRNA, przygotowanie podrozdziału dotyczącego wpływu ncRNA na skuteczność chemio- i radioterapii,
- sprawowanie kontroli edytorskiej nad ostateczną formą manuskryptu.

Tytuł rozdziału: Magnetic Nanoparticles as a Carrier of dsRNA for Gene Therapy

Autorzy: Małgorzata Grabowska, Bartosz F. Grześkowiak, Katarzyna Rolle, Radosław Mrówczyński

Seria wydawnicza: Methods in Molecular Biology

Data opublikowania: luty 2021

Oświadczam, że mój wkład w powstanie wyżej wymienionej pracy naukowej obejmuje:

- znaczny udział w pisaniu manuskryptu, opisanie biologicznej części protokołu,
- sprawowanie kontroli edytorskiej nad ostateczną formą manuskryptu.

Tytuł artykułu naukowego: Down-regulation of tenascin-C inhibits breast cancer cells development by cell growth, migration, and adhesion impairment

Autorzy: Dariusz Wawrzyniak, Małgorzata Grabowska, Paweł Głodowicz P. ,Konrad Kuczyński, Bogna Kuczyńska, Agnieszka Fedoruk-Wyszomirska, Katarzyna Rolle

Czasopismo: PLoS One.

Data opublikowania: sierpień 2020

Oświadczam, że mój wkład w powstanie wyżej wymienionej pracy naukowej obejmuje:

- prowadzenie hodowli komórkowej oraz wprowadzanie do komórek badanej cząsteczki na drodze transfekcji,
- syntezę dsRNA na drodze transkrypcji *in vitro*,
- wykonanie analiz poziomu ekspresji białek metodą Western blot w liniach komórkowych glejaka traktowanych ATN-RNA,
- wykonanie testów *in vitro* migracji, proliferacji oraz adhezji w czasie rzeczywistym z zastosowaniem systemu xCELLigence.

Tytuł artykułu naukowego: Nano-mediated delivery of double-stranded RNA for gene therapy of glioblastoma multiforme

Autorzy: Małgorzata Grabowska, Bartosz F. Grześkowiak, Kosma Szutkowski, Dariusz Wawrzyniak, Paweł Głodowicz, Jan Barciszewski, Stefan Jurga, Katarzyna Rolle, Radosław Mrówczyński

Czasopismo: PLoS One

Data opublikowania: marzec 2019

Oświadczam, że mój wkład w powstanie wyżej wymienionej pracy naukowej obejmuje:

- zgromadzenie i analizę stosownej literatury,
- prowadzenie hodowli komórkowej oraz wprowadzanie do komórek badanej cząsteczki na drodze transfekcji,
- syntezę dsRNA na drodze transkrypcji *in vitro*,
- przygotowanie kompleksów dsRNA z nośnikiem nanocząstkowym,
- wykonanie analiz poziomu ekspresji białek metodą Western blot w liniach komórkowych glejaka traktowanych ATN-RNA,
- wykonanie testów *in vitro* migracji oraz proliferacji w czasie rzeczywistym z zastosowaniem systemu xCELLigence,
- wykonanie analizy migracji komórkowej testem zabliźniania rany.

Małgorzata Grabowska

....
podpis kandydata

Dr hab. Katarzyna Rolle, prof. ICHB PAN   21.05.2022

Zakład Neuroonkologii Molekularnej

Instytut Chemii Bioorganicznej PAN

OŚWIADCZENIE AUTORA KORESPONDENCYJNEGO O WKŁADZIE KANDYDATA W PRACE NAUKOWE WCHODZĄCE W SKŁAD ROZPRAWY DOKTORSKIEJ

Tytuł artykułu naukowego: MiR-218 affects the ECM composition and cell biomechanical properties of glioblastoma cells

Autorzy: Małgorzata Grabowska*, Konrad Kuczyński*, Monika Piwecka, Alicja Rabiasz, Joanna Zemła, Paweł Głodowicz, Dariusz Wawrzyniak, Małgorzata Lekka, Katarzyna Rolle

Czasopismo: Journal of Cellular and Molecular Medicine

Data opublikowania: czerwiec 2022

Oświadczam, że wkład mgr Małgorzaty Grabowskiej w powstanie wyżej wymienionej pracy naukowej obejmuje:

- zgromadzenie i analizę stosownej literatury,
- znaczny udział w pisaniu manuskryptu, opisanie: wstępu teoretycznego, metodyki, wyników i części ich dyskusji,
- przygotowanie większości figur,
- analizę statystyczną danych eksperymentalnych,
- prowadzenie hodowli komórkowej oraz wprowadzanie do komórek badanej cząsteczki na drodze transfekcji,
- wykonanie analiz poziomu ekspresji białek metodą Western blot w liniach komórkowych glejaka nietraktowanych jak i traktowanych syntetycznym miRNA-218,
- wykonanie analiz poziomu ekspresji genów metodą real-time PCR w tkankach GBM pochodzących od pacjentów,

- wykonanie testów *in vitro* migracji, proliferacji oraz adhezji w czasie rzeczywistym z zastosowaniem systemu xCELLigence,
- wykonanie analizy migracji komórkowej testem zabliźniania rany,
- wykonanie analizy proliferacji komórek glejaka metodą inkorporacji znakowanej radioaktywnie tymidyny.

Tytuł rozdziału: Applications of noncoding RNAs in brain cancer patients
Autorzy: Małgorzata Grabowska, Julia O. Misiorek, Żaneta Zarębska, Katarzyna Rolle
Seria wydawnicza: Clinical Applications of Noncoding RNAs in Cancer
Data opublikowania: styczeń 2022

Oświadczam, że wkład mgr Małgorzaty Grabowskiej w powstanie wyżej wymienionej pracy naukowej obejmuje:

- zgromadzenie i analizę stosownej literatury,
- znaczny udział w pisaniu manuskryptu, opisanie: nowotworów mózgu i ich modeli badawczych, eksperymentalnych metod badania interakcji pomiędzy ncRNA a mRNA i białkami, zawartych we wszystkich podrozdziałach informacji dotyczących miRNA, przygotowanie podrozdziału dotyczącego wpływu ncRNA na skuteczność chemio- i radioterapii,
- sprawowanie kontroli edytorskiej nad ostateczną formą manuskryptu.

Tytuł artykułu naukowego: Down-regulation of tenascin-C inhibits breast cancer cells development by cell growth, migration, and adhesion impairment
Autorzy: Dariusz Wawrzyniak, Małgorzata Grabowska, Paweł Głodowicz P, Konrad Kuczyński, Bogna Kuczyńska, Agnieszka Fedoruk-Wyszomirska, Katarzyna Rolle
Czasopismo: PLoS One.
Data opublikowania: sierpień 2020

Oświadczam, że wkład mgr Małgorzaty Grabowskiej w powstanie wyżej wymienionej pracy naukowej obejmuje:

- prowadzenie hodowli komórkowej oraz wprowadzanie do komórek badanej cząsteczki na drodze transfekcji,
- syntezę dsRNA metodą transkrypcji *in vitro*,
- przygotowanie kompleksów dsRNA z nośnikiem nanocząstkowym,
- wykonanie analiz poziomu ekspresji białek metodą Western blot w liniach komórkowych glejaka traktowanych ATN-RNA,
- wykonanie testów *in vitro* migracji oraz proliferacji w czasie rzeczywistym z zastosowaniem systemu xCELLigence,
- wykonanie analizy migracji komórkowej testem zabliźniania rany.

....

podpis autora korespondencyjnego

Dr hab. Radosław Mrówczyński, prof. UAM

Wydział Chemii

Uniwersytet im. Adama Mickiewicza w Poznaniu

21.05.2022

OŚWIADCZENIE AUTORA KORESPONDENCYJNEGO O WKŁADZIE KANDYDATA W PRACE NAUKOWE WCHODZĄCE W SKŁAD ROZPRAWY DOKTORSKIEJ

Tytuł rozdziału: Magnetic Nanoparticles as a Carrier of dsRNA for Gene Therapy

Autorzy: Małgorzata Grabowska, Bartosz F. Grześkowiak, Katarzyna Rolle, Radosław Mrówczyński

Seria wydawnicza: Methods in Molecular Biology

Data opublikowania: luty 2021

Oświadczam, że wkład mgr Małgorzaty Grabowskiej w powstanie wyżej wymienionej pracy naukowej obejmuje:

- znaczny udział w pisaniu manuskryptu, opisanie biologicznej części protokołu,
- sprawowanie kontroli edytorskiej nad ostateczną formą manuskryptu.

Tytuł artykułu naukowego: Nano-mediated delivery of double-stranded RNA for gene therapy of glioblastoma multiforme

Autorzy: Małgorzata Grabowska, Bartosz F. Grześkowiak, Kosma Szutkowski, Dariusz Wawrzyniak, Paweł Głodowicz, Jan Barciszewski, Stefan Jurga, Katarzyna Rolle, Radosław Mrówczyński

Czasopismo: PLoS One

Data opublikowania: marzec 2019

Oświadczam, że wkład mgr Małgorzaty Grabowskiej w powstanie wyżej wymienionej pracy naukowej obejmuje:

- zgromadzenie i analizę stosownej literatury,

- prowadzenie hodowli komórkowej oraz wprowadzanie do komórek badanej cząsteczki na drodze transfekcji,
- syntezę dsRNA metodą transkrypcji *in vitro*,
- przygotowanie kompleksów dsRNA z nośnikiem nanocząstkowym,
- wykonanie analiz poziomu ekspresji białek metodą Western blot w liniach komórkowych glejaka traktowanych ATN-RNA,
- wykonanie testów *in vitro* migracji oraz proliferacji w czasie rzeczywistym z zastosowaniem systemu xCELLigence,
- wykonanie analizy migracji komórkowej testem zabliźniania rany.

podpis autora korespondencyjnego

Grabowska M*, Kuczyński K*, Piwecka M, Rabiasz A,
Zemła J, Głodowicz P, Wawrzyniak D, Lekka M,
Rolle K.

miR-218 affects the ECM composition and cell biomechanical properties of glioblastoma cells

ORIGINAL ARTICLE

WILEY

miR-218 affects the ECM composition and cell biomechanical properties of glioblastoma cells

Małgorzata Grabowska[1] | Konrad Kuczyński[1,2] | Monika Piwecka[1] | Alicja Rabiasz[3] |
Joanna Zemła[4] | Paweł Głodowicz[1] | Dariusz Wawrzyniak[1] | Małgorzata Lekka[4] |
Katarzyna Rolle[1]

[1]Institute of Bioorganic Chemistry, Polish Academy of Sciences, Poznań, Poland

[2]NanoBioMedical Centre, Adam Mickiewicz University, Poznań, Poland

[3]Institute of Human Genetics, Polish Academy of Sciences, Poznań, Poland

[4]Institute of Nuclear Physics, Polish Academy of Sciences, Kraków, Poland

Correspondence
Katarzyna Rolle, Department of Molecular Neurooncology, Institute of Bioorganic Chemistry of the Polish Academy of Sciences, Noskowskiego 12/14, 61-704 Poznan, Poland.
Email: kbug@ibch.poznan.pl

Abstract

Glioblastoma (GBM) is the most common malignant brain tumour. GBM cells have the ability to infiltrate into the surrounding brain tissue, which results in a significant decrease in the patient's survival rate. Infiltration is a consequence of the low adhesion and high migration of the tumour cells, two features being associated with the highly remodelled extracellular matrix (ECM). In this study, we report that ECM composition is partially regulated at the post-transcriptional level by miRNA. Particularly, we show that miR-218, a well-known miRNA suppressor, is involved in the direct regulation of ECM components, tenascin-C (TN-C) and syndecan-2 (SDC-2). We demonstrated that the overexpression of miR-218 reduces the mRNA and protein expression levels of TN-C and SDC-2, and subsequently influences biomechanical properties of GBM cells. Atomic force microscopy (AFM) and real-time migration analysis revealed that miR-218 overexpression impairs the migration potential and enhances the adhesive properties of cells. AFM analysis followed by F-actin staining demonstrated that the expression level of miR-218 has an impact on cell stiffness and cytoskeletal reorganization. Global gene expression analysis showed deregulation of a number of genes involved in tumour cell motility and adhesion or ECM remodelling upon miR-218 treatment, suggesting further indirect interactions between the cells and ECM. The results demonstrated a direct impact of miR-218 reduction in GBM tumours on the qualitative ECM content, leading to changes in the rigidity of the ECM and GBM cells being conducive to increased invasiveness of GBM.

KEYWORDS
AFM, ECM, GBM, glioblastoma, miR-218, tenascin-C

---

1 | INTRODUCTION

Glioblastoma (GBM) is the most malignant astrocytic brain tumour. Despite treatment with advanced therapies, including aggressive surgical intervention, radiotherapy, and systemic chemotherapy, as well as significant advances in the field of oncology, the average survival time for GBM patients is approximately 15 months, with a 5-year survival rate of only 5%.[1,2] The main factor contributing to this poor prognosis is the ability of GBM cells to infiltrate adjacent tissues, resulting in a high rate of tumour recurrence.[3] These notable migration and invasion abilities could be explained by alterations occurring in the structure of cancer cells and their surroundings, defined by mechanobiology.[4]

To promote the invasiveness, cancer cells modify not only themselves but also their environment, namely the extracellular matrix (ECM). It consists of over 300 different proteins, including proteoglycans and glycoproteins.[5] Neoplastic tissues are characterized by the phenomenon of desmoplasia, manifested by the intense formation of a dense ECM consisting of increased levels of total fibrillar collagen, fibronectin, proteoglycans and tenascin-C (TN-C).[6] The capability to synthesize specific and cancer-related ECM components has been shown to be relevant for the high invasiveness of tumour cells. The changed protein profile within ECM increases the stiffness of cancerous tissue,[7,8] which may lead to enhanced cell–ECM adhesion through the involvement of local adhesion proteins. The general trend observed for many types of cells indicates that cell spread and adhesion are improved on harder matrices.[9,10] The effect of the environment on the cells is explained by the mechanotransduction mechanism, in which mechanical and cell-specific signals are actively detected by cells and converted into intracellular biochemical signals. In this manner, the ECM can affect cancer cell behaviour, including invasion and metastasis.[11,12] Therefore, cancer should be considered as a disease with alterations in both cells and their microenvironment, including also the biochemical and biophysical properties of the ECM. Not only proteins suspended in the ECM have an impact on the invasiveness of the tumour, but also transmembrane proteins. The syndecans are a four-member family of evolutionarily conserved small type I transmembrane proteoglycans implicated in the formation of specialized membrane domains, cell adhesion, cytoskeletal organization, migration and wound healing. They have been also related to the pathological conditions, including inflammation and cancer.[13-15] For instance, elevated expression of syndecan-2 (SDC-2) has been correlated with increased invasiveness in various types of cancers, including fibrosarcoma,[16] melanoma,[17] colon,[18] pancreatic[19] and colorectal[20] cancers, while TN-C is overexpressed in brain tumours,[21] breast,[22] lung[23] and colorectal[24] cancers.

In the recent 20 years, microRNAs (miRNAs) have emerged as key regulators of gene expression at the post-transcriptional level. miRNAs are a large family of endogenous, evolutionarily conserved, non-coding RNAs that are ~22 nucleotides long, and they have been implicated in the regulation of nearly every biological process.[25] Deregulated miRNA expression has been shown to play a role in the pathogenesis of a growing list of human diseases, including cancer and cardiovascular, neurodegenerative and autoimmune disorders.[26-29] For example, in GBM, it has been already demonstrated that the downregulation of miR-218 affects cell proliferation, epithelial-to-mesenchymal transition,[30] metabolism of cancer cells[31] and cancer stem cell properties.[32] How miRNAs are involved in the regulation of ECM composition and the mechanobiology of cancer cells in GBM tumours is largely unknown. In principle, miRNAs can exert their control over the ECM either directly by targeting mRNAs encoding ECM proteins or indirectly by modulating the expression of genes involved in the synthesis or degradation of ECM molecules. Here, we have evidenced that miR-218, one of the highly downregulated miRNAs in GBM cells, is involved in the direct regulation of TN-C and SDC-2, two highly overrepresented proteins in GBM and ECM components. Both SDC-2 and TN-C have been previously demonstrated to increase tumour cell migration and invasiveness. In the course of the study, we attempted to validate how miR-218 interaction with its ECM targets affects globally a microenvironment and biomechanical properties of GBM cells; we introduced miR-218 mimic into GBM cells and measured the consequences on the migration, adhesion and stiffness properties of individual cancer cells. As demonstrated by real-time migration analysis and single-cell force spectroscopy (SCFS) measurements using contact-mode atomic force microscopy (AFM), overexpression of miR-218 had a pronounced effect on the mechanical properties of GBM cells, influencing their migration potential, adhesion and overall stiffness. Collectively, our results indicate that miR-218 is a potent tumour suppressor in glioma with a substantial impact on the ECM composition and biomechanical properties of GBM.

2 | MATERIALS AND METHODS

2.1 | Patient sample collection

The GBM samples ($n = 19$) were obtained from the Clinic of Neurosurgery and Neurotraumatology, Karol Marcinkowski University of Medical Sciences in Poznan, Poland, during 2016–2017 based on the approval from the Ethical Committee (Nr. 46/13), and individuals signed an informed consent form.

2.2 | Cell culture

Human glioblastoma cell lines U-118 MG, U-138 MG, U-251 MG and T98-G purchased from American Type Culture Collection (ATCC) were used in the study. Cells were maintained in recommended medium, Eagle's Minimal Essential Medium (EMEM, Corning) or Dulbecco's modified Eagle's medium (DMEM, ATCC) supplemented with 10% foetal bovine serum (FBS, Sigma-Aldrich) and 1% penicillin–streptomycin antibiotic (Sigma-Aldrich) and incubated at 37°C and 5% CO_2 in a humidified atmosphere in an incubator.

2.3 | Transfection

The cells were transfected with *mir*Vana™ hsa-miR-218-5p mimic (Invitrogen) in a final concentration of 10 nM and 50 nM at 70%–80% confluency. Lipofectamine™ 2000 (Invitrogen) was used as a transfection agent according to the manufacturer's protocols. A non-specific scrambled siRNA (Sigma-Aldrich) was used as a control in all transfection experiments. The cells were processed after 24 h for the quantification of transcript levels using qPCR, Western blot, cellular assays or AFM analysis.

2.4 | Luciferase reporter assay

The TargetScan (www.targetscan.org) analysis predicted the 3′UTR segments of TN-C and SDC-2 interacting with hsa-miR-218-5p. Based on them, 22-nucleotides-long fragments were designed, along with corresponding mutants, characterized by one point mutation and one codon change. As a control was used a perfect match sequence, fully complementary to the miR-218. Oligonucleotides were synthesized by Sigma-Aldrich. Fragments were then ligated with the pmirGLO Dual-Luciferase miRNA Target Expression Vector (Promega), transformed by heat shock into TOP10 *Escherichia coli* cells and multiplied. Verified by sequencing, plasmids were transfected together with *mir*Vana™ hsa-miR-218-5p mimic to the U-118 glioblastoma cell line. Luciferase activity was analysed with Dual-Glo® Luciferase Assay System (Promega) by the manufacturer's instructions using the Synergy™ HTX Multi-Mode Microplate Reader (BioTek).

2.5 | Western blots

U-118 MG cells were lysed by sonication for protein isolation in 10 nM Tris–HCl, pH = 7.5 with protease inhibitor cocktail (Sigma-Aldrich). Protein expression glyceraldehyde 3-phosphate dehydrogenase (GAPDH) level was used as an endogenous control. For TN-C, SDC-2 and GAPDH detection, 25 μg of isolated material was used. Protein was denatured, separated by SDS-PAGE (SDS-polyacrylamide gel electrophoresis) on 7,5% for TN-C and 15% gels for SDC-2 and GAPDH detection, with electric current 30 mA and wet transferred to the polyvinylidene fluoride membrane using electric current 130 mA, and blocked with 5% skimmed milk. After incubation with primary and secondary antibodies, proteins of interest were detected with Western Bright Sirius Chemiluminescent Detection Kit (Advansta). The following antibodies were used: polyclonal TN-C H-300 (dilution 1:500; Santa Cruz Biotechnology), monoclonal SDC-267088-1-Ig (dilution 1:500; Proteintech), monoclonal GAPDH 0411 (dilution 1:500; Santa Cruz Biotechnology) and anti-mouse A9044/rabbit A6154 peroxidase (dilution 1:10,000; Sigma-Aldrich). TN-C and GAPDH antibodies were diluted in 3% bovine serum albumin (BSA, Sigma-Aldrich), and others, in skimmed milk.

The intensity of individual bands was analysed quantitively by Multi Gauge ver. 2.0 (Fujifilm). The relative ratio of protein-level expression was determined based on the densitometric measurements of band intensities in relation to the control sample.

2.6 | qRT-PCR

Total RNA was isolated using the TRIzol reagent (Invitrogen) according to the manufacturer's protocol. Afterwards, RNA was purified with the DNA-free™ DNA Removal Kit (Ambion). The reverse transcription reaction was carried out with the Transcriptor High Fidelity cDNA Synthesis Kit (Roche) according to the manufacturer's protocol, using in each case 500 ng of RNA material. The reverse transcription for miRNA was performed by two-step miRNA 1st-Strand cDNA Synthesis Kit (Agilent Technologies). cDNA was used in real-time quantitative reverse transcription PCR (qRT-PCR), with the use of LightCycler®480 (Roche), in three technical replicates. Primers with corresponding probes were designed in the Universal Probe Library Assay Design Center (https://qpcr.probefinder.com/organism.jsp). Relative expression was analysed in the LightCycler®480 Software release 1.5.1.62 (Roche). The level of hypoxanthine phosphoribosyltransferase (HPRT) was used as an endogenous control for analysis of extracellular matrix proteins. In case of miR-218, the level of 18S ribosomal RNA was used for normalization. Sequences of primers 5′-3′ and list of probes were as follows: TN-C forward: GGGATTAATGTCGGAAATGGT; TN-C reverse: CCGGACCAAAACCATCAGT; TN-C probe: 76; SDC-2 forward: TTATCAGATGTCAGCTCTGCTCTC; SDC-2 reverse: GTGGATCCTGCTCACCTTG; SDC-2 probe: 49; HPRT forward: CGAGCAAGACGTTCAGTCCT; HPRT reverse: TGACCTTGATTTATTTTGCATACC; HPRT probe: 73; miR-218: TTGTGCTTGATCTAACCATGT; R18 forward: CATTCTTGGCAAATGCTTTCG; and R18 reverse: CGCCGCTAGAGGTGAAATTC. As a control, RNA from normal, healthy brains (Ambion, First Choice® Human Brain Reference RNA, Cat # 6050, whole brain pooled from 10 females and 13 men, Caucasian, age: 23–86) was used.

2.7 | PCR array of human cell motility, extracellular matrix and adhesion molecules

U-118 MG cells treated with miR218 mimic were collected for total RNA isolation with ExtractME Total RNA Kit (Blirt) according to the manufacturer's protocol. 900 ng of RNA was used in the reverse transcription procedure with RT² Easy First Strand Kit (Qiagen). cDNA mixed with the RT² SYBR Green was then evenly aliquoted onto the RT² profiler plates: Human Cell Motility, and Human Extracellular Matrix and Adhesion Molecules (Qiagen). qRT-PCRs were conducted in LightCycler®480 (Roche), and subsequently analysed by software provided online by Qiagen.

2.8 | Real-time migration

Real-time cell migration monitoring was performed in the xCELLigence® system using the RTCA DP apparatus (ACEA Biosciences). The experiment was carried out on 16-well CIM-Plates, in which culture medium enriched with FBS, served as a chemoattractant, was applied into lower part of the CIM-Plate. To the upper chamber was applied an unsupplemented medium. The first stage of the experiment served to measure the background of electrical impedance. Then, 10,000 U-118 MG cells treated with miR-218 mimic were seeded on the upper chamber of the plate. The CIM-Plate was installed in the RTCA apparatus; from that moment, for further 48 h, the system registered the level of electrical impedance every 15 min. The results of the experiment were presented in the cell index unit of the xCELLigence® system, which corresponded to the measured impedance minus the impedance of the background. The experimental curves were adjusted to the sigmoidal equation and the half-time effective migration values (effective time 50, ET 50) were calculated.

2.9 | Wound healing assay

U-118 MG cells were grown to achieve 90% of confluency on 12-well plates and then transfected with miR-218 mimic. After the medium is changed, scratches were created by scraping cells in a straight line using a 200-µl tip. From that moment on, for 72 h at 12-h intervals, pictures of the culture were taken by a Leica DMI4000 B inverted microscope with 5x magnification objective. The analysis of the degree of the individual scratch area was carried out by the Tscratch software version 1.0 (CSElab). That software is based on novel algorithm for measuring the open image area that utilizes discrete curvelet transform for separating the low-intensity open area and the high-intensity cell-covered area. Then, a grey visible mask is created for cell-free areas. The wound surface area and its change in time are calculated automatically by software.

2.10 | Real-time proliferation

The use of the xCELLigence® system enabled the observation of real-time cell proliferation. In that experiment were used the E-Plates (ACEA Biosciences), whose well bottoms are covered with gold microelectrodes. The test was started by measuring the background impedance of supplemented medium by placing them in the RTCA DP apparatus (ACEA Biosciences) and making the first measurement. Then, 10000 U-118 MG cells were seeded on the same plate and incubated for 24 h under optimal growth conditions. From that moment on, until the end of the experiment, the system performed impedance measurements at 15-min intervals. After 24 h, the cells were transfected with miR-218 mimic, and measurements were continued for the next 48 h. The results are presented by the cell index unit. The normalization time point corresponds to the moment of transfection.

2.11 | Thymidine incorporation assay

The cell culture was transfected and resumed for 20 h. Subsequently, a tritiated thymidine ([methyl-3 H]-thymidine)-labelled solution with final radioactivity of 1 µCi per well was added for another four hours. To detach the cells, they were placed for 30 min at −80°C and then thawed at 37°C. The plate was placed in the MicroBeta FilterMate-96 harvester, where the cells were transferred to the fibreglass filter paper Filtermat A (PerkinElmer) by three washes. Dried Filtermat A was placed in the plastic sample bags, and flooded with Betaplate Scint for Betaplete (PerkinElmer), then moved into the MicroBeta^2 radiometric detector (PerkinElmer), which recorded the number of radioactive pulses per minute (counts per minute, cpm). As a positive control, cells treated with camptothecin (CPT) at a final concentration of 3 µM were used.

2.12 | Real-time adhesion

The xCELLigence® system together with the E-Plates PET (ACEA Biosciences) was used. In each well of them, four rows of microelectrode sensors are removed, creating a window for cell visualization. Plates were covered with poly-L-lysine (Sigma-Aldrich), incubated for one hour in 37°C and rinsed with phosphate-buffered saline (PBS, VWR Life Science). Additionally, some wells were overlaid with 1% BSA for 20 min and acted as a negative control. An unsupplemented medium was analysed as a background. Then, 24 h earlier transfected cells were seeded 10,000 cells per well in serum-free medium. Measurements took place every three minutes for four hours.

2.13 | Single-cell force spectroscopy (SCFS)

Cell deformability and adhesiveness were determined from the AFM measurements carried out in single-cell force spectroscopy (SCFS) mode using CellHesion head (JPK Instruments). In SCFS, adhesion was quantified as a work of adhesion determined as an area under the part of the force curve corresponded to force/work needed to detach a single cell from surface. To prepare a cell force probe, the standard tipless cantilevers (Arrow-TL, NanoWorld) characterized by nominal spring constant of 0.06 N/m were used. The average spring constant was 0.067 ± 0.016 N/m, as verified by the Sader method.[33] First, bare cantilevers were cleaned and activated with an oxygen plasma for 2 min at the maximum power of 100 W (Diener Electronic GmbH, Zepto 1 device). Afterwards, cantilevers were immersed in 2 mg/ml concanavalin A (Con A, Sigma-Aldrich) solution in PBS buffer (Sigma-Aldrich) for 1 h and washed three times in PBS buffer. To use an individual cell as a force probe, the trypsinized solution of transfected cells was added to Petri dish (diameter 3.5 cm, Sarstedt) filled with DMEM with FBS, in which SCFS measurements were performed. Then, Con A-functionalized cantilever was placed above a single cell and moved closer to its surface, followed by pressing it for

about 5 s with the force of 5 nN. Afterwards, a slow cantilever withdrawing was applied until the cell fully detached from the surface. After 15–20 min of a pause time, the cell was usually attached to the cantilever surface. From this moment, the cell was used as a probe to collect force curves. For a single force probe, on average 5 force maps (scan size of 20 μm × 20 μm, on which a grid 6 pixels × 6 pixels was set) were recorded in randomly chosen locations on Petri dish surface. For a given sample type, 8–9 living cell force probes were used. For each sample type, on average 1800 individual force curves were recorded and analysed. The approach and retract speeds were kept at 8 μm/s. The measurement depth was 200 nm. As tipless cantilevers were used and the cell diameter was lower than the width of the cantilever, we treated our system like a single cell in between two fixed and compressive plates. Thus, from the approach part of the force curve, cell stiffness (N/m) was determined from a slope of the approach curve after contact with a cell surface (a linear regression was applied). Cell stiffness is calculated as a slope taking into account the range from the contact point to the maximum load force (maximum cantilever deflection). In parallel, from the retract part of the force curve, work of adhesion was calculated as an area under this part of force curves corresponding to adhesion using the methodology described elsewhere.[34,35]

2.14 | Cytoskeleton imaging

For structural cytoskeleton analysis, U-118 MG cells were cultured on microscope coverslips and transfected under standard conditions as described previously. 24 h post-transfection, cells were fixed with the use of Image-iT™ Fixation/Permeabilization Kit (Invitrogen) according to the manufacturer's protocol. F-actin fibres were visualized by phalloidin conjugated to tetramethylrhodamine (Invitrogen) with simultaneous use of DAPI (Sigma-Aldrich) to visualize cell nuclei. Staining was performed according to the manufacturer's protocol. Pictures were obtained with the use of Leica TCS SP5 confocal microscope and software LAS X SP8 (Leica).

2.15 | Gene expression analysis based on the Gliovis database

TN-C and SDC-2 gene expression analysis for large groups of patients was performed using the Gliovis online tool (gliovis.bioinfo.cnio.es). In order to comprehensively present the expression of these genes in large group of tissues, databases from two independent projects (TCGA and Rembrandt) were used. Data set HG-U133A contained information from 10 non-tumour samples and 528 samples described as GBM. The Agilent-4502A data set contained the same number of healthy samples and 489 samples of glioblastoma. The Rembrandt database, on the contrary, has a set of 28 healthy samples, 225 described as non-tumour glioma and 219 GBM samples. Only the "non-tumour" and "GBM" data sets were used from the Rembrandt database.

2.16 | Statistical analysis

The results are presented as a mean value ± standard deviation (SD). They were averaged depending on the applied methods. For AFM measurements, averaging was performed for 8–9 cell force probes. For other experiments, 3 biological replicates were applied. The statistical significance of the obtained results was evaluated using the Open Office Calc ver. 4.1.1 (Apache) and GraphPad Prism ver. 5.1 (GraphPad Software). Differences between the mean values of the test and the control samples were evaluated using ANOVA variance extended by the Tukey or the Bonferroni post hoc tests. Statistically significant results were assigned as: * for $p < .05$; ** for $p < .01$; and *** for $p < .001$; no statistical significance was found for $p \geq .05$.

3 | RESULTS

3.1 | In glioblastoma, the expression level of miR-218 correlates inversely with the expression levels of the ECM components TN-C and SDC-2

Our previous study revealed that there were 97 miRNAs differentially expressed in glioblastoma compared with those in the healthy brain.[36] Forty-one of these miRNAs showed a reduced expression level in malignant gliomas. Among these miRNAs, we found miR-218 to be significantly downregulated in brain tumour tissues. We further confirmed the expression level of miR-218 in primary and recurrent GBM via qRT-PCR analysis (Figure 1A). The levels of miR-218 expression in primary tumour tissue and recurrent GBM tissue were 56% and 69% lower, respectively, than those in healthy brain tissue.

Given the profound downregulation of miR-218 in GBM, we sought to investigate its putative targets. To identify the binding sites in the 3′UTRs of genes that can be potentially regulated by selected miRNAs, we used prediction software such as ENCORI, miRDB, PicTar and TargetScan. Interestingly, among the predicted targets, we found several genes encoding ECM proteins, such as tenascin-C (TN-C), syndecan-2 (SDC-2), attractin (ATRN), cadherin-2 (CDH-2), cadherin-8 (CDH-8), extracellular leucine-rich repeat and fibronectin type III domain containing 2 (ELFN2), fibronectin leucine-rich transmembrane protein 2 (FLRT2), hyaluronan and proteoglycan link protein 1 (HAPLN1), 5-hydroxytryptamine receptor 7 (HTR7), neurocan (NCAN), proteoglycan (PRG4), reelin (RELN) and sarcoglycan zeta (SGCZ) (Supplementary information 1).

3.2 | TN-C and SDC-2 are direct targets of miR-218

Highly ranked binding targets of miR-218 were subjected to further analysis. We focused specifically on TN-C and SDC-2 and investigated their gene expression levels via qRT-PCR. The tenascin-C level was significantly increased in all examined tumour samples—that is eightfold higher in primary tumour tissue and 21-fold higher in recurrent tumour tissue than in healthy
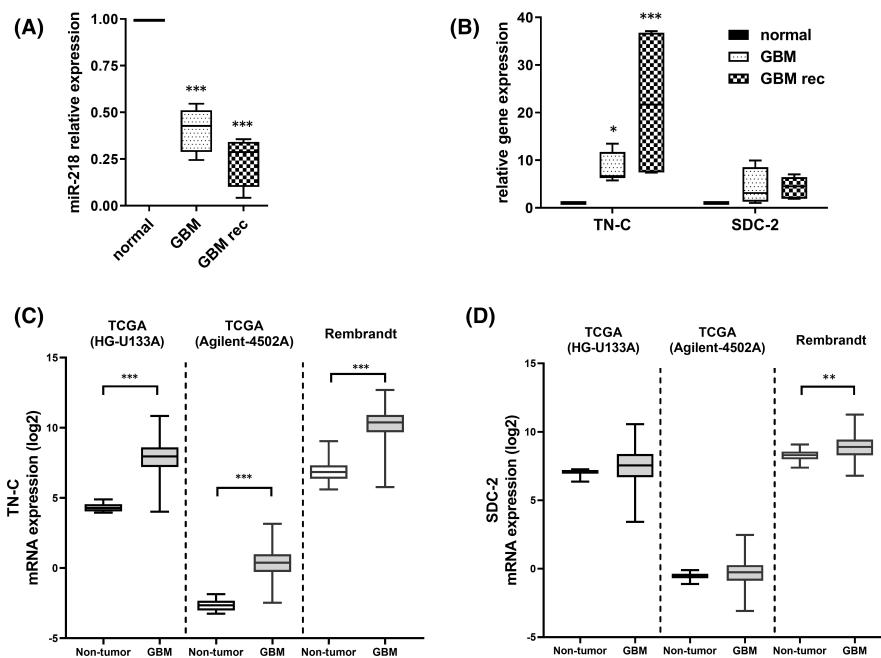
FIGURE 1   miR-218 expression in primary (GBM) and recurrent glioblastoma (GBM rec) tissues and its putative target mRNAs. (A) qRT-PCR analysis of GBM ($n = 10$) and GBM rec samples ($n = 9$) in comparison with a healthy brain RNA sample ($n = 1$). Healthy brain sample consists of RNA pooled from 23 donors. Data are shown as the mean±SD values. One-way ANOVA and the post hoc Bonferroni test, ***$p < .001$. (B) qRT-PCR analysis of the tenascin-C and syndecan-2 mRNA expression levels in GBM and GBM rec tissues in comparison with RNA from healthy brain RNA sample ($n = 1$). Healthy brain sample consists of RNA pooled from 23 people Data are shown as the mean±SD values. Mixed-model analysis and the post hoc Bonferroni test; *$p < .05$ and ***$p < .001$. (C,D) Expression of TN-C and SDC-2 in GBM tumour from TCGA and Rembrandt databases examined using the Gliovis database. Tukey's test, ***$p < .001$ and **$p < .01$

brain tissue. In the case of SDC-2, our analysis indicated an increase of approximately fourfold in GBM (Figure 1B). Our qPCR analysis is additionally supported by the data from large data sets coming from the sequencing of glioblastoma multiforme deposited in TCGA and Rembrandt databases. The expression profile of TN-C and SDC-2 in our experiment is comparable to the expression profile of aforementioned genes in databases (Figure 1C,D). There is a definite difference in TN-C expression levels between normal and tumorous tissue based on the database analysis, what is fully in line with our research and databases. Analogously, the results of our research and the values obtained from databases indicate a statistically significant distinction in the level of TN-C expression between normal tissue and GBM. In the case of SDC-2, differences with a statistical value were observed only in the Rembrandt database.

All algorithms used for miR-218 target prediction showed one binding site within the 3′UTR of both the TN-C and SDC-2 mRNAs. We employed a set of reporter constructs in a luciferase assay to experimentally verify the predicted binding of miR-218 to its target sites within the 3′UTRs of TN-C and SDC-2. The following constructs were tested in parallel: wild-type reporters (WT) containing a single native binding site for either miR-218, constructs with mutations (MUT) disrupting the 5′ seed site (negative controls) and constructs with perfect complementarity (PM) to the miR-218 binding site (positive controls) (Figure 2A). Considering our previous analysis revealing the inverse correlation between miR-218, TN-C and SDC-2

expression, we validated the predicted miRNA–mRNA interactions using a miRNA overexpression system. Specifically, U-118 MG cells were co-transfected with reporter constructs and miRNA-encoding plasmids. Co-transfection experiments showed that cells transfected with miR-218 had significantly inhibited luciferase activity compared to cells transfected with negative control (MUT) miRNA (Figure 2B). The reduction in luciferase activity was reproducible and statistically significant for both WT constructs, with suppression of 33% and 74% for TN-C and SDC-2, respectively. miR-218 did not inhibit the luciferase activity of reporter vectors containing the TN-C and SDC-2 3′UTRs with mutations in the putative miR-218 binding site. This study provides evidence of the direct binding of miR-218 to the TN-C and SDC-2 3′UTRs and positively validates this miRNA as a negative regulator of these ECM molecules.

3.3 | miR-218 regulates TN-C and SDC-2 protein levels

We sought to determine the role of miR-218 in the regulation of TN-C and SDC-2 at the protein level in GBM cells by a gain-of-function approach. We transfected U-118 MG cells with synthetic miRNA (miRNA mimic) at concentrations of 10 and 50 nM. The final miR-218 mimic concentration of 10 nM boosted the expression of miR-218 by almost 500-fold compared with the control level, while 50 nM increased the expression by more than 5000-fold (Figure 2C).
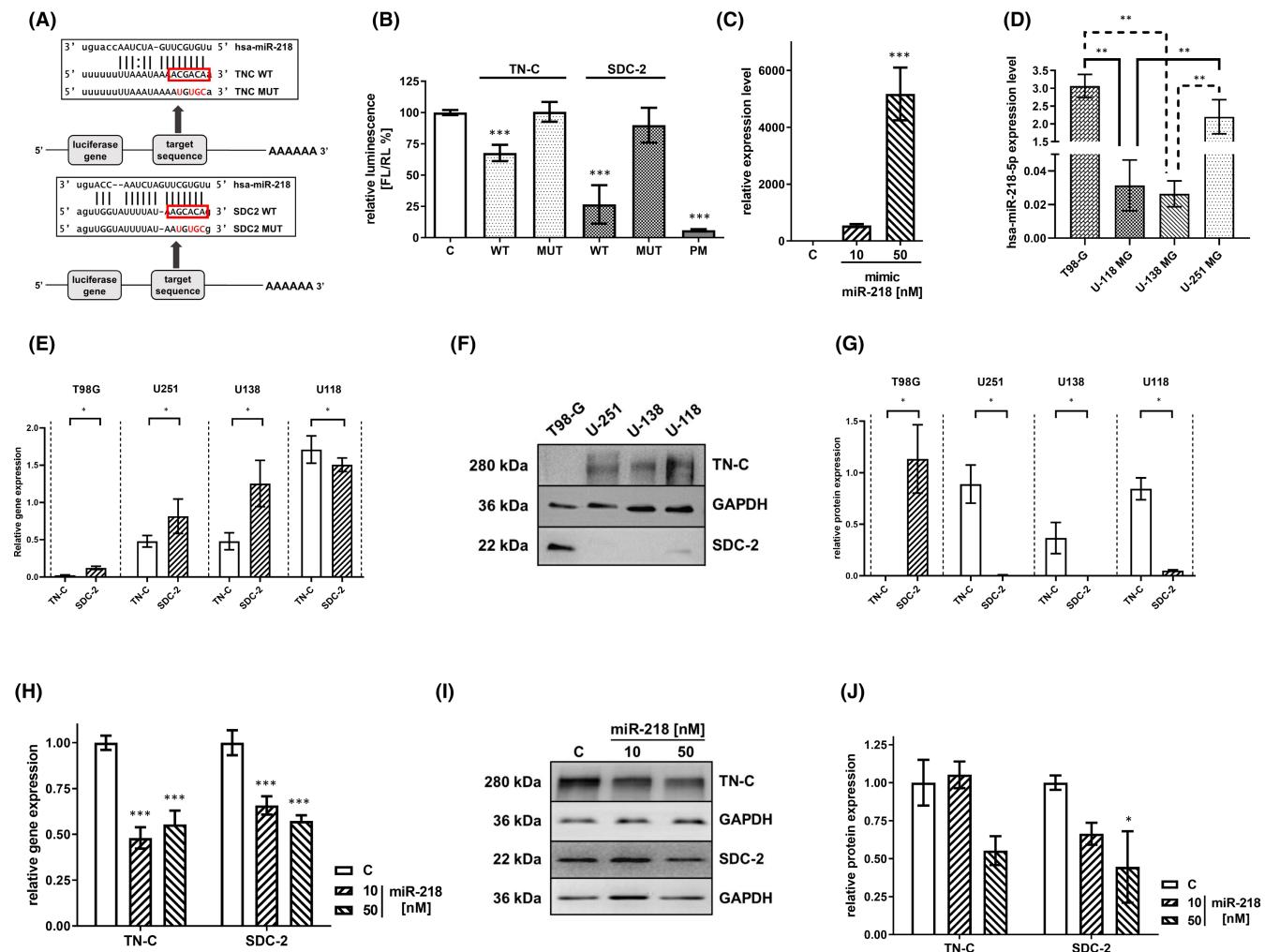
FIGURE 2 Regulation of TN-C and SDC-2 by miR-218. (A) Schematic representation of the interaction between miR-218 and 3′UTRs of its targets. The seed region is enclosed in a red box. The putative conserved sequences in the SDC-2 and TN-C targets are denoted as the wild type (WT). The non-conserved nucleotides within the seed region of the mutant 3′UTRs are marked in red in the construct named "mutant" (MUT). (B) Relative repression of luciferase expression. Reporter constructs carrying a single binding site were tested. miR-218 activity in 5 constructs was measured in parallel (Control U-118 MG cells—C, WT, MUT and perfect match—PT as a positive control in the experiment). Data are shown as the mean ± SD values. ***$p < .001$. (C) Overexpression of miR-218 as a result of miR-218 mimic transfection, as evaluated by qRT-PCR. The measured expression level of TN-C and SDC-2 in different glioma cell lines with the use of qRT-PCR. (D) Expression level of miR-218 in T98-G, U-118 MG, U-138 MG and U-251 MG cell lines. Data are shown as the mean ± SD values. **$p < .01$ (E) and Western blot (F,G). All cell lines were cultured in corresponding cell culture media in the same period of time, and materials for analysis were isolated in the same batch to avoid unnecessary variability. (H) The quantified effects of transfection of U-118 MG cells with the miR-218 mimic at 10 nM and 50 nM concentrations on mRNA levels, as measured by qRT-PCR, and on protein levels, as established by Western blot analysis (I,J). Cells transfected with scrambled siRNA were used as the control—(C). Data are shown as the mean ± SD values. Two-way ANOVA and the post hoc Bonferroni test, *$p < .05$ and ***$p < .001$

In order to select an appropriate research model, we evaluated expression levels of miR-218, TN-C and SDC-2 in four glioblastoma cell lines: T98-G, U-118 MG, U-138 MG and U-251 MG. The U-118 MG and U-138 MG lines represented the lowest miR-218 expression level, with no statistical differences between them (Figure 2D). TN-C was the most expressed on both mRNA and protein levels in U-118 MG cell line, while in T98-G, it was undetectable (Figure 2E). SDC-2 in Western blot analysis was under detection level for U-138 MG and U-251 MG cell lines. qRT-PCR revealed the highest expression of SDC-2 in U-118 MG in relation to other cell lines. We found contradictory results between the levels of SDC-2 mRNA and protein

in T98-G (Figure 2F,G). Summarizing our analyses, we selected the U-118 MG line for further research, taking into account its low expression level of miR-218, high level of TN-C and possible detection of SDC-2.

To further verify the function of miR-218 and its impact on TN-C and SDC-2 expression levels, we performed analyses at both the mRNA and protein levels by qRT-PCR and Western blot, respectively. At the mRNA level, transfection with the miR-218 mimic in two concentrations, 10 nM and 50 nM, resulted in a reduction in the tenascin-C expression level of 45%–52% in comparison with the control level. In the case of syndecan-2, we observed a decrease of

34% for 10 nM and 43% for 50 nM of mimic miR-218 (Figure 2H). Western blot analysis revealed downregulation of SDC2-2 expression by 34–55%. For TN-C, protein level after miR-218 mimic 10 nM supplementation increased by 5% and decreased by 45% after miR-218 mimic 50 nM transfection (Figure 2I,J).

3.4 | miR-218 affects the ECM composition

Given the above results, we have evaluated the miR-218 overexpression on the ECM composition. To test this hypothesis, we used a Human Cell Motility and Extracellular Matrix & Adhesion Molecules RT^2 Profiler PCR Array and profiled the expression of $n = 160$ genes related to the motility and adhesion pathways (Figure 3). More than 95% of the transcripts were detected, but the expression of CDH1, ANOS1, CNTN1 and MMP8 was not detected by this technique in our analysis (data not shown). Quality control parameters (positive PCR controls and reverse transcription controls) showed good reproducibility and efficiency with the web-based RT^2 profiler PCR Array Data Analysis program. In this paper, we include results where p-value is lower than .05 and fold change value is in the range $(\infty, -1) \cup (1, \infty)$. A full set of data obtained from RT^2 profiler plates is included in supplementary materials (Supplementary information 2). Thus, we identified 47 genes displaying significantly different expression as a result of miR-218 overexpression (Supplementary information 3). It became evident that miR-218 overexpression led mostly to decrease in the expression of genes, among which were tenascin-C, as its direct ECM target, as well as the other genes involved in cytoskeletal reorganization. We observed the 1,96-fold reduction in the TN-C expression level. This result is in line with our real-time PCR analyses described above, in which we obtain also almost twofold reduction in TN-C expression level after miR-218 mimic 50 nM transfection. We further hypothesized that changes in the ECM composition due to miR-218 overexpression also affect the mechanobiological properties of cancer cells.

3.5 | Impaired cell migration after miR-218 treatment

To explore the impact of miR-218 on cell migration, we compared the migration rate of miR-218-transfected U-118 MG cells with that of non-treated (negative control) cells (Figure 4A). The mathematical interpretation of the impedance (CI value) for each experimental condition was recorded over time and fitted to a four-parameter logistic non-linear regression model (Figure 4B). Transfection of 10 and 50 nM miR-218 increased the ET$_{50}$ by an average of 4 and 4.7 h, respectively.

As the second independent experiment, we carried out a wound healing assay. 48 h after transfection, the largest unhealed area was observed in the miR-218 50 nM sample and accounted for 25.2% of the original wound area, while in the control sample, it was 0.8% (Figure 4C,D). At a concentration of 10 nM, the unhealed area was
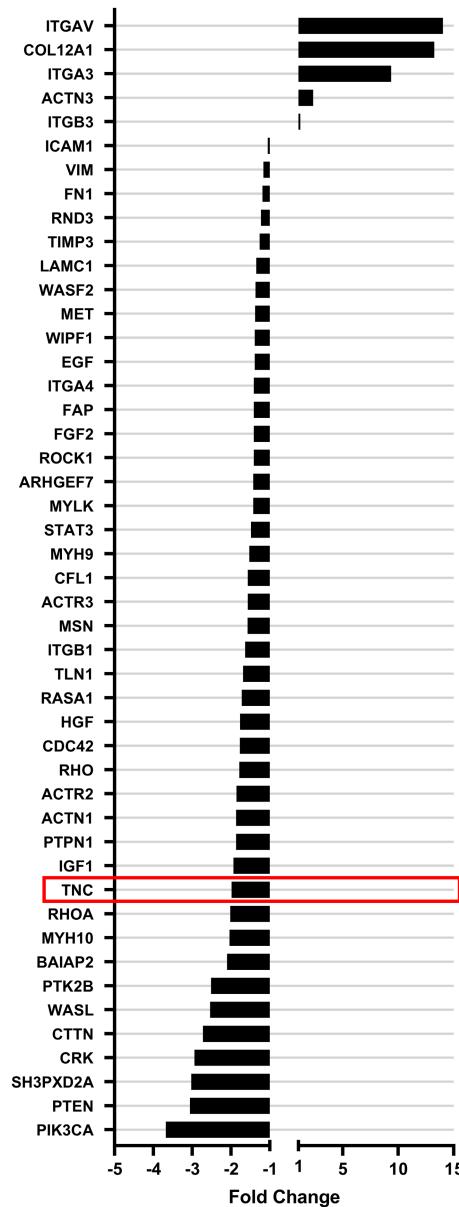

FIGURE 3 Cluster analysis of mRNAs encoding ECM components that were differentially regulated in the GBM cell line after miR-218 transfection. The quantified effects of transfection of U-118 MG cells with the miR-218 mimic at a 50 nM concentration on the expression levels of genes, as determined by qRT-PCR of a Human Cell Motility and Extracellular Matrix & Adhesion Molecules RT2 Profiler PCR Array. Cells transfected with scrambled siRNA were used as the control

2% of the original wound area. The most pronounced difference in the function of miR-218 was revealed at the 24-h time point, when the wound areas in the control and mimic 10 nM and mimic 50 nM samples were 4.4%, 45.3% and 56.2%, respectively. Both experiments indicated a delay in GBM cell migration rate upon miR-218 treatment.

We analysed further the real-time cell proliferation with the xCELLigence system. The graph shows the raw experimental data presented as the dependence of the cell index unit used in the xCELLigence
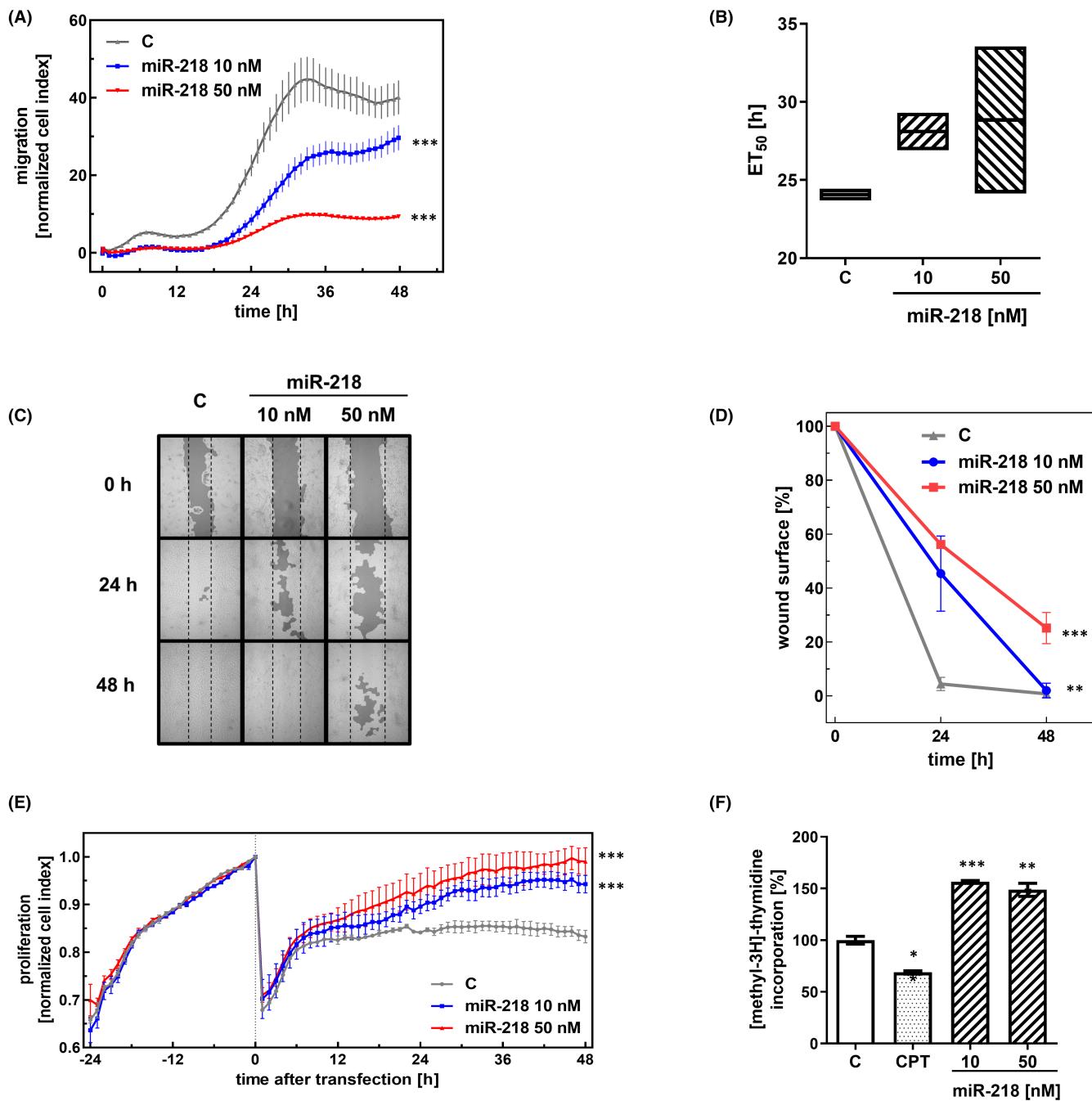
FIGURE 4 Effect of miR-218 on the migration and proliferation of glioblastoma cells. (A) The migration of U-118 MG cancer cells was studied using an xCELLigence system. Cells in serum-depleted medium were transfected with the miR-218 mimic (10 and 50 nM). Control (C)—cells treated with scrambled siRNA. Data are shown as the mean $\pm$ SD values. One-way ANOVA and the post hoc Bonferroni test, ***$p < .001$. (B) The half-maximal effective time (ET50) was calculated for each miR-218 concentration to generate dose–response curves. The ET50 values were normalized to control (C) cells treated with scrambled siRNA and plotted as the normalized ET50 of cell migration against the miR-218 concentration. (C) The wound healing assay after miR-218 mimic transfection. The dark grey areas indicate the surface area of the wound. (D) The calculation of the wound area (%) 24 and 48 h post-transfection. Control U-118 MG cells (C) were treated with scrambled siRNA. Data are shown as the mean $\pm$ SD values. One-way ANOVA and the post hoc Bonferroni test, **$p < .01$ and ***$p < .001$. (E) Proliferation of U-118 MG cancer cells analysed with the xCELLigence system. Cells were transfected with the miR-218 mimic (10 and 50 nM). Control (C)—cells treated with scrambled siRNA. Data are shown as the mean $\pm$ SD values. One-way ANOVA and the post hoc Bonferroni test, *$p < .05$ and **$p < .01$. (F) The thymidine incorporation assay on miR-218 mimic-transfected cells. As the positive control, cells treated with camptothecin were used. One-way ANOVA and post hoc Bonferroni test, *$p < .05$, **$p < .01$ and ***$p < .001$

system on the time (Figure 4E). In this way, the time course of pro-liferation changes with overexpression of miR-218 is illustrated. At the point on the timeline corresponding to 24 h, the curve inflection

indicates the time of transfection. The stimulating effects on prolifer-ation are seen at the final points of the curves, 48 h post-transfection. We observed an increase in the cell index by 14% at a miR-218 mimic

concentration of 10 nM and by as much as 19% at 50 nM. This demonstrates the directly proportional relationship between the increase in the proliferation rate and the expression of miR-218.

A [methyl-3H]-thymidine incorporation assay was performed to complement the proliferation analysis with the xCELLigence system. In this study, the degree of incorporation of radioactively labelled thymidine was evaluated and translated into the replication potential of cells. In addition to the standard trials used, we analysed the effect of 3 μM camptothecin, which has a confirmed pro-apoptotic effect,[37] as a positive control in the experiment. The incorporation rate in CPT-treated cells was 69% compared with that in control cells. miR-218 mimic transfection increased the incorporation of tritiated thymidine by 57% at 10 nM and 49% at 50 nM compared with that in control cells (Figure 4F).

3.6 | miR-218 enhances glioma cell adhesion

To explore the impact of miR-218 on U118-MG cells, the cell surface properties were quantified using AFM in SCFS mode (Figure 5D). These properties are quantified by calculating the work of adhesion, which is defined as the work required to detach a single cell from the surface. In this scenario, each single cell was used as a force probe. For control cells, the work of adhesion ranged from 0.00064 pJ to 0.00315 pJ, with a mean±standard deviation of 0.00186±0.00081 pJ (Figure 5A). The analogous variability in cell adhesion after miR-218 treatment ranged from 0.00191 pJ to 0.00512 pJ (mean±standard deviation = 0.0033±0.00113 pJ) and from 0.00194 pJ to 0.00406 pJ (mean±standard deviation = 0.00297±0.0007 pJ) for concentrations of 10 nM and 50 nM, respectively (Figure 5B,C). Real-time adhesion measurements performed with the xCELLigence system showed changes in the attachment of cells to the plate surface during the observation period (Figure 5E). The cell index of adhesion for cells treated with 10 nM miR-218 mimic was 2.5-fold greater than that of control cells. In the case of 50 nM miR-218 treatment, the observed index was 3 times higher than that measured in the control cells. From the beginning of the experiment to its end, the trends in the particular samples did not change. We assumed that the observed changes were miR-218-dependent, since the negative control cells did not bind to the plate covered with BSA. The untreated cells also showed low adherence compared with the miR-218-treated cells.

Thus, regardless of the technique used for the adhesion study, these two independent experiments demonstrated an increase in the adhesion of GBM cells treated with the miR-218 mimic.

3.7 | Overexpression of miR-218 impacts cell stiffness

Most surface receptors are linked not only to ECM proteins but also to actin filaments forming the actin cortex.[38] Thus, in our next step, we verified whether changes in GBM cell adhesive properties contribute to the overall mechanical properties of these cells. Cell stiffness was measured for cells compressed between the surface and a tipless cantilever; therefore, it was calculated as the slope of the approach part of the recorded force curves and expressed in N/m (Figure 6D).

For all sample types, that is control cells or cells treated either with 10 nM or with 50 nM miR-218, the stiffness of compressed cells remained mildly changed. Here, a smaller variability in mechanical force was observed for a given cellular force probe, as indicated by the standard deviation values. For control cells, the stiffness varied from 0.00425 N/m to 0.00763 N/m with a mean±standard deviation of 0.00568±0.00106 N/m (Figure 6A). Cells treated with miR-218 were characterized by a stiffness ranging from 0.00451 N/m to 0.00927 N/m (mean±standard deviation = 0.00741±0.00155 N/m) and from 0.00535 N/m to 0.00938 N/m (mean±standard deviation = 0.00746±0.00130 N/m) for concentrations of 10 nM and 50 nM, respectively (Figure 6B,C). Regardless of the final values of cell stiffness, an increasing trend was seen. For cells treated with 10 nM miR-218 mimic, the stiffness was increased by 30%, and for cells treated with 50 nM miR-218 mimic, the increase was 31% (Figure 6D). As the cell stiffness measured using AFM is related to the organization of the actin cytoskeleton, it was further visualized using fluorescently labelled F-actin to verify the effect (Figure 6E). Fluorescence images of the actin cortex show differences between control and miR-218-treated cells. Cells treated with miR-218 showed a higher level of actin filament organization. In these cells, the actin filaments became organized more horizontally along the long axis of the cell compared with those in control cells, where they were more dispersed. After treatment with 50 nM miR-218, also small changes in actin structures appeared at the cell surface. The F-actin dynamics and changes in filament organization directly support the increased stiffness of cells treated with the miR-218 mimic. The observed changes confirm then the hypothesis that cell stiffness is related to the cytoskeleton.

4 | DISCUSSION

The malignancy of glioblastoma depends on its ability to infiltrate adjacent tissues and to create secondary lesions.[39] The aggressive growth of glioma tumours and difficulties in developing an effective treatment scheme have led to intense integration of medical and molecular biological research. Remodelling of the ECM and miRNA deregulation are known processes contributing to GBM cell invasion and brain infiltration.[40-42] In this study, we show that miR-218 can play a role in regulation of ECM remodelling in glioblastoma cell line and could be investigated further as a possible important regulator of GBM. We found that TN-C and SDC-2 are directly regulated by miR-218, resulting in alterations in the ECM composition and changes in the mechanical properties of the cells. Although our previous finding identified miR-218 as a potential tumour suppressor in GBM,[36] the mechanism of miR-218 action in GBM is still poorly understood. The sequence of miR-218 is located within intron 15 of the SLIT2 gene, in which promoter region CpG island is hypermethylated in GBM.[43,44]
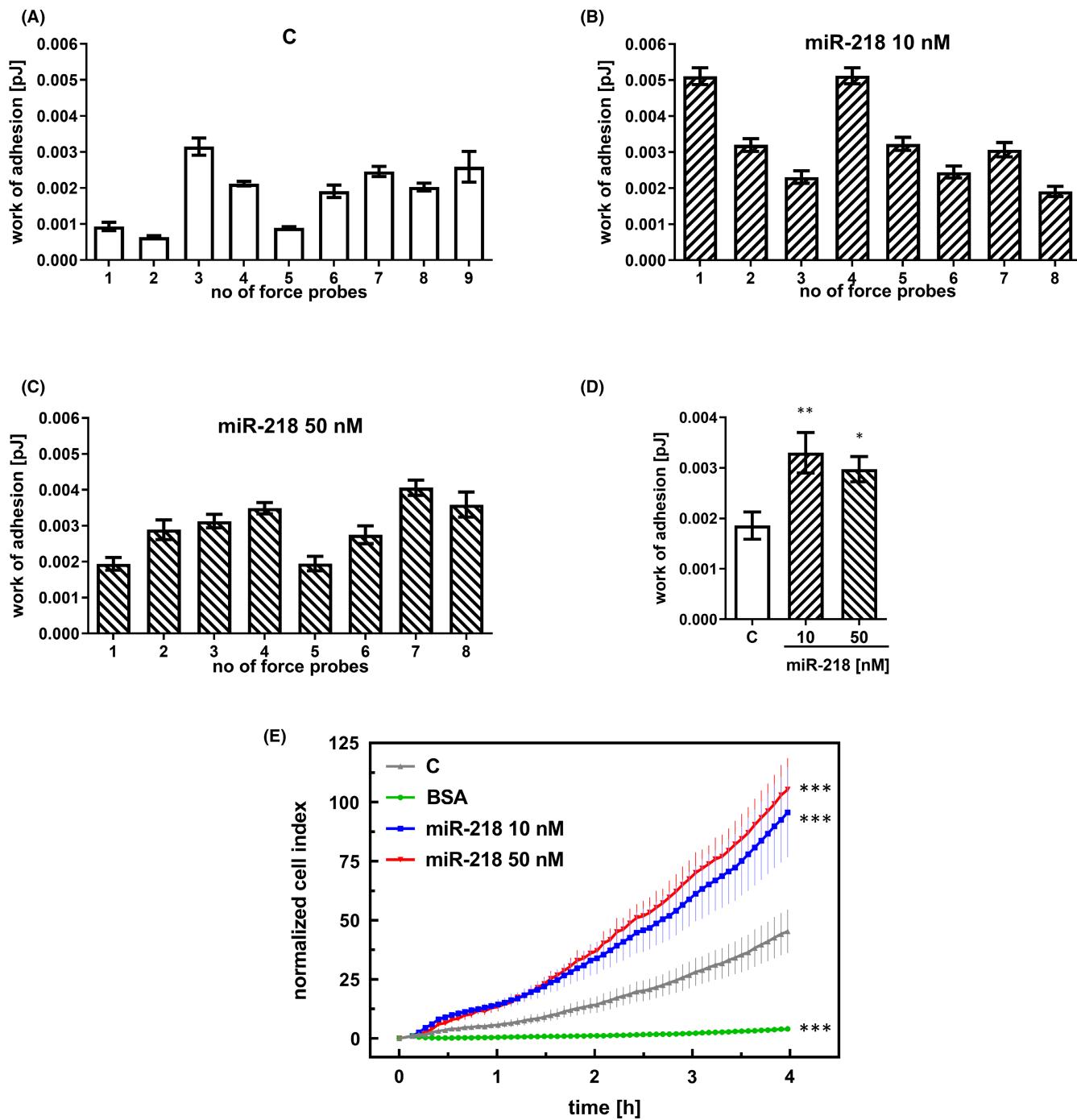
FIGURE 5 Adhesion of GBM cells increases after miR-218 treatment. The adhesive properties of U-118 MG cells were quantified by SCFS using single cells as force probes. Data for control, treated with scrambled siRNA cells (A), cells transfected with the miR-218 mimic at concentrations of 10 nM (B) and 50 nM (C), and the average result over all measurements (D). (E) Real-time adhesion measured with the xCELLigence system. The graph shows the final impedance values minus the initial values for the corresponding samples. Control (C)—cells treated with scrambled siRNA. Cells suspended in bovine serum albumin (BSA) were used as the positive control. Data are shown as the mean ± SD values. One-way ANOVA and the post hoc Bonferroni test, $*p < .05$, $**p < .01$ and $***p < .001$

The positive correlation between SLIT2 and miR-218 expression has been shown, what indicates that these two molecules are transcribed together.[45] The SLIT2 downregulation in GBM in consequence leads to the further decreased expression of miR-218.[46] Moreover, the expression level of miR-218 in GBM might be invoked by the feedback mechanism. The decreased expression of miR-218

can directly increase the expression of effector molecules such as RSK2, 6SK1 and PDGFRα, maintaining then the activity of the RTK pathway at a high level. RTK-conducted signals stimulate the expression of the STAT3 gene, whose product together with BCLAF1 binds directly to the miR-218 locus, thereby suppressing its expression.[47] Our previous finding confirmed then the decreased expression
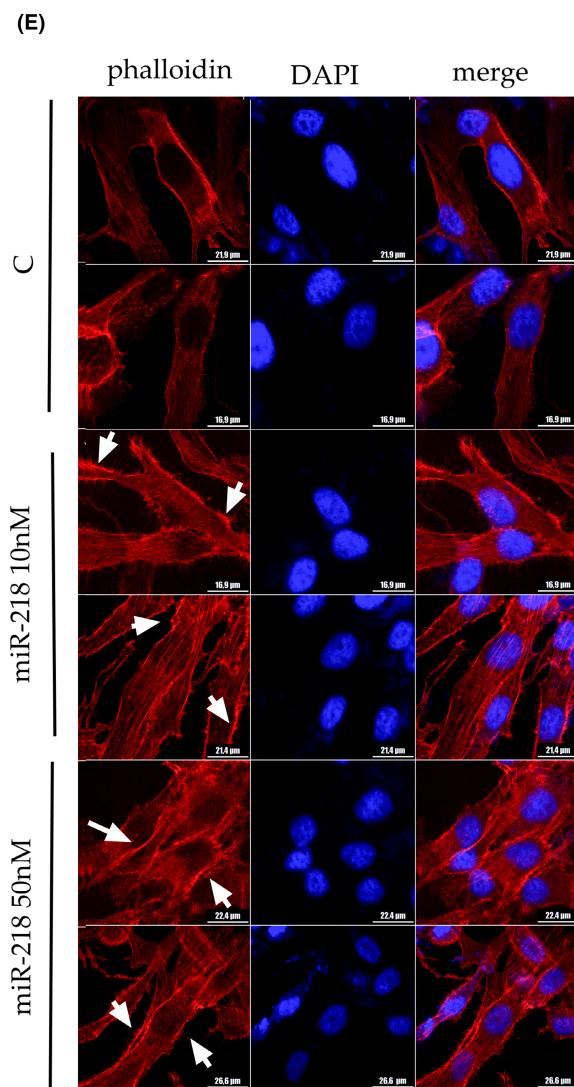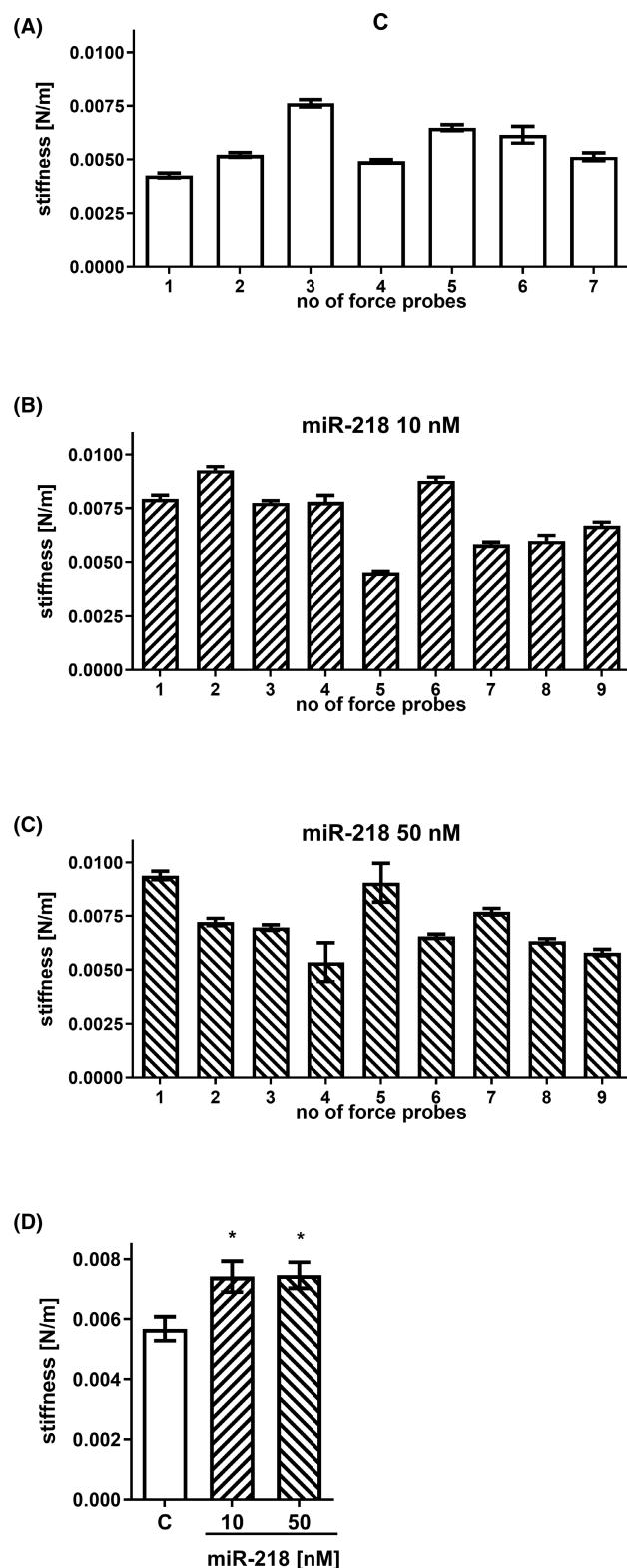
FIGURE 6 Mechanical properties of GBM cells after miR-218 treatment. Stiffness of U-118 MG cells quantified based on AFM elasticity measurements and expressed in N/m. Data for control, treated with scrambled siRNA cells (A), cells transfected with the miR-218 mimic at a 10 nM concentration (B) and a 50 nM concentration (C), and the average result over all measurements (D). (E) Confocal imaging of the actin cortex. Phalloidin (red) staining and DAPI (blue) staining were performed to visualize actin fibres and cell nuclei, respectively. Z-stack images were acquired. White arrows point to visible changes in actin structures. Data are shown as the mean ± SD values. One-way ANOVA and the post hoc Bonferroni test, *$p < .05$

of miR-218 both in primary and in recurrent tumours by 50% and 70%, respectively. Decreased miR-218-5p expression levels have also been reported in other types of human cancer, such as medulloblastoma, thyroid cancer and cervical cancer.[48-50] We confirmed that the predicted miR-218 targets, the ECM components TN-C and SDC-2, are directly regulated by miR-218. We used a dual-luciferase assay and miR-218 mimic to verify these functional interactions. The effects were detectable at both the mRNA and protein levels for both TN-C and SDC-2. Proteins derived from these transcripts are potentially key factors in the ECM of cancer cells.[15,21] The presence of TN-C in cancer tissues was initially considered as a characteristic feature of only gliomas,[51] with its expression increasing in proportion to the degree of brain tumour malignancy.[52] Its presence was found to increase the proliferation and invasiveness of cancer cells and to take part in the process of angiogenesis.[53] The role of TN-C in the neoplastic process is to reduce the adherence of cells, leading to the spread of the tumour. On the surface of healthy fibroblasts, fibronectin (FN) interacts with transmembrane proteins—integrins and syndecan-4 (SDC-4). The Rho protein is activated, and the properties of actin filaments are changed, resulting in cell adhesion. In pathological conditions, tenascin-C blocks the interaction between FN and SDC-4. The Rho protein is not activated, resulting in a lack of cell adhesion signals.[54] Considering the impact of TN-C on cancer cells and its apparent overexpression in glioblastoma tissues, it could be considered as a promising therapeutic target. We have already shown that the treatment with a double-stranded RNA targeting TN-C increased the average survival rate of patients.[55]

An increased level of syndecan-2 is a characteristic of actively migrating cells.[56] Overexpression of this protein in melanoma cells indirectly contributes to an increase in the level of FAK kinase phosphorylation, which has a positive impact on the migration capability of these cells.[17] In lung cancer, SDC-2 deficiency prevents cells from adhering to FN, which blocks their migration.[57]

ECM has become one of the most important focuses of cancer research, as it was shown to play a major role in the development of metastasis.[58] Pronounced ECM remodelling affects the invasion and migration of cancer cells.[59,60] The mechanical properties of the ECM have an impact on fibronectin fibril assembly, cytoskeletal stiffness and the strength of integrin–cytoskeleton linkages, the factors found to be important for cell motility, and thus also on adhesive properties.[61] As demonstrated in previous reports, a more rigid ECM promotes glioma cell migration.[62] On highly rigid ECMs, tumour cells spread extensively, form prominent stress fibres and mature focal adhesions, and migrate rapidly.[62] Our results are in line with these observations, as we showed a decreased cell migration rate after mir-218 overexpression, with subsequent downregulation of TN-C expression. These direct effects were enhanced by the indirect effect of miR-218 on a number of proteins, for example fibronectin, collagens or laminins. Thus, with miR-218 overexpression, we observed changes in the ECM leading to slowed cell migration, most likely induced by changes in overall ECM rigidity.

The obtained data revealed the decrease in the rate of cell migration upon the overexpression of miR-218, but at the same time also an increase in their proliferation potential (Figure 4). Our observations seem to be consistent with the "go-or-grow" hypothesis, according to which the division of neoplastic cells and their movement are two temporally exclusive events.[63] The "go-or-grow" decision is strictly regulated and modulated by changes in the tumour microenvironment, which allows cells to "go" towards more favourable conditions to proliferate at the distant site or to "grow" and to stay at the site of origin, if their current environment provides the proper conditions for tumour growth. Changes in miRNA expression, followed by the ECM remodelling, can modulate the "go-or-grow" decision. As it has already been shown previously, the considerable overexpression of miR-9 in glioma cells inhibits proliferation but concurrently promotes migration.[64] Evidence indicates that mechanical properties and deformability can also be used as biomarkers to distinguish between healthy and cancer cells. The deformability of a whole cell, which depends on the properties of the cytoplasm, the cytoskeleton and the nucleus, can be defined in terms of the response of the cell to an applied stress. One of the techniques that enables the measurement of biophysical properties of cells, such as adhesion and stiffness, is AFM.[65] We evaluated the mechanobiological properties of GBM cells, including adhesion and stiffness, upon miR-218 mimic treatment. We obtained real-time measurements in cell culture (xCELLigence system) and measured physical forces and the work of adhesion[66] by application of AFM in SCFS mode. This approach allowed us to quantify the adhesion of single cells. SCFS analysis revealed strengthened adhesion of GBM cells upon miR-218 overexpression, hence indicating the direct connection between miR-218 and ECM component regulation.

GBM cells, similar to other solid cancers, can remodel the surrounding microenvironment from a normal brain to a stiffer tumour microenvironment through the combination of proteolytic degradation of some ECM components and secretion of other novel ECM components.[67] In our analysis, the stiffness of miR-218-transfected cells as measured by AFM was 30% higher than that of the control cells. Despite the variability observed in the experiment, a clear difference was observed, as the overall stiffness was measured to increase in cells treated with miR-218. The differences observed in the experimental cell group might have stemmed from the distributed contribution of surface receptors on an individual single cell, which can thus impact the adhesion of that cell.[68,69] It has already been shown that tumours can become stiffer than normal tissues due to increased Rho-dependent cytoskeletal pressure, generating excessive growth, focal adhesions, adjacent joint division and tissue disruption.[70] Stiffness also directly depends on the malignancy of the tumour. It is known that invasive GBM tumours produce stiffness-promoting factors such as collagen, fibronectin and laminins, which may suggest that the production of these proteins is disrupted after miR-218 overexpression.[71]

An increase in stiffness has also been observed in many different types of cancer cells, such as breast cancer, melanoma, prostate cancer and cervical cancer cells. An important aspect of cell stiffness is the ratio of cancer to normal cells. While cancer cells are less stiff than normal cells,[72] the same pattern of stiffness is also observed in

malignant versus non-malignant tissues in breast cancer,[73] bladder cancer[74] and prostate cancer.[75] In our research, glioblastoma cells with miR-218 overexpression were approximately 30% stiffer than non-treated cells. Increased stiffness in brain tissues can be correlated with diseases such as brain abscess or with cytoskeletal maturation in brain cells.[76] The correlation of cytoskeletal maturation with an increase in cell stiffness has been observed for astrocytes, in which the AFM-measured stiffness may increase sevenfold in a 5-week observation period during development.[77] In miR-218-treated GBM cells, the actin cytoskeleton was slightly rearranged, which could explain the increase in cell stiffness.

The minor discrepancy in the relation between cell surface adhesive properties and cell stiffness measured in our study can be explained by the different scales of measurements. For cell adhesion, SCFS measurements are limited to local changes occurring on the cell surface, while the stiffness reflects the overall mechanical properties of cells. Thus, we analysed stiffness assuming an indentation depth of 200 nm. This value assures the sensing of a superficial layer of actin filaments. Additionally, brain tissue is much softer than other tissues. The value of Young's modulus ranges from 1 to 1.9 kPa for white matter and from 0.8 to 1.4 kPa for grey matter, depending on the measurement technique.[78,79] Independent methods, that is SCFS and the xCELLigence system, showed similar increases in the adhesive properties of U-118 MG cells upon miR-218 treatment. Collectively, these results demonstrated that miRNA-218 strongly affects the expression of genes encoding cell surface receptors responsible for the adhesive properties of cells.

We also found that miR-218-treated cells are more rigid than non-treated cells, which presumably might prevent them from undergoing extravasation and intravasation during migration and invasion events. We thus hypothesized that miR-218 overexpression can support the maintenance of the non-invasive cell phenotype, which is correlated with differences in mechanical properties. The observation is more important when one realizes the importance of ECM rigidity in the perivascular space. It has already been shown that this part of the brain tissue is more rigid in GBM, thus promoting glioma cell migration.[62]

As we have shown, miR-218-5p deregulation is involved in GBM growth and migration potential. In addition to the direct influence that miR-218 has on transcripts such as TN-C or SDC-2, as shown in this study, it can influence the ECM composition by targeting other molecules, for example the Wnt/β-catenin pathway transcription factors *LEF1* or MMP-9.[80] There are data showing that miR-218 suppresses cell invasion and spheroid formation,[81] arrests GBM cells in G1 phase[31] and can reduce the expression of cancer stem cell markers such as CD133, SOX2 and Nestin.[82] The complex influence that miR-218 has on GBM cells cannot be underestimated and studied only by evaluating direct targets of this miRNA; therefore in search of indirect targets of miR-218 in glioblastoma, we performed an extended-expression analysis and found 47 genes connected to focal adhesion and cell motility. After miR-218 overexpression in glioblastoma cells, we observed a decrease in the expression levels of GBM oncogenes such as *PIK3CA*, *ROCK1*, *LAMC1* and *ICAM1*.

The expression of these genes is increased in GBM compared with healthy tissues.[83-86] Enhanced miR-218 levels also reduced the expression levels of the *CRK*, *RHOA* and *PTPN1* genes involved in GBM progression.[87-89] Our results are supported by data in the literature indicating a decrease in the expression levels of *PIK3CA*,[90] *RHOA*[91] and *STAT3*[50,92] as a consequence of miR-218 overexpression.

Due to the nature of our research, the changes in the expression levels of *CDC42*, *STAT3*, *EGF* and *CTTN* might be particularly important. Previous reports have indicated that *CDC42* is a critical determinant of the migratory and invasive phenotype of malignant gliomas.[93,94] The *STAT3* level is correlated with GBM malignancy, indicating its participation in increasing the migration potential of cancer cells.[95] Additionally, regarding *EGF*, its impact on the migratory nature of GBM cells is known.[96] *CTNN* and the Arp2/3 complex are known for regulating lamellipodia formation, and a decrease in CTNN expression can suppress GBM migration mechanisms.[97,98] Because we showed a decrease in the migration capacity of glioblastoma cells under treatment with miR-218 in our studies, we could conclude then that these changes might be the result of the impact of miR-218 on *CDC42*, *STAT3*, *EGF* and *CTTN*.

The observed increase in GBM cell adhesion may also be associated with a decrease in *ACTN1* expression. It has been shown that after downregulation of *ACTN1*, GBM cells show poor spread but increased focal adhesion.[99] The changes in the cytoskeleton that we observed may be the result of a reduced *HGF* level, which has been demonstrated to affect the distribution of the actin cytoskeleton in glioblastoma cell lines.[100] Both the cancer migration pathway and deregulation of the actin cytoskeleton can be related to downregulation of SH3PXD2A after miR-218 overexpression. SH3PXD2A is a crucial element in the formation of actin-based invadopodia—protrusions of the plasma membrane that are associated with mechanisms of invasiveness.[101,102]

5 | CONCLUSIONS

In this study, we showed that miRNA, as post-transcriptional gene regulator, has a direct impact on the ECM composition and, as a consequence, the mechanobiological properties of glioma cells. We demonstrated that miR-218 can be considered as a potent tumour suppressor that directly participates in post-transcriptional regulation of the expression of the extracellular matrix proteins tenascin-C and syndecan-2. The most intriguing observations in this study are the impact of miR-218 on the mechanical properties of the cells, that is migration and adhesion, followed by the direct changes of cell stiffness as measured with AFM technology. Additionally, our global gene expression analysis revealed changes in a number of genes directly or indirectly involved in cell motility and thus adhesion or cytoskeletal rearrangement. Taken together, our results showed the direct impact of miR-218 on the qualitative ECM content, leading to changes in the rigidity of the ECM and GBM cells. These features impacted by miR-218 overexpression collectively reduce the motility of cancer cells and increase their adhesiveness, thus most

probably conferring a phenotype more closely related to that of normal cells. Collectively, our results indicate that miR-218 is a potent tumour suppressor in glioma with a large impact on the ECM and biomechanical properties of the cells. Additionally, we believe that cell mechanical properties can constitute a broad drug target space, allowing possible corrective modulation of tumour cell behaviour.

AUTHOR CONTRIBUTIONS

Małgorzata Grabowska: Conceptualization (equal); investigation (lead); visualization (equal); writing – original draft (equal); writing – review and editing (equal). **Konrad Kuczyński:** Investigation (lead); methodology (equal); software (equal); visualization (equal); writing – original draft (equal); writing – review and editing (equal). **Monika Piwecka:** Investigation (supporting); methodology (equal); writing – review and editing (equal). **Alicja Rabiasz:** Investigation (supporting). **Joanna Zemła:** Data curation (equal); investigation (supporting); methodology (equal); software (equal). **Paweł Głodowicz:** Investigation (supporting). **Dariusz Wawrzyniak:** Investigation (supporting). **Małgorzata Lekka:** Data curation (equal); methodology (equal); software (equal); writing – original draft (equal); writing – review and editing (supporting). **Katarzyna Rolle:** Funding acquisition (lead); project administration (lead); supervision (lead); writing – original draft (equal); writing – review and editing (equal).

CONFLICT OF INTEREST

The authors confirm that there are no conflicts of interest.

DATA AVAILABILITY STATEMENT

Data available on request from the authors.

INSTITUTIONAL REVIEW BOARD STATEMENT

Tissue samples used in this study were collected based on the approval from the Karol Marcinkowski University of Medical Sciences in Poznan Ethical Committee (Consent nr. 46/13).

ORCID

Konrad Kuczyński https://orcid.org/0000-0002-7664-1045
Katarzyna Rolle https://orcid.org/0000-0002-4175-2490

REFERENCES

1. Sasmita AO, Wong YP, Ling APK. Biomarkers and therapeutic advances in glioblastoma multiforme. *Asia Pac J Clin Oncol.* 2018;14:40-51. doi:10.1111/ajco.12756
2. Vigneswaran K, Neill S, Hadjipanayis CG. Beyond the World Health Organization grading of infiltrating gliomas: advances in the molecular genetics of glioma classification. *Ann Transl Med.* 2015;3:95. doi:10.3978/j.issn.2305-5839.2015.03.57
3. Kim J, Lee IH, Cho HJ, et al. Spatiotemporal evolution of the primary glioblastoma genome. *Cancer Cell.* 2015;28:318-328. doi:10.1016/j.ccell.2015.07.013
4. Wei SC, Yang J. Forcing through tumor metastasis: the interplay between tissue rigidity and epithelial-mesenchymal transition. *Trends Cell Biol.* 2016;26:111-120. doi:10.1016/j.tcb.2015.09.009
5. Naba A, Clauser KR, Hoersch S, Liu H, Carr SA, Hynes RO. The matrisome: in silico definition and in vivo characterization by proteomics of normal and tumor extracellular matrices. *Mol Cell Proteomics.* 2012;11:M111 014647. doi:10.1074/mcp.M111.014647
6. Gkretsi V, Stylianopoulos T. Cell adhesion and matrix stiffness: coordinating cancer cell invasion and metastasis. *Front Oncol.* 2018;8:145. doi:10.3389/fonc.2018.00145
7. Acerbi I, Cassereau L, Dean I, et al. Human breast cancer invasion and aggression correlates with ECM stiffening and immune cell infiltration. *Integr Biol (Camb).* 2015;7:1120-1134. doi:10.1039/c5ib00040h
8. Naba A, Clauser KR, Lamar JM, Carr SA, Hynes RO. Extracellular matrix signatures of human mammary carcinoma identify novel metastasis promoters. *Elife.* 2014;3:e01308. doi:10.7554/eLife.01308
9. Gjorevski N, Sachs N, Manfrin A, et al. Designer matrices for intestinal stem cell and organoid culture. *Nature.* 2016;539:560-564. doi:10.1038/nature20168
10. Rianna C, Kumar P, Radmacher M. The role of the microenvironment in the biophysics of cancer. *Semin Cell Dev Biol.* 2018;73:107-114. doi:10.1016/j.semcdb.2017.07.022
11. Goetz JG, Minguet S, Navarro-Lerida I, et al. Biomechanical remodeling of the microenvironment by stromal caveolin-1 favors tumor invasion and metastasis. *Cell.* 2011;146:148-163. doi:10.1016/j.cell.2011.05.040
12. Levental KR, Yu H, Kass L, et al. Matrix crosslinking forces tumor progression by enhancing integrin signaling. *Cell.* 2009;139:891-906. doi:10.1016/j.cell.2009.10.027
13. Mansouri R, Hay E, Marie PJ, Modrowski D. Role of syndecan-2 in osteoblast biology and pathology. *Bonekey Rep.* 2015;4:666. doi:10.1038/bonekey.2015.33
14. Mytilinaiou M, Nikitovic D, Berdiaki A, et al. Emerging roles of syndecan 2 in epithelial and mesenchymal cancer progression. *IUBMB Life.* 2017;69:824-833. doi:10.1002/iub.1678
15. Vicente CM, Ricci R, Nader HB, Toma L. Syndecan-2 is upregulated in colorectal cancer cells through interactions with extracellular matrix produced by stromal fibroblasts. *BMC Cell Biol.* 2013;14:25. doi:10.1186/1471-2121-14-25
16. Park H, Han I, Kwon HJ, Oh ES. Focal adhesion kinase regulates syndecan-2-mediated tumorigenic activity of HT1080 fibrosarcoma cells. *Cancer Res.* 2005;65:9899-9905. doi:10.1158/0008-5472.CAN-05-1386
17. Lee JH, Park H, Chung H, et al. Syndecan-2 regulates the migratory potential of melanoma cells. *J Biol Chem.* 2009;284:27167-27175. doi:10.1074/jbc.M109.034678
18. Choi S, Choi Y, Jun E, et al. Shed syndecan-2 enhances tumorigenic activities of colon cancer cells. *Oncotarget.* 2015;6:3874-3886. doi:10.18632/oncotarget.2885
19. De Oliveira T, Abiatari I, Raulefs S, et al. Syndecan-2 promotes perineural invasion and cooperates with K-ras to induce an invasive pancreatic cancer cell phenotype. *Mol Cancer.* 2012;11:19. doi:10.1186/1476-4598-11-19
20. Hua R, Yu J, Yan X, et al. Syndecan-2 in colorectal cancer plays oncogenic role via epithelial-mesenchymal transition and MAPK pathway. *Biomed Pharmacother.* 2020;121:109630. doi:10.1016/j.biopha.2019.109630
21. Brosicke N, van Landeghem FK, Scheffler B, Faissner A. Tenascin-C is expressed by human glioma in vivo and shows

a strong association with tumor blood vessels. *Cell Tissue Res.* 2013;354:409-430. doi:10.1007/s00441-013-1704-9

22. Naik A, Al-Yahyaee A, Abdullah N, et al. Neuropilin-1 promotes the oncogenic Tenascin-C/integrin beta3 pathway and modulates chemoresistance in breast cancer cells. *BMC Cancer.* 2018;18:533. doi:10.1186/s12885-018-4446-y

23. Gocheva V, Naba A, Bhutkar A, et al. Quantitative proteomics identify Tenascin-C as a promoter of lung cancer progression and contributor to a signature prognostic of patient survival. *Proc Natl Acad Sci U S A.* 2017;114:E5625-E5634. doi:10.1073/pnas.1707054114

24. Yang Z, Zhang C, Qi W, Cui C, Cui Y, Xuan Y. Tenascin-C as a prognostic determinant of colorectal cancer through induction of epithelial-to-mesenchymal transition and proliferation. *Exp Mol Pathol.* 2018;105:216-222. doi:10.1016/j.yexmp.2018.08.009

25. Ambros V. The functions of animal microRNAs. *Nature.* 2004;431:350-355. doi:10.1038/nature02871

26. Calin GA, Croce CM. MicroRNA signatures in human cancers. *Nat Rev Cancer.* 2006;6:857-866. doi:10.1038/nrc1997

27. van Rooij E, Sutherland LB, Liu N, et al. A signature pattern of stress-responsive microRNAs that can evoke cardiac hypertrophy and heart failure. *Proc Natl Acad Sci U S A.* 2006;103:18255-18260. doi:10.1073/pnas.0608791103

28. O'Connell RM, Rao DS, Chaudhuri AA, Baltimore D. Physiological and pathological roles for microRNAs in the immune system. *Nat Rev Immunol.* 2010;10:111-122. doi:10.1038/nri2708

29. Ciafre SA, Galardi S, Mangiola A, et al. Extensive modulation of a set of microRNAs in primary glioblastoma. *Biochem Biophys Res Commun.* 2005;334:1351-1358. doi:10.1016/j.bbrc.2005.07.030

30. Li Z, Qian R, Zhang J, Shi X. MiR-218-5p targets LHFPL3 to regulate proliferation, migration, and epithelial-mesenchymal transitions of human glioma cells. *Biosci Rep.* 2019;39(3):BSR20180879. doi:10.1042/BSR20180879

31. Zhang Y, Han D, Wei W, et al. MiR-218 inhibited growth and metabolism of human glioblastoma cells by directly targeting E2F2. *Cell Mol Neurobiol.* 2015;35:1165-1173. doi:10.1007/s10571-015-0210-x

32. Wu Z, Han Y, Li Y, et al. MiR-218-5p inhibits the stem cell properties and invasive ability of the A2B5(+)CD133(–) subgroup of human glioma stem cells. *Oncol Rep.* 2016;35:869-877. doi:10.3892/or.2015.4418

33. Sader JE, Larson I, Mulvaney P, White LR. Method for the calibration of atomic force microscope cantilevers. *Rev Sci Instrum.* 1995;66:3789-3798. doi:10.1063/1.1145439

34. Omidvar R, Tafazzoli-Shadpour M, Shokrgozar MA, Rostami M. Atomic force microscope-based single cell force spectroscopy of breast cancer cell lines: an approach for evaluating cellular invasion. *J Biomech.* 2014;47:3373-3379. doi:10.1016/j.jbiomech.2014.08.002

35. Szymon P-B, Joanna R, Jakub R, et al. Adaptability of single melanoma cells to surfaces with distinct hydrophobicity and roughness. *Appl Surf Sci.* 2018;457:881-890. doi:10.1016/j.apsusc.2018.06.251

36. Piwecka M, Rolle K, Belter A, et al. Comprehensive analysis of microRNA expression profile in malignant glioma tissues. *Mol Oncol.* 2015;9:1324-1340. doi:10.1016/j.molonc.2015.03.007

37. Morris EJ, Geller HM. Induction of neuronal apoptosis by camptothecin, an inhibitor of DNA topoisomerase-I: evidence for cell cycle-independent toxicity. *J Cell Biol.* 1996;134:757-770. doi:10.1083/jcb.134.3.757

38. Wang N, Tytell JD, Ingber DE. Mechanotransduction at a distance: mechanically coupling the extracellular matrix with the nucleus. *Nat Rev Mol Cell Biol.* 2009;10:75-82. doi:10.1038/nrm2594

39. Ohgaki H, Kleihues P. Genetic pathways to primary and secondary glioblastoma. *Am J Pathol.* 2007;170:1445-1453. doi:10.2353/ajpath.2007.070011

40. Xu TJ, Qiu P, Zhang YB, Yu SY, Xu GM, Yang W. MiR-148a inhibits the proliferation and migration of glioblastoma by targeting ITGA9. *Hum Cell.* 2019;32:548-556. doi:10.1007/s13577-019-00279-9

41. Lei D, Zhang F, Yao D, Xiong N, Jiang X, Zhao H. MiR-338-5p suppresses proliferation, migration, invasion, and promote apoptosis of glioblastoma cells by directly targeting EFEMP1. *Biomed Pharmacother.* 2017;89:957-965. doi:10.1016/j.biopha.2017.01.137

42. Li Y, Wang Y, Yu L, et al. miR-146b-5p inhibits glioma migration and invasion by targeting MMP16. *Cancer Lett.* 2013;339:260-269. doi:10.1016/j.canlet.2013.06.018

43. Dickinson RE, Dallol A, Bieche I, et al. Epigenetic inactivation of SLIT3 and SLIT1 genes in human cancers. *Br J Cancer.* 2004;91:2071-2078. doi:10.1038/sj.bjc.6602222

44. Dallol A, Krex D, Hesson L, Eng C, Maher ER, Latif F. Frequent epigenetic inactivation of the SLIT2 gene in gliomas. *Oncogene.* 2003;22:4611-4616. doi:10.1038/sj.onc.1206687

45. Tang W, Tang J, He J, et al. SLIT2/ROBO1-miR-218-1-RET/PLAG1: a new disease pathway involved in Hirschsprung's disease. *J Cell Mol Med.* 2015;19:1197-1207. doi:10.1111/jcmm.12454

46. Mertsch S, Schmitz N, Jeibmann A, Geng JG, Paulus W, Senner V. Slit2 involvement in glioma cell migration is mediated by Robo1 receptor. *J Neurooncol.* 2008;87:1-7. doi:10.1007/s11060-007-9484-2

47. Mathew LK, Huangyang P, Mucaj V, et al. Feedback circuitry between miR-218 repression and RTK activation in glioblastoma. *Sci Signal.* 2015;8:ra42. doi:10.1126/scisignal.2005978

48. Shi J, Yang L, Wang T, et al. miR-218 is downregulated and directly targets SH3GL1 in childhood medulloblastoma. *Mol Med Rep.* 2013;8:1111-1117. doi:10.3892/mmr.2013.1639

49. Guan H, Wei G, Wu J, et al. Down-regulation of miR-218-2 and its host gene SLIT3 cooperate to promote invasion and progression of thyroid cancer. *J Clin Endocrinol Metab.* 2013;98:E1334-E1344. doi:10.1210/jc.2013-1053

50. Zhu L, Tu H, Liang Y, Tang D. MiR-218 produces anti-tumor effects on cervical cancer cells in vitro. *World J Surg Oncol.* 2018;16:204. doi:10.1186/s12957-018-1506-3

51. Bourdon MA, Wikstrand CJ, Furthmayr H, Matthews TJ, Bigner DD. Human glioma-mesenchymal extracellular matrix antigen defined by monoclonal antibody. *Cancer Res.* 1983;43:2796-2805.

52. Herold-Mende C, Mueller MM, Bonsanto MM, Schmitt HP, Kunze S, Steiner HH. Clinical impact and functional aspects of tenascin-C expression during glioma progression. *Int J Cancer.* 2002;98:362-369. doi:10.1002/ijc.10233

53. Mustafa DA, Dekker LJ, Stingl C, et al. A proteome comparison between physiological angiogenesis and angiogenesis in glioblastoma. *Mol Cell Proteomics.* 2012;11:M111 008466. doi:10.1074/mcp.M111.008466

54. Chiquet-Ehrismann R, Chiquet M. Tenascins: regulation and putative functions during pathological stress. *J Pathol.* 2003;200:488-499. doi:10.1002/path.1415

55. Rolle K, Nowak S, Wyszko E, et al. Promising human brain tumors therapy with interference RNA intervention (iRNAi). *Cancer Biol Ther.* 2010;9:396-406. doi:10.4161/cbt.9.5.10958

56. Chung H, Lee JH, Jeong D, Han IO, Oh ES. Melanocortin 1 receptor regulates melanoma cell migration by controlling syndecan-2 expression. *J Biol Chem.* 2012;287:19326-19335. doi:10.1074/jbc.M111.334730

57. Munesue S, Kusano Y, Oguri K, et al. The role of syndecan-2 in regulation of actin-cytoskeletal organization of Lewis lung carcinoma-derived metastatic clones. *Biochem J.* 2002;363:201-209. doi:10.1042/0264-6021:3630201

58. He X, Lee B, Jiang Y. Cell-ECM interactions in tumor invasion. *Adv Exp Med Biol.* 2016;936:73-91. doi:10.1007/978-3-319-42023-3_4

59. Lu P, Weaver VM, Werb Z. The extracellular matrix: a dynamic niche in cancer progression. *J Cell Biol*. 2012;196:395-406. doi:10.1083/jcb.201102147

60. Pickup MW, Mouw JK, Weaver VM. The extracellular matrix modulates the hallmarks of cancer. *EMBO Rep*. 2014;15:1243-1253. doi:10.15252/embr.201439246

61. Lo CM, Wang HB, Dembo M, Wang YL. Cell movement is guided by the rigidity of the substrate. *Biophys J*. 2000;79:144-152. doi:10.1016/S0006-3495(00)76279-5

62. Ulrich TA, de Juan Pardo EM, Kumar S. The mechanical rigidity of the extracellular matrix regulates the structure, motility, and proliferation of glioma cells. *Cancer Res*. 2009;69:4167-4174. doi:10.1158/0008-5472.CAN-08-4859

63. Hatzikirou H, Basanta D, Simon M, Schaller K, Deutsch A. "Go or grow": the key to the emergence of invasion in tumour progression? *Math Med Biol*. 2012;29:49-65. doi:10.1093/imammb/dqq011

64. Tan X, Wang S, Yang B, et al. The CREB-miR-9 negative feedback minicircuitry coordinates the migration and proliferation of glioma cells. *PLoS One*. 2012;7:e49570. doi:10.1371/journal.pone.0049570

65. Binnig G, Quate CF, Gerber C. Atomic force microscope. *Phys Rev Lett*. 1986;56:930-933. doi:10.1103/PhysRevLett.56.930

66. Zemla J, Danilkiewicz J, Orzechowska B, Pabijan J, Seweryn S, Lekka M. Atomic force microscopy as a tool for assessing the cellular elasticity and adhesiveness to identify cancer cells and tissues. *Semin Cell Dev Biol*. 2018;73:115-124. doi:10.1016/j.semcdb.2017.06.029

67. Nakada M, Yamada A, Takino T, et al. Suppression of membrane-type 1 matrix metalloproteinase (MMP)-mediated MMP-2 activation and tumor invasion by testican 3 and its splicing variant gene product, N-Tes. *Cancer Res*. 2001;61:8896-8902.

68. Li IT, Ha T, Chemla YR. Mapping cell surface adhesion by rotation tracking and adhesion footprinting. *Sci Rep*. 2017;7:44502. doi:10.1038/srep44502

69. Lomakina EB, Marsh G, Waugh RE. Cell surface topography is a regulator of molecular interactions during chemokine-induced neutrophil spreading. *Biophys J*. 2014;107:1302-1312. doi:10.1016/j.bpj.2014.07.062

70. Paszek MJ, Zahir N, Johnson KR, et al. Tensional homeostasis and the malignant phenotype. *Cancer Cell*. 2005;8:241-254. doi:10.1016/j.ccr.2005.08.010

71. Mahesparan R, Read TA, Lund-Johansen M, Skaftnesmo KO, Bjerkvig R, Engebraaten O. Expression of extracellular matrix components in a highly infiltrative in vivo glioma model. *Acta Neuropathol*. 2003;105:49-57. doi:10.1007/s00401-002-0610-0

72. Hayashi K, Iwata M. Stiffness of cancer cells measured with an AFM indentation method. *J Mech Behav Biomed Mater*. 2015;49:105-111. doi:10.1016/j.jmbbm.2015.04.030

73. Li QS, Lee GY, Ong CN, Lim CT. AFM indentation study of breast cancer cells. *Biochem Biophys Res Commun*. 2008;374:609-613. doi:10.1016/j.bbrc.2008.07.078

74. Ramos JR, Pabijan J, Garcia R, Lekka M. The softening of human bladder cancer cells happens at an early stage of the malignancy process. *Beilstein J Nanotechnol*. 2014;5:447-457. doi:10.3762/bjnano.5.52

75. Lekka M, Gil D, Pogoda K, et al. Cancer cell detection in tissue sections using AFM. *Arch Biochem Biophys*. 2012;518:151-156. doi:10.1016/j.abb.2011.12.013

76. Minelli E, Sassun TE, Papi M, et al. Nanoscale mechanics of brain abscess: An atomic force microscopy study. *Micron*. 2018;113:34-40. doi:10.1016/j.micron.2018.06.012

77. Lee SM, Nguyen TH, Na K, et al. Nanomechanical measurement of astrocyte stiffness correlated with cytoskeletal maturation. *J Biomed Mater Res A*. 2015;103:365-370. doi:10.1002/jbm.a.35174

78. van Dommelen JA, van der Sande TP, Hrapko M, Peters GW. Mechanical properties of brain tissue by indentation: interregional variation. *J Mech Behav Biomed Mater*. 2010;3:158-166. doi:10.1016/j.jmbbm.2009.09.001

79. Budday S, Nay R, de Rooij R, et al. Mechanical properties of gray and white matter brain tissue by indentation. *J Mech Behav Biomed Mater*. 2015;46:318-330. doi:10.1016/j.jmbbm.2015.02.024

80. Liu Y, Yan W, Zhang W, et al. MiR-218 reverses high invasiveness of glioblastoma cells by targeting the oncogenic transcription factor LEF1. *Oncol Rep*. 2012;28:1013-1021. doi:10.3892/or.2012.1902

81. Song L, Huang Q, Chen K, et al. miR-218 inhibits the invasive ability of glioma cells by direct downregulation of IKK-beta. *Biochem Biophys Res Commun*. 2010;402:135-140. doi:10.1016/j.bbrc.2010.10.003

82. Tu Y, Gao X, Li G, et al. MicroRNA-218 inhibits glioma invasion, migration, proliferation, and cancer stem-like cell self-renewal by targeting the polycomb group gene Bmi1. *Cancer Res*. 2013;73:6046-6055. doi:10.1158/0008-5472.CAN-13-0358

83. Liang H, Wang R, Jin Y, Li J, Zhang S. MiR-422a acts as a tumor suppressor in glioblastoma by targeting PIK3CA. *Am J Cancer Res*. 2016;6:1695-1707.

84. Zhou F, Li Y, Hao Z, et al. MicroRNA-300 inhibited glioblastoma progression through ROCK1. *Oncotarget*. 2016;7:36529-36538. doi:10.18632/oncotarget.9068

85. Liu J, Liu D, Yang Z, Yang Z. High LAMC1 expression in glioma is associated with poor prognosis. *Onco Targets Ther*. 2019;12:4253-4260. doi:10.2147/OTT.S205333

86. Gingras MC, Roussel E, Bruner JM, Branch CD, Moser RP. Comparison of cell adhesion molecule expression between glioblastoma multiforme and autologous normal brain tissue. *J Neuroimmunol*. 1995;57:143-153. doi:10.1016/0165-5728(94)00178-q

87. Kumar S, Lu B, Dixit U, et al. Reciprocal regulation of Abl kinase by Crk Y251 and Abi1 controls invasive phenotypes in glioblastoma. *Oncotarget*. 2015;6:37792-37807. doi:10.18632/oncotarget.6096

88. Liu G, Yan T, Li X, et al. Daam1 activates RhoA to regulate Wnt5ainduced glioblastoma cell invasion. *Oncol Rep*. 2018;39:465-472. doi:10.3892/or.2017.6124

89. Li Z, Hu C, Zhen Y, Pang B, Yi H, Chen X. Pristimerin inhibits glioma progression by targeting AGO2 and PTPN1 expression via miR-542-5p. *Biosci Rep*. 2019;39:10.1042/BSR20182389.

90. Mathew LK, Skuli N, Mucaj V, et al. miR-218 opposes a critical RTK-HIF pathway in mesenchymal glioblastoma. *Proc Natl Acad Sci U S A*. 2014;111:291-296. doi:10.1073/pnas.1314341111

91. Meseguer S, Panadero J, Navarro-Gonzalez C, et al. The MELAS mutation m.3243A>G promotes reactivation of fetal cardiac genes and an epithelial-mesenchymal transition-like program via dysregulation of miRNAs. *Biochim Biophys Acta Mol Basis Dis*. 2018;1864:3022-3037. doi:10.1016/j.bbadis.2018.06.014

92. Yang Y, Ding L, Hu Q, et al. MicroRNA-218 functions as a tumor suppressor in lung cancer by targeting IL-6/STAT3 and negatively correlates with poor prognosis. *Mol Cancer*. 2017;16:141. doi:10.1186/s12943-017-0710-z

93. Okura H, Golbourn BJ, Shahzad U, et al. A role for activated Cdc42 in glioblastoma multiforme invasion. *Oncotarget*. 2016;7:56958-56975. doi:10.18632/oncotarget.10925

94. Cheng WY, Chiao MT, Liang YJ, Yang YC, Shen CC, Yang CY. Luteolin inhibits migration of human glioblastoma U-87 MG and T98G cells through downregulation of Cdc42 expression and PI3K/AKT activity. *Mol Biol Rep*. 2013;40:5315-5326. doi:10.1007/s11033-013-2632-1

95. Han D, Yu T, Dong N, Wang B, Sun F, Jiang D. Napabucasin, a novel STAT3 inhibitor suppresses proliferation, invasion and stemness of glioblastoma cells. *J Exp Clin Cancer Res*. 2019;38:289. doi:10.1186/s13046-019-1289-6

96. Chen XC, Wei XT, Guan JH, Shu H, Chen D. EGF stimulates glioblastoma metastasis by induction of matrix metalloproteinase-9 in an EGFR-dependent mechanism. *Oncotarget*. 2017;8:65969-65982. doi:10.18632/oncotarget.19622

97. Zhang S, Qi Q. MTSS1 suppresses cell migration and invasion by targeting CTTN in glioblastoma. *J Neurooncol*. 2015;121:425-431. doi:10.1007/s11060-014-1656-2

98. Wang L, Zhao K, Ren B, et al. Expression of cortactin in human gliomas and its effect on migration and invasion of glioma cells. *Oncol Rep*. 2015;34:1815-1824. doi:10.3892/or.2015.4156

99. Sen S, Dong M, Kumar S. Isoform-specific contributions of alpha-actinin to glioma cell mechanobiology. *PLoS One*. 2009;4:e8427. doi:10.1371/journal.pone.0008427

100. Yu G, Wang Z, Zeng S, et al. Paeoniflorin inhibits hepatocyte growth factor- (HGF-) induced migration and invasion and actin rearrangement via suppression of c-met-mediated RhoA/ROCK signaling in glioblastoma. *Biomed Res Int*. 2019;2019:9053295. doi:10.1155/2019/9053295

101. Stylli SS, Stacey TT, Kaye AH, Lock P. Prognostic significance of Tks5 expression in gliomas. *J Clin Neurosci*. 2012;19:436-442. doi:10.1016/j.jocn.2011.11.013

102. Chen YC, Baik M, Byers JT, Chen KT, French SW, Diaz B. TKS5-positive invadopodia-like structures in human tumor surgical specimens. *Exp Mol Pathol*. 2019;106:17-26. doi:10.1016/j.yexmp.2018.11.005

SUPPORTING INFORMATION

Additional supporting information may be found in the online version of the article at the publisher's website.

SUPPLEMENTARY INFORMATION

gen	adnotacja RefSeq	ENCORI	miRDB	PicTar	TargetScan
ATRN	NM_139321	+	+	-	+
CDH2	NM_001792	+	+	+	-
CDH8	NM_001796	-	+	-	-
ELFN2	NM_052906	-	+	-	+
FLRT2	NM_001346144	+	-	+	+
HAPLN1	NM_001884	-	+	+	+
HTR7	NM_000872	-	+	+	-
NCAN	NM_004386	-	+	-	+
PRG4	NM_001127708	-	+	-	-
RELN	NM_005045	-	+	+	+
SDC2	NM_002998	+	+	+	+
SGCZ	NM_001322879	-	+	+	+
TNC	NM_002160	+	+	-	+

SUPPLEMENTARY INFORMATION

gene	fold change	p-value	RefSeq record
ITGAV	14,0419	0,049032	NM_002210
COL12A1	13,2538	0,043311	NM_004370
ITGA3	9,3718	0,03991	NM_002204
ACTN3	2,32668	0,037733	NM_001104
ITGB3	1,1824	0,045621	NM_000212
ICAM1	-1,0527	0,049994	NM_000201
VIM	-1,16366	0,04722	NM_003380
FN1	-1,1849	0,046053	NM_002026
RND3	-1,2241	0,044132	NM_005168
TIMP3	-1,26043	0,042594	NM_000362
LAMC1	-1,34694	0,048150	NM_002293
WASF2	-1,3645	0,045001	NM_006990
MET	-1,3771	0,013717	NM_000245
WIPF1	-1,3835	0,020224	NM_003387
EGF	-1,3867	0,025987	NM_001963
FAP	-1,4093	0,016415	NM_004460
ITGA4	-1,4093	0,025599	NM_000885
ROCK1	-1,4126	0,006	NM_005406
FGF2	-1,4126	0,014704	NM_002006
ARHGEF7	-1,4224	0,00922	NM_003899
MYLK	-1,4257	0,017474	NM_053025
STAT3	-1,4828	0,042723	NM_003150
MYH9	-1,5245	0,021593	NM_002473
CFL1	-1,5637	0,035133	NM_005507
ACTR3	-1,5674	0,027278	NM_005721
MSN	-1,571	0,001185	NM_002444
ITGB1	-1,6339	0,040562	NM_002211
TLN1	-1,6876	0,000969	NM_006289
RASA1	-1,7231	0,011208	NM_002890
HGF	-1,7634	0,031988	NM_000601
CDC42	-1,7715	0,032539	NM_001791
RHO	-1,7839	0,044098	NM_000539
ACTR2	-1,8553	0,004925	NM_005722
PTPN1	-1,8682	0,000465	NM_002827
ACTN1	-1,8682	0,01462	NM_001102
IGF1	-1,9341	0,020683	NM_000618
TNC	-1,9852	0,031457	NM_002160
RHOA	-2,0162	0,048735	NM_001664
MYH10	-2,035	0,021525	NM_005964
BAIAP2	-2,1019	0,000482	NM_006340
PTK2B	-2,5111	0,018089	NM_004103
WASL	-2,5344	0,00463	NM_003941
CTTN	-2,7226	0,000898	NM_005231
CRK	-2,9383	0,00659	NM_016823
SH3PXD2A	-3,0209	0,000972	NM_014631
PTEN	-3.056	0,044654	NM_000314
PIK3CA	-3,6765	0,042649	NM_006218

Grabowska M, Misiorek JO, Zarębska Ż, Rolle K.

Applications of noncoding RNAs

in brain cancer patients

Applications of noncoding RNAs in brain cancer patients

Małgorzata Grabowska, Julia O. Misiorek, Żaneta Zarębska and Katarzyna Rolle

Department of Molecular Neurooncology, Institute of Bioorganic Chemistry, Polish Academy of Sciences, Poznań, Poland

2.1 Introduction

The number of patients suffering from cancer is constantly growing and, according to the data from the International Agency for Research on Cancer, it reached 18 million new cases worldwide in 2018. Cancer is also a leading cause of death in the world. Over 9 million of cancer patients were reported to die in the year 2018, although the incidence of brain and central nervous system cancers accounted only for 1.6% of all aforementioned cancer cases; high tumor aggressiveness, poor prognosis, and high mortality rate prompt researches to focus especially on this type of cancer (Ferlay et al., 2019). Brain tumors are either developed de novo or less commonly as a result of metastasis. The primary cancers that most frequently metastasize to brain are lung cancer (43.2%), breast cancer (15.7%), melanoma (16.4%), colorectal cancer (9.3%), and renal cell carcinoma (9.1%) (Berghoff et al., 2016).

2.1.1 Types of brain cancer

Brain tumors are generally classified based on the World Health Organization (WHO) system which is primarily focused on tumors' pathological features. Grade I and II tumors are considered benign ones, while grade III and IV tumors belong to malignant ones. Here, we aim to focus on glioblastoma multiforme (GBM) and medulloblastoma (MB), the most malignant brain tumors of grade IV. They are further subclassified based on the tumor location, the predominating type of the neoplastic cells which are either

17

oligodendrocytes or astrocytes, and the major molecular events which contribute to the tumor formation (Louis et al., 2016).

2.1.1.1 Medulloblastoma

MB is defined as an embryonal tumor of the posterior fossa (space located in the bottom of the skull, close to the brainstem and cerebellum) which mainly affects children (Millard & De Braganca, 2016; Udaka & Packer, 2018). MB is classified, according to the WHO guidelines, into five histological subtypes: (1) classic, (2) desmoplastic, (3) anaplastic, (4) large cell, and (5) MB with extensive nodularity (MBEN) (Kijima & Kanemura, 2016; Louis et al., 2016). When considering the molecular events responsible for tumorigenesis, MB is classified into (1) wingless (WNT)-activated, (2) sonic hedgehog (SHH)-activated TP53-mutant, (3) SHH-activated/TP53-wildtype, and (4) non-WNT/non-SHH with further sub-classification into group 3 (G3) and group 4 (G4) of poorly defined pathogenesis and undetermined signaling pathways (Louis et al., 2016).

The most common WNT-MBs display the most promising prognosis among MBs, with the survival rate of 95% (Northcott et al., 2012). WNT-MBs harbor activating somatic mutations in gene-encoding β-catenin (*CTNNB1*) which leads to constitutively active WNT signaling through the stabilization of β-catenin (Northcott et al., 2019). Approximately 30% of all MB cases are SHH-MBs with survival rate of 75% (Northcott et al., 2012). SHH-active tumors are characterized with the dysregulation of SHH signaling. Germline mutations occur in the genes of negative pathway regulators such as *PTCH1* and SUFU. Moreover, aberrations in the copy number of target genes such as *MYCN* and *GLI2* are present (Cavalli et al., 2017). Additional mutations of *TP53* in SHH-MBs are associated with extremely poor outcomes (Northcott et al., 2012). The most aggressive MBs, with 5-year overall survival (OS) of <60%, are within G3 subtype (Northcott et al., 2019). To this group belong 25% of all MBs, nearly half metastatic at the time of diagnosis (Northcott et al., 2012). These tumors are characterized with aberrant expression of *MYC* (**my**elo**c**yto**matosis**) proto-oncogene (Northcott et al., 2019). G4, the most common and least defined subtype, accounts for 35% of all MB tumors and almost 50% of adolescent patients (Northcott et al., 2019). Interestingly, this subtype effects three times more frequently men than women (Northcott et al., 2012).

2.1.1.2 Glioblastoma multiforme

GBM is the most lethal among infiltrating gliomas. The WHO classification of brain tumors from 2016 assigns glioblastoma into a group of diffuse astrocytic and oligoden-droglial tumors (Louis et al., 2016). GBM is characterized by genetic instability and alterations in chromosome structure and copy number. To the most significant, somatically mutated genes in GBM belong *IDH (isocitrate dehydrogenase), TP53, PTEN (phosphatase and tensin homolog), NF1, EGFR, RB1*, and *PIK3R1*. Based on mutations in *IDH1* and *IDH2* genes encoding isocitrate dehydrogenase, GBM is classified into IDH-mutant and IDH wild-type subtypes. The most common GBM is of IDH wild-type since it occurs in 90% of all cases (Louis et al., 2016). On the other hand, tumors with mutations in *IDH1* are less aggressive and have better prognosis (Waitkus et al., 2018). *IDH* mutations together with methylation status of the *O*-methylguanine-DNA methyltransferase (*MGMT*) gene promoter are the main biomarkers used by clinicians for treatment selection so far.

2.1.2 Types of ncRNAs and mechanism of action

One of the most novel, promising biomarkers of brain cancers can be noncoding RNAs (ncRNAs) (International Human Genome Sequencing Consortium, 2004), expression of which is generally dependent on the status of cell development, various pathway activation, response to environmental stimuli, as well as pathological conditions (Hombach & Kretz, 2016; Latowska et al., 2020). What is more important in that context is their cell- and tissue-specific expression pattern. In herein chapter, we focus on three types of ncRNAs: microRNA (miRNA), long noncoding RNA (lncRNA), and circular RNA (circRNA), and describe their applications in MB and GBM patients.

2.1.2.1 MicroRNA

MiRNAs are short [19−25 nucleotide (nt)] ncRNAs. They regulate gene expression of more than 30% mammalian genes at the posttranscriptional level (Lewis et al., 2005). Recent analysis based on combined in silico high- and experimental low-throughput validations indicated the existence of 2300 mature miRNAs (Alles et al., 2019).

The canonical pathway of miRNA biogenesis in mammals begins with the transcription of pri-miRNA, which is then cleaved by a ribonuclease III Drosha to the 60−70 nt long pre-miRNA and exported then to the cytoplasm. RNase III Dicer catalyzes the formation of 19−35 nt double-stranded miRNA duplex, which is subsequently loaded into AGO (Argonaute) protein and proceed in a process named strand selection, when generally a strand with the lower thermodynamic stability at the 5′ end becomes degraded (Denli et al., 2004; Han et al., 2004; Meijer et al., 2014; Schwarz et al., 2003). MiRNAs processing can be also through noncanonical pathways, for example, Dicer-independent ones (Stavast & Erkeland, 2019).

In most cases, miRNA interact with the 3′ UTR (untranslated region) of target messenger RNAs (mRNAs) and suppress gene expression. Nonetheless, it is also possible for miRNAs to interact with the 5′ UTR and the coding sequence (Spengler et al., 2016; Wongfieng et al., 2017). Interaction between miRNA and mRNA occurs based on sequence complementarity. The mRNA response elements (MRE) present on transcript pair with a seed region located at position 2−8 nt on the 5′ end of the miRNA (Kiriakidou et al., 2004; Wang et al., 2006). Many sites that match the seed region, particularly those in the 3′ UTR, are preferentially conserved (Friedman et al., 2009). One miRNA can target many different mRNAs and one transcript can be regulated by multiple miRNAs (Balachandran et al., 2020). Interestingly, almost half of the miRNA target genes are located near genomic regions which are associated with the processes responsible for neoplasm formation (Kozomara & Griffiths-Jones, 2011). Therefore the expression of miRNAs in tumors differs from healthy cells and is usually associated with the characteristics of malignancy. Suppressor miRNAs inhibit cancer cells proliferation (Godlewski et al., 2008; Lee et al., 2014; Ruan et al., 2015) and invasion (Lee et al., 2014; Lv et al., 2017; Que et al., 2015; Ruan et al., 2015) and also make chemotherapy more effective (Shi et al., 2014; Tian et al., 2016; Xiao et al., 2016), while oncomiRs promote metastasis (Esquela-Kerscher & Slack, 2006; Huang et al., 2017; Kaid et al., 2015).

2.1.2.2 Long noncoding RNA

LncRNAs are linear transcripts generally longer than 200 nt. They are mostly transcribed by RNA polymerase II, have cap at their 5′ end, and undergo splicing similar to mRNAs. Some of lncRNAs also have 3′ polyadenylated ends, include promoter regions, and display a coding potential for short peptides. Based on their genomic location, lncRNAs are classified as intergenic (located between protein-coding genes), bidirectional (transcribed form the same promoter in the opposite directions), antisense (transcribed form noncoding strand), and sense-overlapping (located on one or more introns/exons in the coding strand direction) lncRNAs (Balas & Johnson, 2018). The fundamental role of lncRNAs is the regulation of transcription; thus their presence may serve as an indicator of transcription activity of many genes (Quinn & Chang, 2016). Moreover, lncRNAs can also interact, and thus, remodel chromatin structure and be involved in posttranslational regulation. The regulatory role of lncRNA is performed through various mechanisms which still need to be uncovered. LncRNAs have the ability to form secondary structures and are assigned as guides, decoys, precursors of small ncRNAs or miRNA sponges, which all strongly affect gene expression in cells (Jarroux et al., 2017). Not only lncRNA products can be regulative but also the process of lncRNA transcription itself may have a regulatory character. This emphasizes the importance of studies on the regulation of lncRNAs transcription. LncRNAs can be localized and, thus, act in either nucleus or cytoplasm or both localizations (Carlevaro-Fita & Johnson, 2019).

A strong tissue-specific expression pattern of lncRNAs has been observed, especially in testis and brain (Derrien et al., 2012). The importance of lncRNAs in different biological processes has also been demonstrated like development, stress, and tumorigenesis (Carlevaro-Fita et al., 2020; Perry & Ulitsky, 2016; Valadkhan & Valencia-Hipolito, 2016). The pathogenic role of lncRNAs has been reported in diseases often affecting nervous system like Alzheimer's disease or heritable Huntington's disease (Johnson, 2012; Zhou & Xu, 2015). Some data also point to the role of lncRNAs in the pathogenesis and progression of brain tumors, including GBM (Han et al., 2012; Li et al., 2016), in which a strong lncRNA deregulation is observed. LncRNAs are found to act either as promoters or suppressors of GBM by serving as miRNA sponges, modifying chromatin or methylating DNA (Mazor et al., 2019).

2.1.3 Circular RNA

CircRNAs are a class of noncoding, single-stranded RNAs with a characteristic structure of covalently closed loop. Compared to mRNA, they lack typical modifications: a cap at 5′ end and a poly(A) tail at 3′ end (Chen & Yang, 2015). CircRNAs are evolutionary conserved among the species, abundantly expressed in human brain, as well as exhibit cell- and tissue-specific expression pattern (Jeck et al., 2013; Memczak et al., 2013; Rybak-Wolf et al., 2015; Salzman et al., 2013). The basic functions of circRNA include the regulation of gene expression through miRNA sponging, interactions with RNA-binding proteins (RBPs) and their sponging. Moreover, circRNAs act as scaffolds for protein complex assembly, participate in transcription regulation, or serve as templates for protein translation (Bose & Ain, 2018; Huang et al., 2020; Mo et al., 2019; Pamudurti et al., 2017; Panda, 2018; Schneider & Bindereif, 2017; Zang et al., 2020; Zlotorynski, 2015). However, the knowledge regarding their basic mechanisms of action and comprehensive interaction network is still missing. CircRNAs can arise from both exons and introns and, thus, are
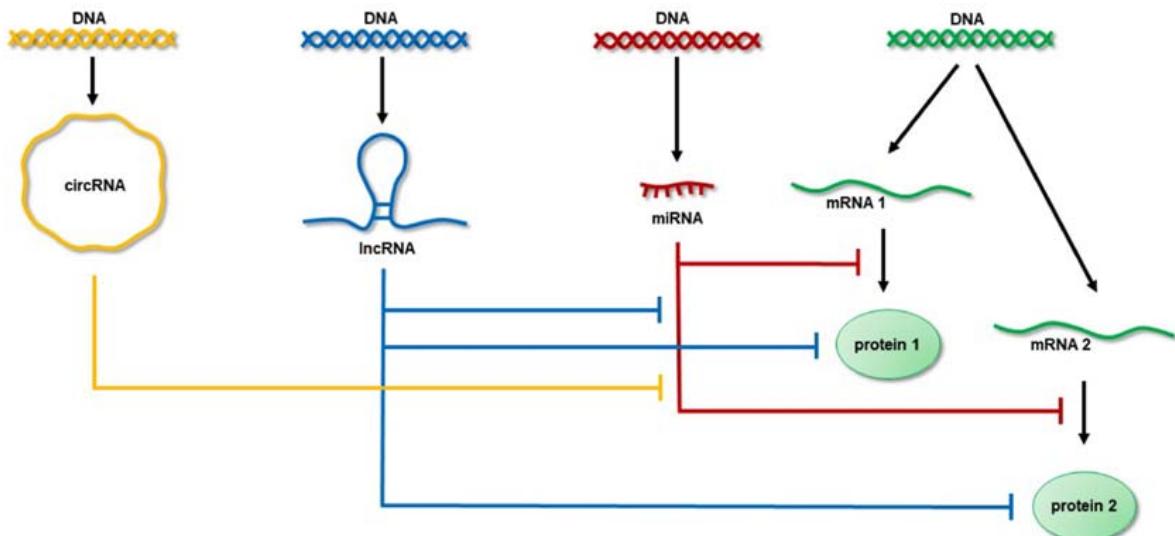
FIGURE 2.1 Competitive endogenous RNA hypothesis. In general, miRNA can inhibit the translation of multiple proteins, circRNAs together with lncRNAs by binding to miRNAs, prevent them from influencing the translation processes. *circRNA*, circular RNA; *lncRNA*, long noncoding RNA; *miRNA*, microRNA.

classified as exonic circRNAs, intronic circRNAs, and exon−intron circRNAs. The biogenesis of exon−intron circRNAs is similar to exon circRNA, except that the intron sequence is preserved and the fusion of circRNA occurs via chromosomal translocations (Greene et al., 2017; Guarnerio et al., 2016; Liu et al., 2019). Most circRNAs are of exonic type, derived from protein-coding genes (Guo et al., 2014). Majority of circRNAs are generated via back-splicing process (Barrett et al., 2015).

CircRNAs are involved in cancer initiation and progression by acting either as tumor suppressors or tumor promoters (also known as oncogenic circRNAs) (Bach et al., 2019). Comprehensive studies on circRNA implicated their role in processes like proliferation, angiogenesis, invasion, metastasis, and senescence (Kristensen et al., 2018). Recent investigations provide evidence for circRNA involvement in human diseases by disrupting circRNA−miRNA−mRNA axis and deregulating signaling of various pathways. NcRNAs like lncRNA or circRNA have a common functionality in their ability to modify gene expression by miRNA titration in a phenomenon known as the competitive endogenous RNA (ceRNA) (Salmena et al., 2011) (Fig. 2.1).

2.2 Data sets for noncoding RNAs analysis

Progressive advancement in the field of bioinformatics enables to deposit and analyze huge amounts of genomic data. Moreover, novel integration methods and developed algorithms facilitate the translation of obtained data into research findings of potential clinical application. In herein section, we aim to present some of commonly used RNA-seq deposit platforms as well as databases that are useful in the analysis of ncRNAs in the studies on brain cancer. Some of commonly used tools for miRNA, lncRNA, and circRNA analyses are listed in Table 2.1.

TABLE 2.1   Deposits and databases for microRNA (miRNA), long noncoding RNA (lncRNA), and circular RNAs (circRNAs) used in brain cancer research.

Databases and tools	Description	Web source	Reference
miRDB	miRNA targets prediction with gene ontology enrichment analysis	http://www.mirdb.org	Chen and Wang (2020)
DIANA	miRNA target prediction, databases of experimentally validated targets and identifying of altered molecular pathways	http://diana.imis.athena-innovation.gr/DianaTools	Paraskevopoulou et al. (2013)
PITA	miRNA targets prediction	https://genie.weizmann.ac.il/pubs/mir07/mir07_prediction.html	Kertesz et al. (2007)
TargetScan		http://www.targetscan.org/vert_72	Agarwal et al. (2015)
RNA22		https://cm.jefferson.edu/rna22	Miranda et al. (2006)
RNAhybrid	Searching for minimal free energy needed for hybridization between long and short RNA	https://bibiserv.cebitec.uni-bielefeld.de/rnahybrid	Rehmsmeier et al. (2004)
LncLocator	lncRNA subcellular localization prediction	http://www.csbio.sjtu.edu.cn/bioinf/lncLocator	Cao et al. (2018)
RNAInter	Gathers experimentally and computationally predicted RNA interactor from over 30 databases	https://www.rna-society.org/rnainter	Lin et al. (2020)
SFPEL-LPI	Prediction of lncRNA-protein interactions	http://www.bioinfotech.cn/SFPEL-LPI	Zhang et al. (2018)
CPPred	Determining lncRNA probability to encode proteins	http://www.rnabinding.com/CPPred	Tong and Liu (2019)
CNIT		http://cnit.noncode.org/CNIT	Guo et al. (2019)
circBase	Unified data sets of circRNAs and scripts to identify known and novel circRNAs	http://www.circbase.org	Glazar et al. (2014)
CIRCpedia v2	Comprehensive circRNA annotation across six different species	http://www.picb.ac.cn/rnomics/circpedia	Dong et al. (2018)
Circbank	Predicting of miRNA binding, coding potential, conservation, circRNA mutation, and methylation	http://www.circbank.cn	Liu et al. (2019)
CircAtlas 2.0	Contains circRNAs expression pattern, conservation, and functional annotation	http://circatlas.biols.ac.cn	Wu et al. (2020)
TSCD	Tissue-specific circRNAs in human and mouse	http://gb.whu.edu.cn/TSCD	Xia et al. (2017)

(*Continued*)

TABLE 2.1   (Continued)

Databases and tools	Description	Web source	Reference
exoRBase	circRNA, lncRNA, and mRNA in human blood exosomes	http://www.exoRBase.org	Li et al. (2018)
CircFunBase	Experimentally validated circRNAs and predicted functions and interactions	http://bis.zju.edu.cn/CircFunBase	Meng et al. (2019)
deepBase v2.0	The decoding evolution, expression patterns, and functions of ncRNAs	http://biocenter.sysu.edu.cn/deepBase	Zheng et al. (2016)
TRCirc	Transcriptional regulation of circRNAs, expression, and methylation levels	http://www.licpathway.net/TRCirc	Tang et al. (2019)
CSCD	Cancer-related circRNAs	http://gb.whu.edu.cn/CSCD	Xia et al. (2018)
MiOncoCirc		https://mioncocirc.github.io	Vo et al. (2019)
circ2GO		https://circ2go.dkfz.de	Lyu et al. (2020)
CircRiC		https://hanlab.uth.edu/cRic	Ruan et al. (2019)
Circ2Traits	Disease-related circRNAs	http://gyanxet-beta.com/circdb	Ghosal et al. (2013)
Circad		http://clingen.igib.res.in/circad	Rophina et al. (2020)
Circ2Disease		http://bioinformatics.zju.edu.cn/Circ2Disease/index.html	Yao et al. (2018)
CircR2Disease		http://bioinfo.snnu.edu.cn/CircR2Disease	Fan et al. (2018)
circRNA disease		http://cgga.org.cn:9091/circRNADisease	Zhao et al. (2018)
LncRNADisease 2.0		http://www.rnanut.net/lncrnadisease	Bao et al. (2019)
CircInteractome	RBP- and miRNA-binding sites mapping, primers design, and siRNAs, with potential IRES identification	http://circinteractome.nia.nih.gov	Dudekula et al. (2016)
circRNAprofiler	circRNAs detected by multiple annotation-based detection tools combining	https://github.com/Aufiero/circRNAprofiler	Aufiero et al. (2020)
Cerina	Inferring the circRNA function based on the competing endogenous RNA model	https://github.com/jcardenas14/CERINA	Cardenas et al. (2020)
CircCode	Investigation of the coding ability of circRNAs	https://github.com/PSSUN/CircCode	Sun and Li (2019)

mRNA, Messenger RNA; *RBP*, RNA-binding protein; *siRNA*, short interfering RNA.

2.2.1 RNA-seq deposits and data sets

Up-to-date next-generation sequencing (NGS) technologies enable to sequence a non-coding transcriptome, including miRNAs, lncRNAs, and circRNAs, even at a single-cell resolution. The raw data obtained from RNA-seq can be deposited in numerous data repositories and easily accessed by other users. For example, The Cancer Genome Atlas (TCGA), supervised by the National Cancer Institute's (NCI), Center for Cancer Genomics, and the National Human Genome Research Institute, has gathered over 2.5 petabytes of genomic, epigenomic, transcriptomic, and proteomic data using processed sequencing data of 33 cancer types with matched samples from healthy individuals so far. Since processing such a large amount of data remains challenging, a platform to search and download cancer data for analysis has been established. Genomic Data Commons is a research program of the NCI, which serves as a unified data repository and enables sharing cancer genomic data. It provides an access to high-quality data sets from NCI programs, like among others TCGA and Therapeutically Applicable Research to Generate Effective Therapies (Grossman et al., 2016).

2.3 Expression of noncoding RNAs in brain cancer patients

In the last few years, new technologies, such as next generation sequencing (NGS), have collected a significant amount of data, making it easier to compare different specimens. Here, we describe the sample types collected from brain cancer patients which are used to determine ncRNA expression for diagnostic and prognostic purposes. We also present different models to evaluate ncRNA expression for research purposes, with a special emphasis on cancer stem cells (CSCs).

2.3.1 Sample types used for analyzing noncoding RNAs in brain

The samples used to determine the ncRNA expression profile in brain cancer patients may come from dissected tumor tissue (both ante- and postmortem) or biopsy, including liquid biopsy, such as cerebrospinal fluid (CSF) and blood (Fontanilles et al., 2018).

The components of blood-derived biomarkers have been described in brain tumor patients and include circulating tumor cells, nucleic acids, and exosomes. CSF, collected during lumbar puncture or surgical operation, contains circulating tumor DNA, exosomes, and proteins derived from the brain tumor (Fontanilles et al., 2018). MiRNA, lncRNA, and circRNA can be detected in both blood plasma (Chen et al., 2020; Li et al., 2019; Liao et al., 2019; Roth et al., 2011; Wang et al., 2019) and in CSF (Akers et al., 2015; He et al., 2019; Kopková et al., 2019; Wang et al., 2018).

2.3.2 Models to study ncRNA expression

Basic research in a cancer field is mainly focused on studying the involvement of individual molecules, as a part of complex pathways, which are involved in tumorigenesis and cancer progression. In vitro studies are usually conducted on primarily established or commercially

available cell lines and organoids. These in vitro models are relatively cheap and easy to cultivate and conducted in a wide range of experiments. Currently, there are 46 human GBM and 4 human MB cell lines banked and available from the American Type Culture Collection (https://www.lgcstandards-atcc.org/). The disadvantage of using GBM established lines, which needs to be considered, is their astrocytic differentiation appearing upon medium supplementation with serum (Robertson et al., 2019). Another drawback is that DNA profile of long-term grown cells may differ from that of the newly purchased cells, which can lead to misidentification of widely used cell lines (Allen et al., 2016). Also, global gene expression revealed that established cell lines display many genomic changes and gene expression fluctuations not present in primary tissues (Li et al., 2008).

To maintain the physiological microenvironment, patient-derived tumor cells can be implanted into immunodeficient mice—an orthotopic patient-derived xenograft model that can arise either by direct inoculation of cell suspension right after surgery, or by inoculation of patient-derived cell cultures with enhanced tumor-initiating potential (Xu et al., 2018).

Another research model possible to be applied in brain cancer studies is genetically engineered mouse model (GEMM) in which tumor is developed de novo via the introduction of gene alterations previously identified in human cancer (Simeonova & Huillard, 2014). This model is obtained by genetic engineering techniques, via utero electroporation and viral gene transfer (Roussel & Stripay, 2020). Unfortunately most of GEMMs possess a *TP53* negative background, whereas *TP53* mutations are observed only in 10% of MB patients (Zhukova et al., 2013). Moreover GBM mouse models lack the intratumor heterogeneity observed in human tumors (Lenting et al., 2017), which indicates the need to adjust the model to the type of cancer under study.

As cell cultures grown in a two-dimensional monolayer do not fully reflect the complexity of tumor mass plus they lack tumor microenvironment which stimuli substantially contribute to tumor initiation and progression, thus there is strong need to introduce the models better reflecting the native tumor (Ivanov et al., 2016). Stem-cell biology has been extensively explored in the past decade, with a special emphasis on CSCs. Along the studies dedicated to CSCs, it has been discovered that these cells display a high proliferation rate (Hamburger & Salmon, 1977) and, thus, can self-renew, as well as are able to differentiate into neurons, astrocytes, and oligodendrocytes (Singh et al., 2004).

GBM stem cells (GSCs) and MB stem cells (MBSCs) could be isolated from primary brain tumor cells using a surface marker of neural stem cells—CD133 (prominin 1) (Ding et al., 2013). Additionally, the pool of stem-cell markers, which gene expression is also increased in CSCs, including NANOG, OCT4, SOX2, BMI1, NESTIN (neuroepithelial stem cell protein), OLIG2, MYC, IDI1, and surface markers CD44, CD15, L1CAM, A2B5 may be used to verify the presence of CSCs (Guo et al., 2011; Ruiz-Garcia et al., 2020). Under neural stem-cell culture conditions, GSC and MBSC grow as 3D culture models—floating multicellular spheroids, neurospheres (Ahmad et al., 2015; Jayakrishnan et al., 2019). Currently, neurospheres are the most commonly used 3D culture model for GBM (Andreatta et al., 2020; Azari et al., 2011; Badodi & Marino, 2019).

GSC have been already shown to be capable of differentiating into endothelial cells allowing for tumor blood vessel formation and may also be involved in the infiltration of GBM into surrounding tissue (Ricci-Vitiani et al., 2010). Furthermore, hypoxia niche for

GSC is hypostatized to promote quiescence, a GSC phenotype that could highly contribute to the enrichment of chemo- and radioresistant subpopulations (Seidel et al., 2010). These features of CSCs have been shown to induce tumor recurrence and progression (Singh et al., 2004). Treatment resistance is widely known phenomenon of glioma patients, as it significantly narrows the possibilities of choosing therapeutic strategy. CSC-mediated resistance response is the subject of wide and comprehensive studies, while this particular fraction of cells is considered to be responsible for glioma aggressive phenotype.

Organoids are 3D structures, commonly derived from patient stem cells, embedded in a matrix. They grow in medium supplemented with a cocktail of growth factors and begin to proliferate and differentiate, self-organizing into an organotypic structure (Andreatta et al., 2020). The first protocol for establishing a culture of cerebral organoids was generated by Lancaster et al. (2013). In a similar way, it is also possible to generate a tumor model directly from patients' biopsies. This method enables to capture the heterogeneity within patients' tumors (Jacob et al., 2020), what makes them a valuable tool for drug screening and precision medicine (Andreatta et al., 2020). Ogawa et al. developed a cancer model of gliomas in human cerebral organoids allowing the observation of tumor initiation. Cells with integrated oncogenic *RAS* (rat sarcoma) expression cassette in the suppressor *TP53* locus rapidly become invasive overwhelming the entire organoid (Ogawa et al., 2018). Another newly proposed model is a neoplastic cerebral organoid, where via transposon- and CRISPR/Cas9-mediated mutagenesis authors introduced into the organoids 18 single gene mutations or amplifications as well as 15 of the most common clinically relevant combinations observed in brain tumors (Bian et al., 2018). Recently, cerebral organoid glioma assembly (GLICO) model has been presented, in which hESC- or iPSC-derived cerebral organoids are cocultured with patient-derived glioma stem cells (Linkous et al., 2019).

2.3.3 NcRNA expression profiles in cancer stem cells and their consequences on tumor development

The presence of CSCs in brain tumors stimulates tumor aggressiveness; thus it is of special interest to identify factors, including ncRNAs, which could shape the specific properties of CSCs and at the same time have potential in therapies. MiRNA expression profile in human neural stem cells and glioma stem cells from patient revealed 116 upregulated and 62 downregulated miRNAs in GSCs. The upregulation of miR-198, miR-146b-5p, miR-152, and miR125a-3p, and downregulation of miR-137 were further confirmed by quantitative reverse transcription polymerase chain reaction (qRT-PCR) analysis (Liu et al., 2014). Studies applying combined microarray and deep sequencing analyses pointed out a set of 10 miRNAs with different expression between GSC and neural stem cells (NSC). Among them, 5 miRNAs were upregulated in GSC including: miR-10a, miR-10b, and miR-140-5p, while downregulated: miR-124 and miR-874 (Lang et al., 2012). Another miRNA microarray research notices 69 differentially expressed miRNAs between the CD133+ and CD133− GBM cells. Lower expression of miR-125b, let-7a, and let-7c, and higher expression of miR-638 and miR-149 were subsequently verified in GSCs. Overexpression of miR-125b inhibited the self-renewal ability of CD133+ cells (Wu et al., 2012).

Global miRNA expression analysis of 10 paired GSC and nonstem GBM cultures concluded with the presentation of 51 most deregulated miRNAs. Total 14 of them correlated to both SOX2 and NESTIN expression: miR-3195, miR-3141, miR-4656, miR-100-5p, miR-4739, miR-3180, miR-1260b, miR-1233-5p, miR4674, miR-328-5p, miR-378h, miR-4505, miR-5787, and miR-1207-5p (Sana et al., 2018). Using the established neurosphere cell lines with and without SOX2-knockdown, the influence of SOX2 on the miRNA profile of GSC was investigated. Forced expression of SOX2 increased levels of miR-128b and miR-425-5p. Additionally an increase in miR-425-5p expression in GBM tumors was proved. Further investigations indicated that miR-425-5p inhibition repressed neurosphere formation, activates apoptosis, and suppress survival pathways in GSCs (de la Rocha et al., 2020).

Studies on the influence of miRNAs on the ability of GSCs to create neurospheres are also a valuable source of information, as they indicate the association of short ncRNAs with the malignant nature of cancer. Overexpression of miR-128 (Godlewski et al., 2008), miR-218 (Tu et al., 2013), and miR-181c (Ruan et al., 2015) decreases the number and volume of neurospheres affecting self-renewal capacity of GSCs.

Expression profiling of MB primary specimens pointed out 21 upregulated and 12 downregulated miRNAs in relative to CD133 + neural stem cells. The most upregulated, with fold change >6, were miR-127-3p, miR-495, miR-409-3p, miR-376c, miR-144*, miR-143, miR-146a, miR-126, miR-126*, and miR-223, while the most downregulated, with the fold change <5, were miR-10a, miR-935, miR-219−2-3p, and miR-504 (Genovesi et al., 2011). Another small RNA sequencing study was performed on SHH MBSCs, and its results were compared to neural stem cells miRNome. In SHH MBSCs, 35 upregulated and 133 downregulated miRNAs were identified. After validation by real-time PCR, higher expression of miR-20a-5p and miR-193a-5p and lower expression of miR-222-5p, miR-34a-5p, miR-345-5p, miR-210-5p, and miR-200a-3p were confirmed (Po et al., 2018). An miRNA profile analysis of the MBSC before and after retinoic acid−induced differentiation revealed 22 miRNAs differentially expressed after 48 h of treatment. It has been confirmed that after differentiation, the levels of miR-195 and miR-145 decrease, while the level of miR-135b increases (Catanzaro et al., 2016).

Total 61 MB patients' analysis indicated higher expression of miR-199b-5p in nonmetastatic cases. Overexpression of that miRNA decreased the MBSC subpopulation in DAOY, medulloblastoma cell line (Garzia et al., 2009). Decrease of CD133 + in DAOY cells, and a reduction in NESTIN staining, was observed also upon miR-34a overexpression (de Antonellis et al., 2011). Studies carried out on various MB cell lines indicated that cells overexpressing miR-367 are more capable of generating expressing CD133 neurospheres than control cells (Kaid et al., 2015). Instead increasing the level of miR-584-5p reduces neurospheres formation together with the reduction of CD133 and MYC markers (Abdelfattah et al., 2018).

An atypical teratoid rhabdoid tumor (ATRT) is a rare, extremally malignant pediatric brain tumor. In CSC subset population isolated from ATRT, miR142-3p downregulation was observed. Overexpression of that miRNA inhibited migration, invasion, and self-renewal of ATRT CD133 + cells (Lee et al., 2014).

lncRNAs have been shown to play essential, regulatory roles in GSCs. Recent studies have revealed differences in splicing and expression profiles of lncRNA present between mesenchymal and proneural subtypes of GSCs, which renders these molecules as

GSC-type specific biomarkers. Moreover, these lncRNAs from differentially expressed pool were found to be associated with GBM prognosis and survival and included CTD-2589M5.5, MYOSLID, CRNDE (Colorectal Neoplasia Differentially Expressed), AC005264.2, SOX21-AS1, RP11−575F12.1 as well as SOX21-AS1 lncRNAs (Guardia et al., 2020). The aberrant lncRNA expression levels have also been identified earlier and showed to affect GSC self-renewal and proliferation processes which, in turn, influence tumor development and progression. Initial microarray studies indicated that uc.283-plus lncRNA was highly expressed in glioma tumors and could affect cell pluripotency (Galasso et al., 2014). Another example is a high expression of lncRNA-ROR (regulator of reprogramming) which has been found in GSCs to negatively correlate to an expression of stemness marker Klf4 and lead to the inhibition of self-renewal and proliferation of these cells (Feng et al., 2015). The expression of other stemness markers SOX2 and nestin was found to be regulated by highly conserved lncRNA MALAT. Its downregulation has been shown to suppress the expression of these two factors and, thus, GSC proliferation (Han et al., 2016). Short interfering RNA (siRNA) downregulation of MALAT1 has also lead to the increased susceptibility of GSC to temozolomide (TMZ) treatment (Kim et al., 2018). Fang et al. (2016) revealed that the downregulation of lncRNA HOTAIR (HOX antisense intergenic RNA) leads to the inhibition of GSC proliferation and a loss of tumor ability to invade adjacent tissues. LncRNAs may also facilitate the interactions between nascent transcripts, like lncRNA FOXM1-AS promoting ALKBH5 and FOXM1 interactions which maintain the pool of GSCs (Zhang et al., 2017). A recent study has indicated TP73-AS1 lncRNA to be clinically significant in GBM. Its high expression levels have been identified specifically in GSCs and linked with poor prognosis as well as resistance to TMZ (Mazor et al., 2019). Current studies related to GSCs biology also explore the function of lncRNAs as "miRNA sponges" since differential expression of lncRNAs has been shown to strongly affect miRNA expression levels. For example, the lncRNA CRNDE has been found highly expressed in GBM tissues, specifically in GSCs, in parallel to downregulated levels of miRNA-186 (Zheng et al., 2015). Further mechanistic studies have revealed that CRNDE binds to and negatively regulates miRNA-186 which, in turn, cannot inhibit the transcription of its target genes *XIAP* and *PAK7*. Thus the overexpression of CRNDE in both in vitro cell culture and in vivo xenograft models promotes GSC proliferation as well as increases cell invasion and migration properties. Described herein studies indicate a strong regulatory role of lncRNA in GSC maintenance and potential to serve as prognostic biomarkers and future targets in therapies against brain cancer.

The expression of circRNA is characterized by dynamic changes during oncogenesis. In cancers and other diseases characterized by increased cell proliferation, decreased circRNA levels are often observed. Presumably, this effect was noticed due to a specific "dilution" caused by high division rate (Bachmayr-Heyda et al., 2015; Moldovan et al., 2019). A growing number of evidence revealed that dysregulated expression of circRNAs is implicated in the onset and development of glioma. A breakthrough event in study of the variability of circRNAs expression was the development of computational pipeline named UROBORUS that allowed for the detection of thousands of circRNAs in RNA-seq data obtained from glioma tissue in comparison with normal tissue samples (Song et al., 2016). The 1411 circRNAs differentially expressed in GBM patients were identified, whereas 1205 were shown to be downregulated and much fewer—206 upregulated

(Zhu et al., 2017). Furthermore, Yuan et al. (2018) took a step further and identified altered expression of 501 lncRNAs, 1999 mRNAs, 2038 circRNAs, and 143 miRNAs between glioblastoma tissue and matched normal brain tissue, revealing their downstream targets in the ceRNA network suggesting that glutamate metabolism might be involved in glioma genesis, development, and infiltration.

circRNAs have been reported to have a role in glioma chemoresistance; however, the detailed underlying mechanisms still needs to be unraveled (Hua et al., 2020; Yin & Cui, 2020; Zhao et al., 2020). The role of exosomes as a new way of circRNAs transfer has been highlighted for cancer diagnosis, therapy, prognosis, and chemoresistance. CircNFIX has been described as upregulated in glioma patient tissues, which is associated with increased glioma cell proliferation and migration by sponging miR-34a-5p. It has been shown that exosomal circNFIX is upregulated in the serum of temozolomide resistant glioma patients and is associated with poor prognosis. Furthermore, the downregulation of circNFIX led to the increase of the TMZ sensitivity in resistant glioma cells in vivo and in vitro. The authors assumed that the regulation of the TMZ resistance in glioma by circNFIX/miR-132 axis might be achieved by the modulation of ABCG2 expression, which have been reported to be a functional target of miR-132 in clear cell renal cell carcinoma (Reustle et al., 2018). Moreover, ABCG2 protein expression is regulated by the circNFIX/miR-132 axis in glioma cells under TMZ exposure and was shown to play a role in the chemoresistance of glioblastoma stem cells (Ding et al., 2020).

The potential role of circASAP1 in glioma chemoresistance has been recently investigated, as the circASAP1 expression was highly upregulated in recurrent GBM patient tissues and TMZ-resistant cell lines. The authors reported increased GBM cell proliferation and the TMZ resistance reduction after circASAP1 knockdown. Moreover, the study showed restored sensitivity to TMZ treatment of TMZ-resistant xenografts obtained by the reduction of circASAP1. The significant regulatory network of circASAP1/miR-502-5p/ neuroblastoma Ras (NRAS) has been identified, which shows that the circASAP1 might increase the expression of NRAS via sponging miR-502-5p (Wei et al., 2021).

Blood−brain barrier (BBB) states one of the major challenges of efficient drug delivery in brain tumors. Therefore surgical resection to the extent feasible following by adjuvant radiation therapy is widely used in the clinics for gliomas treatment (Stupp et al., 2005). Since the use of radiotherapy in glioblastoma treatment is constantly evolving and often used as adjuvant temozolomide therapy, there is a way for personalized treatment implementation taking into account patients' performance status (Barani & Larson, 2015). Since circRNAs are known as regulatory and competing endogenous RNAs, the activation of several pathways might have an impact on the chemo- and radioresistance (Jeyaraman et al., 2019). Su et al. revealed 57 upregulated and 17 downregulated circRNAs in human radioresistant esophageal cancer cell line KYSE-150R in comparison with parental cell line KYSE-150, which clearly shows the association of circRNAs with radioresistance in this type of cancer and might be associated with other types of cancer (Jin et al., 2020; Su et al., 2016).

Up to date much remains to be discovered in the field of circRNAs impact on glioblastoma patients' radioresistance. Zhao et al. identified the upregulation of 63 and downregulation of 48 circRNAs in extracellular vesicles (EVs) of radioresistant U251 cell line in comparison to nontreated U251 cells. CircATP8B4 have been discovered to be significantly
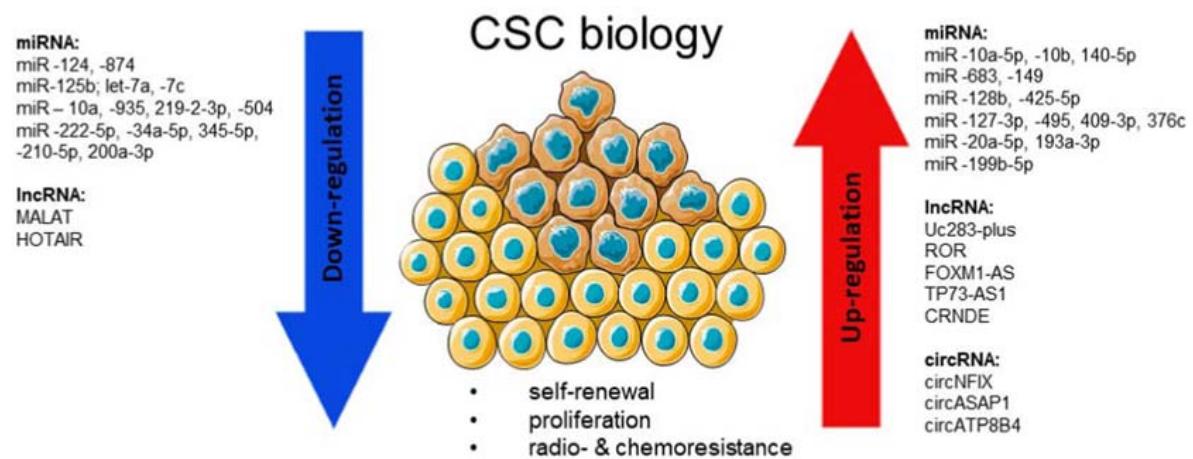
FIGURE 2.2   Aberrant expression profiles of ncRNAs in brain CSCs. The levels of indicated ncRNAs have been found either downregulated (left to the *blue arrow*) or upregulated (right to the *red arrow*) in CSCs isolated from patients' tissues and tissue-derived cell lines. These ncRNAs have been found to influence the biology of CSC, including their ability to self-renew and proliferate. Moreover, modulation in the expression of ncRNA indicated a strong impact of selected ncRNA on tumor resistance to radio- and chemotherapy. *CSC*, cancer stem cell; *ncRNA*, noncoding RNA.

elevated in radioresistant cells and acting as a sponge of miR-766-promoting cell radioresistance. However, future study of the circATP8B4/miR-766/mRNA axis mechanism of action is still needed; hence it is has been discovered that miR-766 acts as a tumor promoter or suppressor in multiple cancer types (Li et al., 2015; Zhao et al., 2019). Fig. 2.2 summarizes the level of different ncRNA expressions in CSC.

2.4 Experimental methods and tools for analyzing noncoding RNAs in brain cancer patients

2.4.1 Studying ncRNA interactions with targets by luciferase assays and ncRNA–protein interactions by immunoprecipitation

Firefly luciferase is commonly used as a reporter to evaluate in vitro transcriptional activity and it is considered the gold standard for the gene regulation studies (Chen et al., 2019; Clément et al., 2015; Jin et al., 2013; Sun et al., 2020; Tomasello et al., 2019; Zhang et al., 2019). The best characterized trait determining miRNA target recognition is pairing within the seed region. However, even 60% of seed interactions could be noncanonical, containing bulged or mismatched nucleotides (Helwak et al., 2013). Therefore target prediction methods based on finding complementarity between the MRE and the seed region may miss a large part of the miRNA–mRNA interaction. Later we present a description of a completely different approach, based on the detection of actually existing miRNA–mRNA interactions, in which the identification of individual elements is the final result, not the initial assumption of the experiment. The use of immunoprecipitation in glioma allowed for the recognition of interactions between lncRNA and miRNA (Fu et al., 2018), as well as circRNA and miRNA (Xu et al., 2018).

Cross-linking immunoprecipitation (CLIP) associated to high-throughput sequencing (CLIP-seq) is a technique used to identify RNA directly bound to RBPs. The application of CLIP-seq to AGO (AGO-CLIP) has been used to identify the miRNA-binding sites (Mato Prado et al., 2016). CLIP protocol begins with ultraviolet (UV) light irradiation of cells, during which covalent bonds between RNA−protein complexes are generated. This reaction only takes place between closely adjacent molecules so that only direct protein−RNA contacts can be cross-linked. Afterword RBPs are purified, mainly by the usage of antibodies. Simultaneously, to facilitate identification of binding sites, cross-linked RNA is partially RNase digested to ∼50 nt. Next proteins are removed with proteinase K leaving pure RNA, which could be used to complementary DNA (cDNA) synthesis and reverse transcription generating templates for sequencing (Jensen & Darnell, 2008). Main disadvantages of CLIP are mutations caused by UV light (Mato Prado et al., 2016). The efficiency of the protein−RNA cross-linking reaction is in the range of 1%−5% (Darnell, 2010). The CLIP technique is undergoing development and currently its new variants are available: the high-throughput sequencing of RNA isolated by CLIP (HITS-CLIP) (Licatalosi et al., 2008), the high-throughput sequencing of RNA isolated from photoactivable−ribonucleoside-enhanced-CLIP (PAR-CLIP) (Hafner et al., 2010), and the individual-nucleotide resolution CLIP (iCLIP) (König et al., 2010).

HITS-CLIP, supplementing the basic technique with bioinformatics approaches, reduces costs and increases the scope of received data by using NGS (Darnell, 2010). In PAR-CLIP a highly photoreactive ribonucleosides, such as 4-thiouridine (4SU) or 6-thioguanosine (6SG), is added into cell culture. As a result during reverse transcription, a characteristic mutation at the position of the cross-linked nucleotide, T−C for 4SU, G−A for 6SG, are introduced, allowing for the separation of cross-linked from noncross-linked input RNAs (Garzia et al., 2018; Spitzer et al., 2014). With HITS-CLIP and PAR-CLIP identification of only the cDNAs that have read through the cross-link site is possible. iCLIP overcoming that limitation by using a primer complementary to the 3′ adaptor, which also contains a 5′ adaptor sequence reducing a mispriming artifacts. Moreover, iCLIP protocol needs relatively low amount of starting material (Gillen et al., 2016; Huppertz et al., 2014).

2.4.2 Validations of RNA-seq results by qRT-PCR and fluorescence in situ hybridization methods

The disease-specific circRNAs have to be not only identified through RNA-seq technique, but they need to be also properly validated. Despite the variety of bioinformatic pipelines using different approaches to identify circular transcripts, there is still a lack of gold standard method for the validation of predicted circRNAs, and the combination of complementary methods is still advised (Holdt et al., 2018). The most widely used methods of circRNAs validation is combination of RNase R treatment and reverse transcription followed by qPCR (qRT-PCR) followed by Sanger sequencing or Northern blotting (Panda & Gorospe, 2018; Xiao & Wilusz, 2019). However, microscopic imaging such as in situ hybridization has become more and more popular method for establishing the abundance and localization of circular transcripts recently (Zaghlool et al., 2018; Hansen et al., 2013). Taking into account the specific closed structure of circRNAs, the basic methods of molecular biology have to be adjusted to differentiate between linear and circular gene transcripts. The presence of both linear and circular transcripts requires precision in experimental

design so that the validation process includes only circular transcripts, excluding linear isoforms. The RNA quality plays key role in validation procedure, as well as RNA-seq library preparation since the characteristic head-to-tail junction might get partially degraded during those steps leading to misinterpreted results (Gallego Romero et al., 2014; Sarantopoulou et al., 2019).

qRT-PCR is considered one of the most powerful tools for a circRNAs validation. The fundamental step is divergent primer design, which spans the characteristic head-to-tail junction sequence characteristic only for circRNAs, allowing to differentiate them from linear counterparts. In some cases, low-abundant circRNAs have to be enriched using RNase R treatment prior to qRT-PCR analysis. RNase R exoribonuclease treatment allows for the hydrolysis of linear transcripts, while circular ones are almost fully resistant for the digestion due to its closed structure. Digital droplet PCR (ddPCR) is particularly useful, as it is based on determining the absolute concentration of circRNA by using the quantitative ratio of positive droplets, in which the qPCR product is present to negative ones, allowing for the elimination of errors related to the formation of exon concatamers (Chen, Zhang, Tan, & Jing, 2017). Therefore ddPCR allows to quantitatively analyze genome-wide data sets, providing highly accurate results, what is valuable in low-abundant RNAs research (Pandey et al., 2020). Despite the fact that this method is widely used and relatively simple, it offers some limitations as most of the reverse transcriptase are known to introduce mutations such as template-switching artifacts occurring while joining two distinct RNA molecules or concatamers generation, what might lead to the misinterpretation of the results (Barrett & Salzman, 2016; Szabo & Salzman, 2016). Additionally, it has been reported by many groups that RNase R might deplete also some circRNA or decay the noncircular RNAs not efficiently due to its complex secondary structure or length (Holdt et al., 2018; Vincent & Deutscher, 2006).

Detection and subcellular localization of circRNAs by microscopy is challenging due to the fact that the only way to distinguish circular transcripts from the linear ones is the presence of a head-to-tail junction. The circRNA molecules can be visualized and quantified using fluorescence in situ hybridization (FISH) coupled with high-resolution microscopy, applying highly sensitive junction-specific probes to avoid simultaneous detection of their linear counterparts (Zirkel & Papantonis, 2018). Variety of available protocols enable high specificity and sensitivity of circRNAs detection, allowing for single RNA molecule visualization. Short transcripts detection might be weak due to the insufficient fluorescence signal from a single bound probe; therefore it can be enhanced by the hybridization of multiple amplifier probes (Itzkovitz & Van Oudenaarden, 2011). However, this approach has been reported to produce less quantitative results (Kocks et al., 2018). FISH, combined with immunohistochemistry, may be applied to examine the colocalization of circRNAs with proteins (Bejugam et al., 2020; Huang et al., 2020).

Northern blotting can be applied to validate circRNAs presence, but it requires probes spanning the head-to-tail junction site. However, Northern blotting is still limited by the circRNAs length, to molecules ranging 0.2−1 kb (Pandey et al., 2020). Circular and linear transcripts vary in the case of migratory potential in polyacrylamide gels, where circRNAs tend to migrate slowly in comparison to the linear one what makes 2D gel methods useful in circRNAs validation process. CircRNAs can be either trapped in agarose gel by sulfide bridges (Gel trap) or reported to migrate slower in polyacrylamide gels. The methods presented in this section contain a number of advantages and disadvantages, which are summarized in Table 2.2.

TABLE 2.2   The advantages and disadvantages of the noncoding RNA (ncRNA) analysis and manipulation methods.

Methods	Advantages	Disadvantages
Approaches used to study and validate the ncRNAs		
NGS	High-throughput method, high sensitivity, and discovery power	High costs and complexity, RNA quality, and RNA-seq library preparation play key role to prevent misleading results
qRT-PCR	Low costs, simultaneous amplification, and detection during amplification	Usage of error-prone reverse transcriptases, limited primer designing in circRNA and miRNA, problems of specificity due to miRNA families similarity, circRNA concatemers formation, low-abundant circRNAs have to be enriched
ddPCR	Absolute quantification of a target with no standard curve requirements provides highly accurate results even in low-abundant RNA sample, lower sensitivity to PCR inhibitors, elimination of errors related to the formation of concatamers in circRNA study	High costs and complexity, limited primer design in circRNA and miRNA
FISH	High sensitivity and specificity in recognizing targeted sequences, visualization of hybridization signals at the single-cell level and ability to detect cell-to-cell variations	Background noises, limitation to cover abundant ncRNAs in cell, off-target hybridization, limited probe design in circRNA and miRNA
Northern blotting	Detection of RNA size and alternative splice products, the membranes can be reprobed long time after blotting	High complexity, requires a large amounts of total RNA, limited probe design in circRNA and miRNA, length limited to molecules ranging 0.2−1 kb
RNase R treatment	Low costs, easy circRNAs enrichment method	Possibility to deplete some circRNA or decay the noncircular RNAs not efficiently
Luciferase assay	Low cost, quickness, and precision of the experiment	Requirement for exogenous substrates, the delay from stimulus to response
CLIP	Determine the binding site with high accuracy, avoid protein−protein cross-links	Mutations caused by UV light
Pull-down	Relatively low input, detection of weak interactions, higher experimental flexibility	Background noises due to nonspecifically binding proteins may occur

(Continued)

TABLE 2.2   (Continued)

Methods		Advantages	Disadvantages
Approaches used to manipulate the expression level of ncRNAs			
miRNA mimics		No or easy available carrier system needed, no vector-based toxicity, easy to use	Relatively high costs, susceptible to ceRNAs and competitive endogenous RNA-binding protein interactions, off-target effects, risk of interferon response
Antisense oligonucleotides	Antagomirs	Nuclease resistant, can be delivered into cells directly without any delivery vehicles	High usage dose, possible off-target effects
	2′-*O*-methyl group−modified AMOs	Less sensitive to degradation in serum or by endogenous cellular exonucleases and endonucleases	2′-*O*-methyl modification decreases the binding of the AMO to its target miRNA
	LNAs	High efficiency of miRNA activity blocking, high stabilization of the LNA/RNA duplex, strongly resistant to nuclease degradation, applied in detection methods	Design requires careful examination, sequences without extensive self-complementary segments
	PMOs	Characterized by stronger steric blocking of nucleases and preventing degradation, highly efficient penetration in multiple tissues in vivo	Requires careful optimization regarding the PMOs length, lower binding affinity than equivalent PNAs
	PNAs	High target affinity, specificity, nucleases resistance, and cell penetration, applied in detection methods	Limitation of solubility and the structural flexibility of nucleic acid recognition
miRNA sponges		Transient and stable miRNA sponges depending on the needs, binding sequences for a family of miRNAs can be constructed together in one vector	Number of binding sequences affects sponge activity, different degrees of inhibition in different contexts, challenging optimization and validation
CRISPR/Cas9		Low costs, high simplicity and efficiency, new CRISPR-Cas13 approach represents a promising method for targeting a specific circRNA	Off-target effects, challenging and time-consuming optimization, single site of gene editing may not be sufficient to manipulate microRNA stem-loop structure and function, depleting the circRNAs without affecting the existing genes remains challenging
siRNAs		Low costs, easily introduced to the cells, predesigned reagents available, many chemical modifications available	Temporary gene silencing, incomplete silencing, off-target effects, transfection difficulties, stimulation of immune response

(*Continued*)

TABLE 2.2 (Continued)

Methods	Advantages	Disadvantages
shRNAs	Permanent gene silencing, high efficiency, reduced off-target effects, predesigned reagents available	Virus-mediated toxic effects, technologically challenging and time-consuming, BSL2 requirement
Small molecule chemical compounds	Typically low costs, easily introduced to the cells, various half-live, and bioavailability	Off-target effects, adverse reactions possible, various half-live, and bioavailability

AMOs, anti-miRNA oligonucleotides; *ceRNA,* competitive endogenous RNA; *circRNA,* circular RNA; *CLIP,* cross-linking immunoprecipitation; *ddPCR,* digital droplet PCR; *FISH,* fluorescence in situ hybridization; *LNA,* locked nucleic acid; *miRNA,* microRNA; *ncRNA,* noncoding RNA; *NGS,* next-generation sequencing; *PMO,* phosphorodiamidate morpholino oligonucleotide; *PNA,* peptide nucleic acid; *qRT-PCR,* quantitative reverse transcription polymerase chain reaction; *shRNA,* short hairpin RNA; *siRNA,* short interfering RNA; *UV,* ultra violet.

2.5 Noncoding RNAs as predictive marker for brain cancer patients

2.5.1 Diagnostic potential of noncoding RNAs in brain cancer patients

Diagnosis of brain cancer is based on neurological examination and confirmed by standard imaging technique—computed tomography and magnetic resonance imaging scans. Other techniques that are used to diagnose brain cancer include diffusion tensor imaging, single photon emission—computerized tomography, positron emission tomography, cerebral angiography, magnetic resonance spectroscopy, and biopsy (Shah & Kochar, 2018; Shahpar et al., 2016). Nowadays, molecular analysis detecting ncRNAs of diagnostic potential in tissue biopsies and body fluids collected from the patients is also possible. By reason of the extensive identification of disease-related ncRNAs and their cell- and tissue specificity, it is believed that they might serve as promising biomarkers and provide new targets for the treatment. Traditional biomarkers currently used in the clinics allow to establish more accurate diagnosis but have disadvantages in the form of lower organ specificity and low positive detection level (Meng et al., 2017). NcRNAs can support the traditionally used diagnostic biomarkers to increase the positive diagnosis rate, as they have been reported to be abundant in saliva, exosomes, blood samples, or CSF. Given in this chapter examples, summarized in the Table 2.3 show the diagnostic and stratification value for brain cancers' patients. Given examples, however, show that the level of ncRNA expression in the tissue does not necessarily correspond to the amount of molecules released into the serum, for example, miR-454-3p.

Determining the degree of malignancy of the neoplasm is important since it allows to decide on the further treatment method and also allows to determine the initial prognosis for the patient. Thus it has become an important aspect to look for biomarkers that help to distinguish low-grade gliomas (LGG) from high-grade gliomas (HGG)—Table 2.3. TCGA data analysis indicated miRNAs that may be considered cerebral LGG prognosis markers: miR-1287, miR-326, and miR-1275 (Liu et al., 2017). Furthermore, comparison of the miRNA profile with the occurrence of mutations in *IDH1/2* genes determined that 74% of 487 considered miRNAs were differentially expressed according to *IDH1/2* mutation status in LGGs (Cheng et al., 2017).

TABLE 2.3   MicroRNA, long noncoding RNA, and circular RNAs with diagnostic potential in brain cancers.

RNA	Tumor type	Expression level	Sample type	Reference
Diagnosis				
miR-129	GBM, MB, ATRT, ependymoma, pilocytic astrocytoma	Down	Fresh tumor tissue	Birks et al. (2011)
miR-142-5p, miR-25		Up		
miR-1259, miR-21, miR-222	Pediatric brain cancers	Up	Fresh tumor tissue	Yuan et al. (2018)
miR-128		Down		
miR-221, miR-222	GBM	Up	Blood	Swellam et al. (2019)
miR-222, miR-7, miR-137	GBM	Down	Formalin-fixed parafin-embedded tissue	Visani et al. (2014)
miR-454-3p	GBM	Down	Fresh tumor tissue and cell lines	Shao et al. (2019)
	GBM	Up	Preoperative exosomes	
	GBM	Down	Postoperative exosomes	
miR-15b	GBM	Up	Cerebrospinal fluid	Baraniskin et al. (2012)
miR210HG	GBM	Up	Fresh tumor tissue and serum	Min et al. (2016)
NFIX	GBM	Up	Fresh tumor tissue	Ding et al. (2020)
ITCH	GBM	Up	Fresh tumor tissue	Li et al. (2018)
SKA3 DTL	MB	Up	Fresh tumor tissue	Lv et al. (2018)
Stratification				
miR-7, miR-10b, miR-137, miR-223	GBM WHO grade I	Down	Fresh tumor tissue	Visani et al. (2014)
miR-21, miR-34a		Up		
miR-7, miR-10b, miR-137, miR-22	GBM WHO grade II	Down		
miR-34a		Up		
miR-7, miR-101, miR-137, miR-22	GBM WHO grade III	Down		
miR-4516	GBM WHO grade IV (compared to grade II and III)	Up	Fresh tumor tissue	Cui et al. (2019)

(*Continued*)

TABLE 2.3 (Continued)

RNA	Tumor type	Expression level	Sample type	Reference
miR-21	HGG and LGG	Up	Cerebrospinal fluid exosomes	Shi et al. (2015)
miR-21	GBM WHO grade IV (compared to WHO grades II–III)	Up	Fresh tumor tissue	Berthois et al. (2014)
miR-200a	GBM WHO grade IV (compared to WHO grades II–III)	Down		
miR-637	GBM	Down	Fresh tissue fresh tumor tissue	Que et al. (2015)
miR-1825	GBM	Down	Serum	Xing and Zeng (2017)
miR-1238	GBM recurrent (compared to primary tumor)	Up	Serum	Yin et al. (2019)
miR-204	MB WNT and 80% of MB G4	Up	Fresh tumor tissue	Bharambe et al. (2019)
	MB SHH and 60% of MB G3	Down		
miR-193a-3p, miR-224, miR-148a, miR-23b, miR-365, miR-10b,	MB WNT	Up	Fresh tumor tissue	Kunder et al. (2013)
miR-182, miR-135b, miR-204	MB SHH	Down		
miR-135b	MB G3 and MB G4	Up		
HOTAIR CRNDE	High-grade astrocytoma	Up	Fresh tumor tissue	Zhang et al. (2012)
LOC286002, C21orf131-A, C21orf131-B	High-grade oligodendrogliomas	Up		

ATRT, an atypical teratoid rhabdoid tumor; *GBM*, glioblastoma multiforme; *HGG*, high-grade gliomas; *LGG*, low-grade gliomas; *MB*, medulloblastoma; *SHH*, sonic hedgehog; *WNT*, wingless.

Noteworthy the diagnostic and prognostic value of miRNA was used to provide the stratification analysis. It allowed to distinguish five subgroups of GBM with different clinical properties and of different origins: (1) oligoneuronal, (2) radial glial, (3) neural, (4) neuromesenchymal, and (5) astrocytic (Kim et al., 2011). Undoubtedly, finding new biomarkers could help in the treatment of GBM at early onset and prevent from disease progression.

2.5.2 Prognostic potential of noncoding RNAs in brain cancer patients

There is a wide relationship between prognostic and predictive biomarkers, which allows to predict the response of the patient to a targeted therapy, as some of them can perform

both functions and distinguishing them can be difficult. In the case of brain tumors, especially gliomas, classical prognostic evaluation is based on the analysis of phenotypical traits, including age, tumor location, histological grade, and performance status. Poor prognosis is associated with older age, where patients aged 70–79 years exhibited a median survival of 2.9 months and patients above 80 years only 1.9 months, poor preoperative performance status, and size and location of the tumor, with the worst outcome for GBM, which is characterized as extensively spreading tumor type (McDonald et al., 2012; Ohgaki et al., 2004). Prognostic markers can predict the course of the disease and help determine which patient should be treated and how. A prime example of a prognostic marker is the tumor histology: LGG have a better prognosis than HGG (Davis, 2018). New affordable methods are needed to help prognosis and to suggest the most appropriate treatment for patients' brain cancer. Recognition of the patient's prognosis could be based on the level of ncRNAs expression in a biopsy or liquid biopsy collected during standard treatment.

Comparing the medical history of patients suffering from brain cancers, with the results of miRNA profiling, allows for the identification of miRNA sets predicting possible outcomes of a disease. Expressions of miR-767-5p and miR-105 are positively correlated to OS, whereas miR-miR-584, miR-296-5p, and miR-196a negatively correlated to OS in anaplastic gliomas regardless of histology type (Yan et al., 2014). Study based on formalin-fixed paraffin-embedded GBM tissue sections developed a four-miRNA signature that could identify GBM patients: let-7a-5p, let-7b-5p, and miR-125a-5p have appositive effect on OS, hsa-miR-615-5p negative (Niyazi et al., 2016). Analysis of microarray data from GBM tissues elicited a set of deregulated miRNA. The expression of miR-124a, miR-129, miR-139, miR-218, and miR-7 was downregulated, and the expression of miR-15b and miR-21 was upregulated. The association with disease-free survival (DFS) demonstrates that the risk score established by those miRNAs was more effective than other criteria that are traditionally used, including Karnofsky Performance Status (KPS), tumor location, recurrence status, *MGMT* methylation, *IDH1* mutation, smoking, and family history of cancer (Chen et al., 2016). High abundance of mentioned well-known oncomiR, miR-21 (Pfeffer et al., 2015), defined a worse prognosis in primary glioma patients also in another study (Shi et al., 2015).

Relapsed GBM tissues were characterized by a lower expression level of miR-203 with simultaneous overexpression of its target, snail family transcriptional repressor 2. OS of patients with higher expression levels of miR-203 was longer (Liao et al., 2015). Better OS was observed as well in patients with higher miR-29c level, which increases chemotherapy efficacy (Xiao et al., 2016). Longer OS together with DFS was related to higher miR-29a/b/c levels. The opposite relation applied to the tumor necrosis factor receptor-associated factor-4 (TRAF4), which promotes apoptosis through the TRAF4/AKT/MDM2 pathway in a p53-dependent manner (Shi et al., 2018). Worse OS prognosis had patients with low expression levels of miRNA-320c, which impair migration and invasion of glioma cells via reducing the expression of matrix metalloproteinases 2 and 9 (MMP2, MMP9) *N*-cadherin and integrin β1 (Lv et al., 2018). The results of Kaplan–Meier analysis revealed that patients with low expression of miR-599 had not only significantly shorter OS but also poorer progression-free survival (PFS). MiR-599 downregulation was significantly correlated to KPS and WHO grading (Zhu et al., 2018). PFS was shorter likewise in patients with lower expression of miR-101, considering it sensitizes resistant GBM cells to chemotherapeutic drug (Tian et al., 2016).

Decreased exosomal miR-151 level in patients' CSF indicated worse prognosis, as induced expression of miR-151 in cell lines inhibited XRCC4 DNA repair mechanism (Zeng et al., 2018). miR-454-3p high expression in serum exosomes or on the other hand low expression in glioma tissue were correlated to a poor survival rate. Forced expression of miR-454-3p in cell lines autophagy as its direct target is mRNA coding autophagy-related 12 protein (ATG12) (Shao et al., 2019). Another prognostic marker was found in a glioma patients' serum—miR-1825. Its level was significantly decreased in patients compared with healthy controls and those with high miR-1825 expression had a longer survival rate (Xing & Zeng, 2017).

For brain tumors other than GBM, research on prognostic miRNAs is not that well developed; however, also here it is worth paying attention to a few examples. In the combined cohort of G3 and G4 MBs, tumors with miR-182 overexpression were found to correlate to worse survival rates, while those with miR-592 overexpression with better survival rates (Kunder et al., 2013). The 5-year OS rate of patients with high miR-495 expression in MB tissue was approximately 25 percentage points higher, compared with patients with low miR-495 expression (Wang et al., 2015). In the case of patients with metastatic inflammatory breast cancer higher serum miR-141 level was found, compared to patients with locally advanced breast cancer. High miR-141 levels were associated with shorter brain metastasis−free survival. Furthermore, knockdown of miR-141 inhibited metastatic colonization to brain in mice (Debeb et al., 2016).

The aberrant expression of lncRNAs has also been shown to correlate to tumor progression and patients' survival which indicates that lncRNA could serve as biomarkers of prognostic potential. Among many the most well-studied is HOTAIR that acts as miR-326 and miR-148b-3p sponge and displays high expression linked to poor prognosis and patient survival (Zhang et al., 2015). While CRNDE stimulates GBM proliferation and migration, serves as a sponge for miR-337-3p, and its elevated levels also correlate to poor prognosis (Gao et al., 2020). Among lncRNAs which act as tumor suppressors and their downregulation that leads to tumor progression and is linked with poor patient survival are MALAT1, TUSC7, and CASC2. MALTA1 executes its function via the deactivation of ERK/mitogen-activated protein kinase (MAPK) pathway, while TUSC7 is known as miR-23b and miR-10a sponge and CASC2 interacts with miR-181a and miR-193-5p affecting WNT signaling (Han et al., 2016; Jiang et al., 2018; Liao et al., 2017; Shang et al., 2016).

The clinicopathological and prognostic value of circRNA in onset and progression of glioma was recently reviewed. Metaanalysis included 24 eligible studies and a total of 1390 patients, with the analysis of two groups of circRNAs—tumor suppressors and carcinogenic tumor promoters. They revealed the correlation between high expression of tumor-promoter circRNAs and significantly poor clinicopathological features, and high expression of tumor-suppressor circRNAs and better clinicopathological features, indicating the circRNAs being related to the occurrence and development of glioma (Ding et al., 2020). Moreover, recent reports indicate that some circRNAs might undergo the translation process generating peptides and proteins. It has been shown that protein products encoded by ncRNA state a promising prognostic biomarker for cancer patients. SHPRH-146aa, encoded by circRNA SHPRH (SNF2 histone linker PHD RING helicase), has been identified as decreased in GBM patients, leading to tumorigenicity reduction through protecting full-length SHPRH, which ubiquitinates proliferating cell nuclear antigen (Zhu et al., 2018).

2.6 Potential of noncoding RNAs in predicting chemoresistance and radioresistance in brain cancer patients

Treatment strategies for brain cancer are either to excise the tumor or stop its propagation. Surgery, chemotherapy, and radiation therapy are paramount therapeutic approaches. Despite the advances in medicine, the treatment results of brain tumors are usually not spectacular since tumors display a strong resistance to radiotherapy and chemotherapy, often infiltrate and recur stimulated by stem cells. CD133 + stem cells in GBM are then considered to be associated with increased resistance to radiation and chemotherapy.

miRNA profiles comparison between two laboratory-derived GBM cell lines with acquired resistance to TMZ and their primary counterparts, together with the comparison between 12 recurrent TMZ-refractory GBM samples and primary tumors, revealed a group of miRNAs with altered expression. TMZ-resistant cell lines and specimens were distinctive for the upregulation of miR-9, miR-182, and downregulation of miR-29c, miR-93, and miR-101. Among them, miR-101 expression rendered glioma cells more sensitive to TMZ both in vitro and in vivo as it has been shown by increased cell apoptosis and decreased tumor growth. Direct target of miR-101 is a glycogen synthase kinase 3 beta (Pyko et al., 2013), which has been reported to affect MGMT expression via promoter methylation (Xiao et al., 2016). As MGMT is the DNA repair protein, it plays a critical role in TMZ resistance. MGMT expression has been shown to be also dependent on miR-29c, which suppresses its expression indirectly via targeting specificity protein 1 (Xiao et al., 2016).

The miRNA expression profiles from 82 primary GBM samples indicated that the TZM chemoresistant subtype is characterized by the overexpression of miR-1280, miR-1238, miR-938, and miR-423-5p and decreased expression of let-7i, miR-151-3p, and miR-93 (Yan et al., 2015). Further research also confirmed that miR-1238 (Yin et al., 2019) and miR-432-5p (Li et al., 2017) expression levels were significantly higher in secondary GBM samples than in primary ones, while miR-151a (Zeng et al., 2018) was significantly decreased in recurrent compared to paired primary GBM samples. Both established and primary human GBM cell line with induced TMZ chemoresistance displayed expressed higher miR-1238 levels than the respective initial cell lines. The proposed mechanism of action presents that loss of CAV1, the direct target of miR-1238, induced the activation of the EGFR-PI3K-Akt-mTOR pathway, leading to enhanced antiapoptosis of TMZ-treated GBM cells (Yin et al., 2019). Overexpression of miR-432-5p in glioma cell lines decreased TMZ chemosensitivity, which could be reversed by forced expression of Ing-4, its validated target (Li et al., 2017). In the case of miR-151a, its overexpression in xenografts decreases a tumor volume translating into better survival of animals (Zeng et al., 2018).

miR-302c was significantly downregulated in glioma brain tissues when compared with control tissue, furthermore its level was decreased in progressive disease samples compared with partial response glioma tissues. miR-302c was also reduced in cell line with induced TMZ resistance, and its overexpression resensitized cells to TMZ by direct targeting of P-glycoprotein known as multidrug resistance protein 1 (Wu et al., 2019). Another study found that tissue specimens are also characterized by the downregulation of miR-124 targeting–related Ras viral oncogene homolog (R-Ras) and NRAS viral oncogene homolog (N-Ras). Forced miR-124 expression in glioma cell lines significantly increased their chemosensitivity to TMZ treatment (Shi et al., 2014). GBM tissue samples and cell

line have lower expression levels of miR-128-3p, which confirmed that target c-Met is responsible for chemoresistance. miR-128-3p enhanced the therapeutic effect of TMZ by the induction of apoptosis from 16% to 28% in vitro and reduction of tumor volume in vivo (Zhao et al., 2020). miR-224-3p induced enhanced chemosensitivity that was observed both in vitro and in vivo. At the molecular level, miR-224-3p downregulated hypoxia-inducible factor 1-alpha and autophagy-related gene 5 (Huang et al., 2019). MiRNA profile of TMZ-resistant glioma cell lines revealed the upregulation of miR-138. Overexpression of that miRNA or knockdown of its target Bcl-2-like protein 11 enhanced autophagy, which increases the chemoresistance of cells (Stojcheva et al., 2016). Significantly upregulated in tumor tissues compared with peritumoral brain edema miR-223 directly targets paired box protein (PAX6) and promotes the proliferation of GSCs after TMZ treatment by PI3K/Akt pathway (Huang et al., 2017).

With reference to CSC, it was observed that miR-29a was significantly downregulated in cisplatin-treated CD133 + GBM cells. Moreover, miR-29a significantly increased apoptosis of CD133 + after cisplatin treatment. Similarly, in xenograft mice, when combined with miRNA-29a overexpression, treatment with cisplatin significantly inhibited tumor growth than treatment with cisplatin alone (Yang et al., 2018). Profiling of glioma cell line with generated cisplatin resistance revealed a set of miRNAs with differential expression, among them let-7b greatly resensitized cells to cisplatin (Guo et al., 2013). miR-873, downregulated miRNA in glioma samples, has also lower expression level in cisplatin-resistant cell lines to the respective wild-type cells. miR-873 increased induced apoptosis in both the cisplatin-resistant and wild-type glioma cells. Its effect could be reversed by the reexpression of its targets, apoptosis regulator protein Bcl-2 (Chen et al., 2015).

miRNA microarray analyses of three pairwise radioresistant and parental GBM cell lines identified between these two groups 113 statistically significant deregulated miRNAs. The most upregulated miRNAs in radioresistant GBM cells were miR-145, miR-10b*, miR-204, miR-1231, miR-4721, miR-4697-3p, miR-10a-star, miR-4725-3p, and miR-4498, while the most downregulated were miR-1271, miR-29b, miR-3065-5p, miR-2467-3p, and miR-1290 (Ondracek et al., 2017).

Expression analysis of glioma tissue specimens from patients treated with radiotherapy for over 6 months showed that miR-320 is notably decreased in radioresistant glioma tumors compared with radiosensitive samples. Overexpression of miR-320 increased caspase-3 activity and DNA double-stranded breaks frequency in irradiated cells. Proposed model of action assumes a direct targeting of forkhead box protein M1 followed by the downregulation of sirtuin type 1 (Li et al., 2018). Another tissue miRNA expression research revealed that the expression of miR-183 was significantly increased in resistant specimens. Cell line transfected with miR-183 mimic and then radiated decreased cell apoptosis, while in vivo miR-183 decreased tumor volume (Fan et al., 2018). Irradiated glioma cell lines were characterized by increased level of miR-21. PI3K-AKT signaling pathway inactivation impairs DNA repair following γ-irradiation. Anti-miR-21 suppressed the phosphorylation of protein kinase B, thus sensitized cells to radiation (Gwak et al., 2012).

GSCs are more radioresistant than glioma cell lines, demonstrating no reactive oxygen species generation after 1 h of 8 Gy X-ray irradiation. miR-153 overexpression made GSCs more radiosensitive and slightly raised their oxygen enhancement ratio (Yang et al., 2015). CSC subset isolated from ATRT was defined by a low expression level of miR142-3p. After an ionizing radiation the proliferation of CD133 + cells with overexpressed miR142-3p was

significantly lower than those with basal expression. Moreover, miR142-3p overexpression markedly reduced tumor growth, and with additional irradiation, reduced the tumor volume to a barely detectable size (Lee et al., 2014).

lncRNAs have also been reported to contribute to brain tumor radio- and chemoresistance. The most distinctive lncRNAs involved in cell resistance presents Table 2.4. The highest potential so far displays lncRNA H19. Its upregulated levels have been noted in glioma cells and its downregulation by shRNA (short hairpin RNA) technology leads to decrease in β-catenin expression and increased susceptibility to TMZ (Jia et al., 2018). Similar, oncogenic features of H19 were reported by Jiang et al. (2016) who silenced H19 with siRNA and also observed tumor decrease in TMZ chemoresistance. H19 has also been shown to activate a key protein of NF-κB (nuclear factor kappa-light-chain-enhancer of activated B cells) signaling which was revealed by both H19 silencing and overexpression experiments (Duan et al., 2018). H19 overexpression and simultaneous treatment with NF-κB inhibitor has led to the eradication of TMZ resistance in glioma cells. As mentioned earlier, lncRNAs often serve as miRNA sponges thus aberrations in lncRNA expression affects also miRNA and its target expression. The expression of lncRNA CASC2 was downregulated in glioma cell lines and tissues, but its overexpression leads to the inhibition of miR-181a expression which affected its target expression PTEN and p-AKT. As a result, the cell resistance to TMZ weakened (Liao et al., 2017). Two clinical studies on glioma tissues have revealed a high expression level of UCA1 lncRNA which ensures chemoresistance. In vitro studies have shown that its knockdown not only suppresses the activity of WNT/β-catenin signaling but can also affect levels of fibronectin, COL5 A1 and ZEB1, by sponging miR-204-5p (Liang et al., 2018; Zhang et al., 2019). The pathway, which involvement has also been noted in glioma chemoresistance, is PI3K/Akt. This pathway can be regulated by two lncRNAs DANCR and MSC-AS1. DANCR increased levels promote resistance to cisplatin treatment, while the increase in MSC-AS1 expression induces TMZ resistance. Less studies are dedicated to the involvement of lncRNAs in radioresistance especially in MB. Recent studies have shown that lncRNA TPTEP1 inhibits glioma radioresistance by competitive interaction with miR-106a-5p and activation of p38 MAPK signaling (Tang et al., 2020). Interesting studies have been performed by Zheng et al. (2016) who first established that lncRNA SNHG18 represses semaphorin 5S and thus promotes radioresistance in glioma cells and xenograft models. Further mechanistic studies revealed that SNHG18 inhibits nucleocytoplasmic transport of ENO1 protein that promotes glioma cell motility (Zheng et al., 2019). In the case of MB, increased chemosensitivity to cisplatin has been observed upon the inhibition of lncRNA CRNDE, which also serves as a sponge of miR-29c-3p (Sun et al., 2020).

CircASAP1 which biogenesis is induced by eukaryotic translation initiation factor 4A3 (EIF4A3) has been shown to promote GBM proliferation and TMZ resistance and to be associated with poor GBM patients' prognosis. Moreover, circASAP1 sponges miR-502-5p, what leads to the deregulation of its target—NRAS expression, enhancing tumor growth and TMZ resistance in vitro and in vivo. NRAS is a member of the RAS family, encoding membrane-bound protein known to function as regulatory element in the signal transduction events of molecules regulating cancer cells survival and proliferation (Wei et al., 2021).

Recently, circRNAs shown to play a relevant role in cancer have been also identified in EVs present in patients' blood. The growing number of evidence shows that

TABLE 2.4 The list of long noncoding RNA (lncRNAs) and circular RNAs (circRNAs) targeting microRNAs (miRNAs) and proteins as well as cross-talked with pathways assuring brain tumor chemo- and radioresistance.

	lncRNA/ circRNA	miRNA sponged	Target protein	Pathway involved	Reference
Chemoresistance in glioma	H19		β-Catenin, c-myc, survivin	Wnt/ β-catenin	Jia et al. (2018)
	H19		MDR, MRP, ABCG		Jiang et al. (2016)
	H19		NF-κB	NF-κB	Duan et al. (2018)
	XIST	miR-29c	SP1, MGMT		Du et al. (2017)
	NCK1-AS1	miR-22-3p	IGF1R		Wang et al. (2020)
	CCAT2	miR-424	CHK1		Ding et al. (2020)
	CASC2	miR-181a	PTEN, p-AKT	PTEN	Liao et al. (2017)
	LINC00174	miR-138-5p	SOX9		Li et al. (2020)
	MALAT1	miR-203	TS		Chen et al. (2017)
	MALAT1	miR-101			Cai et al. (2018)
	HOXD-AS1	miR-130a-3p	ZEB1		Chi et al. (2018)
	KCNQ1OT1	miR-761	PIM1		Wang et al. (2020)
	UCA1			Wnt/ β-catenin	Zhang et al. (2019)
	UCA1	miR-204-5p	Fibronectin, COL5 A1, ZEB1		Liang et al. (2018)
	CASC2	miR-193a-5p	mTOR		Jiang et al. (2018)
	BC200	miR-218-5p			Su et al. (2020)
	DANCR	miR-33a-5p, miR-33b-5p, miR-1-3p, miR-206, miR-613	AXL	PI3K/Akt	Ma et al. (2018)
	AC023115.3	miR-26a	GSK3β		Ma et al. (2017)
	GAS5				Huo and Chen (2019)
	MSC-AS1	miR-373-3p	CPEB4	PI3K/Akt	Li et al. (2020)
	LIFR-AS1	miR-4262	NF-κB		Ding et al. (2020)
	LINC01198		NEDD4−1, PTEN		Chen et al. (2019)
	SBF2-AS1	miR-151a-3p	ZEB1		Zhang et al. (2019)
	ASAP1	miR-502-5p	NRAS		Wei et al. (2021)
	NFIX	miR-132	ABCG2		Ding et al. (2020)

(Continued)

TABLE 2.4   (Continued)

	lncRNA/ circRNA	miRNA sponged	Target protein	Pathway involved	Reference
Radioresistance in glioma	TPTEP1	miR-106a-5p	MAPK14	p38 MAPK	Tang et al. (2020)
	NCK1-AS1	miR-22-3p	IGF1R		Wang et al. (2020)
	TP53TG1	miR-524-5p	RAB5A		Gao et al. (2020)
	RA1				Zheng et al. (2020)
	SNHG18		Semaphorin 5A		Zheng et al. (2016)
	SNHG18		ENO1		Zheng et al. (2019)
	p21	miR-146b-5p	HuR		Yang et al. (2016)
	AHIF				Liao et al. (2019)
	PSMB8-AS1	miR-22-3p	DDIT4		Hu et al. (2020)
	AHIF				Dai et al. (2019)
	ATP8B4	miR-766			Zhao et al. (2019)
	AKT3			PI3K/Akt	Xia et al. (2019)
Chemoresistance inmedulloblastoma	CRNDE	miR-29c-3p			Sun et al. (2020)

tumor-derived exosomes might have a role in a variety of cancer-related processes such as tumor microenvironment remodeling, metastasis, and drug resistance (Mashouri et al., 2019). CircNFIX has been shown to be upregulated in TMZ-resistant patients' serum and enhanced glioma cell migration, invasion, and reduced cancer cell apoptosis under TMZ exposure. Furthermore, authors proved that circNFIX enhances glioma TMZ resistance by sponging miR-132, which has been confirmed in vitro and in vivo. miR-132 is considered tumor-suppressor in glioma and circNFIX knockdown allowed for miR-132 overexpression leading to the inhibition of tumor cell migration, invasion, and the enhancement of cell apoptosis. Authors indicated that the circNFIX/miR-132 axis regulates the ABCG2 expression in glioma cells under TMZ exposure (Ding et al., 2020). Another target—miR-34a-5p has been identified as being sponged by circNFIX, thus directly influences NOTCH1 receptor and Notch signaling pathway, to promote glioma progression (Xu et al., 2018).

CircRNAs expression in EVs isolated both from U251 and radioresistant U251 was established by RNA-seq. Total 63 upregulated and 48 downregulated circRNAs in EVs isolated from radioresistant cell line compared with those untreated cells. CircATP8B4 expression level is significantly upregulated in EV isolated from radioresistant cell line and have been proved to act as a sponge of miR766 to promote cell radioresistance. The

exact mechanism of circATP8B4/miR-766/mRNA still needs to be elucidated; however, miR-766 has been shown to impact the expression level of tumor-suppressor genes in colorectal cancer cell lines by the inhibition of DNMT3B gene (Zhao et al., 2019).

Not only circRNAs itself play a significant role in cancer events. CircRNAs that were considered mainly regulatory molecules have been recently shown to be capable of encoding peptides and proteins (Lei et al., 2020; Shang et al., 2019; Wawrzyniak et al., 2020). Turner et al. (2015) reported a significant role of AKT3—the dominant Akt isoform in promoting glioma progression and activating resistance to radiation and chemotherapy in GBM cases by activating DNA repair pathways of human glioblastoma cells. Interesting example is previously uncharacterized transcript variant of AKT gene—circ-AKT3, encoding a novel protein named AKT3—174aa. The authors showed that circ-AKT3 exhibits lower expression level in comparison to paired adjacent normal brain tissues, and its knockdown enhanced the malignant phenotypes of astrocytoma cells. Furthermore, the overexpression of AKT3—174aa decreased the proliferation, radiation resistance, and tumorigenicity of GBM cells and proved a negative regulatory role of AKT3—174aa in modulating the PI3K/AKT signal intensity via interaction with phosphorylated PDK1 (Xia et al., 2019).

The circRNAs expression profiling in MB tissue in comparison to human normal cerebellum tissues revealed a number of differentially expressed circRNAs. The downregulated circRNAs have been shown to be associated with detection of tumor cells, synaptic transmission, and activation of MAPK. Activation of the RAS/MAPK pathway is crucial in drug resistance, tumor growth, and enhancement of metastatic behavior in patients with Shh pathway-dependent MB (Lv et al., 2018; Zhao et al., 2015).

2.7 Therapeutic potential and targeting of ncRNAs in brain cancer patients—challenges and perspectives

Potential therapies based on the manipulation of ncRNA levels are based on tools which aim to increase the level of tumor suppressors or reduce the level of oncomiRs. Currently the most widely used approach involves delivering synthetic antisense oligonucleotides (ASOs) that imitate the native miRNA, or sequester the endogenous miRNA of interest (Anthiya et al., 2018). MiRNA mimics are synthetic double-stranded RNA molecules with identical sequence as native miRNAs that are able to integrate into the RISC acting as the missing miRNAλ. Antagomirs are single-stranded modified RNA molecules, perfectly complementary to mature miRNAs. They are forming duplexes with their miRNA target, what leads to miRNA degradation and the recycling of the antagomir (Krützfeldt et al., 2005). The discovery of RNA interference (RNAi) has found a new application for ASO—gene silencing, using synthetic, double-stranded, siRNA (Wittrup & Lieberman, 2015). The levels of an miRNA can be deregulated also indirectly, by targeting hypermethylation of miRNA promoter sites (Davalos et al., 2012), restoring a deleted genomic locus at the DNA level using CRISPR/Cas9 (Chang et al., 2016) or by inhibiting possible miRNA sponges like lncRNAs and circRNAs (Petrescu et al., 2019) which were proven to create complex coregulatory networks in brain (Kleaveland et al., 2018; Piwecka et al., 2017). MiRNA biogenesis, maturation, or function could be

prevented by small molecule chemical compounds that bind precursor or mature miRNAs (Monroig et al., 2015).

When designing oligonucleotides with therapeutic potential, several rules should be followed. Molecules must not be toxic to cells, which is related to the use of safe concentrations. The influence of therapeutic oligo on cell proliferation should be individually established. It is accepted to use the concentration not exceeding 50 nM for cells cultured in six well dishes (Matsui & Corey, 2017). Toxicity is also associated with the "off-target" effect, the partial complementarity to unintended targets. Also, one cannot forget about possible interactions of RNA with proteins, as nucleic acids can induce interferon response by binding to proteins on the surface or inside cells (Matsui & Corey, 2017). To avoid confusing the expected effect with the results "off-target," when screening for ASOs or duplexes, it is worth using at least two or three potent compounds at a time that are capable of reducing gene expression and are complementary to the same target RNA by, thus, reducing the possibility that the phenotype is due to nonspecific binding of compounds to unintended targets. It is also crucial to design controls either "scrambled," with swapped groups of bases, or "mismatched," with introduced mismatched bases (Matsui & Corey, 2017).

The most important additional obstacles in ASO therapy are their poor extracellular and intracellular stability, and low efficacy of intracellular delivery. Unmodified ASOs encounter substantial stability and delivery barriers, and to overcome them, modifications protecting against nucleases and enhancing RNA-binding affinity are introduced (Adams et al., 2017). The most basic and widely used RNA modifications include 2′-O-methyl substitution in the sugar of RNA backbone (Meister et al., 2004), change in the 2′-O-methoxyethyl backbone (Khatsenko et al., 2000), locked nucleic acid bases (LNA), and oligomerization with phosphorothioate bonds instead of the canonical phosphodiester bond (Irie et al., 2020). When silencing the circRNA expression, not to disturb the linear version of the transcript, it should also be remembered to design the effector molecule in such a way that it targets the junction site, which is unique for the circular version (Karedath et al., 2019).

Clinical studies with successful lncRNA and circRNA downregulation or upregulation are still missing. However, in the basic research the loss- and gain-of-function studies are often performed, as indicated in examples in previous section. Generally, RNAi platform applies siRNA and shRNA to silence cytoplasmic lncRNAs, while ASOs aim to knockdown lncRNAs located in the nucleus. For example, siRNA knockdown of lncRNA MALAT1 in glioblastoma cell line U87 has been shown to lead to the apoptosis of tumor cells (Liang et al., 2019). On the other hand, shRNA knockdown of lncRNA SCAMP1 has been applied on patient-derived glioma cells and resulted in repression of their proliferation, migration, and invasion (Zong et al., 2019). Studies with xenografted model of glioma, which was intravenously injected with ASOs targeting lncRNA TUG1, showed a significant repression of tumor growth (Katsushima et al., 2016). A more recent approach used is CRISPRi by which the knock-outs and knock-ins of lncRNA are possible (Zhao et al., 2020). Moreover, this tool enables to screen and identify lncRNA of therapeutic potential like in the studies of Liu et al. (2020) CRISPRi screen found lncRNA called lncGRS-1 that sensitizes glioma cells to radiation. ASO-targeting of that lncRNA in brain organoids sensitized cultures to

radiation therapy. However, further studies are needed to apply these tools in clinics. A summary of the advantages and disadvantages of ncRNA expression manipulation methods is provided in Table 2.2.

Expression of miR-10b is higher in GBM than in LGG (Visani et al., 2014) or healthy brains. Inhibition of that miRNA in GSC-derived xenograft using ASO inhibitors attenuated growth and progression tumor without observed systemic toxicity (Teplyuk et al., 2016). miR-10b loss-of-function by CRISPR/Cas9 on cell lines and GBM xenografts led to glioma cell apoptosis and impairs tumor growth (El Fatimy et al., 2017). A decrease in the survival of GBM cells as well as their arrest in G2/M phase upon TMZ treatment was also observed after the coinhibition of miR-21 and miR-10b with their antagomiRs (Ananta et al., 2016). Currently underway clinical trial tests the hypothesis that mir-10b expression patterns could serve as a prognostic and diagnostic marker in primary glioma samples. Tumor tissue, blood, and CSF will be analyzed in terms of the expression level, allowing to link patient survival, tumor grade, and genotypic variation with miR-10b. Moreover, in vitro studies of the sensitivity of individual primary tumors to anti-mir-10b treatment are ongoing (ClinicalTrials.gov Identifier: NCT01849952).

The main challenge that is associated with the use of therapeutics in the treatment of brain tumors is the way of potential drug delivery. One of the approaches enabling drug delivery through the BBB was a monthly repeated opening of the BBB with a pulsed ultrasound in combination with systemically injected microbubbles. Barrier was disrupted at acoustic pressure levels up to 1.1 megapascals with no detectable adverse effects in a clinical trial (Carpentier et al., 2016). This concept was successfully applied in delivery of short hairpin RNA targeting an apoptosis inhibitor Birc5 into rats with orthotopic glioma (Zhao et al., 2018). An effective and noninvasive system for the delivery of drugs to the brain is a transport via nanoparticles. The nanoparticles used to penetrate the BBB are mainly polymer particles composed of poly(butylcyanoacrylate), poly(lactic-*co*-glycolic acid), poly (lactic acid), carbon quantum dots, liposomes, and inorganic composites such as gold, silver, and zinc oxide (Zhou et al., 2018). Natural nanoparticles, which are EVs or exosomes derived from cells, are suitable for the transport of therapeutic nucleic acid molecules. Naturally, they contain endogenous small nucleic acids, although they can also be loaded with synthetic oligonucleotides of tumor suppressive potential (Haraszti et al., 2017; Yuan et al., 2017). Nevertheless, further studies are needed to apply described herein tools in clinical applications. So far, none of lncRNAs and circRNAs have been used in clinical studies.

2.8 Summary and conclusions

As indicated in herein chapter, ncRNAs display a strong diagnostic, prognostic, and therapeutic potential, thus, can be broadly applied in brain cancer field. The process of ncRNA discovery important in brain tumors is shown in Fig. 2.3. This is of a tremendous importance since brain tumors are mostly incurable, highly heterogeneous, and strongly resistant to variable therapies. Tumor heterogeneity constitutes nowadays a major challenge to cancer diagnosis and treatment. Moreover, different tumor stages as well as
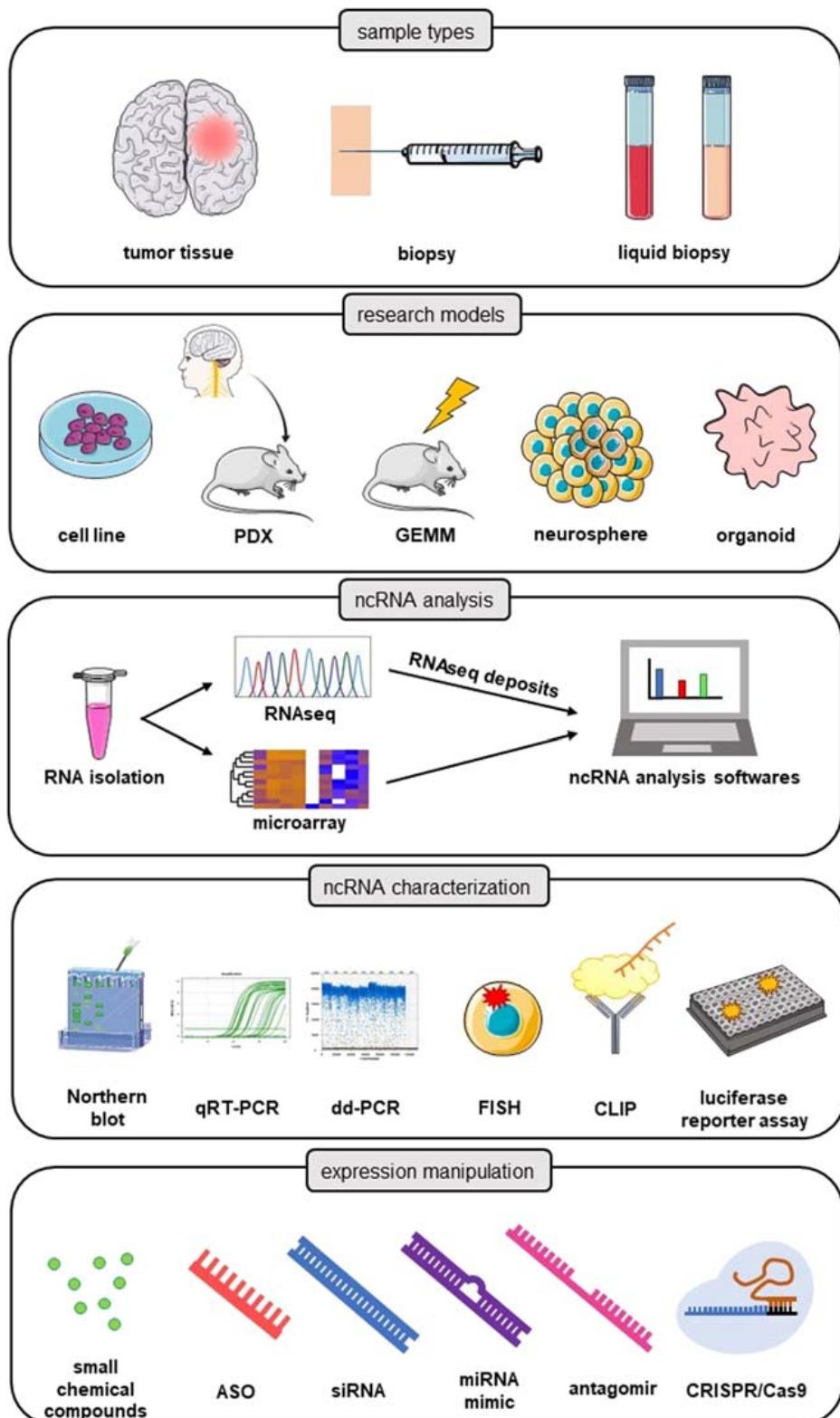
FIGURE 2.3 Pipeline of ncRNA discovery, characterization, and expression-level manipulation. *ASO*, antisense oligonucleotide; *CLIP*, cross-linking immunoprecipitation; *CRISPR/Cas9*, clustered regularly interspaced short palindromic repeats/CRISPR associated protein 9; *dd-PCR*, digital droplet polymerase chain reaction *FISH*, fluorescence in situ hybridization; *GEMM*, genetically modified mouse model; *ncRNA*, noncoding RNA; *PDX*, patient derived xenograft; *qRT-PCR*, quantitative reverse transcription polymerase chain reaction; *RNAseq*, RNA sequencing.

genetic and molecular events in brain tumors are associated with distinct outcomes of therapeutic responses. Specific pattern of ncRNA expression could help to classify these tumors as well as enable for precise treatment selection. Numerous publications focused on ncRNAs also reveal their molecular role in the biology of CSC which are crucial for the development of future successful therapies for brain cancer.

References

Abdelfattah, N., Rajamanickam, S., Panneerdoss, S., Timilsina, S., Yadav, P., Onyeagucha, B. C., ... Rao, M. K. (2018). MiR-584-5p potentiates vincristine and radiation response by inducing spindle defects and DNA damage in medulloblastoma. *Nature Communications*, *9*(1), 4541.

Adams, B. D., Parsons, C., Walker, L., Zhang, W. C., & Slack, F. J. (2017). Targeting noncoding RNAs in disease. *Journal of Clinical Investigation*, *127*(3), 761–771.

Agarwal, V., Bell, G. W., Nam, J. W., & Bartel, D. P. (2015). Predicting effective microRNA target sites in mammalian mRNAs. *Elife*, *4*.

Ahmad, Z., Jasnos, L., Gil, V., Howell, L., Hallsworth, A., Petrie, K., ... Chesler, L. (2015). Molecular and in vivo characterization of cancer-propagating cells derived from MYCN-dependent medulloblastoma. *PLoS One*, *10*(3), e0119834.

Akers, J. C., Ramakrishnan, V., Kim, R., Phillips, S., Kaimal, V., Mao, Y., ... Chen, C. C. (2015). miRNA contents of cerebrospinal fluid extracellular vesicles in glioblastoma patients. *Journal of Neuro-Oncology*, *123*(2), 205–216.

Allen, M., Bjerke, M., Edlund, H., Nelander, S., & Westermark, B. (2016). Origin of the U87MG glioma cell line: Good news and bad news. *Science Translational Medicine*, *8*(354).

Alles, J., Fehlmann, T., Fischer, U., Backes, C., Galata, V., Minet, M., ... Meese, E. (2019). An estimate of the total number of true human miRNAs. *Nucleic Acids Research*, *47*(7), 3353–3364.

Ananta, J. S., Paulmurugan, R., & Massoud, T. F. (2016). Tailored nanoparticle codelivery of antimiR-21 and antimiR-10b augments glioblastoma cell kill by temozolomide: Toward a "Personalized" anti-microRNA therapy. *Molecular Pharmaceutics*, *13*(9), 3164–3175.

Andreatta, F., Beccaceci, G., Fortuna, N., Celotti, M., De Felice, D., Lorenzoni, M., ... Alaimo, A. (2020). The organoid era permits the development of new applications to study glioblastoma. *Cancers (Basel)*, *12*(11), 1–16.

Anthiya, S., Griveau, A., Loussouarn, C., Baril, P., Garnett, M., Issartel, J. P., & Garcion, E. (2018). MicroRNA-based drugs for brain tumors. *Trends Cancer*, *4*(3), 222–238.

Aufiero, S., Reckman, Y. J., Tijsen, A. J., Pinto, Y. M., & Creemers, E. E. (2020). circRNAprofiler: An R-based computational framework for the downstream analysis of circular RNAs. *BMC Bioinformatics*, *21*(1), 164.

Azari, H., Millette, S., Ansari, S., Rahman, M., Deleyrolle, L. P., & Reynolds, B. A. (2011). Isolation and expansion of human glioblastoma multiforme tumor cells using the neurosphere assay. *Journal of Visualized Experiments* (56), e3633.

Bach, D. H., Lee, S. K., & Sood, A. K. (2019). Circular RNAs in cancer. *Molecular Therapy – Nucleic Acids*, *16*, 118–129.

Bachmayr-Heyda, A., Reiner, A. T., Auer, K., Sukhbaatar, N., Aust, S., Bachleitner-Hofmann, T., ... Pils, D. (2015). Correlation of circular RNA abundance with proliferation – Exemplified with colorectal and ovarian cancer, idiopathic lung fibrosis, and normal human tissues. *Scientific Reports*, *5*, 8057.

Badodi, S., Marino, S., & Guglielmi, L. (2019). Establishment and culture of patient-derived primary medulloblastoma cell lines. *Methods in Molecular Biology*, *1869*, 23–36.

Balachandran, A. A., Larcher, L. M., Chen, S., & Veedu, R. N. (2020). Therapeutically significant microRNAs in primary and metastatic brain malignancies. *Cancers (Basel)*, *12*(9), 1–29.

Balas, M. M., & Johnson, A. M. (2018). Exploring the mechanisms behind long noncoding RNAs and cancer. *Noncoding RNA Research*, *3*(3), 108–117.

Bao, Z., Yang, Z., Huang, Z., Zhou, Y., Cui, Q., & Dong, D. (2019). LncRNADisease 2.0: An updated database of long non-coding RNA-associated diseases. *Nucleic Acids Research*, *47*(D1), D1034-D7.

Barani, I. J., & Larson, D. A. (2015). Radiation therapy of glioblastoma. *Cancer Treatment and Research*, *163*, 49–73.

Baraniskin, A., Kuhnhenn, J., Schlegel, U., Maghnouj, A., Zöllner, H., Schmiegel, W., ... Schroers, R. (2012). Identification of microRNAs in the cerebrospinal fluid as biomarker for the diagnosis of glioma. *Neuro-Oncology*, *14*(1), 29−33.

Barrett, S. P., & Salzman, J. (2016). Circular RNAs: Analysis, expression and potential functions. *Development*, *143*(11), 1838−1847.

Barrett, S. P., Wang, P. L., & Salzman, J. (2015). Circular RNA biogenesis can proceed through an exon-containing lariat precursor. *Elife*, *4*, e07540.

Bejugam, P. R., Das, A., & Panda, A. C. (2020). Seeing is believing: Visualizing circular RNAs. *Noncoding RNA*, *6*(4), 45.

Berghoff, A. S., Schur, S., Füreder, L. M., Gatterbauer, B., Dieckmann, K., Widhalm, G., ... Preusser, M. (2016). Descriptive statistical analysis of a real life cohort of 2419 patients with brain metastases of solid cancers. *ESMO Open*, *1*(2), e000024.

Berthois, Y., Delfino, C., Metellus, P., Fina, F., Nanni-Metellus, I., Al Aswy, H., ... Boudouresque, F. (2014). Differential expression of miR200a-3p and miR21 in grade II-III and grade IV gliomas: Evidence that miR200a-3p is regulated by O6-methylguanine methyltransferase and promotes temozolomide responsiveness. *Cancer Biology and Therapy*, *15*(7), 938−950.

Bharambe, H. S., Paul, R., Panwalkar, P., Jalali, R., Sridhar, E., Gupta, T., ... Shirsat, N. V. (2019). Downregulation of miR-204 expression defines a highly aggressive subset of group 3/group 4 medulloblastomas. *Acta Neuropathologica Communications*, *7*(1), 52.

Bian, S., Repic, M., Guo, Z., Kavirayani, A., Burkard, T., Bagley, J. A., ... Knoblich, J. A. (2018). Genetically engineered cerebral organoids model brain tumor formation. *Nature Methods*, *15*(8), 631−639.

Birks, D. K., Barton, V. N., Donson, A. M., Handler, M. H., Vibhakar, R., & Foreman, N. K. (2011). Survey of microRNA expression in pediatric brain tumors. *Pediatric Blood and Cancer*, *56*(2), 211−216.

Bose, R., & Ain, R. (2018). Regulation of transcription by circular RNAs. *Advances in Experimental Medicine and Biology*, *1087*, 81−94.

Cai, T., Liu, Y., & Xiao, J. (2018). Long noncoding RNA MALAT1 knockdown reverses chemoresistance to temozolomide via promoting microRNA-101 in glioblastoma. *Cancer Medicine*, *7*(4), 1404−1415.

Cao, Z., Pan, X., Yang, Y., Huang, Y., & Shen, H. B. (2018). The lncLocator: A subcellular localization predictor for long non-coding RNAs based on a stacked ensemble classifier. *Bioinformatics*, *34*(13), 2185−2194.

Cardenas, J., Balaji, U., & Gu, J. (2020). Cerina: Systematic circRNA functional annotation based on integrative analysis of ceRNA interactions. *Scientific Reports*, *10*(1), 22165.

Carlevaro-Fita, J., & Johnson, R. (2019). Global positioning system: Understanding long noncoding RNAs through subcellular localization. *Molecular Cell*, *73*(5), 869−883.

Carlevaro-Fita, J., Lanzos, A., Feuerbach, L., Hong, C., Mas-Ponte, D., Pedersen, J. S., ... Johnson, R., & PCAWG Consortium. (2020). Cancer LncRNA Census reveals evidence for deep functional conservation of long noncoding RNAs in tumorigenesis. *Communications Biology*, *3*(1), 56.

Carpentier, A., Canney, M., Vignot, A., Reina, V., Beccaria, K., Horodyckid, C., ... Idbaih, A. (2016). Clinical trial of blood−brain barrier disruption by pulsed ultrasound. *Science Translational Medicine*, *8*(343), 343re2.

Catanzaro, G., Besharat, Z. M., Garg, N., Ronci, M., Pieroni, L., Miele, E., ... Ferretti, E. (2016). MicroRNAs-proteomic networks characterizing human medulloblastoma-SLCs. *Stem Cells International*, *2016*, 2683042.

Cavalli, F. M. G., Remke, M., Rampasek, L., Peacock, J., Shih, D. J. H., Luu, B., ... Taylor, M. D. (2017). Intertumoral heterogeneity within medulloblastoma subgroups. *Cancer Cell*, *31*(6), 737−754, e6.

Chang, H., Yi, B., Ma, R., Zhang, X., Zhao, H., & Xi, Y. (2016). CRISPR/cas9, a novel genomic tool to knock down microRNA in vitro and in vivo. *Scientific Reports*, *6*, 22312.

Chen, A., Zhong, L., Ju, K., Lu, T., Lv, J., & Cao, H. (2020). Plasmatic circrna predicting the occurrence of human glioblastoma. *Cancer Management and Research*, *12*, 2917−2923.

Chen, D. F., Zhang, L. J., Tan, K., & Jing, Q. (2017). Application of droplet digital PCR in quantitative detection of the cell-free circulating circRNAs. *Biotechnology & Biotechnological Equipment*, *32*(1), 116−123.

Chen, J., Chen, T., Zhu, Y., Li, Y., Zhang, Y., Wang, Y., ... Ke, Y. (2019). circPTN sponges miR-145-5p/miR-330-5p to promote proliferation and stemness in glioma. *Journal of Experimental & Clinical Cancer Research*, *38*(1), 398.

Chen, L. L., & Yang, L. (2015). Regulation of circRNA biogenesis. *RNA Biology*, *12*(4), 381−388.

Chen, W., Xu, X. K., Li, J. L., Kong, K. K., Li, H., Chen, C., ... Li, F. C. (2017). MALAT1 is a prognostic factor in glioblastoma multiforme and induces chemoresistance to temozolomide through suppressing miR-203 and promoting thymidylate synthase expression. *Oncotarget*, *8*(14), 22783−22799.

Chen, W., Yu, Q., Chen, B., Lu, X., & Li, Q. (2016). The prognostic value of a seven-microRNA classifier as a novel biomarker for the prediction and detection of recurrence in glioma patients. *Oncotarget*, 7(33), 53392−53413.

Chen, W. L., Chen, H. J., Hou, G. Q., Zhang, X. H., & Ge, J. W. (2019). LINC01198 promotes proliferation and temozolomide resistance in a NEDD4-1-dependent manner, repressing PTEN expression in glioma. *Aging (Albany NY)*, 11(16), 6053−6068.

Chen, X., Zhang, Y., Shi, Y., Lian, H., Tu, H., Han, S., . . . He, X. (2015). MiR-873 acts as a novel sensitizer of glioma cells to cisplatin by targeting Bcl-2. *International Journal of Oncology*, 47(4), 1603−1611.

Chen, Y., & Wang, X. (2020). MiRDB: An online database for prediction of functional microRNA targets. *Nucleic Acids Research*, 48(D1), D127−D131.

Cheng, W., Ren, X., Zhang, C., Han, S., & Wu, A. (2017). Expression and prognostic value of microRNAs in lower-grade glioma depends on IDH1/2 status. *Journal of Neuro-Oncology*, 132(2), 207−218.

Chi, C., Mao, M., Shen, Z., Chen, Y., Chen, J., & Hou, W. (2018). HOXD-AS1 exerts oncogenic functions and promotes chemoresistance in cisplatin-resistant cervical cancer cells. *Human Gene Therapy*, 29(12), 1438−1448.

Clément, T., Salone, V., & Rederstorff, M. (2015). Dual luciferase gene reporter assays to study miRNA Function. *Methods in Molecular Biology*, 1296, 187−198.

Cui, T., Bell, E. H., McElroy, J., Becker, A. P., Gulati, P. M., Geurts, M., . . . Chakravarti, A. (2019). miR-4516 predicts poor prognosis and functions as a novel oncogene via targeting PTPN14 in human glioblastoma. *Oncogene*, 38(16), 2923−2936.

Dai, X., Liao, K., Zhuang, Z., Chen, B., Zhou, Z., Zhou, S., . . . Lin, R. (2019). AHIF promotes glioblastoma progression and radioresistance via exosomes. *International Journal of Oncology*, 54(1), 261−270.

Darnell, R. B. (2010). HITS-CLIP: Panoramic views of protein-RNA regulation in living cells. *Wiley Interdisciplinary Reviews: RNA*, 1(2), 266−286.

Davalos, V., Moutinho, C., Villanueva, A., Boque, R., Silva, P., Carneiro, F., . . . Esteller, M. (2012). Dynamic epigenetic regulation of the microRNA-200 family mediates epithelial and mesenchymal transitions in human tumorigenesis. *Oncogene*, 31(16), 2062−2074.

Davis, M. E. (2018). Epidemiology and overview of gliomas. *Seminars in Oncology Nursing*, 34(5), 420−429.

de Antonellis, P., Medaglia, C., Cusanelli, E., Andolfo, I., Liguori, L., De Vita, G., . . . Zollo, M. (2011). MiR-34a targeting of Notch ligand delta-like 1 impairs CD15 + /CD133 + tumor-propagating cells and supports neural differentiation in medulloblastoma. *PLoS One*, 6(9), e24584.

de la Rocha, A. M. A., Gonzalez-Huarriz, M., Guruceaga, E., Mihelson, N., Tejada-Solis, S., Diez-Valle, R., . . . Lopez-Bertoni, H. (2020). miR-425-5p, a SOX2 target, regulates the expression of FOXJ3 and RAB31 and promotes the survival of GSCs. *Archives of Clinical and Biomedical Research*, 4(3), 221−238.

Debeb, B. G., Lacerda, L., Anfossi, S., Diagaradjane, P., Chu, K., Bambhroliya, A., . . . Woodward, W. A. (2016). miR-141-mediated regulation of brain metastasis from breast cancer. *Journal of the National Cancer Institute*, 108 (8), djw026.

Denli, A. M., Tops, B. B. J., Plasterk, R. H. A., Ketting, R. F., & Hannon, G. J. (2004). Processing of primary microRNAs by the microprocessor complex. *Nature*, 432(7014), 231−235.

Derrien, T., Johnson, R., Bussotti, G., Tanzer, A., Djebali, S., Tilgner, H., . . . Guigo, R. (2012). The GENCODE v7 catalog of human long noncoding RNAs: Analysis of their gene structure, evolution, and expression. *Genome Research*, 22(9), 1775−1789.

Ding, B. S., James, D., Iyer, R., Falciatori, I., Hambardzumyan, D., Wang, S., . . . Hormigo, A. (2013). Prominin 1/ CD133 endothelium sustains growth of proneural glioma. *PLoS One*, 8(4), e62150.

Ding, C., Yi, X., Wu, X., Bu, X., Wang, D., Wu, Z., . . . Kang, D. (2020). Exosome-mediated transfer of circRNA CircNFIX enhances temozolomide resistance in glioma. *Cancer Letters*, 479, 1−12.

Ding, H., Cui, L., & Wang, C. (2020). Long noncoding RNA LIFR-AS1 suppresses proliferation, migration and invasion and promotes apoptosis through modulating miR-4262/NF-kappaB pathway in glioma. *Neurological Research*, 1−10.

Ding, J., Zhang, L., Chen, S., Cao, H., Xu, C., & Wang, X. (2020). lncRNA CCAT2 enhanced resistance of glioma cells against chemodrugs by disturbing the normal function of miR-424. *OncoTargets and Therapy*, 13, 1431−1445.

Ding, X., Yang, L., Geng, X., Zou, Y., Wang, Z., Li, Y., . . . Yu, H. (2020). CircRNAs as potential biomarkers for the clinicopathology and prognosis of glioma patients: A *meta*-analysis. *BMC Cancer*, 20(1), 1005.

Dong, R., Ma, X. K., Li, G. W., & Yang, L. (2018). CIRCpedia v2: An updated database for comprehensive circular RNA annotation and expression comparison. *Genomics Proteomics Bioinformatics*, *16*(4), 226−233.

Du, P., Zhao, H., Peng, R., Liu, Q., Yuan, J., Peng, G., & Liao, Y. (2017). LncRNA-XIST interacts with miR-29c to modulate the chemoresistance of glioma cell to TMZ through DNA mismatch repair pathway. *Bioscience Reports*, *37*(5), BSR20170696.

Duan, S., Li, M., Wang, Z., Wang, L., & Liu, Y. (2018). H19 induced by oxidative stress confers temozolomide resistance in human glioma cells via activating NF-kappaB signaling. *OncoTargets and Therapy*, *11*, 6395−6404.

Dudekula, D. B., Panda, A. C., Grammatikakis, I., De, S., Abdelmohsen, K., & Gorospe, M. (2016). CircInteractome: A web tool for exploring circular RNAs and their interacting proteins and microRNAs. *RNA Biology*, *13*(1), 34−42.

El Fatimy, R., Subramanian, S., Uhlmann, E. J., & Krichevsky, A. M. (2017). Genome editing reveals glioblastoma addiction to microRNA-10b. *Molecular Therapy*, *25*(2), 368−378.

Esquela-Kerscher, A., & Slack, F. J. (2006). Oncomirs − MicroRNAs with a role in cancer. *Nature Reviews Cancer*, *6*(4), 259−269.

Fan, C., Lei, X., Fang, Z., Jiang, Q., & Wu, F. X. (2018). CircR2 disease: A manually curated database for experimentally supported circular RNAs associated with various diseases. *Database (Oxford)*, *2018*, bay044.

Fan, H., Yuan, R., Cheng, S., Xiong, K., Zhu, X., & Zhang, Y. (2018). Overexpressed miR-183 promoted glioblastoma radioresistance via down-regulating LRIG1. *Biomedicine and Pharmacotherapy*, *97*, 1554−1563.

Fang, K., Liu, P., Dong, S., Guo, Y., Cui, X., Zhu, X., . . . Wu, Y. (2016). Magnetofection based on superparamagnetic iron oxide nanoparticle-mediated low lncRNA HOTAIR expression decreases the proliferation and invasion of glioma stem cells. *International Journal of Oncology*, *49*(2), 509−518.

Feng, S., Yao, J., Chen, Y., Geng, P., Zhang, H., Ma, X., . . . Yu, X. (2015). Expression and functional role of reprogramming-related long noncoding RNA (lincRNA-ROR) in glioma. *Journal of Molecular Neuroscience*, *56*(3), 623−630.

Ferlay, J., Colombet, M., Soerjomataram, I., Mathers, C., Parkin, D. M., Pineros, M., . . . Bray, F. (2019). Estimating the global cancer incidence and mortality in 2018: GLOBOCAN sources and methods. *International Journal of Cancer*, *144*(8), 1941−1953.

Fontanilles, M., Duran-Peña, A., & Idbaih, A. (2018). Liquid biopsy in primary brain tumors: Looking for stardust!. *Current Neurology and Neuroscience Reports*, *18*(3), 13-.

Friedman, R. C., Farh, K. K. H., Burge, C. B., & Bartel, D. P. (2009). Most mammalian mRNAs are conserved targets of microRNAs. *Genome Research*, *19*(1), 92−105.

Fu, C., Li, D., Zhang, X., Liu, N., Chi, G., & Jin, X. (2018). LncRNA PVT1 facilitates tumorigenesis and progression of glioma via regulation of MiR-128-3p/GREM1 axis and BMP signaling pathway. *Neurotherapeutics*, *15*(4), 1139−1157.

Galasso, M., Dama, P., Previati, M., Sandhu, S., Palatini, J., Coppola, V., . . . Volinia, S. (2014). A large scale expression study associates uc.283-plus lncRNA with pluripotent stem cells and human glioma. *Genome Medicine*, *6*(10), 76.

Gallego Romero, I., Pai, A. A., Tung, J., & Gilad, Y. (2014). RNA-seq: Impact of RNA degradation on transcript quantification. *BMC Biology*, *12*, 42.

Gao, J., Chen, Q., Zhao, Y., & Hou, R. (2020). lncRNA CRNDE is upregulated in glioblastoma multiforme and facilitates cancer progression through targeting miR-337-3p and ELMOD2 axis. *OncoTargets and Therapy*, *13*, 9225−9234.

Gao, W., Qiao, M., & Luo, K. (2020). Long noncoding RNA TP53TG1 contributes to radioresistance of glioma cells via miR-524-5p/RAB5A axis. *Cancer Biotherapy and Radiopharmaceuticals*.

Garzia, A., Morozov, P., Sajek, M., Meyer, C., & Tuschl, T. (2018). PAR-CLIP for discovering target sites of RNA-binding proteins. *Methods in Molecular Biology*, *1720*, 55−75.

Garzia, L., Andolfo, I., Cusanelli, E., Marino, N., Petrosino, G., De Martino, D., . . . Zollo, M. (2009). MicroRNA-199b-5p impairs cancer stem cells through negative regulation of HES1 in medulloblastoma. *PLoS One*, *4*(3), e4998.

Genovesi, L. A., Carter, K. W., Gottardo, N. G., Giles, K. M., & Dallas, P. B. (2011). Integrated analysis of miRNA and mRNA expression in childhood medulloblastoma compared with neural stem cells. *PLoS One*, *6*(9), e23935.

Ghosal, S., Das, S., Sen, R., Basak, P., & Chakrabarti, J. (2013). Circ2Traits: A comprehensive database for circular RNA potentially associated with disease and traits. *Frontiers in Genetics, 4*, 283.

Gillen, A. E., Yamamoto, T. M., Kline, E., Hesselberth, J. R., & Kabos, P. (2016). Improvements to the HITS-CLIP protocol eliminate widespread mispriming artifacts. *BMC Genomics, 17*(1), 338.

Glazar, P., Papavasileiou, P., & Rajewsky, N. (2014). circBase: A database for circular RNAs. *RNA, 20*(11), 1666−1670.

Godlewski, J., Nowicki, M. O., Bronisz, A., Williams, S., Otsuki, A., Nuovo, G., . . . Lawler, S. (2008). Targeting of the Bmi-1 oncogene/stem cell renewal factor by microRNA-128 inhibits glioma proliferation and self-renewal. *Cancer Research, 68*(22), 9125−9130.

Greene, J., Baird, A. M., Brady, L., Lim, M., Gray, S. G., McDermott, R., & Finn, S. (2017). Circular RNAs: Biogenesis, function and role in human diseases. *Frontiers in Molecular Biosciences, 4*, 38.

Grossman, R. L., Heath, A. P., Ferretti, V., Varmus, H. E., Lowy, D. R., Kibbe, W. A., & Staudt, L. (2016). Toward a shared vision for cancer genomic data. *New England Journal of Medicine, 375*(12), 1109−1112.

Guardia, G. D. A., Correa, B. R., Araujo, P. R., Qiao, M., Burns, S., Penalva, L. O. F., & Galante, P. A. F (2020). Proneural and mesenchymal glioma stem cells display major differences in splicing and lncRNA profiles. *NPJ Genomic Medicine, 5*, 2.

Guarnerio, J., Bezzi, M., Jeong, J. C., Paffenholz, S. V., Berry, K., Naldini, M. M., . . . Pandolfi, P. P. (2016). Oncogenic role of fusion-circRNAs derived from cancer-associated chromosomal translocations. *Cell, 165*(2), 289−302.

Guo, J. C., Fang, S. S., Wu, Y., Zhang, J. H., Chen, Y., Liu, J., . . . Zhao, Y. (2019). CNIT: A fast and accurate web tool for identifying protein-coding and long non-coding transcripts based on intrinsic sequence composition. *Nucleic Acids Research, 47*(W1), W516−W522.

Guo, J. U., Agarwal, V., Guo, H., & Bartel, D. P. (2014). Expanded identification and characterization of mammalian circular RNAs. *Genome Biology, 15*(7), 409.

Guo, Y., Liu, S., Wang, P., Zhao, S., Wang, F., Bing, L., . . . Hao, A. (2011). Expression profile of embryonic stem cell-associated genes Oct4, Sox2 and Nanog in human gliomas. *Histopathology, 59*(4), 763−775.

Guo, Y., Yan, K., Fang, J., Qu, Q., Zhou, M., & Chen, F. (2013). Let-7b expression determines response to chemotherapy through the regulation of cyclin D1 in Glioblastoma. *Journal of Experimental and Clinical Cancer Research, 32*(1), 41.

Gwak, H. S., Kim, T. H., Jo, G. H., Kim, Y. J., Kwak, H. J., Kim, J. H., . . . Park, J. B. (2012). Silencing of microRNA-21 confers radio-sensitivity through Inhibition of the PI3K/AKT pathway and enhancing autophagy in malignant glioma cell lines. *PLoS ONE, 7*(10), e47449.

Hafner, M., Landthaler, M., Burger, L., Khorshid, M., Hausser, J., Berninger, P., . . . Tuschl, T. (2010). Transcriptome-wide Identification of RNA-binding protein and microRNA target sites by PAR-CLIP. *Cell, 141*(1), 129−141.

Hamburger, A. W., & Salmon, S. E. (1977). Primary bioassay of human tumor stem cells. *Science, 197*(4302), 461−463.

Han, J., Lee, Y., Yeom, K. H., Kim, Y. K., Jin, H., & Kim, V. N. (2004). The Drosha-DGCR8 complex in primary microRNA processing. *Genes and Development, 18*(24), 3016−3027.

Han, L., Zhang, K., Shi, Z., Zhang, J., Zhu, J., Zhu, S., . . . Kang, C. (2012). LncRNA pro fi le of glioblastoma reveals the potential role of lncRNAs in contributing to glioblastoma pathogenesis. *International Journal of Oncology, 40*(6), 2004−2012.

Han, Y., Wu, Z., Wu, T., Huang, Y., Cheng, Z., Li, X., . . . Du, Z. (2016). Tumor-suppressive function of long noncoding RNA MALAT1 in glioma cells by downregulation of MMP2 and inactivation of ERK/MAPK signaling. *Cell Death & Disease, 7*, e2123.

Han, Y., Zhou, L., Wu, T., Huang, Y., Cheng, Z., Li, X., . . . Du, Z. (2016). Downregulation of lncRNA-MALAT1 affects proliferation and the expression of stemness markers in glioma stem cell line SHG139S. *Cellular and Molecular Neurobiology, 36*(7), 1097−1107.

Hansen, T. B., Jensen, T. I., Clausen, B. H., Bramsen, J. B., Finsen, B., Damgaard, C. K., & Kjems, J. (2013). Natural RNA circles function as efficient microRNA sponges. *Nature, 495*(7441), 384−388.

Haraszti, R., Coles, A., Aronin, N., Khvorova, A., & Didiot, M.-C. (2017). Loading of extracellular vesicles with chemically stabilized hydrophobic siRNAs for the treatment of disease in the central nervous system. *Bio-Protocol, 7*(12), e2338.

He, J., Ren, M., Li, H., Yang, L., Wang, X., & Yang, Q. (2019). Exosomal circular RNA as a biomarker platform for the early diagnosis of immune-mediated demyelinating disease. *Frontiers in Genetics, 10*, 860.

Helwak, A., Kudla, G., Dudnakova, T., & Tollervey, D. (2013). Mapping the human miRNA interactome by CLASH reveals frequent noncanonical binding. *Cell, 153*(3), 654—665.

Holdt, L. M., Kohlmaier, A., & Teupser, D. (2018). Molecular functions and specific roles of circRNAs in the cardiovascular system. *Non-coding RNA Research, 3*(2), 75—98.

Hombach, S., & Kretz, M. (2016). Non-coding RNAs: Classification, biology and functioning. *Advances in Experimental Medicine and Biology, 937*, 3—17.

Hu, T., Wang, F., & Han, G. (2020). LncRNA PSMB8-AS1 acts as ceRNA of miR-22-3p to regulate DDIT4 expression in glioblastoma. *Neuroscience Letters, 728*, 134896.

Hua, L., Huang, L., Zhang, X., & Feng, H. (2020). Downregulation of hsa_circ_0000936 sensitizes resistant glioma cells to temozolomide by sponging miR-1294. *Journal of Biosciences, 45*, 101.

Huang, A., Zheng, H., Wu, Z., Chen, M., & Huang, Y. (2020). Circular RNA-protein interactions: Functions, mechanisms, and identification. *Theranostics, 10*(8), 3503—3517.

Huang, B. S., Luo, Q. Z., Han, Y., Huang, D., Tang, Q. P., & Wu, L. X. (2017). MiR-223/PAX6 axis regulates glioblastoma stem cell proliferation and the chemo resistance to TMZ via regulating PI3K/Akt pathway. *Journal of Cellular Biochemistry, 118*(10), 3452—3461.

Huang, S., Qi, P., Zhang, T., Li, F., & He, X. (2019). The HIF-1α/miR-224-3p/ATG5 axis affects cell mobility and chemosensitivity by regulating hypoxia-induced protective autophagy in glioblastoma and astrocytoma. *Oncology Reports, 41*(3), 1759—1768.

Huo, J. F., & Chen, X. B. (2019). Long noncoding RNA growth arrest-specific 5 facilitates glioma cell sensitivity to cisplatin by suppressing excessive autophagy in an mTOR-dependent manner. *Journal of Cellular Biochemistry, 120*(4), 6127—6136.

Huppertz, I., Attig, J., D'Ambrogio, A., Easton, L. E., Sibley, C. R., Sugimoto, Y., . . . Ule, J. (2014). iCLIP: Protein-RNA interactions at nucleotide resolution. *Methods, 65*(3), 274—287.

International Human Genome Sequencing Consortium. (2004). Finishing the euchromatic sequence of the human genome. *Nature, 431*(7011), 931—945.

Irie, A., Sato, K., Hara, R. I., Wada, T., & Shibasaki, F. (2020). An artificial cationic oligosaccharide combined with phosphorothioate linkages strongly improves siRNA stability. *Scientific Reports, 10*(1), 14845.

Itzkovitz, S., & Van Oudenaarden, A. (2011). Validating transcripts with probes and imaging technology. *Nature Methods, 8*(4 Suppl), S12—S19.

Ivanov, D. P., Coyle, B., Walker, D. A., & Grabowska, A. M. (2016). In vitro models of medulloblastoma: Choosing the right tool for the job. *Journal of Biotechnology, 236*, 10—25.

Jacob, F., Salinas, R. D., Zhang, D. Y., Nguyen, P. T. T., Schnoll, J. G., Wong, S. Z. H., . . . Song, H. (2020). A patient-derived glioblastoma organoid model and biobank recapitulates inter- and intra-tumoral heterogeneity. *Cell, 180*(1), 188—204, e22.

Jarroux, J., Morillon, A., & Pinskaya, M. (2017). History, discovery, and classification of lncRNAs. *Advances in Experimental Medicine and Biology, 1008*, 1—46.

Jayakrishnan, P., Venkat, E., Ramachandran, G., Kesavapisharady, K., Nair, S., Bharathan, B., . . . Gopala, S. (2019). In vitro neurosphere formation correlates with poor survival in glioma. *IUBMB Life, 71*(2), 244—253.

Jeck, W. R., Sorrentino, J. A., Wang, K., Slevin, M. K., Burd, C. E., Liu, J., . . . Sharpless, N. E., et al. (2013). Circular RNAs are abundant, conserved, and associated with ALU repeats. *RNA, 19*(2), 141—157.

Jensen, K. B., & Darnell, R. B. (2008). CLIP: Crosslinking and immunoprecipitation of in vivo RNA targets of RNA-binding proteins. *Methods in Molecular Biology, 488*, 85—98.

Jeyaraman, S., Hanif, E. A. M., Ab Mutalib, N. S., Jamal, R., & Abu, N. (2019). Circular RNAs: Potential regulators of treatment resistance in human cancers. *Frontiers in Genetics, 10*, 1369.

Jia, L., Tian, Y., Chen, Y., & Zhang, G. (2018). The silencing of LncRNA-H19 decreases chemoresistance of human glioma cells to temozolomide by suppressing epithelial-mesenchymal transition via the Wnt/beta-Catenin pathway. *OncoTargets and Therapy, 11*, 313—321.

Jiang, C., Shen, F., Du, J., Fang, X., Li, X., Su, J., . . . Liu, Z. (2018). Upregulation of CASC2 sensitized glioma to temozolomide cytotoxicity through autophagy inhibition by sponging miR-193a-5p and regulating mTOR expression. *Biomedicine & Pharmacotherapy, 97*, 844—850.

Jiang, P., Wang, P., Sun, X., Yuan, Z., Zhan, R., Ma, X., & Li, W. (2016). Knockdown of long noncoding RNA H19 sensitizes human glioma cells to temozolomide therapy. *OncoTargets and Therapy, 9*, 3501—3509.

Jin, X., Yuan, L., Liu, B., Kuang, Y., Li, H., Li, L., ... Li, Q (2020). Integrated analysis of circRNA-miRNA-mRNA network reveals potential prognostic biomarkers for radiotherapies with X-rays and carbon ions in non-small cell lung cancer. *Annals of Translational Medicine*, *8*(21), 1373.

Jin, Y., Chen, Z., Liu, X., & Zhou, X. (2013). Evaluating the MicroRNA targeting sites by luciferase reporter gene assay. *Methods in Molecular Biology*, *936*, 117−127.

Johnson, R. (2012). Long non-coding RNAs in Huntington's disease neurodegeneration. *Neurobiology of Disease*, *46*(2), 245−254.

Kaid, C., Silva, P. B. G., Cortez, B. A., Rodini, C. O., Semedo-Kuriki, P., & Okamoto, O. K. (2015). miR-367 promotes proliferation and stem-like traits in medulloblastoma cells. *Cancer Science*, *106*(9), 1188−1195.

Karedath, T., Ahmed, I., Al Ameri, W., Al-Dasim, F. M., Andrews, S. S., Samuel, S., ... Malek, J. A. (2019). Silencing of ANKRD12 circRNA induces molecular and functional changes associated with invasive phenotypes. *BMC Cancer*, *19*(1), 565.

Katsushima, K., Natsume, A., Ohka, F., Shinjo, K., Hatanaka, A., Ichimura, N., & Kondo, Y. (2016). Targeting the Notch-regulated non-coding RNA TUG1 for glioma treatment. *Nature Communications*, *7*, 13616.

Kertesz, M., Iovino, N., Unnerstall, U., Gaul, U., & Segal, E. (2007). The role of site accessibility in microRNA target recognition. *Nature Genetics*, *39*(10), 1278−1284.

Khatsenko, O., Morgan, R., Truong, L., York-Defalco, C., Sasmor, H., Conklin, B., & Geary, R. S. (2000). Absorption of antisense oligonucleotides in rat intestine: Effect of chemistry and length. *Antisense and Nucleic Acid Drug Development*, *10*(1), 35−44.

Kijima, N., & Kanemura, Y. (2016). Molecular classification of medulloblastoma. *Neurologia Medico-Chirurgica (Tokyo)*, *56*(11), 687−697.

Kim, S. S., Harford, J. B., Moghe, M., Rait, A., Pirollo, K. F., & Chang, E. H. (2018). Targeted nanocomplex carrying siRNA against MALAT1 sensitizes glioblastoma to temozolomide. *Nucleic Acids Research*, *46*(3), 1424−1440.

Kim, T. M., Huang, W., Park, R., Park, P. J., & Johnson, M. D. (2011). A developmental taxonomy of glioblastoma defined and maintained by microRNAs. *Cancer Research*, *71*(9), 3387−3399.

Kiriakidou, M., Nelson, P. T., Kouranov, A., Fitziev, P., Bouyioukos, C., Mourelatos, Z., & Hatzigeorgiou, A. (2004). A combined computational-experimental approach predicts human microRNA targets. *Genes and Development*, *18*(10), 1165−1178.

Kleaveland, B., Shi, C. Y., Stefano, J., & Bartel, D. P. (2018). A network of noncoding regulatory RNAs acts in the mammalian brain. *Cell*, *174*(2), 350−362, e17.

Kocks, C., Boltengagen, A., Piwecka, M., Rybak-Wolf, A., & Rajewsky, N. (2018). Single-molecule fluorescence in situ hybridization (FISH) of circular RNA CDR1as. *Methods in Molecular Biology*, *1724*, 77−96.

König, J., Zarnack, K., Rot, G., Curk, T., Kayikci, M., Zupan, B., & Ule, J. (2010). ICLIP reveals the function of hnRNP particles in splicing at individual nucleotide resolution. *Nature Structural and Molecular Biology*, *17*(7), 909−915.

Kopková, A., šána, J., Večeřa, M., Fadrus, P., Lipina, R., Smrčka, M., ... Slaby, O. (2019). MicroRNAs in cerebrospinal fluid as biomarkers in brain tumor patients. *Klinicka Onkologie*, *32*(3), 181−186.

Kozomara, A., & Griffiths-Jones, S. (2011). miRBase: Integrating microRNA annotation and deep-sequencing data. *Nucleic Acids Research*, *39*. (Database issue):D152-7.

Kristensen, L. S., Hansen, T. B., Veno, M. T., & Kjems, J. (2018). Circular RNAs in cancer: Opportunities and challenges in the field. *Oncogene*, *37*(5), 555−565.

Krützfeldt, J., Rajewsky, N., Braich, R., Rajeev, K. G., Tuschl, T., Manoharan, M., ... Stoffel, M. (2005). Silencing of microRNAs in vivo with "antagomirs". *Nature*, *438*(7068), 685−689.

Kunder, R., Jalali, R., Sridhar, E., Moiyadi, A., Goel, N., Goel, A., & Shirsat, N. V. (2013). Real-time PCR assay based on the differential expression of microRNAs and protein-coding genes for molecular classification of formalin-fixed paraffin embedded medulloblastomas. *Neuro-Oncology*, *15*(12), 1644−1651.

Lancaster, M. A., Renner, M., Martin, C. A., Wenzel, D., Bicknell, L. S., Hurles, M. E., ... Knoblich, J. A. (2013). Cerebral organoids model human brain development and microcephaly. *Nature*, *501*(7467), 373−379.

Lang, M. F., Yang, S., Zhao, C., Sun, G., Murai, K., Wu, X., ... Shi, Y. (2012). Genome-wide profiling identified a set of miRNAs that are differentially expressed in glioblastoma stem cells and normal neural stem cells. *PLoS One*, *7*(4), e36248.

Latowska, J., Grabowska, A., Zarębska, Ż., Kuczyński, K., Kuczyńska, B., & Rolle, K. (2020). Non-coding RNAs in brain tumors, the contribution of lncRNAs, circRNAs, and snoRNAs to cancer development—Their diagnostic and therapeutic potential. *International Journal of Molecular Sciences*, *21*(19), 1−31.

Lee, Y. Y., Yang, Y. P., Huang, M. C., Wang, M. L., Yen, S. H., Huang, P. I., . . . Chen, M. T. (2014). MicroRNA142-3p promotes tumor-initiating and radioresistant properties in malignant pediatric brain tumors. *Cell Transplantation*, *23*(4−5), 669−690.

Lei, M., Zheng, G., Ning, Q., Zheng, J., & Dong, D. (2020). Translation and functional roles of circular RNAs in human cancer. *Molecular Cancer*, *19*(1), 30.

Lenting, K., Verhaak, R., ter Laan, M., Wesseling, P., & Leenders, W. (2017). Glioma: Experimental models and reality. *Acta Neuropathologica*, *133*(2), 263−282.

Lewis, B. P., Burge, C. B., & Bartel, D. P. (2005). Conserved seed pairing, often flanked by adenosines, indicates that thousands of human genes are microRNA targets. *Cell*, *120*(1), 15−20.

Li, A., Walling, J., Kotliarov, Y., Center, A., Steed, M. E., Ahn, S. J., . . . Fine, H. A. (2008). Genomic changes and gene expression profiles reveal that established glioma cell lines are poorly representative of primary human gliomas. *Molecular Cancer Research*, *6*(1), 21−30.

Li, B., Zhao, H., Song, J., Wang, F., & Chen, M. (2020). LINC00174 down-regulation decreases chemoresistance to temozolomide in human glioma cells by regulating miR-138-5p/SOX9 axis. *Human Cell*, *33*(1), 159−174.

Li, C., Feng, S., & Chen, L. (2020). MSC-AS1 knockdown inhibits cell growth and temozolomide resistance by regulating miR-373-3p/CPEB4 axis in glioma through PI3K/Akt pathway. *Molecular and Cellular Biochemistry*, *476*(2), 699−713.

Li, F., Ma, K., Sun, M., & Shi, S. (2018). Identification of the tumor-suppressive function of circular RNA ITCH in glioma cells through sponging miR-214 and promoting linear ITCH expression. *American Journal of Translational Research*, *10*(5), 1373−1386.

Li, Q., Jia, H., Li, H., Dong, C., Wang, Y., & Zou, Z. (2016). LncRNA and mRNA expression profiles of glioblastoma multiforme (GBM) reveal the potential roles of lncRNAs in GBM pathogenesis. *Tumor Biology*, *37*(11), 14537−14552.

Li, S., Li, Y., Chen, B., Zhao, J., Yu, S., Tang, Y., . . . Huang, S. (2018). exoRBase: A database of circRNA, lncRNA and mRNA in human blood exosomes. *Nucleic Acids Research*, *46*(D1), D106−D112.

Li, S., Zeng, A., Hu, Q., Yan, W., Liu, Y., & You, Y. (2017). miR-423-5p contributes to a malignant phenotype and temozolomide chemoresistance in glioblastomas. *Neuro-Oncology*, *19*(1), 55−65.

Li, T., Ma, J., Han, X., Jia, Y., Yuan, H., Shui, S., & Guo, D. (2018). MicroRNA-320 enhances radiosensitivity of glioma through down-regulation of sirtuin type 1 by directly targeting forkhead box protein M1. *Translational Oncology*, *11*(2), 205−M12.

Li, Y., Zhao, J., Yu, S., Wang, Z., He, X., Su, Y., . . . Huang, S. (2019). Extracellular vesicles long RNA sequencing reveals abundant mRNA, circRNA, and lncRNA in human blood as potential biomarkers for cancer diagnosis. *Clinical Chemistry*, *65*(6), 798−808.

Li, Y. C., Li, C. F., Chen, L. B., Li, D. D., Yang, L., Jin, J. P., & Zhang, B. (2015). MicroRNA-766 targeting regulation of SOX6 expression promoted cell proliferation of human colorectal cancer. *OncoTargets and Therapy*, *8*, 2981−2988.

Liang, C., Yang, Y., Guan, J., Lv, T., Qu, S., Fu, Q., & Zhao, H. (2018). LncRNA UCA1 sponges miR-204-5p to promote migration, invasion and epithelial-mesenchymal transition of glioma cells via upregulation of ZEB1. *Pathology − Research and Practice*, *214*(9), 1474−1481.

Liang, Z., Wang, Y., Li, H., Sun, Y., & Gong, Y. (2019). lncRNAs combine and crosstalk with NSPc1 in ATRA-induced differentiation of U87 glioma cells. *Oncology Letters*, *17*(6), 5821−5829.

Liao, H., Bai, Y., Qiu, S., Zheng, L., Huang, L., Liu, T., . . . Guo, H. (2015). MiR-203 downregulation is responsible for chemoresistance in human glioblastoma by promoting epithelial-mesenchymal transition via SNAI2. *Oncotarget*, *6*(11), 8914−8928.

Liao, K., Ma, X., Chen, B., Lu, X., Hu, Y., Lin, Y., . . . Qiu, Y. (2019). Upregulated AHIF-mediated radioresistance in glioblastoma. *Biochemical and Biophysical Research Communications*, *509*(2), 617−623.

Liao, Y., Shen, L., Zhao, H., Liu, Q., Fu, J., Guo, Y., & Cheng, L. (2017). LncRNA CASC2 interacts with miR-181a to modulate glioma growth and resistance to TMZ through PTEN pathway. *Journal of Cellular Biochemistry*, *118*(7), 1889−1899.

Liao, Y., Zhang, B., Zhang, T., Zhang, Y., & Wang, F. (2019). LncRNA GATA6-AS promotes cancer cell proliferation and inhibits apoptosis in glioma by downregulating lncRNA TUG1. *Cancer Biotherapy and Radiopharmaceuticals*, *34*(10), 660−665.

Licatalosi, D. D., Mele, A., Fak, J. J., Ule, J., Kayikci, M., Chi, S. W., . . . Darnell, R. B. (2008). HITS-CLIP yields genome-wide insights into brain alternative RNA processing. *Nature*, *456*(7221), 464−469.

Lin, Y., Liu, T., Cui, T., Wang, Z., Zhang, Y., Tan, P., . . . Wang, D. (2020). RNAInter in 2020: RNA interactome repository with increased coverage and annotation. *Nucleic Acids Research*, *48*(D1), D189–D197.

Linkous, A., Balamatsias, D., Snuderl, M., Edwards, L., Miyaguchi, K., Milner, T., . . . Fine, H. A. (2019). Modeling patient-derived glioblastoma with cerebral organoids. *Cell Reports, 26*(12), 3203–3211, e5.

Liu, J., Zhao, K., Huang, N., & Zhang, N. (2019). Circular RNAs and human glioma. *Cancer Biology & Medicine*, *16*(1), 11–23.

Liu, M., Wang, Q., Shen, J., Yang, B. B., & Ding, X. (2019). Circbank: A comprehensive database for circRNA with standard nomenclature. *RNA Biology*, *16*(7), 899–905.

Liu, S., Yin, F., Zhang, J., Wicha, M. S., Chang, A. E., Fan, W., & Li, Q. (2014). Regulatory roles of miRNA in the human neural stem cell transformation to glioma stem cells. *Journal of Cellular Biochemistry*, *115*(8), 1368–1380.

Liu, S. J., Malatesta, M., Lien, B. V., Saha, P., Thombare, S. S., Hong, S. J., . . . Lim, D. A. (2020). CRISPRi-based radiation modifier screen identifies long non-coding RNA therapeutic targets in glioma. *Genome Biology, 21*(1), 83.

Liu, X., Song, B., Li, S., Wang, N., & Yang, H. (2017). Identification and functional analysis of the risk microRNAs associated with cerebral low-grade glioma prognosis. *Molecular Medicine Reports, 16*(2), 1173–1179.

Louis, D. N., Perry, A., Reifenberger, G., Von Deimling, A., Figarella-Branger, D., Webster, K. C., . . . Ellison, D. W. (2016). The 2016 World Health Organization classification of tumors of the central nervous system: A summary. *Acta Neuropathologica, 131*(6), 803–820.

Lv, Q. L., Du, H., Liu, Y. L., Huang, Y. T., Wang, G. H., Zhang, X., . . . Zhou, H. H. (2017). Low expression of microRNA-320b correlates with tumorigenesis and unfavorable prognosis in glioma. *Oncology Reports, 38*(2), 959–966.

Lv, Q. L., Zhu, H. T., Li, H. M., Cheng, X. H., Zhou, H. H., & Chen, S. H. (2018). Down-regulation of miRNA-320c promotes tumor growth and metastasis and predicts poor prognosis in human glioma. *Brain Research Bulletin, 139*, 125–132.

Lv, T., Miao, Y. F., Jin, K., Han, S., Xu, T. Q., Qiu, Z. L., & Zhang, X. H. (2018). Dysregulated circular RNAs in medulloblastoma regulate proliferation and growth of tumor cells via host genes. *Cancer Medicine, 7*(12), 6147–6157.

Lyu, Y., Caudron-Herger, M., & Diederichs, S. (2020). circ2GO: A database linking circular RNAs to gene function. *Cancers (Basel), 12*(10).

Ma, B., Yuan, Z., Zhang, L., Lv, P., Yang, T., Gao, J., & Zhang, B. (2017). Long non-coding RNA AC023115.3 suppresses chemoresistance of glioblastoma by reducing autophagy. *Biochimica et Biophysica Acta − Molecular Cell Research, 1864*(8), 1393–1404.

Ma, Y., Zhou, G., Li, M., Hu, D., Zhang, L., Liu, P., & Lin, K. (2018). Long noncoding RNA DANCR mediates cisplatin resistance in glioma cells via activating AXL/PI3K/Akt/NF-kappaB signaling pathway. *Neurochemistry International, 118*, 233–241.

Mashouri, L., Yousefi, H., Aref, A. R., Ahadi, A. M., Molaei, F., & Alahari, S. K. (2019). Exosomes: Composition, biogenesis, and mechanisms in cancer metastasis and drug resistance. *Molecular Cancer, 18*(1), 75.

Mato Prado, M., Frampton, A. E., Giovannetti, E., Stebbing, J., Castellano, L., & Krell, J. (2016). Investigating miRNA-mRNA regulatory networks using crosslinking immunoprecipitation methods for biomarker and target discovery in cancer. *Expert Review of Molecular Diagnostics, 16*(11), 1155–1162.

Matsui, M., & Corey, D. R. (2017). *Non-coding RNAs as drug targets* (pp. 167–179). Nature Publishing Group.

Mazor, G., Levin, L., Picard, D., Ahmadov, U., Caren, H., Borkhardt, A., & Rotblat, B. (2019). The lncRNA TP73-AS1 is linked to aggressiveness in glioblastoma and promotes temozolomide resistance in glioblastoma cancer stem cells. *Cell Death & Disease, 10*(3), 246.

McDonald, K. L., Aw, G., & Kleihues, P. (2012). Role of biomarkers in the clinical management of glioblastomas: What are the barriers and how can we overcome them? *Frontiers in Neurology, 3*, 188.

Meijer, H. A., Smith, E. M., & Bushell, M. (2014). Regulation of miRNA strand selection: Follow the leader? *Biochemical Society Transactions, 42*(4), 1135–1140.

Meister, G., Landthaler, M., Dorsett, Y., & Tuschl, T. (2004). Sequence-specific inhibition of microRNA-and siRNA-induced RNA silencing. *RNA, 10*(3), 544–550.

Memczak, S., Jens, M., Elefsinioti, A., Torti, F., Krueger, J., Rybak, A., . . . Rajewsky, N. (2013). Circular RNAs are a large class of animal RNAs with regulatory potency. *Nature, 495*(7441), 333–338.

Meng, S., Zhou, H., Feng, Z., Xu, Z., Tang, Y., Li, P., & Wu, M. (2017). CircRNA: Functions and properties of a novel potential biomarker for cancer. *Molecular Cancer*, *16*(1), 94.

Meng, X., Hu, D., Zhang, P., Chen, Q., & Chen, M. (2019). CircFunBase: A database for functional circular RNAs. *Database (Oxford)*, *2019*, baz003.

Millard, N. E., & De Braganca, K. C. (2016). Medulloblastoma. *Journal of Child Neurology*, *31*(12), 1341−1353.

Min, W., Dai, D., Wang, J., Zhang, D., Zhang, Y., Han, G., . . . Yue, Z. (2016). Long Noncoding RNA miR210HG as a potential biomarker for the diagnosis of glioma. *PLoS One*, *11*(9), e0160451.

Miranda, K. C., Huynh, T., Tay, Y., Ang, Y. S., Tam, W. L., Thomson, A. M., . . . Rigoutsos, I. (2006). A pattern-based method for the identification of microRNA binding sites and their corresponding heteroduplexes. *Cell*, *126*(6), 1203−1217.

Mo, D., Li, X., Raabe, C. A., Cui, D., Vollmar, J. F., Rozhdestvensky, T. S., . . . Brosius, J. (2019). A universal approach to investigate circRNA protein coding function. *Scientific Reports*, *9*(1), 11684.

Moldovan, L. I., Hansen, T. B., Veno, M. T., Okholm, T. L. H., Andersen, T. L., Hager, H., . . . Kristensen, L. S. (2019). High-throughput RNA sequencing from paired lesional- and non-lesional skin reveals major alterations in the psoriasis circRNAome. *BMC Medical Genomics*, *12*(1), 174.

Monroig, Pd. C., Chen, L., Zhang, S., & Calin, G. A. (2015). Small molecule compounds targeting miRNAs for cancer therapy. *Advanced Drug Delivery Reviews*, *81*, 104−116.

Niyazi, M., Pitea, A., Mittelbronn, M., Steinbach, J., Sticht, C., Zehentmayr, F., . . . Unger, K. (2016). A 4-miRNA signature predicts the therapeutic outcome of glioblastoma. *Oncotarget*, *7*(29), 45764−45775.

Northcott, P. A., Jones, D. T. W., Kool, M., Robinson, G. W., Gilbertson, R. J., Cho, Y. J., . . . Pfister, S. M. (2012). Medulloblastomics: The end of the beginning. *Nature Reviews Cancer*, *12*, 818−834.

Northcott, P. A., Robinson, G. W., Kratz, C. P., Mabbott, D. J., Pomeroy, S. L., Clifford, S. C., & Pfister, S. M. (2019). Medulloblastoma. *Nature Reviews Disease Primers*, *5*(1), 11.

Ogawa, J., Pao, G. M., Shokhirev, M. N., & Verma, I. M. (2018). Glioblastoma model using human cerebral organoids. *Cell Reports*, *23*(4), 1220−1229.

Ohgaki, H., Dessen, P., Jourde, B., Horstmann, S., Nishikawa, T., Di Patre, P. L., . . . Kleihues, P. (2004). Genetic pathways to glioblastoma: A population-based study. *Cancer Research*, *64*(19), 6892−6899.

Ondracek, J., Fadrus, P., Sana, J., Besse, A., Loja, T., Vecera, M., . . . Slaby, O. (2017). Global microRNA expression profiling identifies unique microRNA pattern of radioresistant glioblastoma cells. *Anticancer Research*, *37*(3), 1099−1104.

Pamudurti, N. R., Bartok, O., Jens, M., Ashwal-Fluss, R., Stottmeister, C., Ruhe, L., . . . Kadener, S. (2017). Translation of circRNAs. *Molecular Cell*, *66*(1), 9−21, e7.

Panda, A. C., & Gorospe, M. (2018). Detection and analysis of circular RNAs by RT-PCR. *Bio-protocol*, *8*(6).

Panda, A. C. (2018). Circular RNAs act as miRNA sponges. *Advances in Experimental Medicine and Biology*, *1087*, 67−79.

Pandey, P. R., Munk, R., Kundu, G., De, S., Abdelmohsen, K., & Gorospe, M. (2020). Methods for analysis of circular RNAs. *Wiley Interdisciplinary Reviews: RNA*, *11*(1), e1566.

Paraskevopoulou, M. D., Georgakilas, G., Kostoulas, N., Vlachos, I. S., Vergoulis, T., Reczko, M., . . . Hatzigeorgiou, A. G. (2013). DIANA-microT web server v5.0: Service integration into miRNA functional analysis workflows. *Nucleic Acids Research*, *41*(Web Server issue), W169-73.

Perry, R. B., & Ulitsky, I. (2016). The functions of long noncoding RNAs in development and stem cells. *Development*, *143*(21), 3882−3894.

Petrescu, G. E. D., Sabo, A. A., Torsin, L. I., Calin, G. A., & Dragomir, M. P. (2019). MicroRNA based theranostics for brain cancer: Basic principles. *Journal of Experimental & Clinical Cancer Research*, *38*(1), 231.

Pfeffer, S. R., Yang, C. H., & Pfeffer, L. M. (2015). The Role of MIR-21 in cancer. *Drug Development Research*, *76*(6), 270−277.

Piwecka, M., Glazar, P., Hernandez-Miranda, L. R., Memczak, S., Wolf, S. A., Rybak-Wolf, A., . . . Rajewsky, N. (2017). Loss of a mammalian circular RNA locus causes miRNA deregulation and affects brain function. *Science*, *357*(6357), eaam8526.

Po, A., Abballe, L., Sabato, C., Gianno, F., Chiacchiarini, M., Catanzaro, G., . . . Besharat, Z. M. (2018). Sonic hedgehog medulloblastoma cancer stem cells mirnome and transcriptome highlight novel functional networks. *International Journal of Molecular Sciences*, *19*(8), 2326.

Pyko, I. V., Nakada, M., Sabit, H., Teng, L., Furuyama, N., Hayashi, Y., . . . Hamada, J. (2013). Glycogen synthase kinase 3β inhibition sensitizes human glioblastoma cells to temozolomide by affecting O6-methylguanine DNA methyltransferase promoter methylation via c-Myc signaling. *Carcinogenesis*, *34*(10), 2206−2217.

Que, T., Song, Y., Liu, Z., Zheng, S., Long, H., Li, Z., & Qi, S. (2015). Decreased miRNA-637 is an unfavorable prognosis marker and promotes glioma cell growth, migration and invasion via direct targeting Akt1. *Oncogene, 34*(38), 4952−4963.

Quinn, J. J., & Chang, H. Y. (2016). Unique features of long non-coding RNA biogenesis and function. *Nature Reviews Genetics, 17*(1), 47−62.

Rehmsmeier, M., Steffen, P., Höchsmann, M., & Giegerich, R. (2004). Fast and effective prediction of microRNA/target duplexes. *RNA, 10*(10), 1507−1517.

Reustle, A., Fisel, P., Renner, O., Buttner, F., Winter, S., Rausch, S., . . . Schaeffeler, E. (2018). Characterization of the breast cancer resistance protein (BCRP/ABCG2) in clear cell renal cell carcinoma. *International Journal of Cancer, 143*(12), 3181−3193.

Ricci-Vitiani, L., Pallini, R., Biffoni, M., Todaro, M., Invernici, G., Cenci, T., . . . De Maria, R. (2010). Tumour vascularization via endothelial differentiation of glioblastoma stem-like cells. *Nature, 468*(7325), 824−828.

Robertson, F. L., Marqués-Torrejón, M. A., Morrison, G. M., & Pollard, S. M. (2019). Experimental models and tools to tackle glioblastoma. *Disease Models & Mechanisms, 12*(9).

Rophina, M., Sharma, D., Poojary, M., & Scaria, V. (2020). Circad: A comprehensive manually curated resource of circular RNA associated with diseases. *Database (Oxford), 2020*, baaa019.

Roth, P., Wischhusen, J., Happold, C., Chandran, P. A., Hofer, S., Eisele, G., & Keller, A. (2011). A specific miRNA signature in the peripheral blood of glioblastoma patients. *Journal of Neurochemistry, 118*(3), 449−457.

Roussel, M. F., & Stripay, J. L. (2020). Modeling pediatric medulloblastoma. *Brain Pathology, 30*(3), 703−712.

Ruan, H., Xiang, Y., Ko, J., Li, S., Jing, Y., Zhu, X., . . . Han, L. (2019). Comprehensive characterization of circular RNAs in ∼ 1000 human cancer cell lines. *Genome Medicine, 11*(1), 55.

Ruan, J., Lou, S., Dai, Q., Mao, D., Ji, J., & Sun, X. (2015). Tumor suppressor miR-181c attenuates proliferation, invasion, and self-renewal abilities in glioblastoma. *NeuroReport, 26*(2), 66−73.

Ruiz-Garcia, H., Alvarado-Estrada, K., Schiapparelli, P., Quinones-Hinojosa, A., & Trifiletti, D. M. (2020). Engineering three-dimensional tumor models to study glioma cancer stem cells and tumor microenvironment. *Front Cell Neurosci, 14*, 558381.

Rybak-Wolf, A., Stottmeister, C., Glazar, P., Jens, M., Pino, N., Giusti, S., & Rajewsky, N. (2015). Circular RNAs in the mammalian brain are highly abundant, conserved, and dynamically expressed. *Molecular Cell, 58*(5), 870−885.

Salmena, L., Poliseno, L., Tay, Y., Kats, L., & Pandolfi, P. P. (2011). A ceRNA hypothesis: The Rosetta Stone of a hidden RNA language? *Cell, 146*(3), 353−358.

Salzman, J., Chen, R. E., Olsen, M. N., Wang, P. L., & Brown, P. O. (2013). Cell-type specific features of circular RNA expression. *PLOS Genetics, 9*(9), e1003777.

Sana, J., Busek, P., Fadrus, P., Besse, A., Radova, L., Vecera, M., & Slaby, O. (2018). Identification of microRNAs differentially expressed in glioblastoma stem-like cells and their association with patient survival. *Scientific Reports, 8*(1), 2836.

Sarantopoulou, D., Tang, S. Y., Ricciotti, E., Lahens, N. F., Lekkas, D., Schug, J., . . . Grant, G. R. (2019). Comparative evaluation of RNA-Seq library preparation methods for strand-specificity and low input. *Scientific Reports, 9*(1), 13477.

Schneider, T., & Bindereif, A. (2017). Circular RNAs: Coding or noncoding? *Cell Research, 27*(6), 724−725.

Schwarz, D. S., Hutvágner, G., Du, T., Xu, Z., Aronin, N., & Zamore, P. D. (2003). Asymmetry in the assembly of the RNAi enzyme complex. *Cell, 115*(2), 199−208.

Seidel, S., Garvalov, B. K., Wirta, V., von Stechow, L., Schanzer, A., Meletis, K., . . . Acker, T. (2010). A hypoxic niche regulates glioblastoma stem cells through hypoxia inducible factor 2 alpha. *Brain, 133*(Pt 4), 983−995.

Shah, V., & Kochar, P. (2018). Brain cancer: Implication to disease, therapeutic strategies and tumor targeted drug delivery approaches. *Recent Patents on Anti-Cancer Drug Discovery, 13*(1), 70−85.

Shahpar, S., Mhatre, P. V., & Huang, M. E. (2016). *Update on brain tumors: New developments in neuro-oncologic diagnosis and treatment, and impact on rehabilitation strategies* (pp. 678−689). Elsevier Inc.

Shang, C., Guo, Y., Hong, Y., & Xue, Y. X. (2016). Long non-coding RNA TUSC7, a target of miR-23b, plays tumor-suppressing roles in human gliomas. *Frontiers in Cellular Neuroscience, 10*, 235.

Shang, Q., Yang, Z., Jia, R., & Ge, S. (2019). The novel roles of circRNAs in human cancer. *Molecular Cancer, 18*(1), 6.

Shao, N., Xue, L., Wang, R., Luo, K., Zhi, F., & Lan, Q. (2019). MiR-454-3p is an exosomal biomarker and functions as a tumor suppressor in glioma. *Molecular Cancer Therapeutics*, *18*(2), 459−469.

Shi, C., Rao, C., Sun, C., Yu, L., Zhou, X., Hua, D., . . . Yu, S. (2018). miR-29s function as tumor suppressors in gliomas by targeting TRAF4 and predict patient prognosis. *Cell Death & Disease*, *9*(11), 1078.

Shi, R., Wang, P. Y., Li, X. Y., Chen, J. X., Li, Y., Zhang, X. Z., . . . Cheng, S. J. (2015). Exosomal levels of miRNA-21 from cerebrospinal fluids associated with poor prognosis and tumor recurrence of glioma patients. *Oncotarget*, *6*(29), 26971−26981.

Shi, Z., Chen, Q., Li, C., Wang, L., Qian, X., Jiang, C., . . . Jiang, B. H. (2014). MiR-124 governs glioma growth and angiogenesis and enhances chemosensitivity by targeting R-Ras and N-Ras. *Neuro-Oncology*, *16*(10), 1341−1353.

Simeonova, I., & Huillard, E. (2014). In vivo models of brain tumors: Roles of genetically engineered mouse models in understanding tumor biology and use in preclinical studies. *Cellular and Molecular Life Sciences*, *71*(20), 4007−4026.

Singh, S. K., Hawkins, C., Clarke, I. D., Squire, J. A., Bayani, J., Hide, T., . . . Dirks, P. B. (2004). Identification of human brain tumour initiating cells. *Nature*, *432*(7015), 396−401.

Song, X., Zhang, N., Han, P., Moon, B. S., Lai, R. K., Wang, K., & Lu, W. (2016). Circular RNA profile in gliomas revealed by identification tool UROBORUS. *Nucleic Acids Research*, *44*(9), e87.

Spengler, R. M., Zhang, X., Cheng, C., McLendon, J. M., Skeie, J. M., Johnson, F. L., . . . Boudreau, R. L. (2016). Elucidation of transcriptome-wide microRNA binding sites in human cardiac tissues by Ago2 HITS-CLIP. *Nucleic Acids Research*, *44*(15), 7120−7131.

Spitzer, J., Hafner, M., Landthaler, M., Ascano, M., Farazi, T., Wardle, G., . . . Tuschl, T. (2014). PAR-CLIP (Photoactivatable Ribonucleoside-Enhanced Crosslinking and Immunoprecipitation): A step-by-step protocol to the transcriptome-wide identification of binding sites of RNA-binding proteins. *Methods in Enzymology*, *539*, 113−161.

Stavast, C. J., & Erkeland, S. J. (2019). The non-canonical aspects of MicroRNAs: Many roads to gene regulation. *Cells, 8*(11).

Stojcheva, N., Schechtmann, G., Sass, S., Roth, P., Florea, A. M., Stefanski, A., . . . Happold, C. (2016). MicroRNA-138 promotes acquired alkylator resistance in glioblastoma by targeting the Bcl-2-interacting mediator BIM. *Oncotarget*, *7*(11), 12937−12950.

Stupp, R., Mason, W. P., van den Bent, M. J., Weller, M., Fisher, B., Taphoorn, M. J., . . . Mirimanoff, R. O. European Organisation for Research and Treatment of Cancer Brain Tumor and Radiotherapy Groups. National Cancer Institute of Canada Clinical Trials Group. (2005). Radiotherapy plus concomitant and adjuvant temozolomide for glioblastoma. *The New England Journal of Medicine*, *352*(10), 987−996.

Su, H., Lin, F., Deng, X., Shen, L., Fang, Y., Fei, Z., . . . Xie, C. (2016). Profiling and bioinformatics analyses reveal differential circular RNA expression in radioresistant esophageal cancer cells. *Journal of Translational Medicine*, *14*(1), 225.

Su, Y. K., Lin, J. W., Shih, J. W., Chuang, H. Y., Fong, I. H., Yeh, C. T., & Lin, C. M. (2020). Targeting BC200/miR218-5p signaling axis for overcoming temozolomide resistance and suppressing glioma stemness. *Cells, 9*(8), 1859.

Sun, P., & Li, G. (2019). CircCode: A powerful tool for identifying circRNA coding ability. *Frontiers in Genetics*, *10*, 981.

Sun, S. L., Shu, Y. G., & Tao, M. Y. (2020). LncRNA CCAT2 promotes angiogenesis in glioma through activation of VEGFA signalling by sponging miR-424. *Molecular and Cellular Biochemistry*, *468*(1−2), 69−82.

Sun, X. H., Fan, W. J., An, Z. J., & Sun, Y. (2020). Inhibition of long noncoding RNA CRNDE increases chemosensitivity of medulloblastoma cells by targeting miR-29c-3p. *Oncology Research*, *28*(1), 95−102.

Swellam, M., Ezz El Arab, L., Al-Posttany, A. S., & B. Said, S. (2019). Clinical impact of circulating oncogenic MiRNA-221 and MiRNA-222 in glioblastoma multiform. *Journal of Neuro-Oncology*, *144*(3), 545−551.

Szabo, L., & Salzman, J. (2016). Detecting circular RNAs: Bioinformatic and experimental challenges. *Nature Reviews Genetics*, *17*(11), 679−692.

Tang, T., Wang, L. X., Yang, M. L., & Zhang, R. M. (2020). lncRNA TPTEP1 inhibits stemness and radioresistance of glioma through miR106a5pmediated P38 MAPK signaling. *Molecular Medicine Reports*, *22*(6), 4857−4867.

Tang, Z., Li, X., Zhao, J., Qian, F., Feng, C., Li, Y., . . . Li, C. (2019). TRCirc: A resource for transcriptional regulation information of circRNAs. *Briefings in Bioinformatics*, *20*(6), 2327−2333.

Teplyuk, N. M., Uhlmann, E. J., Gabriely, G., Volfovsky, N., Wang, Y., Teng, J., ... Krichevsky, A. M. (2016). Therapeutic potential of targeting microRNA-10b in established intracranial glioblastoma: First steps toward the clinic. *EMBO Molecular Medicine, 8*(3), 268−287.

Tian, T., Mingyi, M., Qiu, X., & Qiu, Y. (2016). MicroRNA-101 reverses temozolomide resistance by inhibition of GSK3β in glioblastoma. *Oncotarget, 7*(48), 79584−79595.

Tomasello, L., Cluts, L., & Croce, C. M. (2019). Experimental validation of microRNA targets: Luciferase reporter assay. *Methods in Molecular Biology, 1970*, 315−330.

Tong, X., & Liu, S. (2019). CPPred: Coding potential prediction based on the global description of RNA sequence. *Nucleic Acids Research, 47*(8), e43.

Tu, Y., Gao, X., Li, G., Fu, H., Cui, D., Liu, H., ... Zhang, Y. (2013). MicroRNA-218 inhibits glioma invasion, migration, proliferation, and cancer stem-like cell self-renewal by targeting the polycomb group gene Bmi1. *Cancer Research, 73*(19), 6046−6055.

Turner, K. M., Sun, Y., Ji, P., Granberg, K. J., Bernard, B., Hu, L., ... Zhang, W. (2015). Genomically amplified Akt3 activates DNA repair pathway and promotes glioma progression. *Proceedings of the National Academy of Sciences of the United States of America, 112*(11), 3421−3426.

Udaka, Y. T., & Packer, R. J. (2018). Pediatric brain tumors. *Neurologic Clinics, 36*(3), 533−556.

Valadkhan, S., & Valencia-Hipolito, A. (2016). lncRNAs in stress response. *Current Topics in Microbiology and Immunology, 394*, 203−236.

Vincent, H. A., & Deutscher, M. P. (2006). Substrate recognition and catalysis by the exoribonuclease RNase R. *Journal of Biological Chemistry, 281*(40), 29769−29775.

Visani, M., de Biase, D., Marucci, G., Cerasoli, S., Nigrisoli, E., Bacchi Reggiani, M. L., ... Pession, A. PERNO study group. (2014). Expression of 19 microRNAs in glioblastoma and comparison with other brain neoplasia of grades I-III. *Molecular Oncology, 8*(2), 417−430.

Vo, J. N., Cieslik, M., Zhang, Y., Shukla, S., Xiao, L., Zhang, Y., ... Chinnaiyan, A. M. (2019). The landscape of circular RNA in. *Cancer Cell, 176*(4), 869−881, e13.

Waitkus, M. S., Diplas, B. H., & Yan, H. (2018). Biological role and therapeutic potential of IDH mutations in cancer. *Cancer Cell, 34*(2), 186−195.

Wang, B., Love, T. M., Call, M. E., Doench, J. G., & Novina, C. D. (2006). Recapitulation of short RNA-directed translational gene silencing in vitro. *Molecular Cell, 22*(4), 553−560.

Wang, B., Wang, K., Jin, T., Xu, Q., He, Y., Cui, B., & Wang, Y. (2020). NCK1-AS1 enhances glioma cell proliferation, radioresistance and chemoresistance via miR-22-3p/IGF1R ceRNA pathway. *Biomedicine & Pharmacotherapy, 129*, 110395.

Wang, C., Yun, Z., Zhao, T., Liu, X., & Ma, X. (2015). MIR-495 is a predictive biomarker that downregulates GFI1 expression in medulloblastoma. *Cellular Physiology and Biochemistry, 36*(4), 1430−1439.

Wang, J., Zhou, T., Wang, T., & Wang, B. (2018). Suppression of lncRNA-ATB prevents amyloid-β-induced neurotoxicity in PC12 cells via regulating miR-200/ZNF217 axis. *Biomedicine and Pharmacotherapy, 108*, 707−715.

Wang, L. Q., Sun, W., Wang, Y., Li, D., & Hu, A. M. (2019). Downregulation of plasma miR-124 expression is a predictive biomarker for prognosis of glioma. *European Review for Medical and Pharmacological Sciences, 23*(1), 271−276.

Wang, W., Han, S., Gao, W., Feng, Y., Li, K., & Wu, D. (2020). Long noncoding RNA KCNQ1OT1 confers gliomas resistance to temozolomide and enhances cell growth by retrieving PIM1 from miR-761. *Cellular and Molecular Neurobiology*.

Wawrzyniak, O., Zarebska, Z., Kuczynski, K., Gotz-Wieckowska, A., & Rolle, K. (2020). Protein-related circular RNAs in human pathologies. *Cells, 9*(8), 1841.

Wei, Y., Lu, C., Zhou, P., Zhao, L., Lyu, X., Yin, J., ... You, Y. (2021). EIF4A3-induced circular RNA ASAP1 promotes tumorigenesis and temozolomide resistance of glioblastoma via NRAS/MEK1/ERK1-2 signaling. *Neuro-Oncology, 23*(4), 611−624.

Wittrup, A., & Lieberman, J. (2015). Knocking down disease: A progress report on siRNA therapeutics. *Nature Reviews Genetics, 16*(9), 543−552.

Wongfieng, W., Jumnainsong, A., Chamgramol, Y., Sripa, B., & Leelayuwat, C. (2017). 5′-UTR and 3′-UTR regulation of MICB expression in human cancer cells by novel microRNAs. *Genes, 8*(9), 213.

Wu, N., Xiao, L., Zhao, X., Zhao, J., Wang, J., Wang, F., ... Lin, X. (2012). MiR-125b regulates the proliferation of glioblastoma stem cells by targeting E2F2. *FEBS Letters, 586*(21), 3831−3839.

Wu, W., Ji, P., & Zhao, F. (2020). CircAtlas: An integrated resource of one million highly accurate circular RNAs from 1070 vertebrate transcriptomes. *Genome Biology*, *21*(1), 101.

Wu, Y., Yao, Y., Yun, Y., Wang, M., & Zhu, R. (2019). MicroRNA-302c enhances the chemosensitivity of human glioma cells to temozolomide by suppressing P-gp expression. *Bioscience Reports*, *39*(9), BSR20190421.

Xia, S., Feng, J., Chen, K., Ma, Y., Gong, J., Cai, F., ... He, C. (2018). CSCD: A database for cancer-specific circular RNAs. *Nucleic Acids Research*, *46*(D1), D925-D9.

Xia, S., Feng, J., Lei, L., Hu, J., Xia, L., Wang, J., ... He, C. (2017). Comprehensive characterization of tissue-specific circular RNAs in the human and mouse genomes. *Briefings in Bioinformatics*, *18*(6), 984–992.

Xia, X., Li, X., Li, F., Wu, X., Zhang, M., Zhou, H., ... Zhang, N. (2019). A novel tumor suppressor protein encoded by circular AKT3 RNA inhibits glioblastoma tumorigenicity by competing with active phosphoinositide-dependent Kinase-1. *Molecular Cancer*, *18*(1), 131.

Xiao, M. S., & Wilusz, J. E. (2019). An improved method for circular RNA purification using RNase R that efficiently removes linear RNAs containing G-quadruplexes or structured 3' ends. *Nucleic Acids Research*, *47*(16), 8755–8769.

Xiao, S., Yang, Z., Qiu, X., Lv, R., Liu, J., Wu, M., ... Liu, Q. (2016). MiR-29c contribute to glioma cells temozolomide sensitivity by targeting O6-methylguanine-DNA methyltransferases indirectly. *Oncotarget*, *7*(31), 50229–50238.

Xing, W., & Zeng, C. (2017). A novel serum microRNA-based identification and classification biomarker of human glioma. *Tumor Biology*, *39*(5), 1010428317705339.

Xu, H., Zhang, Y., Qi, L., Ding, L., Jiang, H., & Yu, H. (2018). NFIX circular RNA promotes glioma progression by regulating miR-34a-5p via notch signaling pathway. *Frontiers in Molecular Neuroscience*, *11*, 225.

Xu, Z., Kader, M., Sen, R., & Placantonakis, D. G. (2018). Orthotopic patient-derived glioblastoma xenografts in mice. *Methods in Molecular Biology*, *1741*, 183–190.

Yan, W., Li, R., Liu, Y., Yang, P., Wang, Z., Zhang, C., ... Jiang, T. (2014). MicroRNA expression patterns in the malignant progression of gliomas and a 5-microRNA signature for prognosis. *Oncotarget*, *5*(24), 12908–12915.

Yan, W., Liu, Y., Yang, P., Wang, Z., You, Y., & Jiang, T. (2015). MicroRNA profiling of Chinese primary glioblastoma reveals a temozolomide-chemoresistant subtype. *Oncotarget*, *6*(13), 11676–11682.

Yang, L., Li, N., Yan, Z., Li, C., & Zhao, Z. (2018). MiR-29a-mediated CD133 expression contributes to cisplatin resistance in CD133 + glioblastoma stem cells. *Journal of Molecular Neuroscience*, *66*(3), 369–377.

Yang, W., Shen, Y., Wei, J., & Liu, F. (2015). MicroRNA-153/Nrf-2/GPx1 pathway regulates radiosensity and stemness of glioma stem cells via reactive oxygen species. *Oncotarget*, *6*(26), 22006–22027.

Yang, W., Yu, H., Shen, Y., Liu, Y., Yang, Z., & Sun, T. (2016). MiR-146b-5p overexpression attenuates stemness and radioresistance of glioma stem cells by targeting HuR/lincRNA-p21/beta-catenin pathway. *Oncotarget*, *7*(27), 41505–41526.

Yao, D., Zhang, L., Zheng, M., Sun, X., Lu, Y., & Liu, P. (2018). Circ2Disease: A manually curated database of experimentally validated circRNAs in human disease. *Scientific Reports*, *8*(1), 11018.

Yin, H., & Cui, X. (2020). Knockdown of circHIPK3 facilitates temozolomide sensitivity in glioma by regulating cellular behaviors through miR-524-5p/KIF2A-mediated PI3K/AKT pathway. *Cancer Biotherapy and Radiopharmaceuticals*.

Yin, J., Zeng, A., Zhang, Z., Shi, Z., Yan, W., & You, Y. (2019). Exosomal transfer of miR-1238 contributes to temozolomide-resistance in glioblastoma. *EBioMedicine*, *42*, 238–251.

Yuan, D., Zhao, Y., Banks, W. A., Bullock, K. M., Haney, M., Batrakova, E., & Kabanov, A. V. (2017). Macrophage exosomes as natural nanocarriers for protein delivery to inflamed brain. *Biomaterials*, *142*, 1–12.

Yuan, Y., Jiaoming, L., Xiang, W., Yanhui, L., Shu, J., Maling, G., & Qing, M. (2018). Analyzing the interactions of mRNAs, miRNAs, lncRNAs and circRNAs to predict competing endogenous RNA networks in glioblastoma. *Journal of Neuro-Oncology*, *137*(3), 493–502.

Zaghlool, A., Ameur, A., Wu, C., Westholm, J. O., Niazi, A., Manivannan, M., ... Feuk, L. (2018). Expression profiling and in situ screening of circular RNAs in human tissues. *Scientific Reports*, *8*(1), 16953.

Zang, J., Lu, D., & Xu, A. (2020). The interaction of circRNAs and RNA binding proteins: An important part of circRNA maintenance and function. *Journal of Neuroscience Research*, *98*(1), 87–97.

Zeng, A., Wei, Z., Yan, W., Yin, J., Huang, X., Zhou, X., ... You, Y. (2018). Exosomal transfer of miR-151a enhances chemosensitivity to temozolomide in drug-resistant glioblastoma. *Cancer Letters*, *436*, 10–21.

Zhang, B., Fang, S., Cheng, Y., Zhou, C., & Deng, F. (2019). The long non-coding RNA, urothelial carcinoma associated 1, promotes cell growth, invasion, migration, and chemo-resistance in glioma through Wnt/beta-catenin signaling pathway. *Aging (Albany NY)*, *11*(19), 8239–8253.

Zhang, C., Chen, Q., Zhu, J. W., & Liu, Z. F. (2019). MicroRNA-199a-5p regulates glioma progression via targeting MARCH8. *European Review for Medical and Pharmacological Sciences*, *23*(17), 7482–7487.

Zhang, K., Sun, X., Zhou, X., Han, L., Chen, L., Shi, Z., . . . Kang, C. (2015). Long non-coding RNA HOTAIR promotes glioblastoma cell cycle progression in an EZH2 dependent manner. *Oncotarget*, *6*(1), 537–546.

Zhang, S., Zhao, B. S., Zhou, A., Lin, K., Zheng, S., Lu, Z., . . . Huang, S. (2017). m(6)A demethylase ALKBH5 maintains tumorigenicity of glioblastoma stem-like cells by sustaining FOXM1 expression and cell proliferation program. *Cancer Cell*, *31*(4), 591–606, e6.

Zhang, W., Yue, X., Tang, G., Wu, W., Huang, F., & Zhang, X. (2018). SFPEL-LPI: Sequence-based feature projection ensemble learning for predicting LncRNA-protein interactions. *PLOS Computational Biology*, *14*(12), e1006616.

Zhang, X., Sun, S., Pu, J. K., Tsang, A. C., Lee, D., Man, V. O., . . . Leung, G. K. K. (2012). Long non-coding RNA expression profiles predict clinical phenotypes in glioma. *Neurobiology of Disease*, *48*(1), 1–8.

Zhang, Z., Yin, J., Lu, C., Wei, Y., Zeng, A., & You, Y. (2019). Exosomal transfer of long non-coding RNA SBF2-AS1 enhances chemoresistance to temozolomide in glioblastoma. *Journal of Experimental & Clinical Cancer Research*, *38*(1), 166.

Zhao, C., Gao, Y., Guo, R., Li, H., & Yang, B. (2020). Microarray expression profiles and bioinformatics analysis of mRNAs, lncRNAs, and circRNAs in the secondary temozolomide-resistant glioblastoma. *Investigational New Drugs*, *38*(5), 1227–1235.

Zhao, C., Guo, R., Guan, F., Ma, S., Li, M., Wu, J., . . . Yang, B. (2020). MicroRNA-128-3p enhances the chemosensitivity of temozolomide in glioblastoma by targeting c-Met and EMT. *Scientific Reports*, *10*(1), 9471.

Zhao, G., Huang, Q., Wang, F., Zhang, X., Hu, J., Tan, Y., . . . Cheng, Y. (2018). Targeted shRNA-loaded liposome complex combined with focused ultrasound for blood brain barrier disruption and suppressing glioma growth. *Cancer Letters*, *418*, 147–158.

Zhao, M., Xu, J., Zhong, S., Liu, Y., Xiao, H., Geng, L., & Liu, H. (2019). Expression profiles and potential functions of circular RNAs in extracellular vesicles isolated from radioresistant glioma cells. *Oncology Reports*, *41*(3), 1893–1900.

Zhao, X., Ponomaryov, T., Ornell, K. J., Zhou, P., Dabral, S. K., Pak, E., . . . Segal, R. A. (2015). RAS/MAPK activation drives resistance to Smo inhibition, metastasis, and tumor evolution in SHH pathway-dependent tumors. *Cancer Research*, *75*(17), 3623–3635.

Zhao, Y., Teng, H., Yao, F., Yap, S., Sun, Y., & Ma, L. (2020). Challenges and strategies in ascribing functions to long noncoding RNAs. *Cancers (Basel)*, *12*(6), 1458.

Zhao, Z., Wang, K., Wu, F., Wang, W., Zhang, K., Hu, H., . . . Jiang, T. (2018). circRNA disease: A manually curated database of experimentally supported circRNA-disease associations. *Cell Death & Disease*, *9*(5), 475.

Zheng, J., Li, X. D., Wang, P., Liu, X. B., Xue, Y. X., Hu, Y., . . . Liu, Y. (2015). CRNDE affects the malignant biological characteristics of human glioma stem cells by negatively regulating miR-186. *Oncotarget*, *6*(28), 25339–25355.

Zheng, J., Wang, B., Zheng, R., Zhang, J., Huang, C., Zheng, R., & Yuan, Y. (2020). Linc-RA1 inhibits autophagy and promotes radioresistance by preventing H2Bub1/USP44 combination in glioma cells. *Cell Death & Disease*, *11*(9), 758.

Zheng, L. L., Li, J. H., Wu, J., Sun, W. J., Liu, S., Wang, Z. L., . . . Qu, L. (2016). deepBase v2.0: Identification, expression, evolution and function of small RNAs, LncRNAs and circular RNAs from deep-sequencing data. *Nucleic Acids Research*, *44*(D1), D196-202.

Zheng, R., Yao, Q., Li, X., & Xu, B. (2019). Long noncoding ribonucleic acid SNHG18 promotes glioma cell motility via disruption of alpha-enolase nucleocytoplasmic transport. *Frontiers in Genetics*, *10*, 1140.

Zheng, R., Yao, Q., Ren, C., Liu, Y., Yang, H., Xie, G., . . . Yuan, Y. (2016). Upregulation of long noncoding RNA small nucleolar RNA host gene 18 promotes radioresistance of glioma by repressing semaphorin 5A. *International Journal of Radiation Oncology, Biology, Physics*, *96*(4), 877–887.

Zhou, X., & Xu, J. (2015). Identification of Alzheimer's disease-associated long noncoding RNAs. *Neurobiology of Aging*, *36*(11), 2925–2931.

Zhou, Y., Peng, Z., Seven, E. S., & Leblanc, R. M. (2018). Crossing the blood-brain barrier with nanoparticles. *Journal of Controlled Release*, *270*, 290–303.

Zhu, J., Ye, J., Zhang, L., Xia, L., Hu, H., Jiang, H., . . . Luo, C. (2017). Differential expression of circular RNAs in glioblastoma multiforme and its correlation with prognosis. *Translational Oncology*, *10*(2), 271–279.

Zhu, S., Wang, J., He, Y., Meng, N., & Yan, G. R. (2018). Peptides/proteins encoded by non-coding RNA: A novel resource bank for drug targets and biomarkers. *Frontiers in Pharmacology*, *9*, 1295.

Zhu, X. Y., Li, G. X., & Liu, Z. L. (2018). miR-599 as a potential biomarker for prognosis of glioma. *European Review for Medical and Pharmacological Sciences*, *22*(2), 294–298.

Zhukova, N., Ramaswamy, V., Remke, M., Pfaff, E., Shih, D. J. H., Martin, D. C., . . . Tabori, U. (2013). Subgroup-specific prognostic implications of TP53 mutation in medulloblastoma. *Journal of Clinical Oncology*, *31*(23), 2927–2935.

Zirkel, A., & Papantonis, A. (2018). Detecting circular RNAs by RNA fluorescence in situ hybridization. *Methods in Molecular Biology*, *1724*, 69–75.

Zlotorynski, E. (2015). Non-coding RNA: Circular RNAs promote transcription. *Nature Reviews Molecular Cell Biology*, *16*(4), 206.

Zong, Z., Song, Y., Xue, Y., Ruan, X., Liu, X., Yang, C., . . . Liu, Y. (2019). Knockdown of LncRNA SCAMP1 suppressed malignant biological behaviours of glioma cells via modulating miR-499a-5p/LMX1A/NLRC5 pathway. *Journal of Cellular and Molecular Medicine*, *23*(8), 5048–5062.

Grabowska M, Grześkowiak BF, Rolle K,

Mrówczyński R.

Magnetic Nanoparticles as a Carrier
of dsRNA for Gene Therapy

Magnetic Nanoparticles as a Carrier of dsRNA for Gene Therapy

Małgorzata Grabowska, Bartosz F. Grześkowiak, Katarzyna Rolle, and Radosław Mrówczyński

Abstract

Glioma belongs to the most aggressive and lethal types of cancer. Glioblastoma multiforme (GBM), the most common type of malignant gliomas, is characterized by a poor prognosis and remains practically incurable despite aggressive treatment such as surgery, radiotherapy, and chemotherapy. Brain tumor cells overexpress a number of proteins that play a crucial role in tumorigenesis and may be exploited as therapeutic targets. One such target can be an extracellular matrix glycoprotein—tenascin-C (TN-C). Downregulation of TN-C by RNA interference (RNAi) is a very promising strategy in cancer therapy. However, the successful delivery of naked double-stranded RNA (dsRNA) complementary to TN-C sequence (ATN-RNA) requires application of delivery vehicles that can efficiently overcome rapid degradation by nucleases and poor intracellular uptake. Here, we present a protocol for application of MNP@PEI as a carrier for ATN-RNA to GBM cells. The obtained complexes consisted of polyethyleneimine (PEI)-coated magnetic nanoparticles combined with the dsRNA show high efficiency in ATN-RNA delivery, resulting not only in significant TN-C expression level downregulation, but also impairing the tumor cells migration.

Key words Magnetic nanoparticles, RNAi, Tenascin-C, Glioblastoma, Gene therapy, Cytotoxicity, Transfection, Double-stranded RNA

1 Introduction

The most common type of glioma, accounting for 55% of brain tumors, is glioblastoma multiforme (GBM). It is rated as the most aggressive, a fourth grade cancer, according to the World Health Organization classification [1]. Recommended therapies include surgical resection, radiotherapy, and systemic chemotherapy with oral prodrug temozolomide. Depending on the therapy, a median survival rate amounts 12–15 months, while failure to attempt treatment results in patient's death within 3 months [2].

None of the current state-of-the-art treatments for malignant glioma can be regarded as effective. Complete surgical resection of

GBM is often not feasible due to its location in significant areas of the brain. GBM, characterized by high degree of invasiveness, readily infiltrate surrounding tissues, leading to later disease progression or recurrence [3]. It is therefore important to limit the migration potential of GBM cells. To initiate the migration process glioma cells degrade the surrounding extracellular matrix (ECM) into a migration favorable microenvironment [4].

Tenascin-C (TN-C), one of the ECM proteins responsible for adhesion and invasiveness of cancer cells, is highly overexpressed in GBM compared to healthy tissues, what makes it a great therapeutic target [5]. The identification of new molecular biomarkers in GBM as well as new drug delivery strategies are now a major therapeutic challenge. One of the most promising cancer treatment methods is gene therapy based on RNA interference (RNAi), referring to post-transcriptional gene silencing mediated by either degradation or translation inhibition of target RNA.

RNAi is triggered by the introduction of double-stranded RNA (dsRNA) into a cell [6]. In experimental approach, dsRNA with sequence homologous to TN-C mRNA was used to reduce TN-C expression [7]. Use of this RNA agent, named ATN-RNA, administrated locally into the tumor's cavity during standard neurosurgical procedure, results in increased survival and better quality of life of patients [8]. To overcome the lack of an effective delivery method for dsRNA and the instability of the nucleic acids during the delivery, we successfully tested the magnetic nanoparticles modified with polyethyleneimine (MNP@PEI) as a therapeutics' carrier [9].

Here, we present a protocol for application of MNP@PEI as a carrier for ATN-RNA to GBM cells. We demonstrate the protocols for magnetic nanoparticles synthesis, for assessment of cytotoxicity of obtained materials, preparation of nanoparticles-dsRNA complexes and their application in delivery of dsRNA to GBM cells. We also describe a method for assessing the gene silencing level and an approach for detection of the cell migration impairment.

2 Materials

2.1 Magnetic Nanoparticles Synthesis

1. Working solution: 0.5 g of 25-kDa branched polyethyleneimine (PEI-25$_{Br}$), 250 μL of Capstone FS-65 (Du Pont) fluorosurfactant, 2.5 mL of NH_4OH, 10 mL of water.

2.2 Preparation of ATN-RNA

2.2.1 In Vitro Transcription of ATN-RNA

1. pT7/T3α18 plasmid harboring ATN-RNA sequence. ATN-RNA was chemically synthesized form eight short (approximately 40 nt) overlapping oligodeoxynucleotides: four homologous to target fragment, and four complementary to it. Complementary fragments overlap with a shift of 10 nt. Resulting 5′ overhangs contain sites recognized by restriction enzymes *Hind*III for sense strand and *EcoR*I for template strand.

2. T3 transcription kit (Thermo Fisher Scientific).

3. T7 transcription kit (Thermo Fisher Scientific).

4. Gel DNA purification kit.

5. DNA gel loading dye.

6. 10× TBE buffer: 1 M Tris base, 1 M boric acid, 0.02 M EDTA, in H_2O.

7. 1% agarose gel.

8. Horizontal gel electrophoresis system.

9. Transilluminator.

2.2.2 dsRNA Hybridization

1. Hybridization buffer: 20 mM Tris–HCl pH 7.5, 50 mM NaCl, in H_2O.

2. 10% PAGE with 7 M urea: 4 mL of 10× TBE buffer, 10 mL of 20% acrylamide/bisacrylamide, 19.2 g of urea, up to 40 mL of H_2O.

3. RNA gel loading dye.

4. SYBR Safe.

5. Transilluminator.

2.3 MNP@PEI/dsRNA Complex Preparation

1. ATN-RNA solution in water at a concentration of 100 ng/μL.

2. MNP@PEI solution in water at a concentration of 1000 μg Fe/mL.

2.3.1 Gel Retardation Assay

1. DNA gel loading dye.

2. 10× TBE buffer: 1 M Tris base, 1 M boric acid, 0.02 M EDTA.

3. 1% agarose gel.

4. Horizontal gel electrophoresis system.

5. System for gel documentation.

6. Multidimensional images software (e.g., Digital Imaging and Analysis System II, Serva).

2.3.2 UV–Vis Spectrophotometry

1. Microvolume spectrophotometer (e.g. NanoDrop 2000, Thermo Scientific).

2.4 Cell Culture Maintenance

1. U-118 MG cell line (ATCC).
2. Dulbecco's Modified Eagle Medium (DMEM) High Glucose.
3. Fetal bovine serum (FBS).
4. Penicillin-streptomycin.
5. Trypsin.
6. Phosphate-buffered saline (PBS).
7. T-75 flasks.
8. CO_2 incubator.

2.5 Visualization of Transfection Complexes in the Cells

1. Atto 550 NHS solution (10 mg/mL): 1 mg of Atto 550 NHS, 100 μL of DMSO. Store at −20 °C.
2. Borate buffer: 0.1 M borate, pH 8.5, 1 M NaOH in H_2O.
3. Slide-A-Lyzer G2 Dialysis Cassettes, 3.5 k MWCO, 3 mL (Thermo Fisher Scientific).
4. 8-well Nunc Lab-Tek Chamber Slide (Thermo Fisher Scientific).
5. Label IT Tracker Intracellular Nucleic Acid Localization Kit, Fluorescein (Mirus).
6. 4% formaldehyde solution: 1 mL of 16% formaldehyde, 3 mL of Dulbecco's phosphate-buffered saline containing $MgCl_2$ and $CaCl_2$ (DPBS).
7. Concanavalin A-FITC (Thermo Fischer) solution (1 mg/mL): 10 mg of Concanavalin A-FITC, 10 mL of 0.1 M sodium bicarbonate. Aliquot and store at −20 °C.

2.6 Cytotoxicity Assays

1. Black polystyrene 96-well flat bottom μClear plate with the transparent bottom (Greiner Bio-One GmbH).
2. Live/Dead assay solution: 2 μM calcein AM, 2 μM ethidium homodimer-1, 8 μM Hoechst 33342 in DPBS. Protect from light, storing in a tube wrapped with aluminum foil.

2.7 Transfection

1. DMEM High Glucose.
2. PBS.
3. 12-well cell culture plate.

2.8 Establishing TNC-C Expression Level

2.8.1 Total RNA Isolation from Cell Culture

1. TRIzol Reagent.
2. Chloroform.
3. 2-Propanol.
4. 75% ethanol.
5. Refrigerated microfuge.
6. Microvolume spectrophotometer.

2.8.2 Removal of Residual DNA and Reverse Transcription	1. DNA removal kit (Ambion).
	2. cDNA reverse transcription kit (Roche).
	3. RNA gel loading dye.
	4. 10× TBE buffer: 1 M Tris base, 1 M boric acid, 0.02 M EDTA.
	5. 1% agarose gel.
	6. Vertical gel electrophoresis system.
	7. Transilluminator.
	8. Microvolume spectrophotometer.

2.8.3 Real-Time Polymerase Chain Reaction

1. RT-PCR probe mix 2×.
2. Primers for the gene of interest.
3. Primers for the endogenous gene.
4. Probe from the Universal Probe Library (UPL, Roche).
5. 96-well PCR plates.
6. Adhesive PCR plate foils.
7. Real-time PCR detection system.

2.9 Cell-Migration Analysis

1. DMEM High Glucose.
2. PBS.
3. 12-well cell culture plate.
4. 200 μL micropipette tip.
5. Microscope with ×5 magnification.
6. Software with edge-detection algorithm to wound-healing assays analysis (e.g., TScratch, CSElab).

3 Methods

3.1 Synthesis and Functionalization of Magnetic Nanoparticles

1. Mix $FeCl_3 \cdot 6H_2O$ (135 mg, 0.5 mmol) with $FeCl_2 \cdot 4H_2O$ (50 mg, 0.25 mmol) in 5 mL of water and degassed with N_2 (*see* **Note 1**).
2. Heat the mixture up to 80 °C. Add 1 mL of working solution and continue heating for 120 min. Cool down the mixture and collect nanoparticles by an external magnet (*see* **Note 2**).
3. Wash nanoparticles with water (2 × 150 mL) and collected by an external magnet. Finally, redisperse nanoparticles in 10 mL of water.

3.2 Preparation of ATN-RNA

3.2.1 In Vitro Transcription of ATN-RNA

1. Digest 50 μg of plasmid harboring ATN-RNA construct separately with restriction enzymes *EcoR*I and *Hind*III.

2. Carry out the digestion process by minimum 8 h or overnight.

3. Separate the whole reaction on the 1% agarose gel and examine it on the transilluminator.

4. From agarose gel cut out the digested form of plasmid and purify the plasmid from the gel using gel DNA purification kit.

5. Independently transcribe the two strands of RNA with T3 and T7 polymerases for 1 μg of EcoRI and HindIII digested plasmids, respectively. Incubate the reaction overnight.

6. Purify the reaction loading whole mixture onto spin column plugged into sterile 1.5 mL collection tubes, then centrifuge at $750 \times g$, 2 min.

7. Apply 20 μL of nuclease-free H_2O on spin tubes and repeat centrifugation to new collection tubes.

8. Store transcripts in $-20\,^{\circ}C$.

3.2.2 dsRNA Hybridization

1. Mix equal quantities of T3 and T7 transcripts. Add 20 μL of $5\times$ hybridization buffer and fill up with H_2O to 100 μL.

2. Incubate: $95\,^{\circ}C$, 3 min, then follow the incubation for $75\,^{\circ}C$, 30 min.

3. Slowly cool down the reaction for minimum 4 h or overnight to $25\,^{\circ}C$.

4. Check the quality of dsRNA by separating with accompanying T3 and T7 non-hybridized transcripts on 10% polyacrylamide denaturing gel.

5. Rinse the gel for half an hour in SYBR Safe in water solution to visualize the bands.

3.3 MNP@PEI/dsRNA Complexes Preparation

1. Thaw dsRNA on ice and stir it gently by pipetting.

2. Vortex vigorously nanoparticles to break up the sediment and scatter nanoparticles in ultrasonic disperser for 15 min.

3. Mix dsRNA with MNP@PEI in a series of Fe to RNA weight ratios (1, 2, 3, 4, 5, 8, 10 Mag@PEI to ATN-RNA wt:wt ratios). Manipulate only with the amount of nanoparticles, as each complex must have an identical amount of dsRNA.

4. Adjust the volume of the complexes up to 50 μL with nuclease-free water.

5. Incubate: room temperature, 30 min.

6. Determine the rate of binding by gel retardation assay (Subheading 3.3.1) or UV-VIS spectrophotometry (Subheading 3.3.2). Use the free RNA as a control.

3.3.1 Gel Retardation Assay	1. Mix 15 μL of the complexes with 3 μL of gel loading dye solution and load MNP@PEI/dsRNA complexes on 1% agarose gel. As a control use the pure dsRNA.

2. Run electrophoresis in $1\times$ TBE buffer at a constant voltage 10 V/cm for 30 min.

3. Visualize the samples using gel imaging system.

4. Calculate the binding efficiency by comparing density data obtained for complexes to those for the pure dsRNA.

3.3.2 UV-Vis Spectrophotometry

1. Centrifuge MNP@PEI/dsRNA complexes: $9300 \times g$, 10 min.

2. Measure the concentration of RNA contained in the supernatant at A260 on the spectrophotometer. Load 1 μL of the supernatant on the measurement pedestal and measure the absorbance.

3. Measure the concentration of pure dsRNA sample.

4. Calculate binding efficiency by comparing concentrations obtained for complexes to those for the pure dsRNA.

3.4 Cell Culture Maintenance

1. Grow adherent U-118 MG glioblastoma multiforme cell line in T-75 flask. Use culture medium supplemented with 10% FBS and 1% antibiotic solution, then replace it at intervals 24–36 h.

2. To passage the culture detach cells using trypsin. Carry out the culture in CO_2 incubators at temperature 37 °C, humidity 95%, CO_2 concentration 5% (*see* **Note 3**).

3.5 Visualization of Transfection Complexes in the Cells

3.5.1 Cellular Uptake of Transfection Complexes

1. To obtain fluorescently labeled MNP@PEI, mix 2 mL of magnetic NPs suspension (2 mg Fe/mL) with 490 μL 0.1 M borate buffer and 10 μL solution of Atto 550 NHS.

2. Incubate the suspension overnight at room temperature with continuous stirring.

3. Dialyze the suspension against water using a Slide-A-Lyzer G2 cassette with a cut-off at 3500 MW. Determine the iron concentration in obtained sample on a spectrophotometer.

4. Seed U118-MG cells into 8-well Nunc Lab-Tek Chamber Slide at 2.5×10^4 cells/well (300 μL) and incubate under standard tissue culture conditions for 24 h.

5. Prepare working dilution of transfection complexes containing fluorescently labeled NPs with an iron-to-RNA ratio of 3:1 (w/w). Transfer 50 μL of the transfection complexes corresponding to the ATN-RNA final concentration of 100 nM into the well of slide with the seeded cells. Incubate the cells with complexes for 24 h.

6. Wash the cells 1× with DPBS and then fix the cells by adding 200 μL of 4% formaldehyde and incubate for 15 min at room temperature.

7. Wash the cells 1× with DPBS and label the cellular membranes by adding 200 μL of Concanavalin A-FITC at the concentration of 25 μg/mL and incubate for 30 min at room temperature. Protect from light.

8. Wash the cells 1× with DPBS and label the nuclei by adding 200 μL of Hoechst 33342 at the concentration of 8 μM and incubate for 10 min at room temperature. Protect from light.

9. Wash the cells 1× with DPBS. Samples may be stored in 300 μL at 4 °C.

10. Visualize the cells using confocal laser scanning microscope. For the experiments detailed in this section, the images were acquired on the Olympus FV1000 with a ×60 objective, a 1.4 oil immersion lens, and analyzed using the FV10-ASW software (*see* **Note 4**).

3.5.2 Colocalization of Magnetic Nanoparticles and RNA Inside the Cells

1. To obtain fluorescently labeled ATN-RNA with Label IT Tracker Intracellular Nucleic Acid Localization Kit, mix 5 μg of RNA with 10× Labeling Buffer A, *Label* IT® Reagent and DNase-, RNase-free water in a volume of 50 μL.

2. Quantify the final concentration on a spectrophotometer.

3. Seed U-118 MG cells into 8-well Nunc Lab-Tek Chamber Slide at 2.5×10^4 cells/well (300 μL) and incubate under standard tissue culture conditions for 24 h.

4. Prepare working dilution of transfection complexes containing Atto 550 NHS-labeled NPs (red) and fluorescein-labeled RNA (green) with an iron-to-RNA ratio of 3:1 (w/w). Transfer 50 μL of the transfection complexes corresponding to the ATN-RNA final concentration of 100 nM into the well of slide with the seeded cells. Incubate the cells with complexes for 24 h.

5. Wash the cells 1× with DPBS and then fix the cells by adding 200 μL of 4% formaldehyde and incubate for 15 min at room temperature. Protect from light.

6. Remove fixative from the cells and then wash the cells 1× with DPBS.

7. Label the nuclei by adding 200 μL of Hoechst 33342 at the concentration of 8 μM and incubate for 10 min at room temperature. Protect from light. Samples may be stored in 300 μL at 4 °C.

8. Visualize the cells using confocal laser scanning microscope. For the experiments detailed in this section, the images were

acquired on the Olympus FV1000 with a $\times 60$ objective, a 1.4 oil immersion lens, and analyzed using the FV10-ASW software (*see* **Note 5**).

3.6   Cytotoxicity Assays

3.6.1   WST-1 Cell Proliferation Assay

1. Seed U-118 MG cells into 96-well plate at 1×10^4 cells/well (150 µL) and incubate under standard tissue culture conditions for 24 h.

2. Prepare dilutions of transfection complexes with an iron-to-RNA ratio of 3:1 (w/w) corresponding to the ATN-RNA final concentration of 100, 50, 25, 12.5, and 6.25 nM. Transfer 50 µL each of the transfection complexes into the culture plates with the seeded cells. Incubate the cells with complexes for 24 h. Test each dilution of transfection complex in triplicate.

3. Add 10 µL WST-1 Cell Proliferation Reagent to each well and incubate at 37 °C for 4 h. Use cell culture medium as a blank.

4. Transfer 100 µL medium to the fresh wells on 96-well plate and record the absorbance at 450 nm (reference wavelength 620 nm) using a multiwell plate reader. Use untransfected cells as a reference.

5. Express the cell viability as: Cell viability (%) = $(Abs_{sample} - Abs_{blank})/(Abs_{ref} - Abs_{blank}) * 100$. Abs_{sample}, Abs_{blank}, and Abs_{ref} are absorbances at the maximum of the WST-1 absorption spectrum registered for a sample, blank, and reference sample, respectively.

3.6.2   Live/Dead Cell Viability Assay

1. Seed U-118 MG cells into 96-well µClear plate at 1×10^4 cells/well (150 µL) and incubate under standard tissue culture conditions for 24 h.

2. Prepare dilutions of transfection complexes with an iron-to-RNA ratio of 3:1 (w/w) corresponding to the ATN-RNA final concentration of 100, 50, 25, 12.5, and 6.25 nM. Transfer 50 µL each of the transfection complexes into the culture plates with the seeded cells. Incubate the cells with complexes for 24 h. Test each dilution of transfection complex in triplicate.

3. Remove medium from all wells and replace with 100 µL of Live/Dead assay solution. Incubate at 37 °C for 30 min.

4. Scan the plate using a high-content imaging system. For the experiments detailed in this section, the images were acquired on the IN Cell Analyzer 2000 with a $\times 20$ objective and analyzed using the IN Cell Developer Toolbox software using in-house developed protocol (*see* **Note 6**).

3.7   Transfection

1. Calculate the volumes of nanoparticles and dsRNA needed for transfection based on binding efficiency obtained from Subheadings 3.3.1 and 3.3.2. Determine what volume of dsRNA

should be delivered to the cells to obtain the desired concentration of RNA and the amount of nanoparticles needed to bind them.

2. Seed U-118 MG cells into 12-well plate at 1.5×10^5 cells/well (1 mL) and incubate under standard tissue culture conditions for 24 h to obtain 75–90% confluence.

3. Remove medium from the cells, then wash the cells with PBS and add the supplemented medium in volume reduced by the amount of the transfection mixture.

4. Prepare MNP@PEI and dsRNA and form the MNP@PEI/dsRNA complexes as described in Subheading 3.3.

5. Add prepared transfection complexes to the cells, slowly spotting them on the surface of the whole well and incubate the cells for 24 h.

6. Depending on the purpose of the experiment, go to Subheading 3.8 or 3.9.

3.8 Establishing TNC-C Expression Level

1. Remove medium from the cells, then wash the cells with PBS.

2. Add 250 μL of TRIzol reagent per one well from 12-well plate.

3. Incubate plate: 10 min, room temperature.

3.8.1 Total RNA Isolation from Cell Culture

4. Transfer the lysate to a sterile 1.5 mL tube. Add 50 μL of chloroform and mix by shaking for 15 s to extract RNA.

5. Incubate: 10 min, room temperature and centrifuge at $12{,}000 \times g$, 4 °C, 15 min.

6. Transfer the upper, aqueous phase containing the RNA into a new sterile 1.5 mL tube.

7. Add 125 μL of 2-propanol and mix by inverting the tube several times.

8. Incubate for 10 min at room temperature and centrifuge at $12{,}000 \times g$, 4 °C, 8 min.

9. Remove the supernatant and add 0.5 mL of cold 75% ethanol. Mix by vortexing and centrifuge at $7500 \times g$, 4 °C, 10 min.

10. Remove the supernatant. Leave the tube open for 5–10 min to evaporate the ethanol. Do not let the sediment to dry out completely.

11. Dissolve RNA in 20 μL of nuclease-free water. Keep the RNA on ice (*see* **Note 7**).

12. Measure the amount of obtained RNA at A260 on the spectrophotometer.

3.8.2 Removal of Residual DNA and Reverse Transcription

1. Dispense 5 μg of isolated RNA.

2. Remove the residual DNA from sample using DNA removal kit.

3. Measure the amount of purified RNA at A260 on the spectrophotometer.

4. Investigate the quality of RNA by electrophoretic separation in the 1% agarose gel. If the resulting material does not contain any degradation or DNA residue, go to **step 5**. If not then repeat DNA removal or reisolate the RNA.

5. Using the cDNA reverse transcription kit and the isolated, pure total RNA, perform the reverse transcription according to the manufacturer's instructions.

6. Use the final product as a template in Subheading 3.8.3.

3.8.3   Real-Time
Polymerase Chain Reaction

1. Design primers and probes for endogenous gene and gene of interest by the Universal Probe Library Assay Design Center.

2. Dilute primers to the concentration 10 µM.

3. Estimate the efficiency of primers on the standard curve with series of two-fold dilutions. Only primers not differing by more than 10% of efficiency can be subjected to one analysis.

4. Prepare the reaction mix: 5 µL of RT-PCR probe mix 2×, 1 µL of forward primer, 1 µL of reverse primer, 0.1 µL of probe, 1.9 µL of sterile water. Make three technical replicates for each experiment.

5. Pipette the reaction mixture onto 96-well plate and add 1 µL of template cDNA to the proper wells.

6. Seal the plate with adhesive PCR plate foil, centrifuge at 1800 × g, 3 min and place the plate in a real-time PCR detection system.

7. Proceed reaction under the following conditions: 5 min of preincubation at 95 °C, 40 cycles of denaturation in 95 °C for 10 s, annealing at proper to primers temperature for 30 s and extension at 72 °C for 10 s.

8. Calculate the level of gene expression in the test samples by first comparing the Ct values obtained for the test gene to those obtained for the endogenous gene, and then comparing the test samples to the control.

3.9   Cell-Migration
Analysis

1. Remove the transfection mix from the cells, then wash the cells with PBS.

2. Add 1 mL of supplemented medium.

3. Create a "wound" by scratching the straight line in monolayer of cells by 200 µL tip.

4. Using the ×5 magnification take an image of scratch area at 12 h intervals. The image needs to be taken at exactly the same place of the well.

5. Observe for 48 h or until the scars are healed.

6. Analyze the degree of scarring of individual "wounds" at subsequent time points using wound-healing assays analysis software.

4   Notes

1. Bubbling N_2 at for 20 min in order to prevent unwanted oxidation of nanoparticles during the synthesis. Remember to keep the mixture all the time under N_2 atmosphere during the synthesis.

2. The collection of nanoparticles by external magnet can be performed in the beaker rather than in round bottom flask. The flat bottom of beaker gives bigger surface to collect nanoparticles and allows to handle them during the washing steps.

3. All activities related to cell culture perform under sterile conditions underneath a laminar flow cabinet.

4. Images of the Mag@PEI NPs were visualized using 559 nm excitation and 570–590 nm emission filters. To visualize the cell membranes, 488 nm excitation and 495–545 nm emission filters were applied. The Hoechst fluorescence was detected using 405 nm excitation source and 425–475 nm emission filters.

5. Images of the Mag@PEI NPs were visualized using 559 nm excitation and 570–590 nm emission filters, whereas ATN-RNA was visualized using 488 nm excitation and 495–545 nm emission filters. The Hoechst fluorescence was detected using 405 nm excitation source and 425–475 nm emission filters.

6. Perform all operations involving RNA manipulations on ice, using nuclease-free water.

7. Using a real-time PCR system based on probes allows for greater specificity of detection than a system based on fluorescent dyes.

Acknowledgments

References

1. Dunn GP, Rinne ML, Wykosky J et al (2012) Emerging insights into the molecular and cellular basis of glioblastoma. Genes Dev 26:756–784

2. Stupp R, Mason WP, van den Bent MJ et al (2005) Radiotherapy plus concomitant and adjuvant temozolomide for glioblastoma. N Engl J Med 352:987–996

3. Davis ME (2016) Glioblastoma: overview of disease and treatment. Clin J Oncol Nurs 20: S2–S8

4. Lefranc F, Brotchi J, Kiss R (2005) Possible future issues in the treatment of glioblastomas: special emphasis on cell migration and the resistance of migrating glioblastoma cells to apoptosis. J Clin Oncol 23:2411–2422

5. Brösicke N, Faissner A (2015) Role of tenascins in the ECM of gliomas. Cell Adhes Migr 9:131–140

6. Mathupala SP, Guthikonda M, Sloan AE (2006) RNAi based approaches to the treatment of malignant glioma. Technol Cancer Res Treat 5:261–269

7. Zukiel R, Nowak S, Wyszko E et al (2006) Suppression of human brain tumor with interference RNA specific for tenascin-C. Cancer Biol Ther 5:1002–1007

8. Wyszko E, Rolle K, Nowak S et al (2008) A multivariate analysis of patients with brain tumors treated with ATN-RNA. Acta Pol Pharm 65:677–684

9. Grabowska M, Grześkowiak BF, Szutkowski K et al (2019) Nano-mediated delivery of double-stranded RNA for gene therapy of glioblastoma multiforme. PLoS One 14:e0213852

Wawrzyniak D, Grabowska M, Głodowicz P,
Kuczyński K, Kuczyńska B, Fedoruk-Wyszomirska A,
Rolle K.

**Down-regulation of tenascin-C inhibits breast cancer
cells development by cell growth, migration,
and adhesion impairment**

PLOS ONE

Down-regulation of tenascin-C inhibits breast cancer cells development by cell growth, migration, and adhesion impairment

Dariusz Wawrzyniak[1], **Małgorzata Grabowska**[1], **Paweł Głodowicz**[1], **Konrad Kuczyński**[1,2], **Bogna Kuczyńska**[1], **Agnieszka Fedoruk-Wyszomirska**[3], **Katarzyna Rolle**[1]*

1 Department of Molecular Neurooncology, Institute of Bioorganic Chemistry of the Polish Academy of Sciences, Poznan, Poland, **2** NanoBioMedical Centre, Adam Mickiewicz University, Poznan, Poland, **3** Laboratory of Subcellular Structures Analysis, Institute of Bioorganic Chemistry of the Polish Academy of Sciences, Poznan, Poland

* kbug@ibch.poznan.pl

Abstract

Tenascin-C (TNC) is an extracellular matrix (ECM) glycoprotein that plays an important role in cell proliferation, migration, and tumour invasion in various cancers. TNC is one of the main protein overexpressed in breast cancer, indicating a role for this ECM molecule in cancer pathology. In this study we have evaluated the TNC loss-off-function in breast cancer cells. In our approach, we used dsRNA sharing sequence homology with *TNC* mRNA, called ATN-RNA. We present the data showing the effects of ATN-RNA in MDA-MB-231 cells both in monolayer and three-dimensional culture. Cells treated with ATN-RNA were analyzed for phenotypic alterations in proliferation, migration, adhesion, cell cycle, multi-caspase activation and the involvement in epithelial to mesenchymal transition (EMT) processes. As complementary analysis the oncogenomic portals were used to assess the clinical implication of TNC expression on breast cancer patient's survival, showing the TNC overexpression associated with a poor survival outcome. Our approach applied first in brain tumors and then in breast cancer cell lines reveals that ATN-RNA significantly diminishes the cell proliferation, migration and additionally, reverses the mesenchymal cells phenotype to the epithelial one. Thus, TNC could be considered as the universal target in different types of tumors, where TNC overexpression is associated with poor prognosis.

Introduction

The tumor microenvironment is composed of the surrounding stromal cells, such as endothelial cells in blood vessels, immune cells, fibroblasts, and the extracellular matrix (ECM) [1, 2]. During carcinogenesis is often perturbed and deregulated, while during embryonic development is strictly controlled to maintain homeostasis [3]. In tumors, the composition of the ECM differs from that of normal tissue and enables new interactions that affect the function of cancer cells and are critical in modulating invasion associated with cell migration and growth. The tumor-associated ECM presents several tumor-associated antigens that are generally more abundant

and possibly more stable than those of the cell surface [4–6]. Consequently, these proteins represent possible valuable targets for tumor imaging and therapy [4, 5]. ECM proteins such as fibronectin (FN) and tenascin have isoforms that are expressed in a tissue specific manner generated by alternative splicing of their primary transcripts. One of the most consistent isoform changes in the ECM of many tumors is the up-regulation of the glycoprotein, tenascin-C (TNC). TNC alongside tenascin-X (TNX), tenascin-R (TNR) and tenascin-W (TNN) are members of, well conserved among vertebrates, tenascin family (TN) [7–12]. Numerous isoforms of TNC can be produced through alternative splicing of nine fibronectin type III regions between repeats 5 and 6 at the pre-mRNA level. There is a considerable amount of literature on the contribution of different splicing-dependent TNC domains in specific biological functions [13]. Changes in the TNC isoforms expression pattern have been then described in a number of malignancies, and their nature appears to be tumor-type specific. Recent studies have demonstrated that some splice variants are specific to diseased tissues [14–16]. In breast tissues, expression of two TNC variants, one containing domain D and the other both B and D, was found to be associated with invasive phenotype [17]. TNC promotes cell migration, angiogenesis, inhibit focal contact formation, and also act as a cell survival factor [18–22]. Its importance was found in the development and progression of different types of neoplasm, including: colon and breast cancer, fibrosarcoma, lung cancer, melanoma, squamous cell carcinoma, bladder cancer, and prostatic adenocarcinoma [23, 24]. TNC is also highly expressed in high-grade gliomas which correlates as well with the invasiveness of glioma cells [25–27]. In the brain, it is important for the development of neural stem cells [28, 29] and moreover is suspected to be a potential marker for glioblastoma multiforme (GBM) stem cells (GSC) [30].

Previously, we have shown that TNC is overexpressed in GBM and can be a good target in RNAi approach. With 164-nt long dsRNA complementary to the mRNA of TNC, which we called ATN-RNA, we conducted the experimental therapy for GBM patients [25]. The discovery that TNC presents a dominant epitope in glioblastoma prompted us to investigate the potential of ATN-RNA to block the TNC expression and its effect on the growth of human breast cancers, where TNC overexpression was also established and linked with the highest malignancy, invasion capability and metastasis ability. This view is supported by Mock et al., who showed that GBM patients with antibodies against the EGF-like repeats of TNC (antibody target: VCEDGFTGPDCAE) have a significantly better prognosis than other patients [31]. Thus we assumed, that in the light of the satisfactory results of brain tumors experimental therapy, breast cancer could be the next possible object of interest to establish the ATN-RNA approach.

Here, we demonstrate that ATN-RNA approach can be successfully used in breast cancer cells, impairing the basic hallmarks of tumor cells. With the performed analysis of proliferation, migration rate, multi-caspases induction pathway, cell cycle analysis, spheroids viability and the involvement of TNC in EMT induction, we have then interrogated the impact of TNC on breast cancer growth showing its potency to be also the promising therapeutic target in breast cancer treatment.

Results

Oncogenomic *in silico* analysis reveals the TNC correlation with poor survival of breast-cancer patients

To look deeper into the TNC function we performed the analysis of genome-wide breast cancer data with available oncogenomic portals such as GEPIA, the Human Protein Atlas, cBioPortal, and PPISURV. Based on the status of three important receptors conventionally used for breast cancer subtyping, i.e., estrogen receptor (ER), progesterone receptor (PR), and human epithelial receptor 2 (HER2), breast cancer is classified as luminal A, luminal B, HER2 positive and triple-

negative ("basal-like"). Triple-negative and HER2-overexpressing breast cancer yields a poor patient prognosis because of a high incidence of metastases, disease progression, and resistance to current chemotherapy regimens [32]. We first compared the expression level of tenascin-C in 4 subtypes of breast cancer using GEPIA program (Fig A in S1 File). mRNA level of TNC were higher in triple-negative and HER2 subtypes compared to the luminal A and luminal B subtypes, which have a better prognosis for patient survival. Therefore, we chose MDA-MB-231 cells as a model for *in vitro* experiments because it is the most invasive cell line from breast cancer models. MDA-MB-231 cell genome clusters with the basal subtype of breast cancer. Since the cells also lack the growth factor receptor HER2, they represent a good model of triple-negative breast cancer [33]. What is important, Adams et al. [17] showed that only invasive cell lines such as MDA-MB-231 or MDA-MB-468 express tenascin-C, whereas the tumor cell lines with a low invasive capacity, MCF-7 and T47D do not.

As a next step we compared the expression levels of tenascin genes (*TNC*, *TNN*, *TNR*, *TNXB*) in invasive breast cancer using GEPIA program (Fig 1A). mRNA level of TNC was highly expressed in breast cancer tissue (BRCA). Interestingly, expression levels of *TNN* and *TNXB* were significantly lower in breast cancer tissues (Fig 1A). There was no significant difference in *TNR* gene expression between breast cancer and non-tumor tissues.

We also examined the expression of tenascin proteins in normal and malignant tissues by querying data from the Human Protein Atlas. TNC in most cases and partly TNN were expressed at medium levels, whereas TNR was not detected (Fig 1B and 1C). TNC and TNR levels were undetectable in samples from normal breast (adipocytes, glandular and myoepithelial cells). Taken together, our results demonstrate that mRNA and protein levels of TNC is relatively higher in invasive breast cancer tissues than those in normal tissues.

The cBioPortal analysis enabled to look for the mutations in the *TNC* gene. It appeared that *TNC* gene mutations measured for 2051 breast cancer patients, are present as somatic mutation only in 11 cases (0.5%). Since these mutations seem to be irrelevant for breast cancer, we did not perform any further analysis.

With PPISURV portal we looked through the transcriptomic data to correlate the TNC expression with the different clinical parameters, such as survival or prognosis of the cancer.

As the initial step of analysis we performed the alignment of TNC and other proteins from the tenascin family, such as tenascin-X (TNX) looking for the homology between these two proteins. At the top of that we made the analysis of the homology between the TNC and TNX with the relation to ATN-RNA sequence. The alignment of these two ECM proteins shows that they share only limited number of nucleotides (query cover 5% and 22%, for short and long transcriptional variants in the protein N-terminus region, respectively. The sequence alignment analysis clearly show the ATN-RNA matching exclusively to the TNC sequence (100% identity) (Fig 2A).

PPISURV analysis based on the Kaplan-Meier statistics showed very clearly the strong correlation with TNC expression and patients survival. The high expression level has a great impact on the shorter survival for the patients, thus suggesting also that TNC can be also considered as the prognostic factor for breast cancers ($P = 0.0196$) (Fig 2B). At the same time, we analyzed also the available data for the TNX. The results showed an inverse correlation of *TNXB* mRNA expression and survival ($P = 0.00179$) (Fig 2C). Analysis was carried out on the group of patient N = 196 for *TNC* and N = 232 for *TNXB*.

ATN-RNA mediates the down-regulation of TNC mRNA and protein expression in breast cancer cells

To achieve down-regulation of TNC expression in breast cancer cell line, transfection with various concentration of ATN-RNA (10; 25; 50 and 100 nM) was performed. 48 h after

A

B

Protein level	Number of breast cancer cases				Healthy breast			
	TNC	TNN	TNR	TNXB	TNC	TNN	TNR	TNXB
High	0	0	0	N/A	-	N/A	-	N/A
Medium	8	5	0	N/A	-	N/A	-	N/A
Low	3	1	1	N/A	-	N/A	-	N/A
N.D.	1	6	11	N/A	+	N/A	+	N/A

C
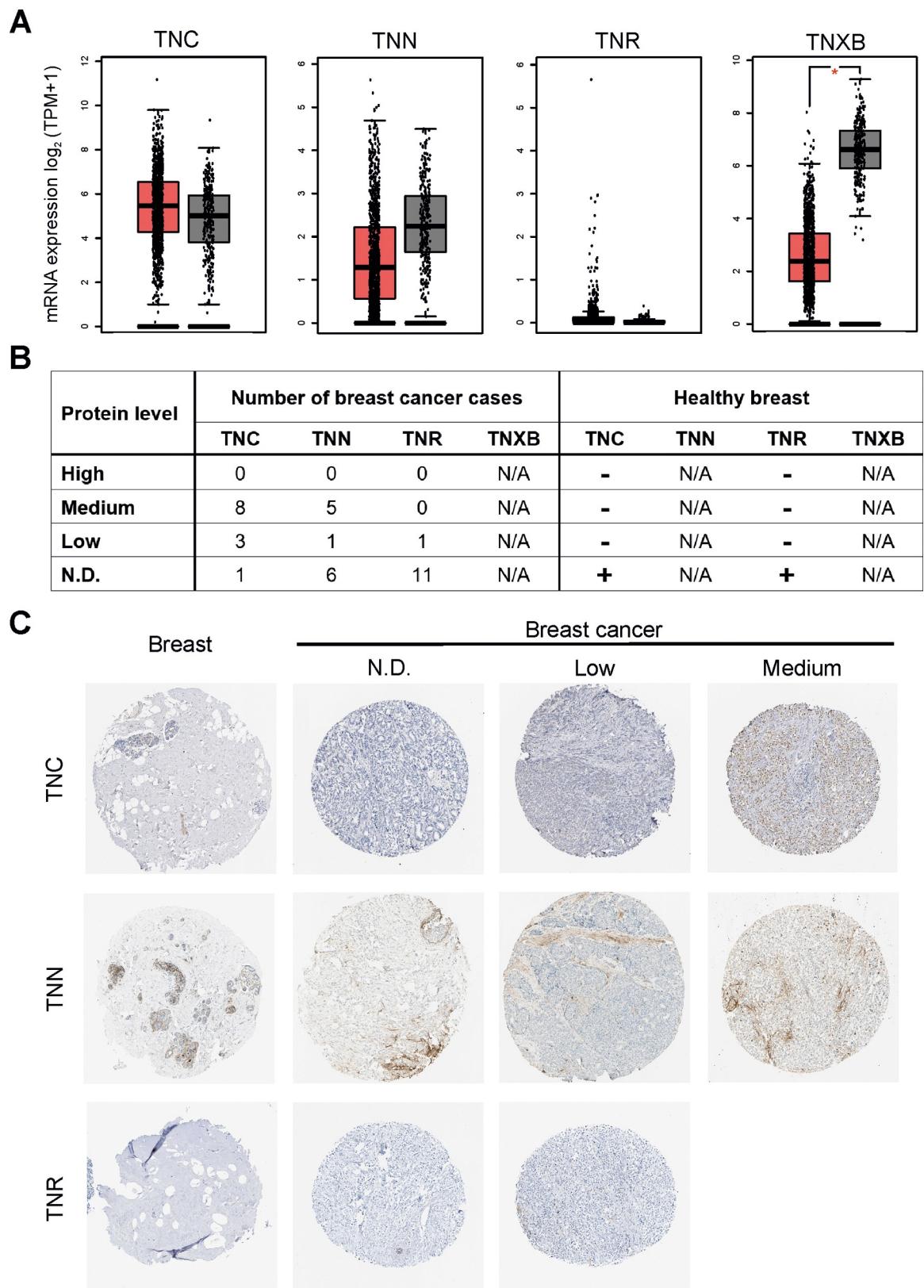
Fig 1. Tenascin is highly expressed in breast invasive carcinoma (TCGA-BRCA). (A) Messenger RNA levels of TNC (tenascin-C), TNN (tenascin-W), TNR (tenascin-R), TNXB (tenascin-X) genes in 1085 specimens from patients with invasive carcinoma of the breast

(*vs*. 291 non-tumor samples). RNA sequencing data were retrieved from the database of TCGA and analysed using the GEPIA (Gene Expression Profiling Interactive Analysis) online web server (http://gepia.cancer-pku.cn/). The red boxes represent cancer specimens, grey boxes represent healthy breast specimens. Significance value: * *P* < 0.05. **(B)** Summary of tenascin expression patterns in breast cancer tissues and healthy breast determined by immunohistochemical staining. Data were retrieved from the Human Protein Atlas database. Case numbers of invasive breast cancer are shown. N/A: not available; N.D.: not detectable. In "Healthy breast" column "+" means that TNC and TNR are not detected in non-tumor samples. Results in normal breast are based on immunohistochemical staining of a single sample. **(C)** Representative images of immunohistochemical staining for TNC, TNN, and TNR in breast (healthy tissue) and invasive breast carcinoma specimens. The images shown here are of the tissue sections from tissue microarray arrays (TMAs) stained with appropriate antibodies; TNC–CAB004592, TNN–CAB010907, TNR–CAB022343. All the images were taken at 200× magnification.

https://doi.org/10.1371/journal.pone.0237889.g001

transfection the expression level of TNC was examined by qRT-PCR analyses. Significant down-regulation of TNC mRNA expression was observed compared to control treated with scrambled RNA. The level of TNC was decreased from 15% at a concentration of 10 nM ATN-RNA up to 55% for cells treated with 100 nM ATN-RNA in comparison to the control (*P* < 0.001) (Fig 3A).
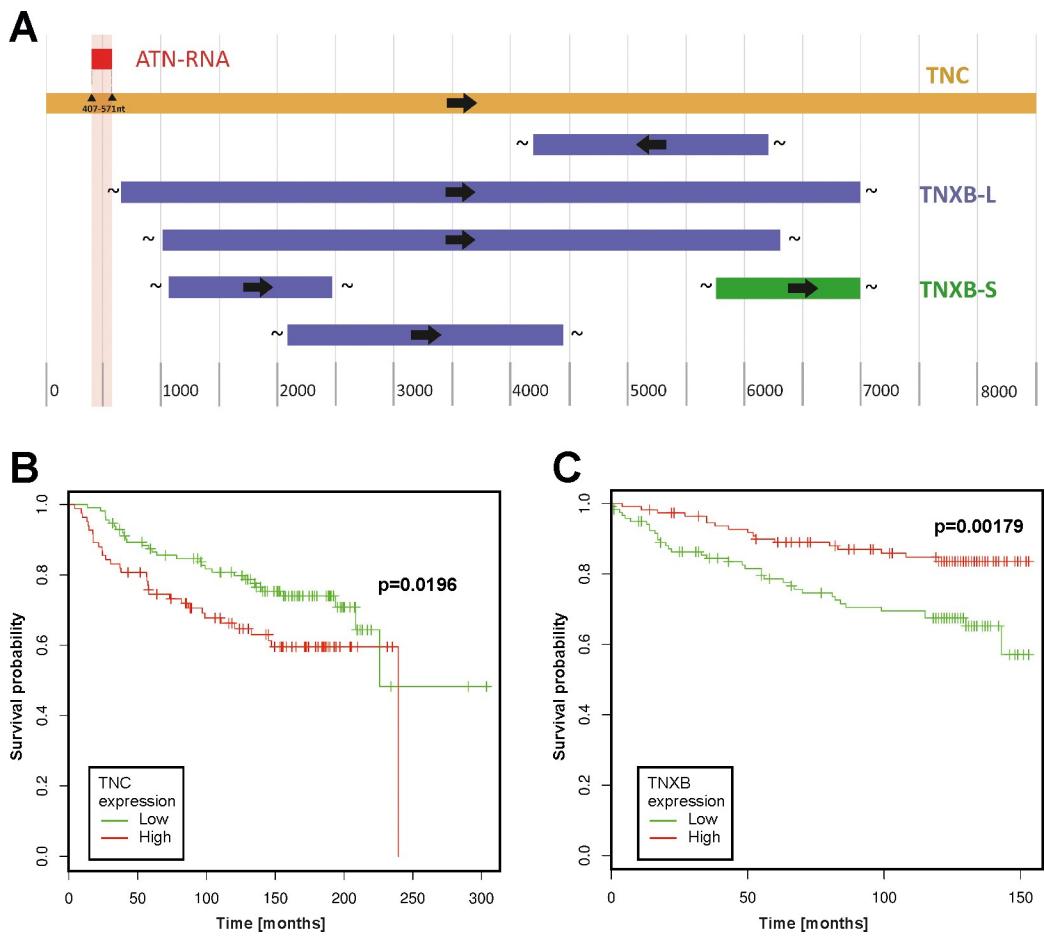
Fig 2. The oncogenomic analysis of the survival association with tenascin-C and tenascin-X in breast cancer. (A) Sequence alignment of tenascin-C versus tenascin-X with their relation to ATN-RNA. The sequence alignment analysis clearly show the ATN-RNA matching exclusively to the TNC sequence (100% identity). Relation of TNC **(B)** and TNXB **(C)** gene expression to survival of breast cancer patients. Survival analysis performed with the use of a dataset (breast cancer; GEO: GSE7390 and GSE3494) deposited in and tools available from the PPISURV web portal. TNXB-L- long transcription variant; TNXB-S- short transcription variant.

https://doi.org/10.1371/journal.pone.0237889.g002
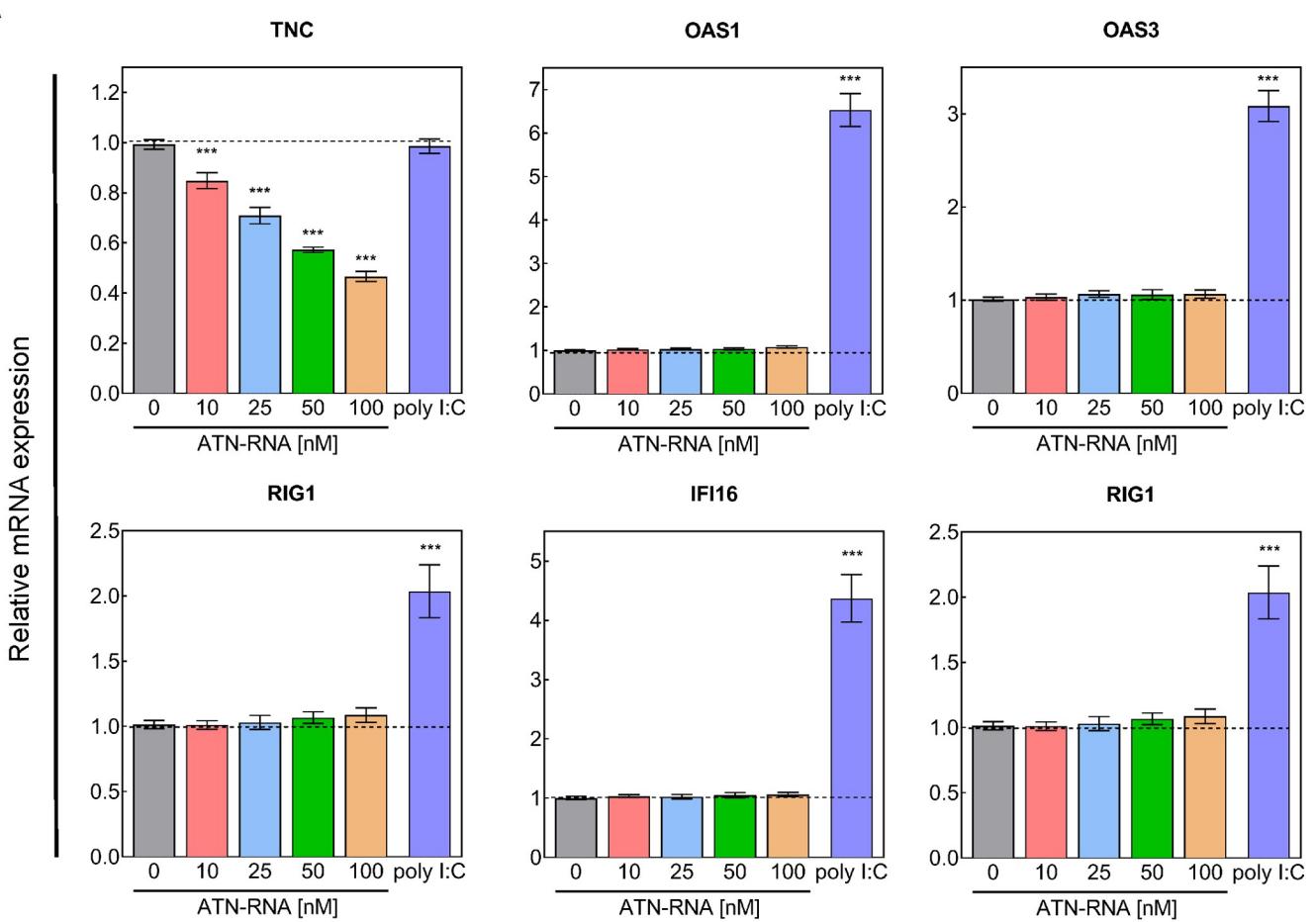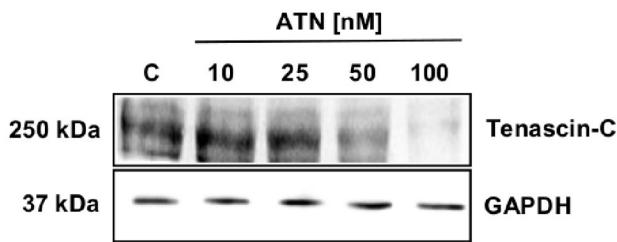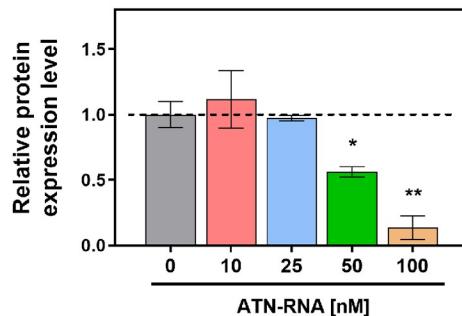
Fig 3. Expression level of TNC and immune response genes after ATN-RNA treatment in MDA-MB-231 cell line. (**A**) Relative expression level of the expression of *TNC*, *OAS1*, *OAS3*, *RIG1*, *IFI16* and *TLR3* established by qRT-PCR. Relative expression was calculated using the–ΔΔC_P method. Statistical evaluation of ATN-RNA *versus* scrambled siRNAs (C-control) cells was performed using one-way ANOVA followed by Tukey's post-hoc test. Effect of poly I:C (100 μg/ml) on immune response genes (*OAS1*, *OAS3*, *RIG1*, *IFI16*, *TLR3*) in the figure presented as purple bars. The results for *HPRT*-normalized expression of mRNA are expressed as fold change of target gene expression relative to the control (without poly I:C treatment, which is defined as 1). (**B**) The protein expression levels of *TNC* and *HPRT*. (**C**) Western blot analysis reveals efficient TNC silencing in MDA-MB-231 cells with ATN-RNA, compared to cells treated with siRNAs (C-control). The data represents the means ± SD from 3 independent experiments. Significance value: * $P < 0.05$, ** $P < 0.01$, *** $P < 0.001$.

The qRT-PCR analysis was also supported by direct analysis of the protein expression level. We have observed already a 44% decrease in TNC protein expression upon 50nM ATN-RNA treatment. The highest concentration (100nM) used led to the dramatic drop of the protein

expression measured as the 86% of the decrease (Fig 3B and 3C). These observations were fully consistent with relative TNC expression level measured by qRT-PCR.

Interferon response to ATN-RNA

To establish interferon induction in breast cancer MDA-MB-231 cultured cells, we looked for interferon stimulated genes (ISG) including: *OAS1*, *OAS3*, *RIG1*, *TLR3* and *IFI16* genes. The analysis was carried out with the qRT-PCR (Fig 3A). Changes after ATN-RNA measured by qRT-PCR were not significant, as shown basically for all of the genes in the concentration range of 10–100 nM. In parallel, a synthetic form of dsRNA, poly(I):poly(C) (poly I:C), was transfected as a positive control. Poly I:C has been used extensively as a TLR3 ligand to induce antiviral response [34–36]. We showed that transfection with poly I:C (100 μg/ml) efficiently induced the expression of immune response genes (*OAS1*, *OAS3*, *RIG1*, *IFI16*, *TLR3*) in MDA-MB-231 cells. This enhancement in mRNA expression was 2–7-fold higher in poly I:C treated cells than in untreated cells (Fig 3A, purple bars).

TNC knockdown inhibits cells proliferation and leads to the changes in migration rate and adhesion potential of breast cancer cells

In order to investigate the involvement of TNC on breast cancer cells proliferation, MDA-MB-231 cell line was treated with ATN-RNA and the real-time cell proliferation assay was performed. The cells ability to proliferate was measured for 72 h. We have noticed time- and concentration-dependent decrease in proliferation rate. The most effective concentration of ATN-RNA was 100 nM, with decrease from 32–45% after 24 and 72 h, respectively (Fig 4A). Noteworthy, 25 nM and 50 nM of ATN-RNA was already sufficient concentration for the efficient inhibition of breast cancer cells proliferation. The dose-dependent effect of ATN-RNA in MDA-MB-231 proliferation potential resulted in standard sigmoidal dose-responses with IC_{50} of 97.6 ± 8.2 nM after 24 h, 92.1 ± 7.8 nM after 48 h and 88.4 ± 5.2 nM after 72 h of treatment (Fig 4B).

To get more insight into the down-regulation of TNC expression by ATN-RNA on the mobility of breast cancer cells, real-time measurements of migration was carried out. We found that down-regulation of TNC expression by ATN-RNA significantly impaired the cell migration in breast cancer cell lines (Fig 4C). The results were quantitatively assessed during 72 h of experiment and showed that MDA-MB-231 cells transfected with ATN-RNA had the lowest motility beginning from 12 h post transfection. It was established that ATN-RNA delayed the migration of MDA-MB-231 cells by 22.45 ± 2.7 h, 20.80 ± 2.5 h, 15.44 ± 1.9 h and 12.40 ± 2.5 h with 10, 25, 50 and 100nM concentration, respectively. Notably, the most effective concentration which affected the migration potential of the cells was 10nM. When compared to the control, the observed delay was 22.45 ± 2.7 h.

Since TNC is implicated also in cell-matrix attachment, we further looked at the adhesion ability of ATN-RNA treated cells. The cells were conducted to real-time adhesion assay with *xCELLigence* system. Compared with the controls, TNC knockdown resulted in increased cells adhesion 15% on average (Fig 4D).

TNC promotes apoptosis and is involved in cell cycle regulation in breast cancer cells

To determine additionally the effect of ATN-RNA on the cell cycle progression, the MDA-MB-231 cells were treated with different concentrations of ATN-RNA for 24–48 h, and the cell cycle analysis was assessed by Muse® Cell Analyzer. Cells transfected with ATN-RNA
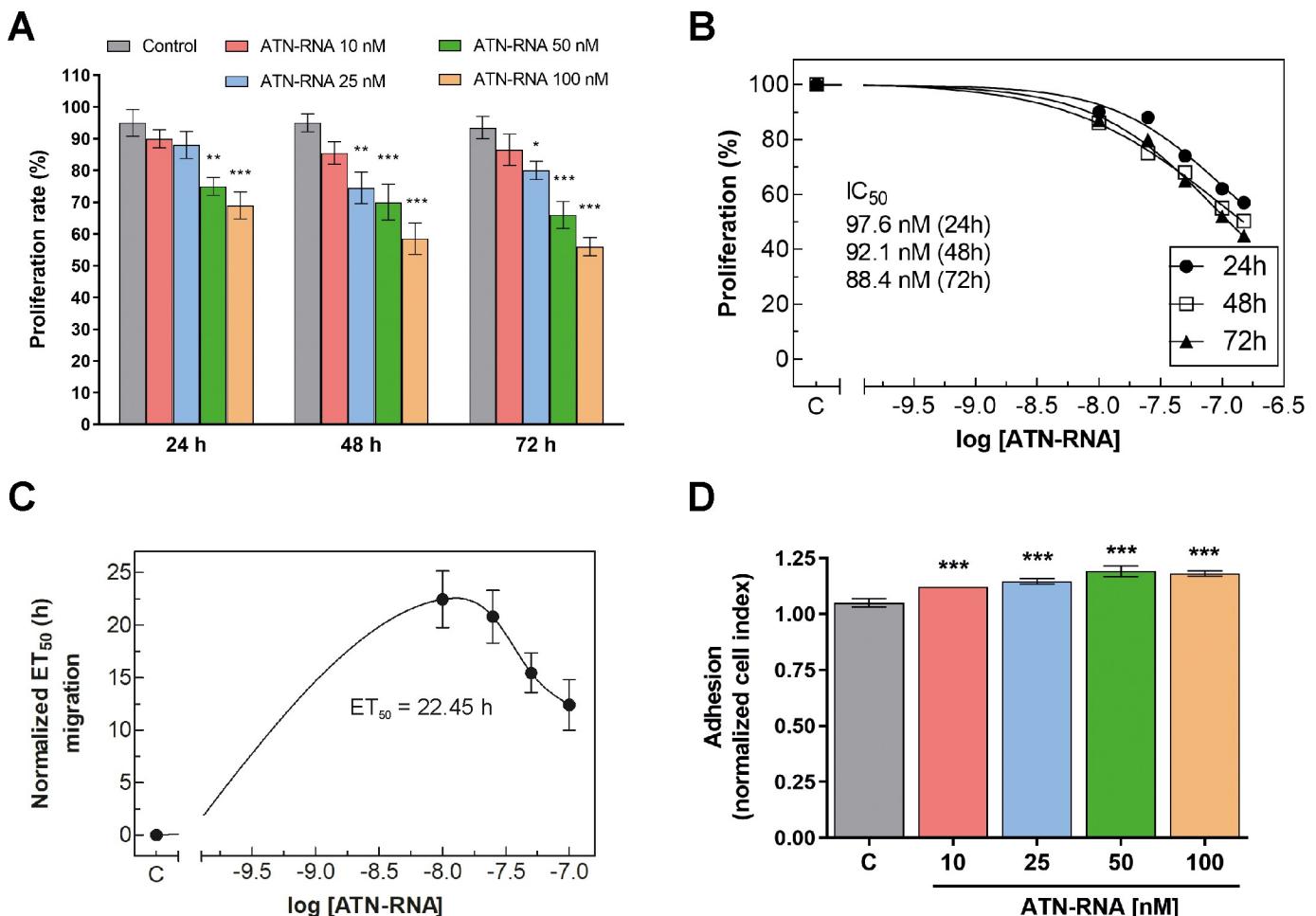
Fig 4. Activity of ATN-RNA in proliferation, migration and adhesion. Proliferation of breast cancer in culture was monitored in real-time using *xCELLigence* system. **(A)** Impedance was recorded every 15 min, but to improve the clarity of the graphs only every fourth readout was plotted. Data show the mean ± SD of three independent measurements. **(B)** Dose-dependent effects of ATN-RNA on proliferation was evaluated using non-linear regression by fitting experimental values to sigmoidal, bell-shaped equation. **(C)** Migration of MDA-MB-231 cancer cells was studied using *xCELLigence* system. Serum-depleted cells were transfected with increasing concentrations of ATN-RNA (from 10 to 100 nM) or scrambled siRNAs (C-control). Impedance (CI values) of each experimental condition was recorded over time, plotted against time, fitted to four-parameter logistic non-linear regression model and ET_{50} was calculated for each ATN-RNA concentration to generate dose-response curves. ET_{50} value was normalized to the data obtained for untreated cells and plotted as normalized half maximal effective time (ET_{50}) of cell migration against ATN-RNA concentrations. **(D)** Adhesion of MDA-MB-231 cell line was observed in real-time using *xCELLigence* system. Graph shows the final impendence values minus the initial values for the respective samples. Differences between CI values for ATN-RNA treated and control cells were statistically evaluated using one-way ANOVA followed by Tukey's post-hoc test (symbols above the bars). Significance value: *** $P < 0.001$ compared to cells treated with scrambled siRNAs (C-control).

https://doi.org/10.1371/journal.pone.0237889.g004

showed the cell cycle distribution with the concentration-dependent decrease in cell number in G_0/G_1 phase, increased in S phase and unchanged in G_2/M phase compared to the cells transfected with unspecific control RNA (Fig 5A). ATN-RNA impacted the cell cycle by almost doubling the cells S-phase fraction from 18% to 34% for the highest ATN-RNA concentration, thus resulted with the cells arrest in S phase. The cell cycle analysis proved the non-toxic effect of ATN-RNA, since we did not observe the increase in G_1 population. S phase arrest persists following up to 48 h of ATN-RNA treatment (Fig 5B).

Thus, to examine whether ATN-RNA-induced apoptosis would be associated with the caspases activation, the expression levels and activity of caspases such as: caspase-1, -3, -4, -5, -6, -7, -8 and -9 in the ATN-RNA-treated MDA-MB-231 cells were assessed using Muse® Cell
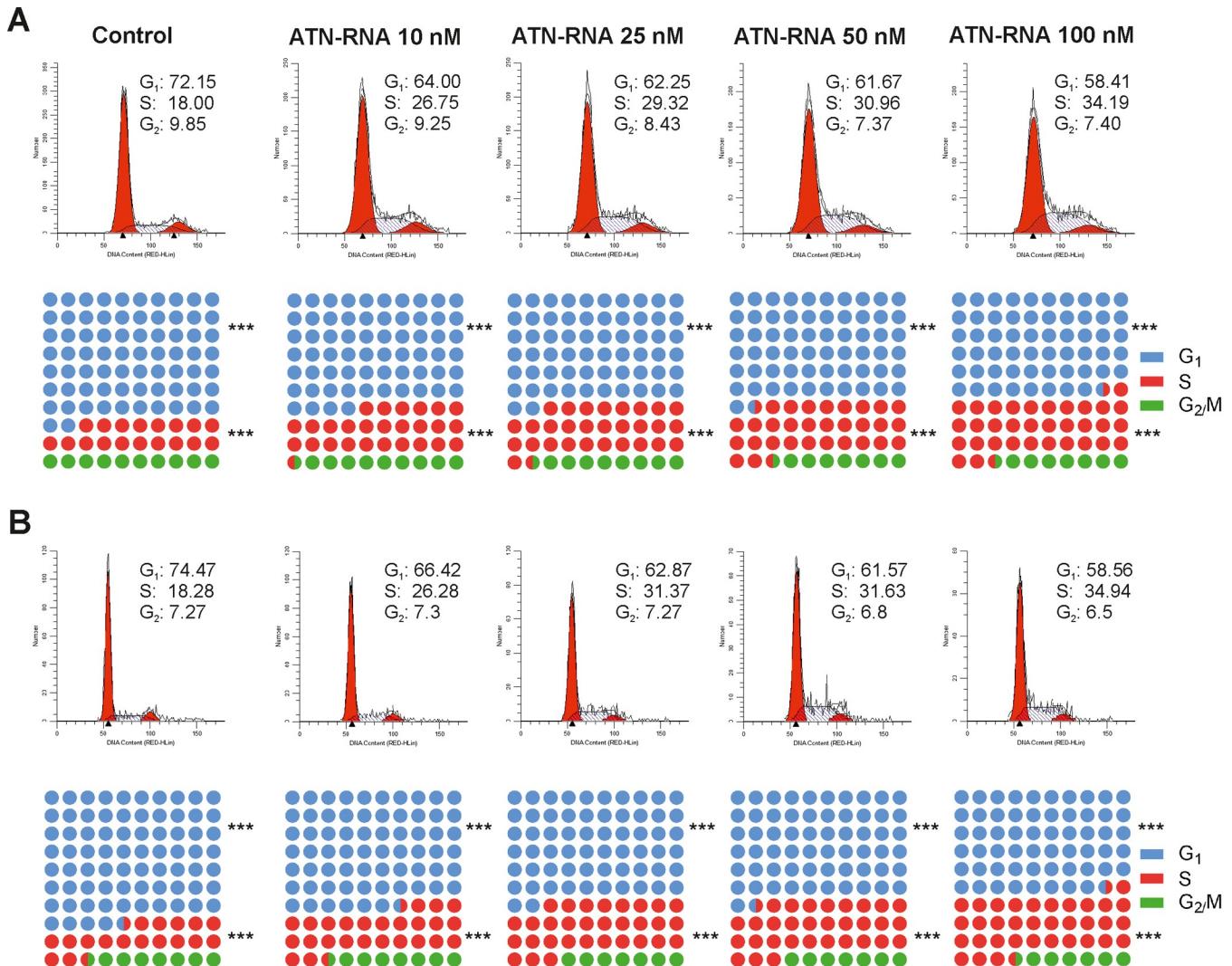
Fig 5. Effect of ATN-RNA on breast cancer cell cycle phase analysis. MDA-MB-231 cells were transiently transfected with increasing concentrations of ATN-RNA (from 10 to 100 nM) or scrambled siRNA (C-control) for 24 **(A)** and 48 h **(B)**. The cells were then fixed and added with Propidium Iodide (PI)/ RNase A staining solution and analyzed in Muse® Cell Analyzer using ModFit LT™ software. A percentage of cell distribution in each cell cycle phase was summarized and shown. The cell cycle distribution profile image is shown as a representative result of three independent experiments.

https://doi.org/10.1371/journal.pone.0237889.g005

Analyzer. As shown in Fig 6A, breast cancer cells treated with ATN-RNA exhibited enhanced multi-caspase activity in a concentration-dependent manner. The multi-caspase activity was 17.48 ± 3.22, 28.73 ± 3.15, 33.15 ± 2.90 and $42.95 \pm 4.03\%$ respectively, at 10; 25; 50 and 100 nM ATN-RNA concentration compared with the control (Fig 6B). Thus, we observed almost 5-fold increase of the population of the apoptotic cells with the lowest ATN-RNA concentration, whereas almost 12-fold with the highest one.

ATN-RNA has an impact on spheroids integrity

To visualize the involvement of TNC in tumor formation, the 3D culture model was applied. Since 3D cell culture models mimic better the *in vivo* behavior of cells in tumour tissues and are excellent surrogates to predict tumorigenic potential *in vivo*, the ability to spheroid maintenance of breast cancer cells was assessed after ATN-RNA treatment. We have observed that
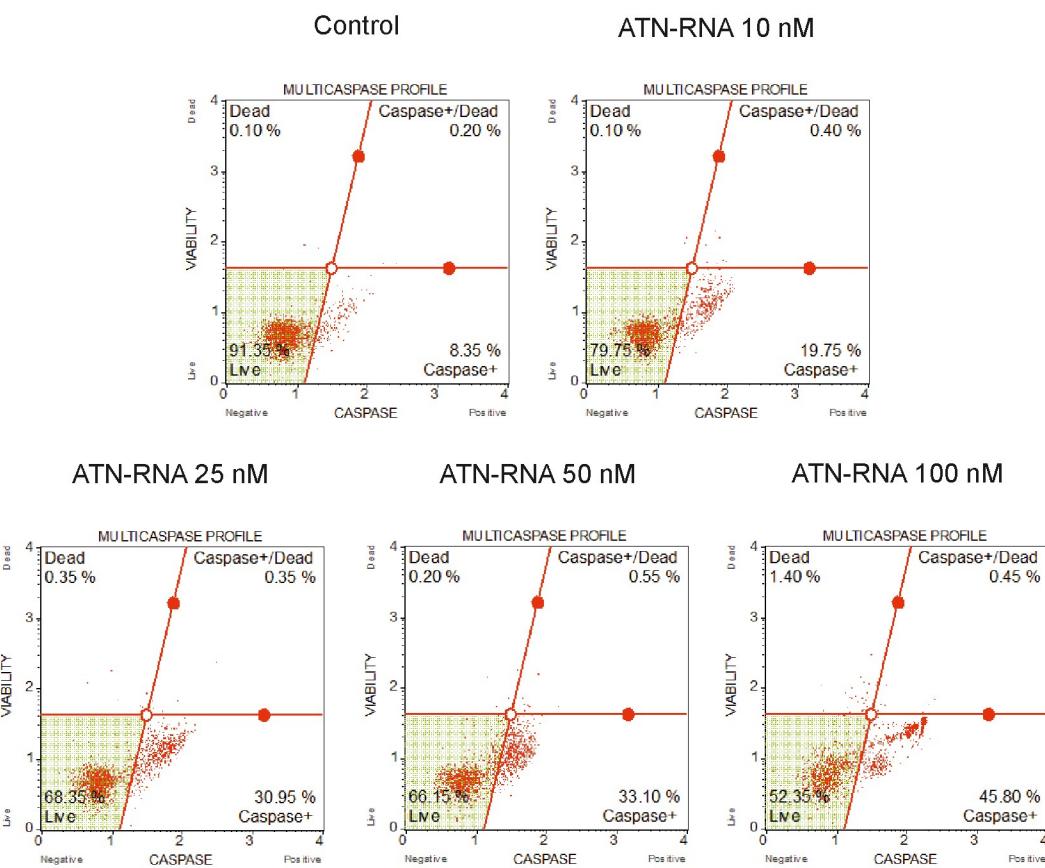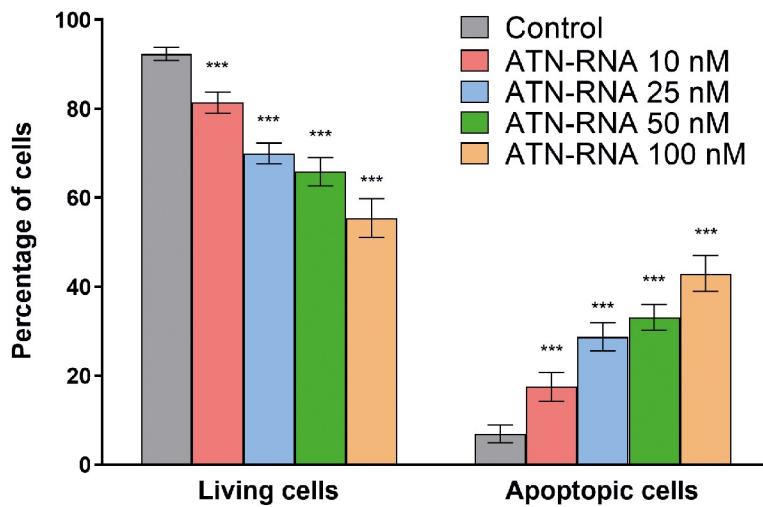
Fig 6. Effect of ATN-RNA on multiple caspase activation (caspase-1, 3, 4, 5, 6, 7, 8, and 9) in MDA-MB-231 cell line.
Breast cancer cells were transiently transfected with increasing concentrations of ATN-RNA (from 10 to 100 nM) or scrambled siRNAs (C-control) for 24 h. The transfected cells were then incubated with Muse® MultiCaspase reagent followed by analysis of the percentage of cell population in live, caspase+, caspase+/dead and dead in Muse® Cell Analyzer. **(A)** The percentage of live, caspase+, caspase+/dead and dead cells profile image is shown as a representative result from one of three independent experiments. **(B)** The graphical representation of percentage of live and exhibiting caspase activity cell population transfected with ATN-RNA and scrambled siRNAs. Statistical evaluation of ATN-RNA *versus* scrambled cells

down-regulation of TNC led to the disintegration of the spontaneously forming spheroids of MDA-MB-231. The clearly visible effect on the spheroid viability was observed even with the lowest ATN-RNA concentration. The increased concentrations of dsRNA had a great impact on spheroids integrity, resulting in structure disintegration at the highest concentration of 100 nM (Fig 7A). The ATN-RNA application influenced the spheroid volume and shape, displaying the total shrinking of the compact structure into the small fragments with the highest ATN-RNA concentration (Fig 7A).

To have a better insight into the MDA-MB-231 spheroids structure and the ATN-RNA impact on their viability, the confocal microscopy imaging was assessed. The analysis of fluorescent labelling with green-fluorescent calcein-AM of living and dead cells within the spheroid with the Live/Dead Viability/Cytotoxicity Kit was carried out. As revealed by the image of the untreated MDA-MB-231 cells, compact multicellular spheroids were obtained. Fluorescence images revealed the overall morphology of the MDA-MB-231 spheroids (Fig 7B). The cell density in the core of the untreated spheroid was high and no dead cells were identified. The similar pictures were obtained for the control. Furthermore, all conditions with different ATN-RNA concentrations resulted with losing the spheroid density, increased dimensions and appearing a higher population of dead cells. It is worthy of note, that the spheroids treated with increasing ATN-RNA concentrations did not display a smooth contour following 24 h of treatment and subsequently, their round shape was markedly altered by the treatments. After the treatment with 50nM concentrations, the spheroids showed the strong overrepresentation of dead cells (Fig 7B). Thus, the 100nM concentration of ATN-RNA was most likely too high for the cells viability and we were not able to keep the spheroids in shape, that would allow for the imaging.

TNC is involved in EMT processes

As the consequence of these finding we analyzed the expression level of proteins involved in EMT processes. We took into account two main EMT markers, E-cadherin and vimentin. Western blot analysis shows the significant increase of E-cadherin level followed by the drop of the expression of vimentin protein (Fig 8A). These observations were concentration-dependent, showing the highest efficacy for ATN-RNA at the concentration of 100nM for E-cadherin expression. Similarly, for vimentin we have observed the highest decrease of expression upon ATN-RNA transfection at 100nM concentration (Fig 8B).

Discussion

TNC is the main ECM protein of various tumors and its over-expression is repeatedly observed in breast cancer cells both *in vitro* and *in vivo*, indicating a role for this extracellular matrix glycoprotein in neoplastic pathology. Moreover, its high expression correlates with worsened patient survival prognosis in several cancer types [37]. In breast cancers, several studies demonstrate that high expression of TNC is not only an indicator of poor prognosis, but also correlates with metastasis to distinct organs such as lymph nodes, liver and lung [38–40]. TNC plays a substantial role in EMT, that is believed to be a key mechanism in cancer progression whereby cancer cells acquire more aggressive behavior [4, 39]. In human breast cancer specimens, TNC is co-expressed with the mesenchymal marker vimentin [41]. The mechanistic role of TNC in the process of EMT remains poorly defined, however, studies
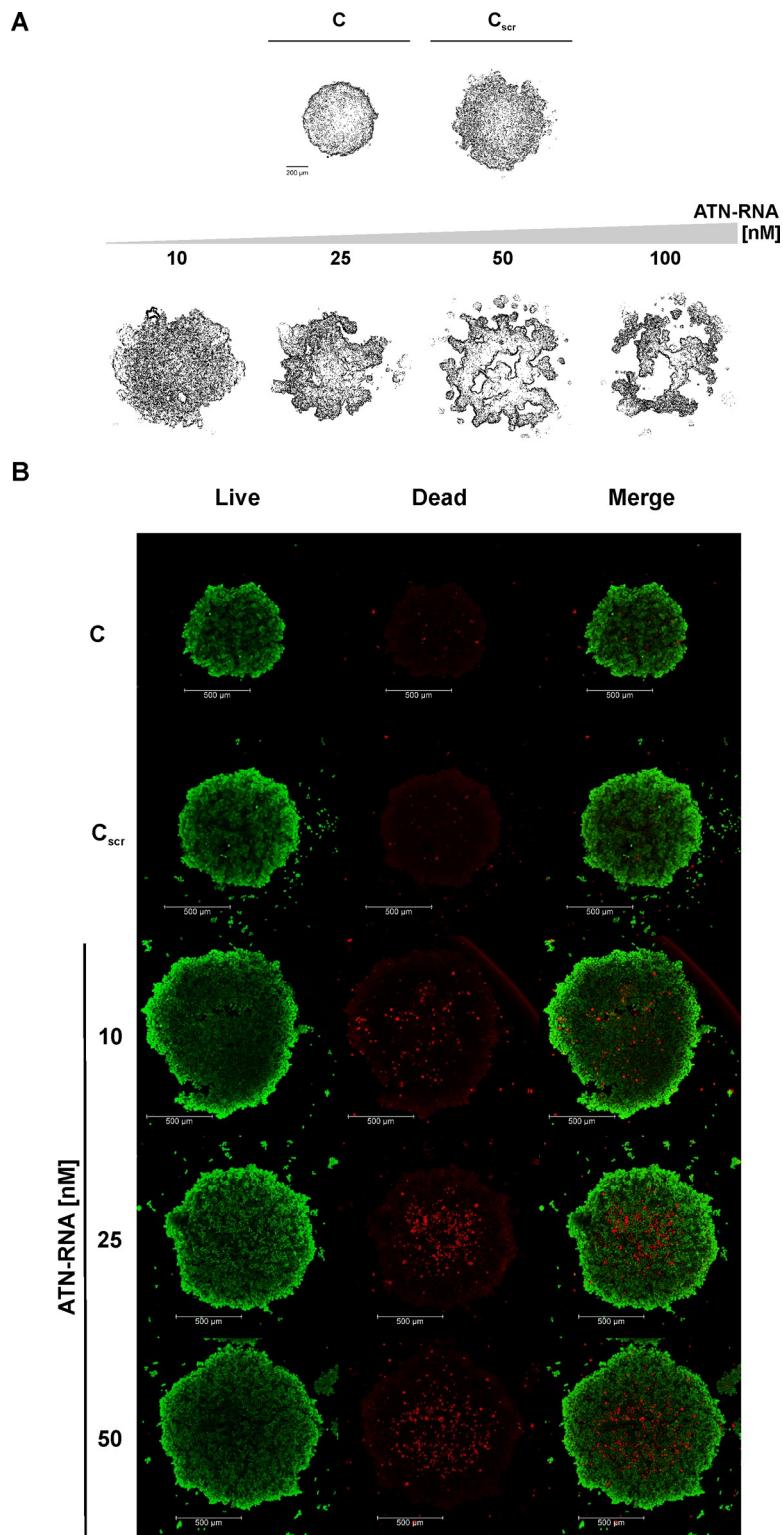
Fig 7. Effects of ATN-RNA on viability and spheroid structure in MDA-MB-231 cells. (A) Monolayer cultures were transfected with indicated amounts of ATN-RNA oligonucleotides and after 24 hrs, cellular spheroids of MDA-MB-231 cells were generated from 5000 cells in Perfecta3D® 96-well Hanging Drop Plate and cultured for up to 120 hours. Scale bars, 200 μm. Scrambled siRNAs (C_{scr}). **(B)** The viability of the ATN-RNA transfected cells within spheroids using LIVE/DEAD Cell Imaging Kit. Left and middle panels present live cells (green) and dead cells (red), respectively.

The right panels show merge of two fluorescent images. Scrambled siRNAs (C$_{scr}$), 10, 25, 50 concentrations of ATN-RNA used for transfection. Fluorescence images were taken using Leica TCS SP5 confocal laser scanning microscope and Plan Apo 63×1.4 NA oil-immersion objective. Scale bars, 500 μm.

https://doi.org/10.1371/journal.pone.0237889.g007

suggest that TNC can induce an EMT like phenotype in MCF-7 breast cancer cells *via* the αVβ6 and αVβ1 integrins [42, 43]. Many studies on various cancer tissues have demonstrated down-regulation of epithelial markers including E-cadherin, plakoglobin and cytokeratin, as well as the up-regulation of mesenchymal markers such as N-cadherin and vimentin and expression of EMT transcription factors SNAI 1/2 and TWIST. Since these changes towards mesenchymal phenotype could correlate with invasiveness, metastatic potential and poor patient's outcome, we have investigated the effect of TNC knockdown on the expression levels of EMT markers. Our results show that down regulation of TNC reverses the malignant phenotype of the cancer cells. As the experimental result we observed the down-regulation of mesenchymal marker—vimentin followed by the up-regulation of epithelial marker—E-cadherin. This indicates ATN-RNA as a potential therapeutic agent, which could switch the mesenchymal phenotype of breast cancer cells to the epithelial one, inhibiting the ability to metastasis and invasion. Additionally, it has been also shown that TNC as the ECM component plays also
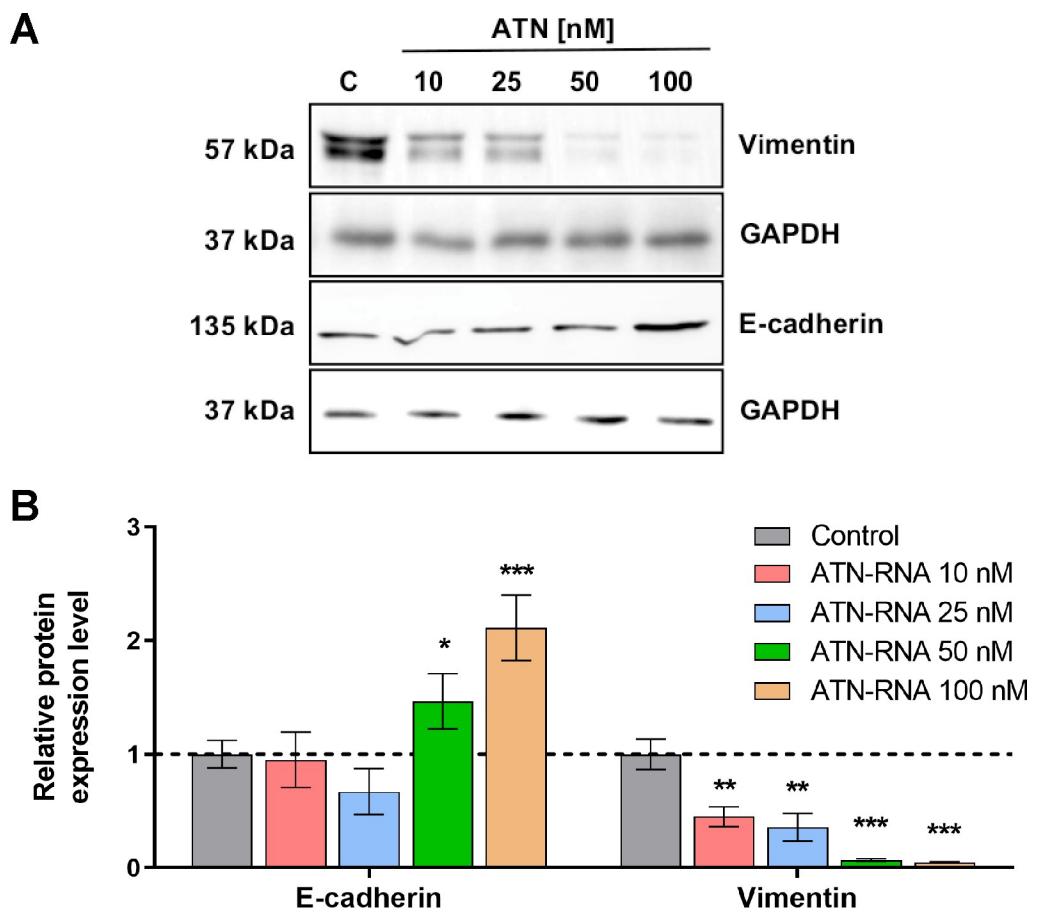
Fig 8. The effect of TNC down-regulation on EMT process of MDA-MB-231 cells. (A) The protein expression levels of E-cadherin, vimentin and GAPDH. **(B)** Western blot analysis of ATN-RNA effects on the EMT process revealed a significant increase in E-cadherin level followed by the drop of the expression of vimentin protein. The data represents the means ± SD from 3 independent experiments.

https://doi.org/10.1371/journal.pone.0237889.g008

a role in cell to cell or cell-matrix attachment most probably inhibiting the cells' migration. In approach with ATN-RNA, it seems that TNC in breast cancer cell line plays an anti-adhesive role, which would affect the cell migration and invasion ability in addition to EMT processes. Thus, TNC down-regulation seems to enhances the adhesiveness of cancer cells, showing the direct involvement of TNC in cell adhesive properties. Targeting the TNC in potential therapy might be also highly beneficial since it has been already established, that TNC maintain a stem cell niche in the brain tumors, thus could promote the tumor cell invasion. Therefore, its over-expression largely contributes to radio/chemotherapy resistance and tumor recurrence. In fact, it has been shown that targeting GBM invasion increases tumor sensitivity to temozolomide [44]. TNC also promotes stromal events such as the angiogenic switch and the formation of more but leaky blood vessels involving Wnt signaling and inhibition of Dickkopf1 (DKK1) in a neuroendocrine tumor model [45].

We observed significant ATN-RNA–mediated down-regulation of TNC was in concordance with the observed changes in proliferation and migration rates. The results show that the ATN-RNA transfected cells lose their ability to migrate, thus showing the involvement of TNC in breast cancer invasiveness. Our data indicate also that, the down-regulation of TNC expression in MDA-MB-231 cancer cell lines inhibits proliferation along with induction of cell death. We were able to determine the TNC impact on the apoptosis by measuring level of both caspases initiating intracellular events (caspase-2, -8, -9) and effector caspases-3, -6 and -7.

Orend et al. [46] demonstrated that TNC causes cdk2 inactivation and blocks cell cycle progression from G_1 phase to S phase of anchorage-dependent fibroblasts by interfering with fibronectin–syndecan-4 interactions. For the proliferation of anchorage-dependent cells, attachment to the ECM is required. Detachment of fibroblasts by a pure tenascin-C substratum results in G_1-phase arrest by inactivation of the cdk2 complex in a CKI-dependent manner [46]. In contrast to fibroblasts, proliferation of most tumor cells is stimulated by TNC [47]. This shows that the effect of TNC on proliferation is cell type-specific and suggests that in cancer cells, the cdk2 complex is not repressed in the presence of TNC. In leukemia, breast carcinoma and glioma were found subpopulations of stem-like cells that support tumor growth [48]. In such cells, adhesion on the TNC substratum may override the G_0/G_1 and G_1/S cell cycle checkpoints, which may explain the increased proliferation rate [47]. The G_1/S transition is enforced by cyclin E/cdk2 activation *via* syndecan-4 related signalling. It has been shown that TNC in tumor cells binds to the syndecan-4 binding site in fibronectin, thereby blocking syndecan-4 ligation, releasing the tumor cells from the suppressive effect of fibronectin on their proliferation [49]. This would appear to indicate that TNC indirectly blocks some signalling pathways by inactivating syndecan-4 and activating cdk2. In the present study, we observed the induced accumulation of cells in S-phase with a concomitant decrease in number of cells in G_1-phase. Since this phenomenon was not observed in untreated cells, we concluded that the accumulation of cells in S-phase was largely attributed to the presence of ATN-RNA. The dose-related S-phase cell cycle accumulation described here appears to be primarily the result of TNC down-regulation. Since, inhibitory phosphorylation of cdk2 is maximal during S- and G_2-phase it is likely that decreased level of TNC caused by ATN-RNA negatively affects cdk2 activation in S-phase and inhibition of the cell cycle in this phase. However, the exact mechanism should be the subject of future investigations. It seems likely that, down-regulation of TNC mRNA may be a unique approach to sensitizing cancer cells with S-phase chemotherapy. It has been already shown, that S-phase cell arrest can be impacted by the potential therapeutic agent incorporation into DNA during replication e.g. nucleosides analogous [50–52]. Mechanistically, cell cycle analysis revealed that ATN-RNA reduces cell proliferation primarily *via* cell cycle arrest in S-phase. The desirability of targeting S-phase as a mode of action of

breast cancer therapeutics is underlined by the topoisomerase I (TOP1) inhibitor irinotecan, which is a clinically effective pharmaceutical for advanced and metastatic breast cancer [53].

Since we used RNAi technology and dsRNA for TNC downregulation that as has been shown may also induce various sequence-dependent and sequence-independent events including immune response activation, we have also looked at the expression level of the genes possibly stimulated by the dsRNA. The stimulation of cytoplasmic IFN-inducible dsRNA-activated protein kinase (PKR), retinoid acid-inducible gene-I (RIG-I), 2′-5′-oligoadenylate synthetase (OAS), interferon gamma inducible factor 16 (IFI16) and endosomal Toll-like receptors TLR3, TLR7, TLR8 leads to the activation of interferon regulatory factors and secretion of type I and III interferons. These molecules *via* autocrine/paracrine signaling activate (STAT) signaling pathway and lead to sequence-independent changes in cell division, growth or apoptosis [54–56].

However, our results did not show the ability to induce the immune response in breast cancer cell line at the level of the selected genes expression. Thus, our collected data of apoptosis and cell cycle analysis, together with the immune response analysis allowed us to hypothesize that ATN-RNA is specifically involved in apoptosis induction, without possible off-target effect and immune response activation.

Closely mimicking the tumor environment 3D cell line spheroids model of breast cancer confirmed TNC direct involvement in tumor spheroids viability, thus the down-regulation of this protein results in disintegration of spheroid morphology. One can however observe, that the application of 100 nM concentration of ATN-RNA in some cases impacts the unexpected changes and the discrepancy regarding to lower concentrations. 100nM ATN-RNA concentrations seems to be too high for the viability of cells resulting with the more likely unspecific effects. This would suggest, that the dose of ATN-RNA applied to cancer cells must be then carefully established to avoid any toxic or unspecific effects. In our approach we established then the TNC loss-off-function MDA-MB-231 cell line, what resulted in a response to abrogate potency to tumor growth. We have found that the viability of microtumor is abolished in a dose-dependent manner, especially at the tumor borders, but also with the predominant presence of dead cells in the spheroid core (Fig 8). Since a large number of dead cells was observed in all spheroids treated with ATN-RNA, we could suspect the possible diffusion of the ATN-RNA agent and high levels of cellular stress inside the 3D structure.

Our results share a number of similarities with Xia et al.'s [57] findings with glioma "go-or-grow" phenomenon which represents characteristic, fast growing tumor cores and diffuse tumor borders with a low proliferation rate. The cellular mechanisms of this phenotypic switch in intracranial tumor xenografts are associated with decreased tumor invasion and increased tumor proliferation due to decreased TNC level in tumor microenvironment [57]. Taken together our observations, we conclude that, even when we observe the cells diffusion from the periphery of the spheroids, it more likely cannot be connected to the possible invasive cells potential.

There is a large body of literature that highlights the role of TNC in tumor expansion and metastasis [46, 47, 49, 58, 59]. Although, participation in pathological processes of other tenascin family proteins, especially tenascin-X (TNX, encoded by the *TNXB* gene) is still controversial. Liot et al. [58] conducted a large meta-analysis using the Gene Expression Omnibus and The Cancer Genome Atlas databases and immunohistochemistry staining of Tissue MicroArrays to analyze TNX expression in 13 types of cancer in the context of tumor progression. Their results show that TNX mRNA and protein levels are down-regulated in most cancers, except for glioma. Discrepancies between gene and protein expressions were observed for stomach adenocarcinoma, ovary cancer and malignant mesothelioma. Survival differences between the established *TNXB*^low and *TNXB*^high subgroups were evaluated with Kaplan–Meier survival curves. As expected, the expression level of *TNXB* mRNA were significantly associated

with the clinical outcomes of lung adenocarcinoma ($P = 0.0014$) and breast carcinoma ($P = 0.0234$) patients. These results indicate that high expression of *TNXB* correlates with good prognosis and survival rate in the breast and lung carcinomas which have the highest incidence and mortality in the world among all of cancers.

Our experimental data are in concordance with the oncogenomic portals deep analysis showing the association of the TNC over-expression and the poor survival of the breast cancer patients. The analogous analysis of the TNX expression level shows the opposite effect on the survival. The over-expression of *TNXB* mRNA correlates with the long survival of the breast cancers patients, whereas its down-regulation is linked to shorter time of survival. The finding is consistent with previous research by Matsumoto et al. [60], which found that the absence of TNX may promote tumor cell behaviour. In particular, B16-BL6 melanoma cell growth and metastasis was increased in tenascin-X double knockout mice (TNX-/-) in comparison to littermates. Cells in natural state express TNX reciprocal to TNC, so therapy based on silencing expression should target only one of those proteins to not disturb functionality of the second one. The alignment of these two ECM proteins—TNC and TNX shows that they share only a limited number of nucleotides, avoiding the ATN-RNA sequence overlap with the *TNXB*. Therefore the ATN-RNA therapeutic tool only matches to the *TNC* sequence (Fig 2A). The down-regulation of TNC with ATN-RNA prolongs then patients' survival protecting the suppressive activity of TNX. Regarding the presence of the TNC isoforms, almost universal and high level of expression of all these isoforms in breast carcinomas coupled with their tumor-restricted distribution make them still a plausible therapeutic target for ATN-RNA, since the sequence of ATN-RNA is directed to the EGF–like domains present always in all splicing variants.

Looking at the data, one can however see the discrepancy between gene and protein expression of the isoforms at the breast and breast cancer tissue level in our analysis. The repositories in the data bases allowed us to clearly show the expression of the TNC and TNX at the mRNA level which was detected for 1085 patients. The Human Protein Atlas at the same time shows the data for only 11 breast cancer patients at the protein level. Thus, we assume the discrepancy might arise from the highly different number of the samples with the relevant data. The data on the mRNA and protein level, although differ in the number of the samples, still keep, in our mind, the tendency which shows the overexpression of TNC in breast cancer samples.

Additionally, the performed analysis including the TNC impact on the patient survival, with the data for 196 breast cancer patients, provides, in our mind, strong premise for considering the TNC as the good candidate as the therapeutic target and the malignancy predictor for breast cancer patients.

Our results as well as the oncogenomic data, both correlate TNC expression with the poor patients survival and enhance the utility of TNC as a kind of universal therapeutic target for other tumors types, where TNC overexpression is associated with poor prognosis.

However, we also emphasize the fact that no ECM protein exists in isolation and suggest that, even targeting such potent molecule as TNC alone, may not be sufficient to completely damage the neoplasm and benefit patient outcome. Therefore, targeting TNC may be potentially supportive in designing more effective anticancer treatments when used in conjunction with radiotherapy, and chemotherapy.

Materials and methods

Cell culture conditions

Human MDA-MB-231 breast cancer cells triple negative–ER-; PR-; HER2- were purchased from ATCC (American Type Cell Collection, Manassas, VA, USA). Cells were maintained in

DMEM medium supplemented with 10% foetal bovine serum (FBS), 100 U/ml penicillin and 0.1 mg/ml streptomycin (all from Sigma-Aldrich, MO, USA). Cell line was cultured in humidified incubator with 5% CO_2 at 37˚C.

dsRNA preparation

ATN-RNA was prepared as previously described [25, 61]. Briefly, ATN-RNA was generated by *in vitro* transcription of ATN-DNA flanked by T7 and T3 RNA polymerase promoter regions. The two strands were synthesized individually, purified, and then added together for annealing and renaturation (50 mM Tris-HCl pH 7.5, 50 mM NaCl, 95˚C for 3 min, 75˚C for 30 min and slow cooling down for 4 h to 25˚C) [62]. Hybridization was analysed on 6% polyacrylamide gel electrophoresis with 7M urea.

In vitro transfection

Transfection of dsRNA was performed with a commercial reagent, Lipofectamine® 2000 (Thermo Fisher Scientific, MA, USA) in 24-well plates according to manufacturer's instructions. Briefly, the day before transfection, confluent layers of cells were trypsinized, counted and resuspended. Cell suspension was plated into each well of the 24-well plates, so that they could become about 70% confluent next day at the time of transfection. The cells were then incubated with dsRNA (10; 25; 50 and 100 nM–final concentration) for 48 h.

3D spheroid culture

MDA-MB-231 cells were initially maintained as a monolayer culture and transfected with 10; 25; 50; 100 nM (final concentration) of ATN-RNA and Lipofectamine® 2000 (Invitrogen, CA, USA). After 24 h cells were seeded in Perfecta3D® 96-well Hanging Drop Plate (3D Biomatrix, Ann Arbor, MI, USA). Spheroids in hanging drops were formed by pipetting 5×10^3 cells in 50 μl of complete growth medium. The cell culture medium was supplemented on the third day of culture by adding 7 μl fresh growth media to each drop. Spheroids were grown for 5 days.

RNA isolation

Total RNA from breast cell lines was isolated with TRIzol® Reagent (Thermo Fisher Scientific, MA, USA), then purified using the Ambion® DNA-*free*™ Kit (Applied Biosystems, CA, USA) according to the manufacturer's instructions. The reverse transcription was carried out using 1 μg RNA, random primer and RevertAid™ H Minus M-MuLV reverse transcriptase (Thermo Fisher Scientific, MA, USA).

Quantitative RT-PCR

Real-time qPCR was performed to assess transcripts of TNC (Tenascin-C; `TNC-R:GGGATT AATGTCGGAAATGGT, TNC-L: CCGGACCAAAACCATCAGT`), OAS1 (2'5'-oligoadenylate synthetase 1; `OAS1-R: CAGGAGCTCCAGGGCATAC, OAS1-L: CATCCGCCTAGTCAAGC ACT`), OAS3 (2'-5'-oligoadenylate synthetase 3; `OAS3-R: ACGAGGTCGGCATCTGAG, OAS3-L: TCCCATCAAAGTGATCAAGGT`), RIG1 (retinoic acid-inducible gene I; `RIG1-R: TTGGTATCTCCTAATCGCAAAAG, RIG1-L: GGCAAGTCCCGCTGTAAAC`), IFI16 (interferon gamma inducible factor 16; `IFI16-R: TTTGGATGCTCTGGTCATCTT, IFI16-L: GGCATTTTGAAGAATTGGAAAG`), TLR3 (Toll-like receptor 3; `TLR3-R: ATCTTCCAATTGC GTGAAAAC, TLR3-L: TGGATATCTTTGCCAATTCATCT`) expression relative to HPRT (hypoxanthine phosphoribosyltransferase; `HPRT-R: CGAGCAAGACGTTCAGTCCT,`

HPRT-L: TGACCTTGATTTATTTTGCATACC), ACTB (β-actin; ACTB-R: CCAGAGGCGT
ACAGGGATAG; ACTB-L: CCAACCGCGAGAAGATGA) using the thermocycler LightCy-
cler® 480 (Roche Applied Science, Germany). The reaction mixture was prepared with the
LightCycler® 480 Probes Master Kit (Roche Applied Science, Germany) and included 1x Mas-
ter Mix, 0.1 μM of probes, 1 μM of each primer, 1 μl of template cDNA and water to a final vol-
ume of 10 μl. The PCR conditions for all genes were as follows: initial incubation step at 95˚C
for 5 min followed by 45 cycles of amplification for 15 s at 95˚C, 30 s at 55˚C and 30 s at 72˚C.
the final cooling step was 40˚C for 30 s. All standard curves were generated by amplifying a
series of 2-fold dilution of cDNA.

Protein isolation

MDA-MB-231 3D spheroid cells treated with ATN-RNA were sonicated in 50 mM Tris-HCl
buffer pH 7.5 with 1x protease inhibitors cocktail (Sigma-Aldrich, MO, USA) for 3×15 s and
centrifugated 5 min at 10000 rpm. Supernatant containing soluble proteins was spectrophoto-
metrically measured at a wavelength of 280 nm to assess the protein concentration and then
used for Western blot analysis.

Western blot analysis

100, 50 and 10 μg of protein extracts were separated by 15% SDS-PAGE for TNC, EMT pro-
teins and GAPDH, respectively. PageRuler™ Plus Prestained Protein Ladder (Thermo Fisher
Scientific, MA, USA) was used as the size marker. The electrophoresis was run at a current of
30 mA and a voltage of 250 V. Transfer was carried out for 30 min at a current of 130 mA and
a voltage of 100 V in wet transfer blotter (Bio-Rad, CA, USA) onto PVDF membrane of
0.45 μm pore size (GE Healthcare, IL, USA) in transfer buffer (25 mM Tris base, 190 mM gly-
cine, 20% methanol). Blots were rinsed once in PBST20 (PBS, 0.05% Tween 20). The mem-
branes were placed in the SNAP i.d.® 2.0 apparatus (EMD Milipore, MA, USA), where it was
blocked for 10 min with a 0.5% solution of skimmed milk in PBST20 (Sigma-Aldrich, MO,
USA). Hybridization was done with polyclonal Tenascin-C antibody (Santa Cruz Biotechnol-
ogy, TX, USA), E-cadherin and vimentin from the Epithelial-Mesenchymal Transition (EMT)
Antibody Sampler Kit (Cell Signaling Technology, MA, USA), while for detection of glyceral-
dehyde 3-phosphate dehydrogenase (GAPDH) monoclonal antibody was used (Santa Cruz
Biotechnology, TX, USA). Antibodies were diluted 1:500 in 3% BSA. Membranes were incu-
bated with the primary antibody for 10 min or overnight, depending on the level of detection
of the protein then washed 3 times with PBST20. Secondary anti-rabbit IgG and anti-mouse
IgG antibodies conjugated with horseradish peroxidase (HRP) were used (Sigma-Aldrich,
MO, USA). Detection of proteins was carried out with WesternBright Sirius Chemilumines-
cent Detection Kit (Advansta, CA, USA). Intensity of individual bands was analyzed qualita-
tively by Multi Gauge ver. 2.0 (Fujifilm, Tokio, Japan). Final expression levels of Tenascin-C,
E-cadherin and vimentin were compared to GAPDH expression level.

Real-time proliferation assay

Experiments were carried out using the *xCELLigence* Real-Time Cell Analyzer (RTCA) DP
instrument (Roche Applied Science, Germany). The system measures time-resolved electrical
impedance changes resulting from cell proliferation to electrodes located on the plate surface
(E-plate, ACEA Biosciences, San Diego, CA, USA). Initially, 100 μl of cell-free complete
growth medium (10% FBS) was added to the wells. After leaving the 16-well E-plates at room
temperature for 10 min in tissue culture hood, the background impedance for each well was
measured. Transfected with 10; 25; 50; 100 and 150 nM (final concentration) of ATN-RNA,

MDA-MB-231 cells were seeded in E-plates at a density of 10×10^4 per well in complete growth medium (100 μl). After leaving the plates at room temperature for 30 min to allow cell attachment, they were placed in RTCA DP instrument and the impedance value of each well was monitored by the *xCELLigence* system and defined as a *Cell Index* value (CI), a dimensionless parameter, which was directly proportional to the total area of microelectrodes populated by the cells. Impedance was measured for 72 h. CI was monitored every 15 min during the experiment. Obtained CI values were entered to the GraphPad Prism v5.01 (GraphPad Software, La Jolla, CA, USA) software and used to calculate half maximal inhibitory concentrations (IC_{50}).

Transwell migration assay

Transwell cell migration experiments were performed using *xCELLigence* RTCA DP Analyzer in Cell Invasion and Migration (CIM) plates (ACEA Biosciences, San Diego, CA, USA) with each well consisting of an upper and a lower chamber separated by a microporous polyethylene terephthalate (PET) membrane containing randomly distributed 8 μm-pores. Prior to migration assay, MDA-MB-231 cells were transfected with ATN-RNA. Initially, 160 μl of complete growth medium (supplemented with 10% FBS) was added to the lower chamber and 25 μl of serum-free growth medium to the upper chambers of CIM-plate. To initiate a transwell migration experiment, cells were detached, resuspended in serum-free growth medium and seeded in the upper chamber at a density of 5×10^4 cells in 175 μl per well, treated with ATN-RNA (in 10; 25; 50 and 100 nM concentration). After cell addition, CIM-plates were incubated during 30 min at room temperature in tissue culture hood to allow the cells to embed onto the PET membrane. Impedance of the microelectrode array attached to the bottom side of the microporous membrane was monitored and converted by RTCA DP software to CI. Readouts were performed every 15 min for up to 72 h. Using GraphPad Prism v5.01 obtained CI values from each experimental condition were plotted against time, fitted to four-parameter logistic non-linear regression model and the half-time of migration (half maximal effective time, ET_{50}) was calculated [63].

Adhesion assay

Cellular reattachment from suspension was monitored by the *xCELLigence* system based on RTCA DP instrument. Experiment was carried out in 16-well E-Plates VIEW (ACEA Biosciences, San Diego, CA, USA) with electrode-free viewing strip which allows for microscopy observations. MDA-MB-231 cell transfections with ATN-RNA at final concentrations of 10; 25; 50; 100 nM were done 24 h prior to the reattachment assay. 1 h before test, E-Plates VIEW were coated with 0.5% BSA dissolved in PBS, left at 37°C and 5% CO_2. Then wells were washed with PBS and filled with 50 μl of serum-free growth medium supplemented with 0.25% BSA. Plate was next plugged in the RTCA DP instrument for first measurement of the background impedance. Afterwards the same plate was seeded at the density of 5×10^4 cells in 150 μl medium per well. System was subsequently re-inserted into the RTCA and left for 10 min to stop movements of media in well. The impedance measurements lasted for 4 h with readout at 3 minute intervals. The resulting IC data depends on the number of adherent cells.

Cell cycle

MDA-MB-231 cells (6×10^4 per 6-well plate) were seeded and exposed to ATN-RNA (0; 10; 25; 50 and 100 nM) for 24 h and 48 h. The harvested cells were washed in PBS and 200 μl of Muse® cell cycle reagent (EMD Millipore, MA, USA) was added. The cells were incubated for 30 min at RT in the dark. Cell cycle distribution was analyzed by Muse® Cell Analyzer (Merck Millipore, MA, USA).

Multi-caspase assay

The activity of caspase-1, -3, -4, -5, -6, -7, -8 and -9 was measured using a Muse® Multi-caspase kit (MCH100109, Merck Millipore, MA, USA) according to the manufacturer's instructions. MDA-MB-231 cells were incubated with various concentrations of ATN-RNA (0; 10; 25; 50 and 100 nM) for 24 h. Cells were harvested and incubated with 5 μl of Muse® Multi-Caspase reagent working solution at 37˚C for 30 min. Then, 150 μl of Muse® Caspase 7-AAD working solution was added to each sample. Multi-caspase assay was performed with Muse® Cell Analyzer (Merck Millipore, MA, USA).

Microscopy and image analysis

The morphology of the spheroids was visualized by a Leica DMI4000 B inverted microscope (Leica Microsystems, Wetzlar, Germany) with 5× magnification objective. For assessment of ATN-RNA effects in 3D cultures on spheroid morphology we applied author's spheroid-edge detection method. In brief, for each ATN-RNA concentration at experimental endpoint (72 h) high magnification microscopy images were taken with a Leica Application Suite (Leica Microsystems, Wetzlar, Germany) with a 1 ms exposure time. Central micro tumours were cropped into the final images for spheroid-contour processing. The size of each cropped image in all experiments was 567 x 567 pixels (24 Bit Color RGB), with resolution of 96 dpi. In next step, the contour of spheroids was identified, followed by *Contour Tool* in Corel® PHOTO--PAINT X5 (Corel Corporation, Ottawa, ON, Canada). The size of the spheroids was analysed using the analysis tools in Photoshop CS5 software (Adobe Systems, San Jose, CA, USA).

Viability analysis of spheroids

The viability of MDA-MB-231 spheroids treated with 10; 25 and 50 nM of ATN-RNA was analyzed using LIVE/DEAD Cell Imaging Kit (488/570) (Thermo Fischer Scientific, MA, USA). MDA-MB-231 cells were transfected with ATN-RNA and seeded onto 96-well U-bottom plates at a density of 5×10^3 cells/well in the 100 μl of DMEM growth medium supplemented with 10% of FBS and 1% of antibiotic solution and cultured at 37˚C and 5% CO_2 saturation. After 3 days, spheroids were replaced into prewarmed (37˚C) fresh medium containing LIVE/DEAD reagent (calcein-AM/ethidium homodimer 1) prepared according to the manufacturer's protocol and incubated for 30 min under growth conditions. Next spheroids were moved to the glass-bottom dishes and placed in FluoroBrite DMEM (ThermoFisher Scientific). Life-cell imaging was done using Leica TCS SP5 confocal laser scanning microscope equipped with White Light Laser (470–670 nm) and environmental cell culture chamber provides controlled conditions of temperature, CO_2 saturation and humidity. Sequentially scanned images were collected at Ex: 488 nm/Em: 515 nm for live cells and Ex: 570 nm/Em: 602 nm for dead cell, respectively, using a Plan Apo 63×1.4 NA oil-immersion objective. Image processing and analysis was done in Leica LAS AF software.

Databases

The expression data of *TNC*, *TNN*, *TNR* and *TNXB* genes were retrieved from The Cancer Genome Atlas (TCGA) and the Human Protein Atlas. The GEPIA (Gene Expression Profiling Interactive Analysis) online web server (http://gepia.cancer-pku.cn/) [64] collects data from the database of TCGA. The tenascin genes expression data from TCGA were retrieved using the GEPIA program. mRNA levels ($\log_2$ TPM+1) of tenascin genes were replotted. The survival analyses of the cancer patients with high and low levels of *TNC*, and *TNXB* expression were performed with the use of datasets and tools available in the PPISURV portal (http://

www.bioprofiling.de/GEO/PPISURV/ppisurvD.html) [65]. The data for analysis of the relationship between copy number category and expression level of TNC were obtained from cBioPortal for Cancer Genomics (Memorial Sloan-Kettering Cancer Center, New York, NY, USA; http://www.cbioportal.org/) [66, 67]. Sequence alignment of tenascin-C versus tenascin-X with their relation to ATN-RNA was performed with BLASTN 2.6.1+ [68]. Accession numbers for analysed genes used in this alignment: Homo sapiens tenascin-C (TNC), mRNA—NM_002160.3; Homo sapiens tenascin-X (TNXB-S), transcript variant XB-S, mRNA—NM_032470.3; Homo sapiens tenascin-X (TNXB-L), transcript variant XB-L, mRNA—NM_019105.6. Immunohistochemical staining of tumor and normal tissues were retrieved from the Human Protein Atlas. Samples with different scales of protein staining in tumor or normal tissues were counted.

Statistical analysis

Statistical analyses were performed using GraphPad Prism v5.01. Data was collected as triplicate from at least 3 independent experiments. The results were shown as mean ± standard deviation (SD). Differences between the means of treatments were evaluated using one-way analysis of variance (ANOVA) followed by Tukey's test. The half-maximal inhibitory concentrations (IC_{50}) were calculated by fitting experimental values to a sigmoidal bell-shaped equation. Statistical significance was designated as * $P < 0.05$, ** $P < 0.01$ and *** $P < 0.001$.

Supporting information

S1 File.
(DOCX)

S1 Raw images.
(PDF)

Acknowledgments

We thank Dr. Patrick McDevitt Perrigue for critical reading the manuscript and language editing. We would like to thank the Laboratory of Subcellular Structures Analysis of the Institute of Bioorganic Chemistry, Polish Academy of Sciences in Poznan, for the facilitating the cell culture maintaining and the microscopic analysis.

Author Contributions

Conceptualization: Dariusz Wawrzyniak, Katarzyna Rolle.

Data curation: Dariusz Wawrzyniak, Paweł Głodowicz, Konrad Kuczyński, Bogna Kuczyńska, Agnieszka Fedoruk-Wyszomirska, Katarzyna Rolle.

Formal analysis: Dariusz Wawrzyniak, Małgorzata Grabowska, Paweł Głodowicz, Konrad Kuczyński, Bogna Kuczyńska, Agnieszka Fedoruk-Wyszomirska.

Funding acquisition: Katarzyna Rolle.

Investigation: Dariusz Wawrzyniak, Małgorzata Grabowska, Paweł Głodowicz, Konrad Kuczyński, Bogna Kuczyńska, Katarzyna Rolle.

Methodology: Dariusz Wawrzyniak, Małgorzata Grabowska, Agnieszka Fedoruk-Wyszomirska.

Project administration: Katarzyna Rolle.

Resources: Katarzyna Rolle.

Supervision: Katarzyna Rolle.

Validation: Dariusz Wawrzyniak, Małgorzata Grabowska, Katarzyna Rolle.

Visualization: Agnieszka Fedoruk-Wyszomirska.

Writing – original draft: Dariusz Wawrzyniak, Katarzyna Rolle.

Writing – review & editing: Dariusz Wawrzyniak, Katarzyna Rolle.

References

1. Charles NA, Holland EC, Gilbertson R, Glass R, Kettenmann H. The brain tumor microenvironment. Glia. 2011; 59(8):1169–80. https://doi.org/10.1002/glia.21136 PMID: 21446047.

2. Lorger M. Tumor microenvironment in the brain. Cancers (Basel). 2012; 4(1):218–43. https://doi.org/10.3390/cancers4010218 PMID: 24213237; PubMed Central PMCID: PMC3712675.

3. Quirico-Santos T, Fonseca CO, Lagrota-Candido J. Brain sweet brain: importance of sugars for the cerebral microenvironment and tumor development. Arq Neuropsiquiatr. 2010; 68(5):799–803. https://doi.org/10.1590/s0004-282x2010000500024 PMID: 21049197.

4. Ioachim E, Charchanti A, Briasoulis E, Karavasilis V, Tsanou H, Arvanitis DL, et al. Immunohistochemical expression of extracellular matrix components tenascin, fibronectin, collagen type IV and laminin in breast cancer: their prognostic value and role in tumour invasion and progression. Eur J Cancer. 2002; 38(18):2362–70. https://doi.org/10.1016/s0959-8049(02)00210-1 PMID: 12460779.

5. Jahkola T, Toivonen T, Virtanen I, von Smitten K, Nordling S, von Boguslawski K, et al. Tenascin-C expression in invasion border of early breast cancer: a predictor of local and distant recurrence. Br J Cancer. 1998; 78(11):1507–13. https://doi.org/10.1038/bjc.1998.714 PMID: 9836485; PubMed Central PMCID: PMC2063217.

6. Orimo A, Gupta PB, Sgroi DC, Arenzana-Seisdedos F, Delaunay T, Naeem R, et al. Stromal fibroblasts present in invasive human breast carcinomas promote tumor growth and angiogenesis through elevated SDF-1/CXCL12 secretion. Cell. 2005; 121(3):335–48. https://doi.org/10.1016/j.cell.2005.02.034 PMID: 15882617.

7. Probstmeier R, Nellen J, Gloor S, Wernig A, Pesheva P. Tenascin-R is expressed by Schwann cells in the peripheral nervous system. J Neurosci Res. 2001; 64(1):70–8. https://doi.org/10.1002/jnr.1055 PMID: 11276053.

8. Pesheva P, Spiess E, Schachner M. J1-160 and J1-180 are oligodendrocyte-secreted nonpermissive substrates for cell adhesion. J Cell Biol. 1989; 109(4 Pt 1):1765–78. https://doi.org/10.1083/jcb.109.4.1765 PMID: 2477380; PubMed Central PMCID: PMC2115782.

9. El Ayachi I, Baeza N, Fernandez C, Colin C, Scavarda D, Pesheva P, et al. KIAA0510, the 3'-untranslated region of the tenascin-R gene, and tenascin-R are overexpressed in pilocytic astrocytomas. Neuropathol Appl Neurobiol. 2010; 36(5):399–410. https://doi.org/10.1111/j.1365-2990.2010.01074.x PMID: 20202125.

10. Lethias C, Carisey A, Comte J, Cluzel C, Exposito JY. A model of tenascin-X integration within the collagenous network. FEBS Lett. 2006; 580(26):6281–5. https://doi.org/10.1016/j.febslet.2006.10.037 PMID: 17078949.

11. Veit G, Hansen U, Keene DR, Bruckner P, Chiquet-Ehrismann R, Chiquet M, et al. Collagen XII interacts with avian tenascin-X through its NC3 domain. J Biol Chem. 2006; 281(37):27461–70. https://doi.org/10.1074/jbc.M603147200 PMID: 16861231.

12. Minamitani T, Ikuta T, Saito Y, Takebe G, Sato M, Sawa H, et al. Modulation of collagen fibrillogenesis by tenascin-X and type VI collagen. Exp Cell Res. 2004; 298(1):305–15. https://doi.org/10.1016/j.yexcr.2004.04.030 PMID: 15242785.

13. Meiners S, Geller HM. Long and short splice variants of human tenascin differentially regulate neurite outgrowth. Mol Cell Neurosci. 1997; 10(1–2):100–16. https://doi.org/10.1006/mcne.1997.0643 PMID: 9361291.

14. Mighell AJ, Thompson J, Hume WJ, Markham AF, Robinson PA. Human tenascin-C: identification of a novel type III repeat in oral cancer and of novel splice variants in normal, malignant and reactive oral mucosae. Int J Cancer. 1997; 72(2):236–40. https://doi.org/10.1002/(sici)1097-0215(19970717)72:2<236::aid-ijc6>3.0.co;2-s PMID: 9219826.

15. Carnemolla B, Castellani P, Ponassi M, Borsi L, Urbini S, Nicolo G, et al. Identification of a glioblastoma-associated tenascin-C isoform by a high affinity recombinant antibody. Am J Pathol. 1999; 154

(5):1345–52. https://doi.org/10.1016/S0002-9440(10)65388-6 PMID: 10329587; PubMed Central PMCID: PMC1866608.

16. Dueck M, Riedl S, Hinz U, Tandara A, Moller P, Herfarth C, et al. Detection of tenascin-C isoforms in colorectal mucosa, ulcerative colitis, carcinomas and liver metastases. Int J Cancer. 1999; 82(4):477–83. https://doi.org/10.1002/(sici)1097-0215(19990812)82:4<477::aid-ijc2>3.0.co;2-5 PMID: 10404058.

17. Adams M, Jones JL, Walker RA, Pringle JH, Bell SC. Changes in tenascin-C isoform expression in invasive and preinvasive breast disease. Cancer Res. 2002; 62(11):3289–97. PMID: 12036947.

18. Chung CY, Murphy-Ullrich JE, Erickson HP. Mitogenesis, cell migration, and loss of focal adhesions induced by tenascin-C interacting with its cell surface receptor, annexin II. Mol Biol Cell. 1996; 7 (6):883–92. https://doi.org/10.1091/mbc.7.6.883 PMID: 8816995; PubMed Central PMCID: PMC275940.

19. Murphy-Ullrich JE, Lightner VA, Aukhil I, Yan YZ, Erickson HP, Hook M. Focal adhesion integrity is downregulated by the alternatively spliced domain of human tenascin. J Cell Biol. 1991; 115(4):1127–36. https://doi.org/10.1083/jcb.115.4.1127 PMID: 1720121; PubMed Central PMCID: PMC2289958.

20. Phillips GR, Krushel LA, Crossin KL. Domains of tenascin involved in glioma migration. J Cell Sci. 1998; 111 (Pt 8):1095–104. PMID: 9512505.

21. Jones PL, Jones FS. Tenascin-C in development and disease: gene regulation and cell function. Matrix Biol. 2000; 19(7):581–96. https://doi.org/10.1016/s0945-053x(00)00106-2 PMID: 11102748.

22. Pas J, Wyszko E, Rolle K, Rychlewski L, Nowak S, Zukiel R, et al. Analysis of structure and function of tenascin-C. Int J Biochem Cell Biol. 2006; 38(9):1594–602. https://doi.org/10.1016/j.biocel.2006.03.017 PMID: 16698307.

23. Chiquet-Ehrismann R, Chiquet M. Tenascins: regulation and putative functions during pathological stress. J Pathol. 2003; 200(4):488–99. https://doi.org/10.1002/path.1415 PMID: 12845616.

24. Leins A, Riva P, Lindstedt R, Davidoff MS, Mehraein P, Weis S. Expression of tenascin-C in various human brain tumors and its relevance for survival in patients with astrocytoma. Cancer. 2003; 98 (11):2430–9. https://doi.org/10.1002/cncr.11796 PMID: 14635078.

25. Rolle K, Nowak S, Wyszko E, Nowak M, Zukiel R, Piestrzeniewicz R, et al. Promising human brain tumors therapy with interference RNA intervention (iRNAi). Cancer Biol Ther. 2010; 9(5):396–406. https://doi.org/10.4161/cbt.9.5.10958 PMID: 20118657.

26. Daniels DA, Chen H, Hicke BJ, Swiderek KM, Gold L. A tenascin-C aptamer identified by tumor cell SELEX: systematic evolution of ligands by exponential enrichment. Proc Natl Acad Sci U S A. 2003; 100(26):15416–21. https://doi.org/10.1073/pnas.2136683100 PMID: 14676325; PubMed Central PMCID: PMC307582.

27. Hancox RA, Allen MD, Holliday DL, Edwards DR, Pennington CJ, Guttery DS, et al. Tumour-associated tenascin-C isoforms promote breast cancer cell invasion and growth by matrix metalloproteinase-dependent and independent mechanisms. Breast Cancer Res. 2009; 11(2):R24. https://doi.org/10.1186/bcr2251 PMID: 19405959; PubMed Central PMCID: PMC2688953.

28. Jurga M, Lipkowski AW, Lukomska B, Buzanska L, Kurzepa K, Sobanski T, et al. Generation of functional neural artificial tissue from human umbilical cord blood stem cells. Tissue Eng Part C Methods. 2009; 15(3):365–72. https://doi.org/10.1089/ten.tec.2008.0485 PMID: 19719393.

29. von Holst A. Tenascin C in stem cell niches: redundant, permissive or instructive? Cells Tissues Organs. 2008; 188(1–2):170–7. https://doi.org/10.1159/000112848 PMID: 18160825.

30. He J, Liu Y, Xie X, Zhu T, Soules M, DiMeco F, et al. Identification of cell surface glycoprotein markers for glioblastoma-derived stem-like cells using a lectin microarray and LC-MS/MS approach. J Proteome Res. 2010; 9(5):2565–72. https://doi.org/10.1021/pr100012p PMID: 20235609; PubMed Central PMCID: PMC2866009.

31. Mock A, Warta R, Geisenberger C, Bischoff R, Schulte A, Lamszus K, et al. Printed peptide arrays identify prognostic TNC serumantibodies in glioblastoma patients. Oncotarget. 2015; 6(15):13579–90. Epub 2015/05/07. https://doi.org/10.18632/oncotarget.3791 PMID: 25944688; PubMed Central PMCID: PMC4537035.

32. Hoeferlin LA, C EC, Park MA. Challenges in the Treatment of Triple Negative and HER2-Overexpressing Breast Cancer. J Surg Sci. 2013; 1(1):3–7. Epub 2014/05/13. PMID: 24818173; PubMed Central PMCID: PMC4012677.

33. Dai X, Cheng H, Bai Z, Li J. Breast Cancer Cell Line Classification and Its Relevance with Breast Tumor Subtyping. J Cancer. 2017; 8(16):3131–41. Epub 2017/11/22. https://doi.org/10.7150/jca.18457 PMID: 29158785; PubMed Central PMCID: PMC5665029.

34. Matsumoto M, Seya T. TLR3: interferon induction by double-stranded RNA including poly(I:C). Adv Drug Deliv Rev. 2008; 60(7):805–12. Epub 2008/02/12. https://doi.org/10.1016/j.addr.2007.11.005 PMID: 18262679.

35. Ichinohe T, Watanabe I, Ito S, Fujii H, Moriyama M, Tamura S, et al. Synthetic double-stranded RNA poly(I:C) combined with mucosal vaccine protects against influenza virus infection. J Virol. 2005; 79 (5):2910–9. Epub 2005/02/15. https://doi.org/10.1128/JVI.79.5.2910-2919.2005 PMID: 15709010; PubMed Central PMCID: PMC548446.

36. Kumar A, Zhang J, Yu FS. Toll-like receptor 3 agonist poly(I:C)-induced antiviral response in human corneal epithelial cells. Immunology. 2006; 117(1):11–21. Epub 2006/01/21. https://doi.org/10.1111/j.1365-2567.2005.02258.x PMID: 16423036; PubMed Central PMCID: PMC1782193.

37. Midwood KS, Chiquet M, Tucker RP, Orend G. Tenascin-C at a glance. J Cell Sci. 2016; 129(23):4321–7. Epub 2016/11/23. https://doi.org/10.1242/jcs.190546 PMID: 27875272.

38. Minn AJ, Gupta GP, Siegel PM, Bos PD, Shu W, Giri DD, et al. Genes that mediate breast cancer metastasis to lung. Nature. 2005; 436(7050):518–24. https://doi.org/10.1038/nature03799 PMID: 16049480; PubMed Central PMCID: PMC1283098.

39. Oskarsson T, Acharyya S, Zhang XH, Vanharanta S, Tavazoie SF, Morris PG, et al. Breast cancer cells produce tenascin C as a metastatic niche component to colonize the lungs. Nat Med. 2011; 17(7):867–74. https://doi.org/10.1038/nm.2379 PMID: 21706029; PubMed Central PMCID: PMC4020577.

40. Tavazoie SF, Alarcon C, Oskarsson T, Padua D, Wang Q, Bos PD, et al. Endogenous human micro-RNAs that suppress breast cancer metastasis. Nature. 2008; 451(7175):147–52. https://doi.org/10.1038/nature06487 PMID: 18185580; PubMed Central PMCID: PMC2782491.

41. Dandachi N, Hauser-Kronberger C, More E, Wiesener B, Hacker GW, Dietze O, et al. Co-expression of tenascin-C and vimentin in human breast cancer cells indicates phenotypic transdifferentiation during tumour progression: correlation with histopathological parameters, hormone receptors, and oncoproteins. J Pathol. 2001; 193(2):181–9. Epub 2001/02/17. https://doi.org/10.1002/1096-9896(2000)9999:9999<::AID-PATH752>3.0.CO;2-V PMID: 11180164.

42. Katoh D, Nagaharu K, Shimojo N, Hanamura N, Yamashita M, Kozuka Y, et al. Binding of alphavbeta1 and alphavbeta6 integrins to tenascin-C induces epithelial-mesenchymal transition-like change of breast cancer cells. Oncogenesis. 2013; 2:e65. Epub 2013/08/21. https://doi.org/10.1038/oncsis.2013.27 PMID: 23958855; PubMed Central PMCID: PMC3759126.

43. Nagaharu K, Zhang X, Yoshida T, Katoh D, Hanamura N, Kozuka Y, et al. Tenascin C induces epithelial-mesenchymal transition-like change accompanied by SRC activation and focal adhesion kinase phosphorylation in human breast cancer cells. Am J Pathol. 2011; 178(2):754–63. Epub 2011/02/02. https://doi.org/10.1016/j.ajpath.2010.10.015 PMID: 21281808; PubMed Central PMCID: PMC3069868.

44. Siebzehnrubl FA, Silver DJ, Tugertimur B, Deleyrolle LP, Siebzehnrubl D, Sarkisian MR, et al. The ZEB1 pathway links glioblastoma initiation, invasion and chemoresistance. EMBO Mol Med. 2013; 5 (8):1196–212. https://doi.org/10.1002/emmm.201302827 PMID: 23818228; PubMed Central PMCID: PMC3944461.

45. Saupe F, Schwenzer A, Jia Y, Gasser I, Spenle C, Langlois B, et al. Tenascin-C downregulates wnt inhibitor dickkopf-1, promoting tumorigenesis in a neuroendocrine tumor model. Cell Rep. 2013; 5 (2):482–92. Epub 2013/10/22. https://doi.org/10.1016/j.celrep.2013.09.014 PMID: 24139798.

46. Orend G, Huang W, Olayioye MA, Hynes NE, Chiquet-Ehrismann R. Tenascin-C blocks cell-cycle progression of anchorage-dependent fibroblasts on fibronectin through inhibition of syndecan-4. Oncogene. 2003; 22(25):3917–26. Epub 2003/06/19. https://doi.org/10.1038/sj.onc.1206618 PMID: 12813465.

47. Orend G. Potential oncogenic action of tenascin-C in tumorigenesis. Int J Biochem Cell Biol. 2005; 37 (5):1066–83. Epub 2005/03/04. https://doi.org/10.1016/j.biocel.2004.12.002 PMID: 15743679.

48. Marx J. Cancer research. Mutant stem cells may seed cancer. Science. 2003; 301(5638):1308–10. Epub 2003/09/06. https://doi.org/10.1126/science.301.5638.1308 PMID: 12958339.

49. Huang W, Chiquet-Ehrismann R, Moyano JV, Garcia-Pardo A, Orend G. Interference of tenascin-C with syndecan-4 binding to fibronectin blocks cell adhesion and stimulates tumor cell proliferation. Cancer Res. 2001; 61(23):8586–94. Epub 2001/12/04. PMID: 11731446.

50. Shi Z, Azuma A, Sampath D, Li YX, Huang P, Plunkett W. S-Phase arrest by nucleoside analogues and abrogation of survival without cell cycle progression by 7-hydroxystaurosporine. Cancer Res. 2001; 61 (3):1065–72. Epub 2001/02/28. PMID: 11221834.

51. Szymanska-Michalak A, Wawrzyniak D, Framski G, Stawinski J, Barciszewski J, Kraszewski A. New antiglioma zwitterionic pronucleotides with an FdUMP framework. Eur J Med Chem. 2018; 144:682–91. Epub 2018/01/01. https://doi.org/10.1016/j.ejmech.2017.12.070 PMID: 29289891.

52. Szymanska-Michalak A, Wawrzyniak D, Framski G, Kujda M, Zgola P, Stawinski J, et al. New 3'-O-aromatic acyl-5-fluoro-2'-deoxyuridine derivatives as potential anticancer agents. Eur J Med Chem. 2016; 115:41–52. Epub 2016/03/21. https://doi.org/10.1016/j.ejmech.2016.03.010 PMID: 26994842.

53. Ramnath N, Khushalani N, Toth K, Litwin AM, Intengan ME, Slocum HK, et al. S-phase modulation by irinotecan: pilot studies in advanced solid tumors. Cancer Chemother Pharmacol. 2005; 56(5):447–54. Epub 2005/06/11. https://doi.org/10.1007/s00280-004-0951-6 PMID: 15947933.

54. Sledz CA, Holko M, de Veer MJ, Silverman RH, Williams BR. Activation of the interferon system by short-interfering RNAs. Nat Cell Biol. 2003; 5(9):834–9. https://doi.org/10.1038/ncb1038 PMID: 12942087.

55. Bridge AJ, Pebernard S, Ducraux A, Nicoulaz AL, Iggo R. Induction of an interferon response by RNAi vectors in mammalian cells. Nat Genet. 2003; 34(3):263–4. https://doi.org/10.1038/ng1173 PMID: 12796781.

56. Jackson AL, Burchard J, Schelter J, Chau BN, Cleary M, Lim L, et al. Widespread siRNA "off-target" transcript silencing mediated by seed region sequence complementarity. RNA. 2006; 12(7):1179–87. https://doi.org/10.1261/rna.25706 PMID: 16682560; PubMed Central PMCID: PMC1484447.

57. Xia S, Lal B, Tung B, Wang S, Goodwin CR, Laterra J. Tumor microenvironment tenascin-C promotes glioblastoma invasion and negatively regulates tumor proliferation. Neuro Oncol. 2016; 18(4):507–17. https://doi.org/10.1093/neuonc/nov171 PMID: 26320116; PubMed Central PMCID: PMC4799677.

58. Liot S, Aubert A, Hervieu V, Kholti NE, Schalkwijk J, Verrier B, et al. Loss of Tenascin-X expression during tumor progression: A new pan-cancer marker. Matrix Biology Plus. 2020; 6–7:100021. https://doi.org/10.1016/j.mbplus.2020.100021.

59. Orend G, Chiquet-Ehrismann R. Tenascin-C induced signaling in cancer. Cancer Lett. 2006; 244 (2):143–63. https://doi.org/10.1016/j.canlet.2006.02.017 PMID: 16632194.

60. Matsumoto K, Takahashi K, Yoshiki A, Kusakabe M, Ariga H. Invasion of melanoma in double knockout mice lacking tenascin-X and tenascin-C. Jpn J Cancer Res. 2002; 93(9):968–75. Epub 2002/10/03. https://doi.org/10.1111/j.1349-7006.2002.tb02472.x PMID: 12359049; PubMed Central PMCID: PMC5927135.

61. Zukiel R, Nowak S, Wyszko E, Rolle K, Gawronska I, Barciszewska MZ, et al. Suppression of human brain tumor with interference RNA specific for tenascin-C. Cancer Biol Ther. 2006; 5(8):1002–7. https://doi.org/10.4161/cbt.5.8.2886 PMID: 16775434.

62. Fish RJ, Kruithof EK. Short-term cytotoxic effects and long-term instability of RNAi delivered using lentiviral vectors. BMC Mol Biol. 2004; 5:9. https://doi.org/10.1186/1471-2199-5-9 PMID: 15291968; PubMed Central PMCID: PMC514603.

63. Wnorowski A, Sadowska M, Paul RK, Singh NS, Boguszewska-Czubara A, Jimenez L, et al. Activation of beta2-adrenergic receptor by (R,R')-4'-methoxy-1-naphthylfenoterol inhibits proliferation and motility of melanoma cells. Cell Signal. 2015; 27(5):997–1007. https://doi.org/10.1016/j.cellsig.2015.02.012 PMID: 25703025; PubMed Central PMCID: PMC4361792.

64. Tang Z, Li C, Kang B, Gao G, Li C, Zhang Z. GEPIA: a web server for cancer and normal gene expression profiling and interactive analyses. Nucleic Acids Res. 2017; 45(W1):W98–W102. Epub 2017/04/14. https://doi.org/10.1093/nar/gkx247 PMID: 28407145; PubMed Central PMCID: PMC5570223.

65. Antonov AV, Krestyaninova M, Knight RA, Rodchenkov I, Melino G, Barlev NA. PPISURV: a novel bioinformatics tool for uncovering the hidden role of specific genes in cancer survival outcome. Oncogene. 2014; 33(13):1621–8. https://doi.org/10.1038/onc.2013.119 PMID: 23686313.

66. Cerami E, Gao J, Dogrusoz U, Gross BE, Sumer SO, Aksoy BA, et al. The cBio cancer genomics portal: an open platform for exploring multidimensional cancer genomics data. Cancer Discov. 2012; 2(5):401–4. https://doi.org/10.1158/2159-8290.CD-12-0095 PMID: 22588877; PubMed Central PMCID: PMC3956037.

67. Gao J, Aksoy BA, Dogrusoz U, Dresdner G, Gross B, Sumer SO, et al. Integrative analysis of complex cancer genomics and clinical profiles using the cBioPortal. Sci Signal. 2013; 6(269):pl1. https://doi.org/10.1126/scisignal.2004088 PMID: 23550210; PubMed Central PMCID: PMC4160307.

68. Altschul SF, Madden TL, Schaffer AA, Zhang J, Zhang Z, Miller W, et al. Gapped BLAST and PSI-BLAST: a new generation of protein database search programs. Nucleic Acids Res. 1997; 25 (17):3389–402. https://doi.org/10.1093/nar/25.17.3389 PMID: 9254694; PubMed Central PMCID: PMC146917.

SUPPLEMENTARY MATERIALS
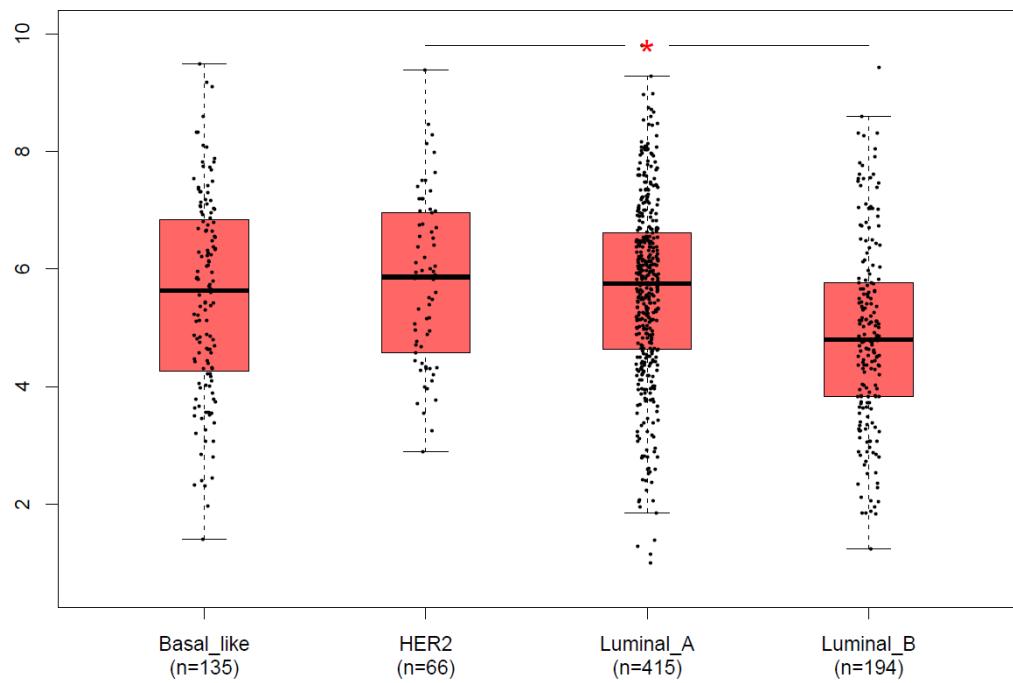
Figure A. Messenger RNA level of TNC (tenascin-C) gene in 4 subtypes of invasive carcinoma of the breast (N = 810 samples). RNA sequencing data were retrieved from the database of BRCA-TCGA and analysed using the GEPIA (Gene Expression Profiling Interactive Analysis) online web server (http://gepia.cancer-pku.cn/).

Grabowska M, Grześkowiak BF, Szutkowski K,
Wawrzyniak D, Głodowicz P, Barciszewski J, Jurga S,
Rolle K, Mrówczyński R.

Nano-mediated delivery of double-stranded RNA for gene therapy of glioblastoma multiforme

Nano-mediated delivery of double-stranded RNA for gene therapy of glioblastoma multiforme

Małgorzata Grabowska[1], Bartosz F. Grześkowiak[2], Kosma Szutkowski[2], Dariusz Wawrzyniak[1], Paweł Głodowicz[1], Jan Barciszewski[3], Stefan Jurga[2], Katarzyna Rolle[1,4]*, Radosław Mrówczyński[2]*

1 Department of Molecular Neurooncology, Institute of Bioorganic Chemistry Polish Academy of Science, Poznan, Poland, 2 NanoBioMedical Centre, Adam Mickiewicz University in Poznan, Poznan, Poland, 3 Department of Epigenetics, Institute of Bioorganic Chemistry Polish Academy of Science, Poznan, Poland, 4 Centre for Advanced Technologies, Poznan, Poland

* radoslaw.mrowczynski@amu.edu.pl (RM); kbug@man.poznan.pl (KR)

Abstract

Glioblastoma multiforme (GBM) is the most common type of malignant gliomas, characterized by genetic instability, intratumoral histopathological variability and unpredictable clinical behavior. Disappointing results in the treatment of gliomas with surgery, radiation and chemotherapy have fueled a search for new therapeutic targets and treatment modalities. Here we report new approach towards RNA interference therapy of glioblastoma multiforme based on the magnetic nanoparticles delivery of the double-stranded RNA (dsRNA) with homological sequences to mRNA of tenascin-C (TN-C), named ATN-RNA. The obtained nanocomposite consisted of polyethyleneimine (PEI) coated magnetic nanoparticles conjugated to the dsRNA show high efficiency in ATN-RNA delivery, resulting not only in significant TN-C expression level suppressesion, but also impairing the tumor cells migration. Moreover, synthesized nanomaterials show high contrast properties in magnetic resonance imaging (MRI) and low cytotoxicity combining with lack of induction of interferon response. We believe that the present work is a successful combination of effective, functional, non-immunostimulatory dsRNA delivery system based on magnetic nanoparticles with high potential for further application in GBM therapy.

Introduction

Although accounting for less than 2% of adult cancers, gliomas are the most common form of malignant primary brain tumor in adults.[1] Glioblastoma multiforme constitutes 25% of all malignant nervous system tumors and the median overall survival remains around 12–15 months, even after combination treatments of cytoreductive surgical resection, radiotherapy, and adjuvant oral chemotherapy with temozolomide[2,3,4,5] The recent medical treatment strategies have been progressing toward individualized therapy and many targeted drugs have

been investigated, but the identification of molecular biomarkers in GBM as well as the novel drugs delivery strategies are still of considerable therapeutic importance.

Among recently developed new methods towards GBM treatment, a lot of attention has been drawn to gene therapy.[6,7,8] One of the strategy is RNA interference (RNAi), a general term referring to post-transcriptional gene silencing mediated by either degradation or translation arrest of target RNA. RNAi is triggered by gene silencing mechanism that is initiated with the introduction of dsRNA into a cell.[9] Specifically designed RNAi molecules can target mRNAs and initiate their degradation. We have previously reported that dsRNA synthesized by *in vitro* method can cleave the targeted mRNA and silenced the gene of interest expression. [10,11] We used double-stranded 164 nucleotides long double stranded RNA specific for tenascin-C (TN-C) mRNA. That agent, called ATN-RNA, induces RNAi pathway to degradation of TN-C, the extracellular matrix (ECM) protein which is highly overexpressed in brain tumor tissue. The technology was coined interference RNA intervention (iRNAi). With the approach ATN-RNA was administrated locally into the tumor's cavity during standard neurosurgical procedures. Although the obtained clinical outcome from the experimental therapy has been found as the very promising, resulting with the improving of the quality of patients life, as well as the increasing of the overall survival, we are still far from the conclusion that the used approach can be the most effective GBM treatment. Lack of an effective delivery method for dsRNA and the instability of the nucleic acids during and/or after the delivery are still the major difficulties in gene silencing studies.

In the last decade, nanotechnology has been widely applied in synthesis of nanoscale materials with main focus on cancer therapy.[12,13,14] Especially a lot of work has been put on the development of new, multifunctional delivery systems which could overcome drawbacks of conventional treatment methods and improve existing therapies by selective enrichment of active substances in diseased tissue structures, an increase in bioavailability, the decrease of the active substance degradation and, above all, the reduction and/or avoidance of unwanted side effects.[15,16] Magnetic nanoparticles, mostly based on magnetite (Mag) have drawn so much considerable attention in the field of smart materials due to their unique advantages over other materials.[17,18] They are easy to produce and the synthesis cost is relatively small in comparison to other nanomaterials.[19] Moreover, they are physically and chemically stable, biocompatible and environmentally friendly. Therefore, they have been frequently used in gene therapy as non-viral gene carriers.[20] Another important point in the application of magnetic nanoparticles is the fact that they can be employed as contrast agents in MRI (Magnetic Resonance Imaging) what makes them a very powerful diagnostic tool.[21] Indeed, the magnetic nanoparticles have been successfully applied also in MRI of a brain tumor as well as in magnetic hyperthermia resulting in reducing of brain tumor mass.[22,23] Recently, they have been also used in gene therapy for delivery of siRNA against survivin but reported results showed moderate mortality of the cells.[24]

In the paper, we demonstrate application of magnetic nanoparticles as a multifunctional carrier for a double-stranded RNA with contrast properties in MRI. We used a previously reported ATN-RNA sequence shown to significantly reduce the expression level of TN-C. The conjugation of nanoparticles with ATN-RNA showed the more effective TN-C downregulation followed by the substantial impairment of the migration properties of cancer cells regarding the routinely used transfection agent. Furthermore, obtained nanocomposites and their complexes with ATN-RNA did not show the toxic properties and consequently, they do not stimulate the interferon induction and innate immune response. Therefore, our results shed new light on application of multifunctional magnetic nanoparticles in gene therapy of GBM utilizing RNAi approach and point promising candidate for further studies.

Materials and methods

All reagents and solvents were of reagent-grade quality. For all experiments, Milli-Q deionized water (resistivity 18 M$\Omega \times$cm^{-1}) was used.

Synthesis and labeling of Mag@PEI nanoparticles

Magnetic nanoparticles coated with PEI (Mag@PEI) were synthesized according to a previously reported protocol with small modifications. Briefly, FeCl$_3 \cdot$6H$_2$O (Sigma-Aldrich) (135 mg, 0.5 mmol) were mixed with FeCl$_2 \cdot$4H$_2$O (Sigma-Aldrich) (50 mg, 0.25 mmol) in water (5 mL) and degassed with N$_2$. The mixture was heated up to 80˚C followed by addition of 1 mL of working solution (0.5 g of 25-kDa branched polyethyleneimine (PEI-25$_{Br}$), 250 µL of Capstone FS-65 fluorosurfactant (Du Pont) and 2.5 mL of NH$_4$OH dissolved in 10 mL of Milli-Q water) and constant heating was maintained for 120 min. After cooling down the mixture of nanoparticles was washed with water (2 x 150 mL) and collected by an external magnet. Finally, the NPs were redispersed in 10 mL of water. The Mag@PEI concentration was determined spectrophotometrically in terms of the iron content in an aqueous suspension of the stock nanomaterial by complexation with 1,10-phenanthroline (Sigma-Aldrich) as described previously.[25]

Nanoparticles conjugated with fluorescent dye ATTO 550 were prepared as described elsewhere [26] Briefly, 2 mL of Mag@PEI nanoparticle suspension in water (2.25 mg Fe/mL) was mixed with 490 µL 0.1 M borate buffer, pH 8.5, and 10 µL solution of ATTO 550 NHS-ester (Sigma-Aldrich) in DMSO (10 mg/mL). The resulting suspension was incubated o/n at room temperature and dialyzed against water using Slide-A-Lyzer Dialysis Cassette G2 (Thermo Fisher Scientific) with a cut-off at 3500 MW.

Physical characterization

For transmission electron microscopy (TEM) a small amount of the sample was placed on a copper measuring grid (Formvar/Carbon 200 Mesh made by TedPella (USA)) after 5 minutes of sonication in deionized water. Then, the sample was dried in a vacuum desiccator for 24 hours. TEM images were recorded on a JEM-1400 microscope made by JEOL (Japan) at an accelerating voltage of 120 kV. The ImageJ software (Bethesda, MD, USA) was used to process TEM micrographs in order to analyze the size of nanoparticles. Magnetic measurements were performed on SQUID magnetometer at 5 K and 300 K. FT-IR spectra were recorded on Bruker Tensor 27 spectrometer in KBr pallets. Multiple light scattering (MLS) measurements were performed on Turbiscan Lab produced by Formulaction SA in 10 mL vials. Zeta (ζ) potential measurements were carried out using Zetasizer Nano-ZS ZEN 3600 produced by Malvern Instruments Ltd (UK). The experimental setup for magnetic resonance imaging studies consisted of an Agilent 9.4 T MRI preclinical scanner equipped with a 120 mm gradient coil (2 mT/m/A) and 30 mm millipede coil. In order to perform a quantitative T$_2$ relaxation experiment (at 18˚C) we employed MEMS protocol. Each echo is acquired after an excitation pulse with an increasing echo time. The parameters of the data acquisition were as follows: field of view 15 mm (FOV), matrix size 128 × 128, Gaussian-shaped pulse with 2048 µs length. The echo time was set to 4 and 10 ms in two separate experiments. In total, 16 consecutive images with varied echo time were acquired for each sample. The initial analysis was performed in VnmrJ 4.2 revision software (Santa Clara, CA, USA). The raw relaxation data points were collected from an average intensity obtained from circular Region of Interests (ROIs) and then analyzed using Origin 8.5 software (Origin Lab, Northampton, MA, USA) using simple single exponential decay function. In order to prepare MRI agarose-based phantom, nanoparticles were suspended in a hot 2% agarose solution. The hot solution was finally transferred to 10 mm plastic vials and left for full agarose gelation.

ATN-RNA preparation

ATN-RNA was synthesized *in vitro* as it has been already published.[11] ATN DNA harboring plasmid was cleaved by EcoRI and HindIII restriction enzymes (Promega). The two strands of RNA were transcribed separately with T3 and T7 RNA polymerases from MEGAscript Transcription Kits (Ambion). Hybridization of RNA was performed in a buffer containing 20 mM Tris-HCl, pH 7.5 and 50 mM NaCl. The reaction was carried out for 3 min at 95°C, 30 min at 75°C and at the end slowly cooled down to the room temperature.

Sequence of ATN-RNA (US Patent US 8,946.400 B2)

5' CAAGCGACAGAGUGGGGUGAACGCCACCCUGCCAGAAGAGAACCAGCCAGUGGUGUU UAACCACGUUUACAACAUCAAGCUGCCAGUGGGAUCCCAGUGUUCGGUGGAUCUGGAGUCA GCCAGUCCCCUCUUCUGGACCGGGCGGAAGUCUCGGGCGCU 3'

3' GUUCGCUGUCUCACCCCACUUGCGGUGGGACGGUCUUCUCUUGGUCGGUCACCACAA AUUGGUGCAAAUGUUGUAGUUCGACGGUCACCCUAGGGUCACAAGCCACCUAGACCUCAGU CGGUCACCCCUCUUCUGGACCGGGCGGAAGUCUCGGGCGCU 5'

Preparation of Mag@PEI/ATN-RNA complexes

The binding ability of ATN-RNA to Mag@PEI was performed by the gel retardation assay and UV-Vis spectrophotometry. To prepare Mag@PEI/ATN-RNA complexes, 1 μg of ATN-RNA was mixed with Mag@PEI with a series of Fe weight ratios (1, 2, 3, 4, 5, 8, 10 Mag@PEI to ATN-RNA wt:wt ratio) in the nuclease-free water, and incubated for 30 min at RT, allowing for sufficient binding of dsRNA molecules with the Mag@PEI. The Mag@PEI/ATN-RNA complexes were loaded onto 1% agarose gel for electrophoresis in TAE buffer at a constant voltage of 70 V for 30 min to visualize the ATN-RNA bands using a Digital Imaging and Analysis System II (Serva). SimplySafe fluorescent stain was used for detecting RNA in agarose gel. Meanwhile, the formed Mag@PEI/RNA complexes suspension was centrifuged (10000 rpm, 10 min) and the prepared supernatant was analyzed spectrophotometrically (NanoDrop 2000, Thermo Scientific) at A260 nm to reveal ATN-RNA content.

Cell culture

The study was performed on a human U-118 MG cell line (ATTC) derived from a glioblastoma multiforme. Adherent cell growth was carried out in a Dulbecco's Modified Eagle Medium (DMEM, Gibco) High Glucose supplemented with 10% fetal bovine serum (FBS, Sigma-Aldrich) and 1% penicillin-streptomycin antibiotic (Sigma-Aldrich). Cells were grown at 37°C in a 95% humidified chamber with 5% CO_2.

Transfection of GBM cells

ATN-RNA transfection was performed with Mag@PEI or Lipofectamine (Invitrogen) as a carrier. The procedure was carried out on the day-old cell culture seeded on 12 or 96-well plates in the supplemented medium. In a case of the 12-well plate, 150,000 cells were seeded in 1 mL of medium, for 96-well it was 10,000 cells in 200 μL. Once the cells have reached 75–90% confluency, the medium was removed, cells were washed with phosphate-buffered saline (PBS, Sigma-Aldrich) buffer and an unsupplemented culture medium in the amount reduced by the volume of the transfection mixture was added. Transfection complexes containing Mag@PEI nanoparticles were prepared by mixing Mag@PEI suspension (100 μg Fe/mL) with ATN-RNA solution (100 ng/μL) in serum and supplement-free DMEM with an iron-to-RNA ratio of 3:1 (w/w). The mixture was further incubated at RT for 30 min to allow the components to

assemble. After this time, the volumes of the prepared complexes corresponding to the proper ATN-RNA final concentration (10, 25, 50 and 100 nM) were transferred to the wells.

Lipofection was performed according to the manufacturer's recommendations. Two separate mixtures, OptiMEM (Gibco) with Lipofectamine and OptiMEM with ATN-RNA, were incubated for 5 min at the room temperature. After that, both solutions were combined. The prepared reaction mixture was incubated 20 min at the room temperature and then transferred to the appropriate wells. In addition, cells treated with Lipofectamine or Mag@PEI carriers only were used as controls.

Cellular uptake of transfection complexes

To track the magnetic complexes in the cell, ATN-RNA was fluorescently labelled with fluorescein, according to the manufacturer's protocol (Label IT Tracker Intracellular Nucleic Acid Localization Kits, Mirus Bio, USA). The final concentration of the fluorescein containing RNA was quantified on a spectrophotometer (NanoDrop 2000). The fluorescently labelled Mag@-PEI nanoparticles were then used to assemble complexes with fluorescently labelled ATN-RNA, as described in the previous section. U-118 cells (2.5×10^4 cells/well) were plated onto an 8-well Nunc Lab-Tek Chamber Slide (Thermo Fisher Scientific) and cultured for 24 h. Next, 50 μL of Mag@PEI/ATN-complexes (100 nM) was added and incubated with the cells at 37˚C for 24 h.

For visualization under a confocal microscope, the cells were fixed with 4% formaldehyde (Sigma-Aldrich) in phosphate-buffered saline (PBS) for 15 min. The cell membranes were stained with ConcanavalinA-FITC (Life Technologies) at a concentration of 50 μg/mL, the F-actin fibers were stained with Oregon Green 488 phalloidin (Molecular Probes) at a concentration of 165 nM and the cell nuclei were stained with Hoechst 33342 (Molecular Probes) at a concentration of 8 μM. Cells were imaged using a confocal laser scanning microscope (Olympus FV1000, Japan). Image acquisition and analysis were performed with a 60x objective, a 1.4 oil immersion lens and FV10-ASW software (Olympus). Images of the Mag@PEI were visualized using 559 nm excitation and 570–590 nm emission filters, whereas ATN-RNA was visualized using 488 nm excitation and 495–545 nm emission filters. To visualize the cell membranes or cytoskeleton, 488 nm excitation and 495–545 nm emission filters were applied. The Hoechst fluorescence was detected using 405 nm excitation source and 425–475 nm emission filters. The 3D-scan of the sample was performed using Z-stack mode measurements and analyzed with Imaris software (Bitplane).

Cytotoxicity assays

The WST-1 cell proliferation assay, as well as fluorescent cell viability assay, were carried out to assess the cytotoxicity of the nanoparticles and complexes with ATN-RNA.

In WST-1 assay (Takara), U-118 cells were seeded at the density of 10,000 cells per well in the 96-well plate. After 24 hours, medium containing an increasing concentration of tested Mag@PEI/ATN-RNA complexes (in terms of RNA concentration) was added to each well and the cells were incubated for 24 h. After incubation, 10 μL of the WST-1 Cell Proliferation Reagent was added to each well and incubated for 4 hours. After this time, the absorbance at 450 nm (reference wavelength 620 nm) was recorded against the background control, using a multiwell plate reader (Zenyth, Biochrom) and the cell viability was expressed as the respiration activity normalized to untreated cells.

In Live/Dead assay, the U-118 cells were seeded in black polystyrene 96-wells flat bottom plate with the transparent bottom (Greiner Bio-One GmbH) at densities of 10 000 cells per well. After 24 h, medium containing an increasing concentration of tested Mag@PEI/

ATN-RNA complexes (in terms of RNA concentration) was added to each well. Following 24 h exposure to the complexes, cells were incubated with 2 μM calcein AM (Thermo Fisher Scientific), 2 μM ethidium homodimer-1 (Thermo Fisher Scientific) and 8 μM Hoechst 33342 containing PBS (100 μL/well) during 30 minutes at 37˚C. Finally, the cells were analyzed with the IN Cell Analyzer 2000 (GE Healthcare Life Sciences, UK). Viable cells were imaged using the FITC/FITC excitation/emission filters while for the dead cells the TexasRed/TexasRed ex/em filter combination was applied. DAPI/DAPI was applied to detect the Hoechst 33342 blue signal. A minimum of 20 fields was imaged per well with a 20x magnification. Analysis of the collected images was performed with the IN Cell Developer Toolbox software (GE Healthcare Life Sciences, UK) using in-house developed protocol. First, the total cell number was retrieved from the DAPI images by means of defining and counting the nuclei. Subsequently, the number of viable cells from the FITC images and the number of dead cells from the TexasRed images were determined.

Nucleic acid extraction and quantification

Total RNA was extracted from cell lines with TRIZOL solution (Invitrogen) according to the Chomczynski's procedure.[27] Obtained RNA was purified from DNA residues with the DNA-free DNA Removal Kit (Ambion) following the manufacturer's instructions. The procedure was completed by examining the quantity and quality of the resulting RNA solution. The concentration was measured spectrophotometrically at a wavelength of λ = 260 nm by Nano-Drop 2000. The degree of possible material degradation was verified by an electrophoretic separation in the 1% agarose gel. Purified RNA was a template for complementary DNA (cDNA) synthesis. Reverse transcription was performed using 500 ng of material with the Transcriptor High Fidelity cDNA Synthesis Kit (Roche) according to the attached procedure.

qRT-PCR

The quantitative reverse transcriptase real-time PCR (qRT-PCR) was performed with the Light-Cycler480 using LightCycler480 Probes Master and Universal Probe Library (UPL) Set for Human (Roche). Primers with probes were designed by the Universal Probe Library Assay Design Center (https://qpcr.probefinder.com/organism.jsp). Primers sequences are given in Table 1. The efficiency of primers was estimated on the standard curve with series of 2-fold dilutions. The qRT-PCR proceeded under the following conditions: an initial 5 min preincubation at 95˚C, 45 cycles of denaturation in 95˚C for 10 sec, annealing at 55˚C for 30 sec and extension at 72˚C for 10 sec. Hypoxanthine phosphoribosyltransferase (HPRT) was used as the endogenous control. The LightCycler480 Software release 1.5.1.62 allowed for an analysis basing on the E-method (Roche) expression level. All experiments were performed in triplicates.

Western blot analysis

Transfected cells were lysed by sonication. 150 μg and 10 μg of denaturated protein extracts were separated on 12% and 15% SDS-PAGE (SDS-polyacrylamide gel electrophoresis) for tenascin-C and glyceraldehyde 3-phosphate dehydrogenase (GAPDH) detection respectively. Spectra Multicolor Broad Range Protein Ladder (Thermo Fisher Scientific) was used as the size marker. Subsequently the wet transfer onto PVDF membrane with 0.45 μm pore size (GE Healthcare) was performed in transfer buffer (25 mM Tris base, 190 mM glycine, 20% methanol). The membranes were placed in the SNAP i.d. 2.0 apparatus (EMD Milipore), where it was blocked with a 0.5% solution of skimmed milk in PBS. For detection of tenascin-C the TNC polyclonal antibody (H-300, Santa Cruz) was used, while GAPDH was detected using monoclonal antibody (0411, Santa Cruz). Antibodies were diluted 1:500 in 3% BSA (Sigma-

Table 1. Primer sequences for qRT-PCR.

Primer Sequence 5' → 3'	UPL
RIG1_L GGCAAGTCCCGCTGTAAAC	42
RIG1_R TTGGTATCTCCTAATCGCAAAAG	
OAS1_L CATCCGCCTAGTCAAGCACT	87
OAS1_R CAGGAGCTCCAGGGCATAC	
OAS3_L TCCCATCAAAGTGATCAAGGT	41
OAS3_R ACGAGGTCGGCATCTGAG	
TLR3_L TGGATATCTTTGCCAATTCATCT	80
TLR3_R ATCTTCCAATTGCGTGAAAAC	
INTγ_L GGCATTTTGAAGAATTGGAAAG	21
INTγ_R TTTGGATGCTCTGGTCATCTT	
GPX_L CAACCAGTTTGGGCATCAG	77
GPX_R TCTCGAAGAGCATGAAGTTGG	
TNC_L CCGGACCAAAACCATCAGT	76
TNC_R GGGATTAATGTCGGAAATGGT	
HPRT_L TGACCTTGATTTATTTTGCATACC	73
HPRT_R CGAGCAAGACGTTCAGTCCT	

https://doi.org/10.1371/journal.pone.0213852.t001

Aldrich). Membranes were incubated with the primary antibody for 10 min or overnight,. Afterwards, secondary anti-rabbit IgG and anti-mouse IgG antibodies conjugated with horseradish peroxidase (HRP) (Sigma-Aldrich) were used. Detection of a protein was carried out with WesternBright Sirius Chemiluminescent Detection Kit (Advansta). Intensity of individual bands was analyzed qualitatively by Multi Gauge ver. 2.0 (Fujifilm).

Cell proliferation and migration assays

Real-time cell proliferation and migration were monitored by measuring changes in electrical impedance using xCELLigence RTCA DP system (ACEA Biosciences). In the first step, the background impedance of a culture medium in plates was measured. In proliferation experiments, the 16-well plate with incorporated sensor electrode arrays (E-plate) were seeded with 10,000 cells per well in a final volume of 200 μL of medium. Next, the impedance was measured at 15-minute intervals for 72 h. The transfection was performed 24 h after cell seeding. For migration assays, the 16-well plate consisting of two chambers with a microporous polyethylene terephthalate (PET) membrane containing microfabricated gold electrode arrays on the bottom side of the membrane between them (CIM-plate) was used. 10,000 cells per well were seeded in an upper chamber in unsupplemented medium and moved towards a bottom chamber filled with supplemented medium. The impedance was measured at 15-minute intervals for 96 h. The seeded cells were transfected 24 h before experiment. Obtained cell index (CI) values were entered to the GraphPad Prism ver. 5.1 (GraphPad Software, Inc., La Jolla, CA, USA) software and used to calculate half maximal inhibitory concentrations (IC_{50}) of effecting cell proliferation. In case of transwell migration assay, obtained CI values from each experimental condition were plotted against time, fitted to four-parameter logistic non-linear regression model and the half-time of migration (half maximal effective time, ET_{50}) was calculated.

Scratch assay

Cell migration scratch assay was performed on 12-well plate, with 200,000 cells per well seeded in a supplemented medium. Cells were grown for 24 h under optimal growth conditions.

Next, the transfection was performed and the plate was incubated for another 24 h. After this time the medium was replaced and "wound" was created in the monolayer of cells covering the well. The scar effect was obtained by scraping cells in a straight line using a 200 µL tip. From that moment, images of the cultured cells at 12 h intervals were taken for 48 h using a fluorescence microscope at 5x magnification. The analysis of the degree of scarring of individual "wounds" was carried out by computer using the Tscratch program (CSElab).

Statistical analysis

Experimental results were subjected to statistical evaluation using GraphPad Prism ver. 5.1. Values presented are an average of three biological along with three technical replicates as mean values ± standard error of the mean (SEM). Differences between mean values of tested samples and controls were compared with the analysis of variance (ANOVA) extended by Tukey or Bonferroni post-hoc tests. Statistically significant results were obtained at the level of: * for $p < 0.05$; ** for $p < 0.01$; *** for $p < 0.001$; no statistical significance for $p \geq 0.05$.

Results and discussion

Synthesis and characterization of nanoparticles

In the first step (Fig 1), the PEI coated magnetic nanoparticles (Mag@PEI) were prepared in a straightforward manner *via* previously reported procedure in one step protocol from iron III and II chlorides in the molar ratio 2:1 in the presence of polyethyleneimine and surfactant.[25]

The morphology of obtained nanocomposites was investigated by means of TEM. The particles were spherical in shape, however, some aggregations were observed (Fig 2A). The obtained average size of magnetic nanomaterials ranged between 8 to 12 nm. In order to confirm the successful coating with PEI, the FT-IR spectrum was recorded. The spectrum showed a peak at 585 cm^{-1} which was assigned Fe-O bond. Characteristic signals at 1080 cm^{-1} and 1330cm^{-1} were attributed to C-N stretching vibration from the PEI. The peak observed at 1575cm^{-1} corresponds to N-H bending vibration from amine moieties present in polyethylenimine structure. Moreover, the signals from CH_2 groups were observed at 2820 cm^{-1} and 2950 cm^{-1}, respectively. Thus, FT-IR proved attachment of PEI at the surface of magnetic nanoparticles (Fig 2B).

Since PEI molecules bound to magnetite nanoparticles by electrostatic interaction and the negative charge on the surface of the particles is converted to positive charge, zeta potential of Mag@PEI NPs was measured. Performed studies revealed that zeta potential of Mag@PEI NPs was +40.6 mV what indicated the high colloidal stability of nanocomposites and additionally confirmed successful functionalization of magnetic nanoparticles (Fig 2D). Encouraged by the results obtained from zeta potential measurement we also investigated the colloidal stability of Mag@PEI NPs in real-time by Multiple Light Scattering (MLS) using Turbiscan apparatus.

This technique provides the information about TSI global index which is a sum of all destabilization processes occurring in the sample. However, one needs to take into account that the lower the TSI index, the more stable the sample. The investigation of kinetic destabilization for Mag@PEI NPs in water was monitored over a period of 24 h. The TSI index changed over time from 0.6 to 6.8 for 4 h and 24 h, respectively, what proved that the Mag@PEI NPs had high colloidal stability and sedimentation process occurred only in small extent (Figure A in S1 File). The magnetic properties of obtained materials were measured by means of SQUID. The sample exhibited superparamagnetic behavior, as evidenced by the lack of hysteresis loop and blocking temperature of 155 K. Obtained nanomaterial had high magnetic saturation above 40 emu/g at 300 K, which is important for its further guidance by external magnetic
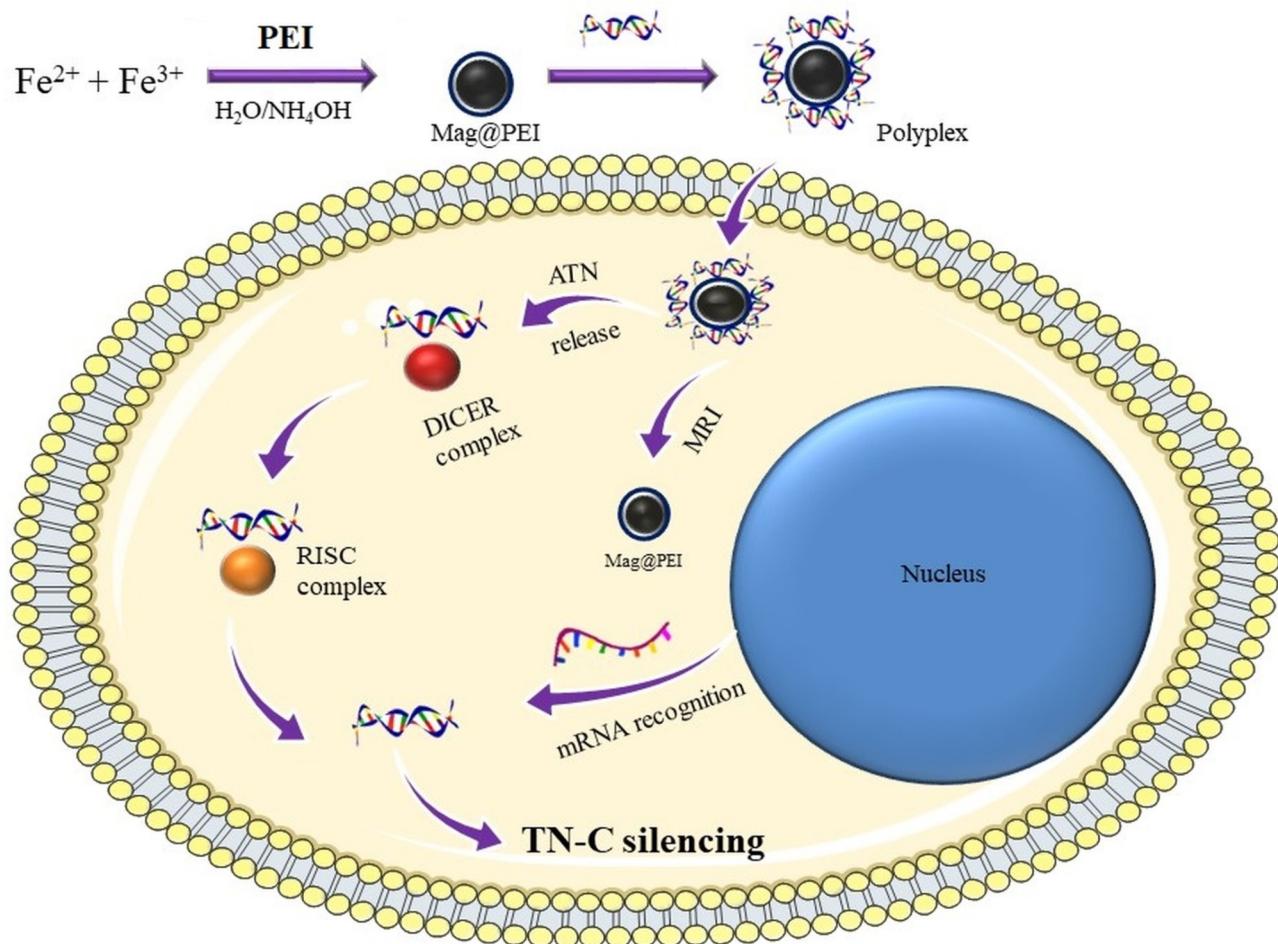
Fig 1. Schematic diagram of preparation of Mag@PEI /ATN-RNA complexes and its application in RNAi therapy of GBM cells.

field and during magnetic separation. Moreover, the sample was easy handled by an external magnet (Fig 2C).

Furthermore, contrast properties of synthesized magnetic nanocarriers and their potential application in magnetic resonance imaging were assessed. In order to avoid drift of magnetic nanomaterial in the high magnetic field, the suspensions of nanoparticles in an agarose gel (2 mg/mL) were prepared, according to recently reported protocol.[28] The spin echo (MEMS) imaging results obtained for Mag@PEI NPs are shown in Fig 3. The relaxivity value measured for our nanocarrier was as high as 225 $mM^{-1}s^{-1}$ proving high contrast properties of synthesized nanoparticles. Moreover, this value is much higher than the relaxivity values reported for commercial contrast agents based on magnetic nanoparticles like Feridex (120 $mM^{-1}s^{-1}$), Resovist (186 $mM^{-1}s^{-1}$) and Combidex (65 $mM^{-1}s^{-1}$).[29] Thus, our nanoparticles exhibited strong application potential in further MRI studies.

The characterized nanocarrier was further used to determine its binding capability towards ATN-RNA. In this experiment, ATN RNA was mixed with Mag@PEI NPs for 30 minutes at different weight ratios varied from 1:1 to 10:1. We expected that negatively charged ATN-RNA will interact with positively charged Mag@PEI NPs resulting in polyplexes formation. This type of structure is often postulated in literature when PEI is used as a carrier for nucleic acids
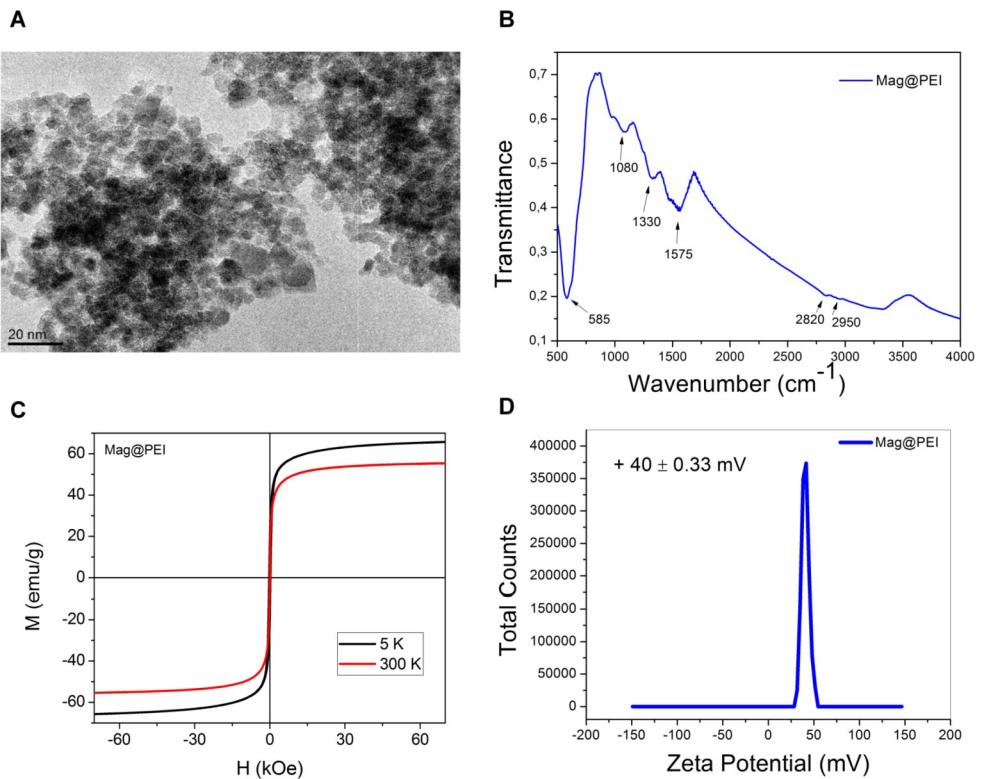
Fig 2. Characteristics of Mag@PEI. A. TEM picture of Mag@PEI NPs B. FTIR spectra of Mag@PEI NPs C. Hysteresis loop recorded for Mag@PEI NPs by means of SQUID D. Zeta potential of synthesized Mag@PEI NPs.

https://doi.org/10.1371/journal.pone.0213852.g002

delivery.[30] In the next step, obtained Mag@PEI/ATN-RNA complexes were submitted to agarose gel electrophoresis assay to visualize the linking of ATN-RNA to Mag@PEI NPs (Fig 4A). It is worth to highlight that the total amount of iron in the sample was first determined to
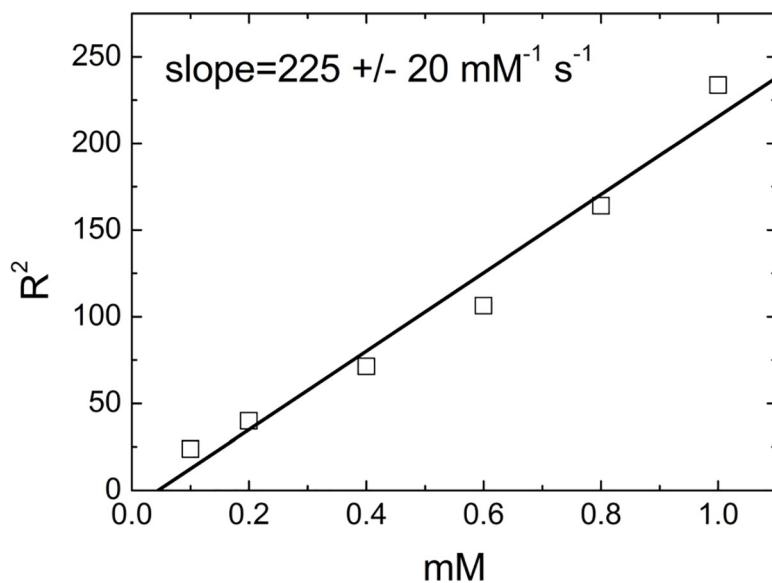
Fig 3. Contrast properties of Mag@PEI. Relaxation rates R^2 as well as relaxivity obtained from MRI experiment for Mag@PEI NPs in agarose gel 2 wt %.

https://doi.org/10.1371/journal.pone.0213852.g003
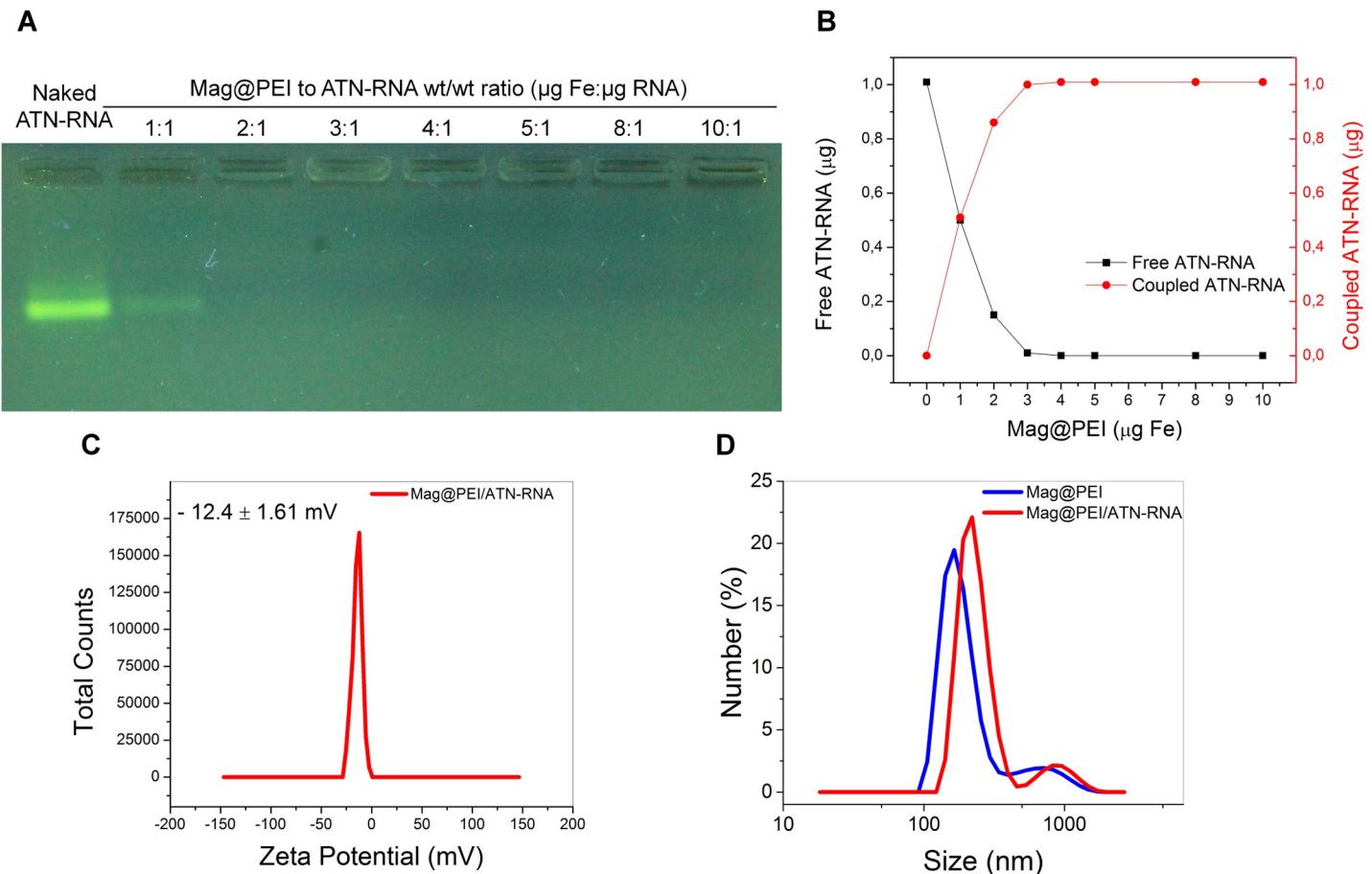
Fig 4. Binding of ATN-RNA to Mag@PEI NPs. A. Agarose gel electrophoresis of Mag@PEI/ATN-RNA complexes at the different mass ratio. B. Binding capability of Mag@PEI NPs towards ATN-RNA recorded using Nanodrop. C. Zeta potential of complexes obtained between Mag@PEI NPs and ATN-RNA at ratio 3:1. D. DLS size distribution for Mag@PEI NPs and Mag@PEI/ATN-RNA complexes at ratio 3:1.

https://doi.org/10.1371/journal.pone.0213852.g004

keep this value constant in order to repeat the experiments with different batches of nanoparticles which could slightly differ between each other. Analysis revealed that 2 weight equivalents were sufficient to bind almost all of the ATN-RNA used in the experiment. However, to get a deeper insight into this process, ATN-RNA concentration in the supernatant was investigated by UV-Vis spectroscopy. This technique has higher sensitivity than the gel electrophoresis. The data are presented in Fig 4B. UV-Vis experiments revealed that at Mag@PEI NPs to ATN-RNA ratio of 2:1, free ATN-RNA was still present in the supernatant and the loading was around 90%. However, at the ratio 3:1, the ATN-RNA was completely linked to Mag@PEI NPs. Furthermore, at this ratio, a change in zeta potential from +40 mV for Mag@PEI NPs to −12 mV for Mag@PEI/ATN-RNA complexes was observed (Fig 4C). This clearly proved that negatively charged ATN-RNA bind to the surfaces of Mag@PEI NPs.

The DLS measurements were performed to investigate the size of synthesized nanoparticles and prepared complexes in water. The Mag@PEI NPs had the hydrodynamic diameter of ~150 nm while the hydrodynamic diameter of Mag@PEI/ATN-RNA complexes increased slightly to around 200 nm after nucleic acid binding (Fig 4D).

The uptake of Mag@PEI/ATN-RNA complexes by U-118 cells was investigated by means of confocal microscopy. First, Mag@PEI nanoparticles were labelled with ATTO 550 dye. As illustrated in Fig 5, glioma cells could be successfully transfected with nanoparticles since the
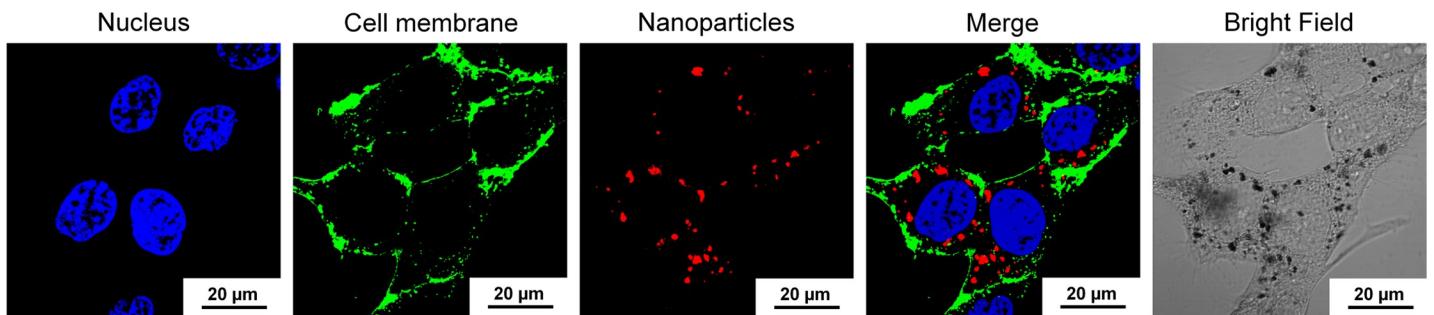
Fig 5. Cellular uptake of complexes containing fluorescently labelled Mag@PEI NPs into U-118 cells. The representatives of the colors are blue (Hoechst 33342) for nuclei, green (Concanavalin A-FITC) for cell membranes, and red (ATTO550) for Mag@PEI nanoparticles.

https://doi.org/10.1371/journal.pone.0213852.g005

red fluorescence from the dye was observed in the cytoplasm. Moreover, the analysis of the 3D reconstruction further confirmed their internalization capacity of obtained complexes. (S1 Video). The bright field images show the presence of black dots corresponding to the aggregated complexes containing fluorescently labelled Mag@PEI NPs.

A colocalization analysis was also performed to further demonstrate transfection of Mag@-PEI/ATN-RNA complexes into glioblastoma cells. As shown in Fig 6, there is a visible colocalization between the ATTO 550 labelled Mag@PEI nanoparticles (red color) and the FITC labelled ATN-RNA (green color) in the cytoplasm suggesting high transfection efficiency of the synthesized nanoparticles.

Cytotoxicity of magnetic nanocarierr and complexes with ATN-RNA

Cytotoxicity of both Mag@PEI NPs and polyplexes bearing ATN-RNA on GBM U-118 cells were determined by two cytotoxicity tests, namely WST-1 and LIVE/DEAD assays. In the first step, the toxicity of Mag@PEI NPs without bounded ATN-RNA at the concentrations of NPs corresponding to the concentrations used in further transfection experiments (Figure B in S1 File). Mag@PEI carrier did not cause any significant toxic effect in the investigated concentration range and the data from both tests were consistent. Also, SRB test did not show any
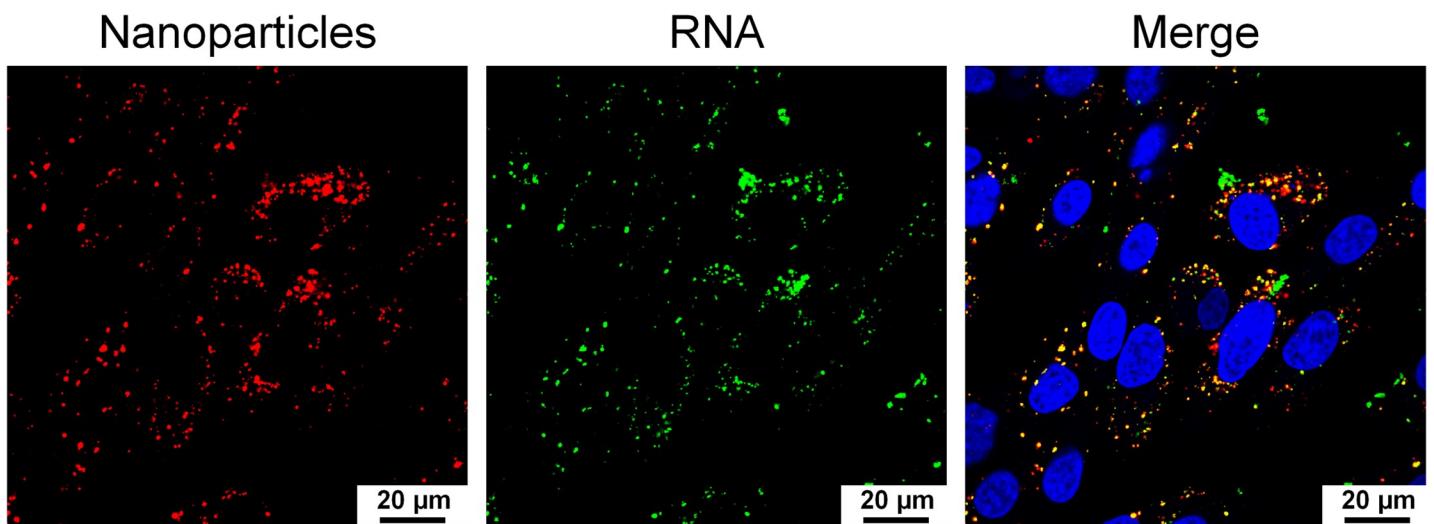

Fig 6. Colocalization of Mag@PEI NPs and ATN-RNA in U-118 cells. The representatives of the colours are blue (Hoechst 33342) for nuclei, green (FITC) for ATN-RNA, and red (ATTO550) for Mag@PEI nanoparticles.

https://doi.org/10.1371/journal.pone.0213852.g006
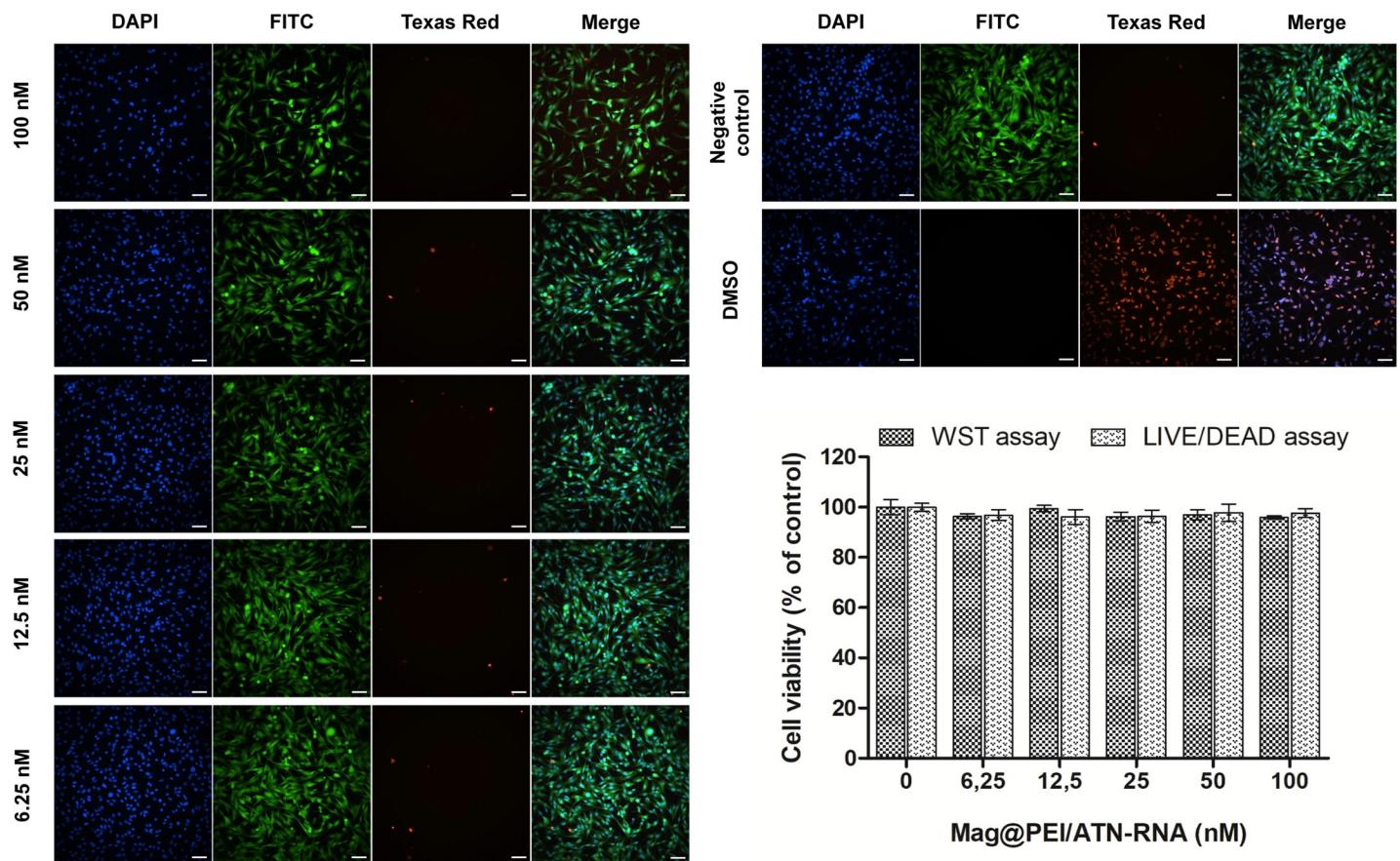
Fig 7. Representative high-content images of U-118 cells exposed to Mag@PEI/ATN-RNA complexes (6.25–100 nM). 10% DMSO was used as a positive control. Images were obtained using different filters to detect nuclei (DAPI), live cells (FITC), and dead cells (TexasRed). The scale bars denote 100 µm. Cell viability of U118 cells exposed to Mag@PEI/ATN-RNA complexes (6.25–100 nM) for 24 h. The value at X-axis in Fig 7 corresponds to concertation of free ATN-RNA on the carrier.

https://doi.org/10.1371/journal.pone.0213852.g007

toxicity of our carrier (Figure C in S1 File). Subsequently, we assessed the cytotoxicity of Mag@PEI/ATN-RNA complexes (Fig 7). To keep the same range of concentrations as previously used in RNAi approach [10], we used the ATN-RNA concentration between 10 to 100 nM. Both cytotoxicity assays revealed high viability of glioblastoma cells in the investigated concertation range. So we could exclude undesired side effects coming from the nanoparticles.

Immune response

Taking into account the possible use of nanoparticles as the therapeutic tool in GBM treatment, the analysis of expression level of the genes involved in innate immune response was performed. We examined whether our nanoparticles delivery system would elicit an innate immune response *in vitro*. Undesired immune responses are an important consideration in gene therapy and in the development of gene delivery systems because the introduction of exogenous genes can activate the innate immune system of human cells to combat foreign gene or pathogen invasion.[31] For example, siRNA can provoke an immune response *via* its interactions with Toll-like receptors (TLRs) and trigger an interferon (IFN) response.[32] Additionally, systemically introduced lipid nanoparticles have been reported to induce an immune response in mice.[33] Thus, the potential immunostimulatory properties of a proposed gene delivery system are important. We characterized U-118 GBM cells for their innate
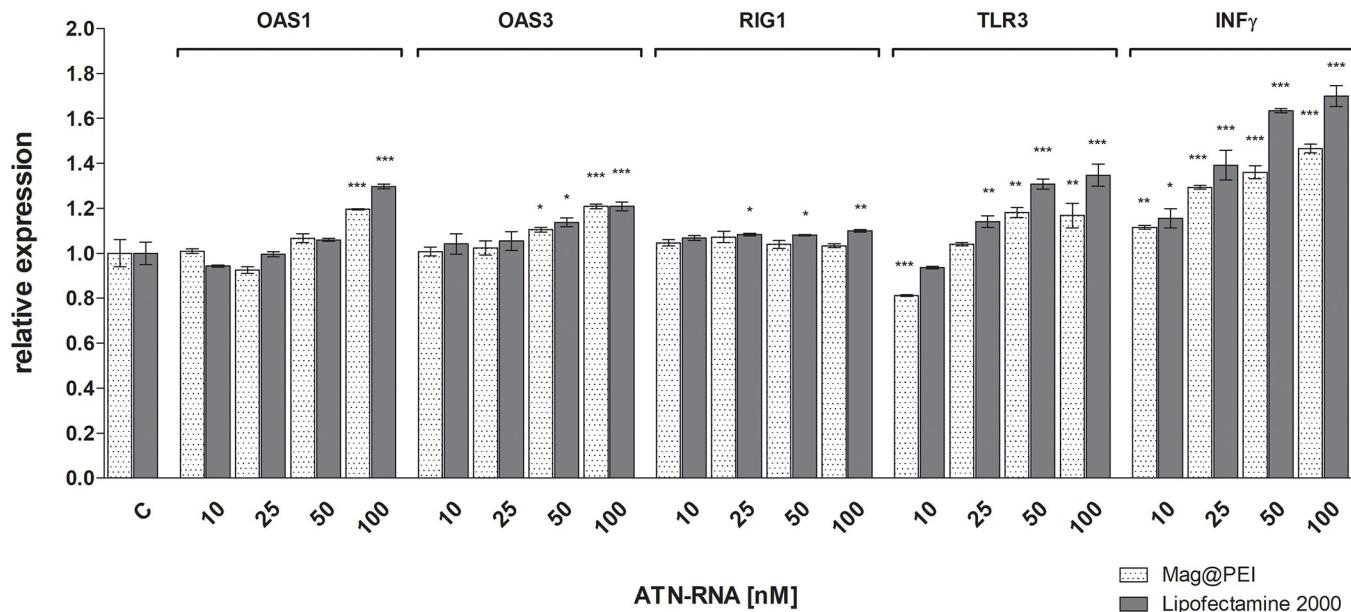
Fig 8. The expression level of immune response genes after lipo- and nano-mediated ATN-RNA delivery to U-118 cell line. The relative expression level of the expression of OAS1, OAS3, RIG1, INFγ and TLR3 established by qRT-PCR calculated wit the −ΔΔCp method. Statistical evaluation of ATN-RNA versus control (Clipo or Cnano, respectively) cells was performed using one-way ANOVA followed by Tukey's posthoc test. Significance value: * $p < 0.05$, ** $p < 0.01$, *** $p < 0.001$ compared to untreated cells (Clipo or Cnano, respectively). Legend: Mag@PEI- nano-mediated ATN-RNA delivery; Lipofectamine—lipo mediated ATN-RNA delivery.

https://doi.org/10.1371/journal.pone.0213852.g008

immune response to the nanoparticle complexes. We measured the expression of OAS1, OAS3, RIG1, TLR3 and INFγ using the qRT-PCR (Fig 8). The changes after ATN-RNA treatment were either not observed, as for the RIG1 gene or negligible, as for OAS3 gene. However, the highest concentration of ATN-RNA (50, 100 nM) caused the weak activation of interferon response of above mentioned genes, but this activation was slightly higher in case of lipofection when compared to magnetic nanocarrier—about 8% ($p < 0.01$ and $p < 0.005$, respectively). The higher activation of OAS 1 gene was measured both in case of lipofectamine and nanoparticles treatment, but it needs to be highlighted, that at 100nM ATN-RNA working concentration the expression level of that gene was about 30% higher for lipofection, what gives 10% increase in relation to the nanoparticles-mediated delivery ($p < 0.005$).

The highest activation with ATN-RNA both with lipofectamine and using Mag@PEI nanocarrier was observed for TLR3 and INFγ genes. The ATN-RNA delivered with lipofectamine caused the TLR3 gene expression activation at the level from 16% to 37%, starting from the 25 nM ATN-RNA concentration ($p < 0.005$). The Mag@PEI NPs used as the ATN-RNA carrier resulted in the lowest activation of the TLR3 gene expression with the observed 8–15% level, for 25–100 nM ATN-RNA concentrations ($p < 0.01$).

INFγ gene was significantly upregulated both by the lipofectamine and Mag@PEI NPs. However, with the same ATN-RNA concentration, the gene expression was elevated at the higher level by the lipofectamine-mediated ATN-RNA delivery. With the already lowest concentration, we observed 10–12% overexpression by the lipofection and Mag@PEI NPs ($p < 0.01$). However, starting from the 25 nM ATN-RNA concentrations we noticed the growing differences with the effect of lipofectamine versus Mag@PEI NPs. With this concentration, we observed the INFγ gene overexpression of about 27 and 42% for Mag@PEI NPs and lipofection, respectively. The highest concentrations caused –for 50 nM: 28 and 63%, for 100 nM: 44 and 75% in case of use of Mag@PEI NPs and lipofection, respectively.

RNA interference therapy

To achieve down-regulation of TN-C expression in U-118 glioblastoma cell line, lipofection along with Mag@PEI NPs with various concentration of ATN-RNA– 10, 25, 50 and 100 nM was performed. 24 hours after transfection the expression level of tenascin-C was examined by qRT-PCR analyses. The downregulation of TN-C mRNA expression was observed compared to controls treated with the transfection agent or with scrambled RNA. The level of TN-C was decreased from 2% at a concentration of 10 nM ATN-RNA to 34% for cells treated with 100 nM ATN-RNA in comparison to the untreated cells ($p < 0.005$) in case of samples where ATN-RNA was delivered with lipofectamine (Fig 9). At the same time, the above mentioned range of ATN-RNA concentration was delivered with Mag@PEI nanoparticles resulted in the significant drop of the TN-C expression level. The downregulation effect was visible already with the lowest concentration with the decrease at 20%. The highest concentrations: 25, 50 and 100 nM caused the TN-C downregulation about 43, 48 and 80%, respectively ($p < 0.005$) (Fig 9A).

The qRT-PCR analysis was also supported by the direct analysis of the protein expression level. The Western blot detection reveled again with the more significant drop of the TN-C expression caused by the nanoparticles-mediated ATN-RNA delivery. We observed already 40% decrease of the protein expression with the 10 nM ATN-RNA. The highest concentration used caused the dramatic drop of the protein expression measured as the 85% of the decrease. The lipofectamine mediated ATN-RNA delivery at the same time caused only about 40% decrease of the expression level with ATN-RNA concentrations 50 and 100 nM (Fig 9B). These observations were fully consistent with the obtained relative TN-C expression level measured by qRT-PCR.

These results clearly support the idea of nanoparticles mediated delivery in order to achieve the significant biological effect along with the lowest concentration of therapeutic agent. The Mag@PEI mediated ATN-RNA delivery was already efficient with the lowest- 10 nM concentration- 20% of TNC downregulation, while the lipofectamine at the same time was not able yet to deliver the RNA. During the whole experiment, we observed about 30–50% higher efficiency of nanomediated delivery compared to the lipofectamine-driven one.
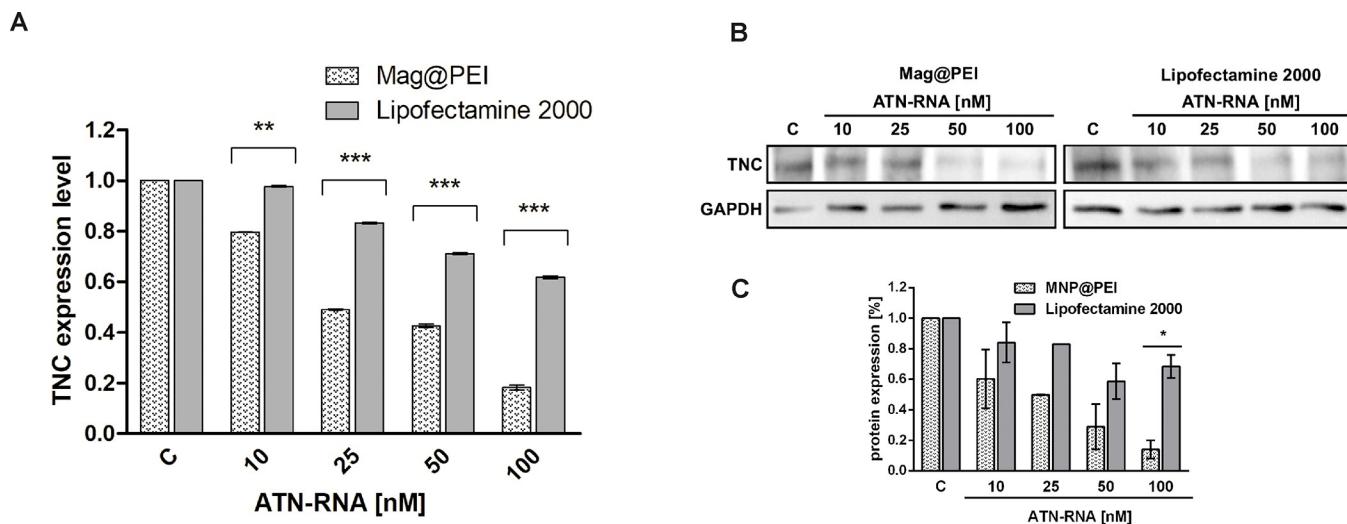

Fig 9. The expression level of TN-C after lipo- and nano-mediated ATN-RNA delivery to U-118 cell line. A. The relative expression level of the expression of TN-C established by qRT-PCR calculated with the ΔΔCp method. B. The protein expression level measured by Western blot with densitometric analysis (C.) Statistical evaluation of ATN-RNA versus control (Clipo or Cnano, respectively) cells was performed using one-way ANOVA followed by Tukey's posthoc test. Significance value: ** $p < 0.01$, *** $p < 0.001$. Legend: Mag@PEI- nano-mediated ATN-RNA delivery; Lipofectamine- lipo mediated ATN-RNA delivery.
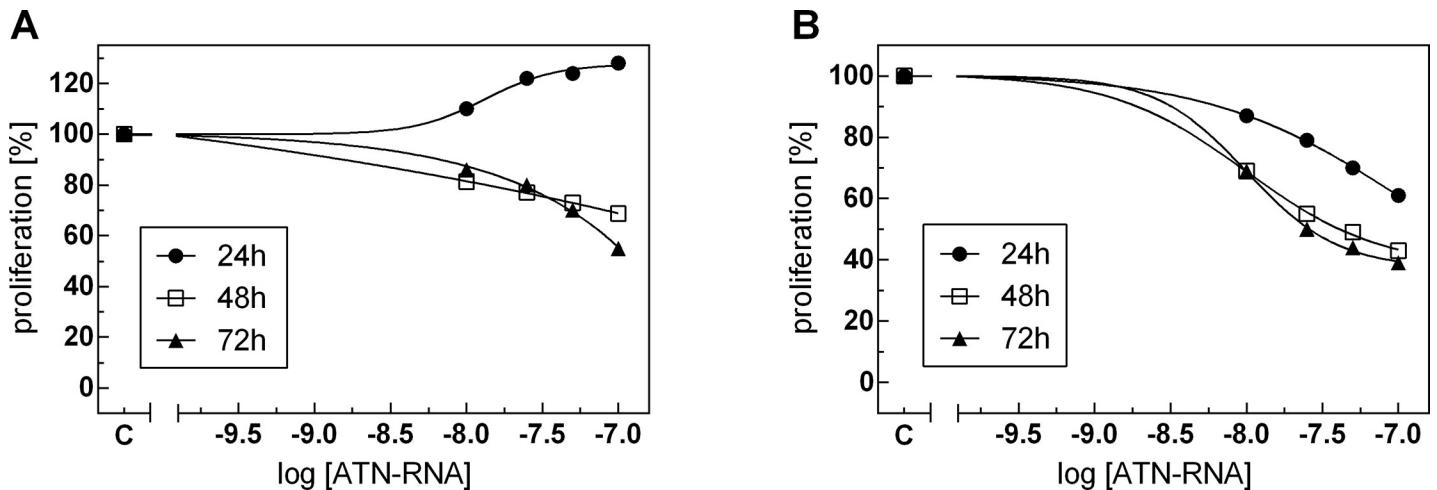
Fig 10. Anti-proliferative activity of ATN-RNA, after nano- (A) and lipo-mediated (B) delivery. Proliferation was monitored in real-time using the xCELLigence system. Differences between CI values for ATN-RNA treated and control cells were statistically evaluated using one-way ANOVA followed by Tukey's posthoc test. Dose-dependent effects of ATN-RNA on proliferation was evaluated using non-linear regression by fitting experimental values to sigmoidal, bell-shaped equation. Legend: Mag@PEI- nano-mediated ATN-RNA delivery; Lipofectamine—lipo mediated ATN-RNA delivery.

https://doi.org/10.1371/journal.pone.0213852.g010

Proliferation and migration of GBM cells

In order to investigate the delivery efficacy of the carriers, we measured the cells proliferation rate. U-118 glioblastoma cell line was treated with Mag@PEI NPs and Lipofectamine combined with ATN-RNA followed by the real-time cell proliferation assay with the xCELLigence system. The cell's ability for proliferation was measured for 72 h. We noticed ATN-RNA concentration-dependent decrease of proliferation rate both for Lipofectamine carrier with the significant decrease of proliferation with 100 nM–ATN-RNA concentration. The proliferation rate dropped for ATN-RNA delivered with the cationic carrier from 40–61% (Fig 10B). However, for Mag@PEI NPs we observed the opposite effect, resulting in the increase of proliferation- most effective concentration of ATN-RNA was 100 nM, with an increase from 10–28% after 24 h, respectively (Fig 10A). Noteworthy, 25 nM and 50 nM of ATN-RNA was already sufficient concentration for the efficient changes of GBM cells proliferation. After 48 and 72 h post transfection we observed again the inhibition of proliferation, from 7–45%, respectively. This allowed us to assume that the most effective delivery of ATN-RNA is achieved after first 24 h from transfection. We also would postulate that the significant drop of the proliferation rate both for Lipofectamine and for nanoparticles mediated delivery 48 and especially 72 h post transfection is more likely due to the simple death of the cells, rather than the ATN-RNA action.

To get more insight into the down-regulation of TN-C expression by ATN-RNA on the mobility of glioblastoma cancer cells, real-time measurements of migration was carried out. In this approach, U-118 cells were treated again with Mag@PEI NPs and Lipofectamine and ATN-RNA and allowed to migrate through microporous polyethylene terephthalate (PET) membrane towards chemoattractant. The number of cells that crossed the membrane was continuously recorded.

We found that down-regulation of TN-C expression by ATN-RNA delivered by Mag@PEI NPs significantly impaired the cell migration in GBM cells (Fig 11). The results were quantitatively assessed during 72 h of experiment and showed that U-118 cells transfected with ATN-RNA had the lowest motility beginning from 12 h post transfection. It was established that Mag@PEI NPs with ATN-RNA delayed the migration of U-118 cells by 5.76 ± 1.02,
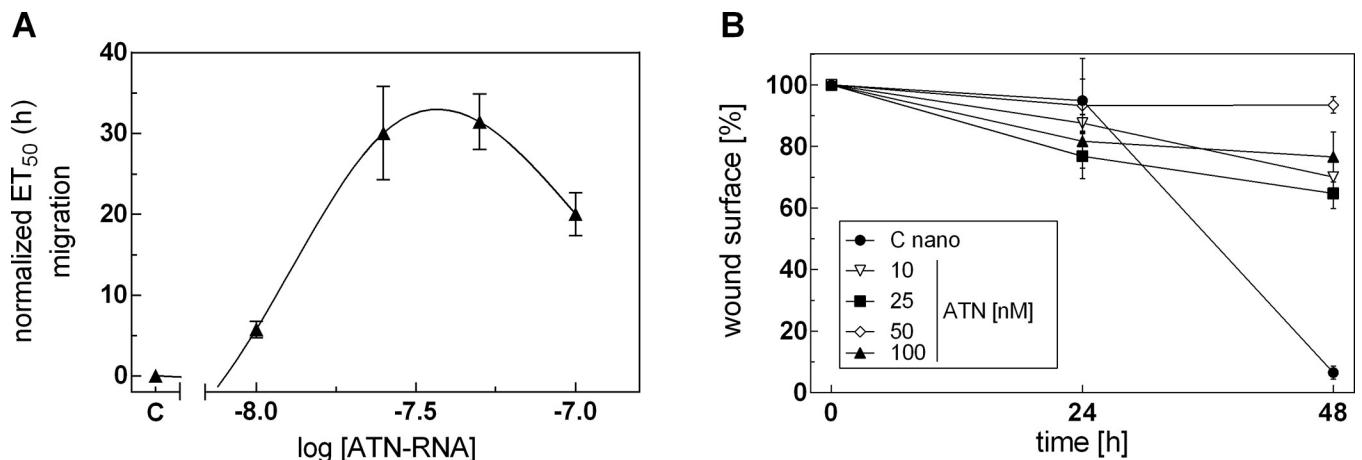
Fig 11. The effect of nano-mediated delivery of ATN-RNA on the migration processes. (A) Migration of U-118 GBM cancer cells was studied using the xCELLigence system. Serum-depleted cells were transfected with increasing concentrations of ATN-RNA (from 10 to 100 nM) or vehicle (Opti-MEM, C-control). Impedance (CI values) of each experimental condition was recorded over time, plotted against time, fitted to four-parameter logistic non-linear regression model and ET50 was calculated for each ATN-RNA concentration to generate dose-response curves. The ET50 value was normalized to the data obtained for cells treated with native Mag@PEI and plotted as normalized half maximal effective time (ET50) of cell migration against ATN-RNA concentrations. (B) The scratch assay analysis. U-118 GBM cells were transfected with Mag@PEI/ATN-RNA complexes. Images were captured after 24 and 48 h (Figure D in S1 File). The rate of migration was measured by quantifying the total distance that the U-118 cells moved from the edge of the scratch toward the centre of the scratch.

30.06 ± 5.78, 31.46 ± 3.41 and 20.03 ± 2.65 h with 10, 25, 50 and 100 nM concentration, respectively (Fig 11A). Notably, the most effective concentration influencing the migration potential of the cells is 50 nM, while 100 nM seems to cause the elevated cells death. One can notice the entirely different results observed for the ATN-RNA delivery driven by Lipofectamine. During the experiment, we were not able to detect the specific migration impairment, most probably due to the high toxicity of Lipofectamine. To get more insight into the problem, we performed also the scratch assay. Again, with the lipofectamine delivered ATN-RNA we were not able to quantify the existing wound since the transfection resulted in the cells death. Conversely, the results from nanoparticles-mediated ATN-RNA delivery in the wound-healing assay demonstrated that U-118 ATN-RNA treated cells migrate into the scratched area more slowly than the control cells- 18% after 24 and 24% after 48 h, respectively (Fig 11B).

Notably, the infection did not change substantially also the viability of the cells, what was observed in terms of lipofection (Figure D in S1 File) Thus, taking together the independent experiments proved the significant impairment of migration rate of the Mag@PEI/ATN-RNA treated U-118 cells, suggesting the therapeutic potential of the used nanocomposite. This extremely interesting observation could suggest either the gradual release of the dsRNA from the nanoparticles surface, resulting in the best effect already at the higher concentration or the highest stability of dsRNAs. At the same time, one can notice the significant migration impairment is already established with the 25 nM concentration. This could suggest that the nanoparticles-mediated delivery would use the lowest concentration of the therapeutic agent allowed for an efficient silencing of the tenascin-C. Observed migration delay as the results with the nanoparticles delivery is fully consistent with the tenascin-C expression level measured by qRT-PCR. The highest TN-C downregulation has functional consequences with the migration rate of U-118 glioblastoma cells.

Our functional studies with using both nano- and lipo- carriers showed the potential of nanoparticles with dsRNA delivery. ATN-RNA in our previous studies had a great impact on the migration and proliferation properties of cancer's cells resulted in the decrease of both of

these potentials. In the present study, however, we observed surprisingly the increase of the proliferation potential caused by the ATN-RNA delivery with nanoparticles. Since we observed the enhanced TN-C downregulation followed by the ATN-RNA delivery with nanoparticles, our results seem to be in concordance with the results in intracranial xenografts.[34]

The TN-C knockdown in the tumor microenvironment modulated the behavior of a tumor stromal cells, inhibited tumor invasion, and increased tumor cell proliferation. The combination of this phenotypic phenomenon is similar to the go-or-grow glioma growth phenotype found in human neoplasms, which represent characteristic, highly proliferative tumor cores and diffuse borders with a low proliferation rate.[34]

Conclusions

We have successfully demonstrated a new dsRNA delivery system that harnesses well- characterized magnetic nanoparticles coated with PEI to effectively silence expression of tenascin-C in glioblastoma multiforme cell line. Both mere nanoparticles and their complexes with dsRNA do not show toxicity and do not provoke undesired immune responses in U-118 GBM cell line. Additionally, we proved by confocal microscopy imaging, that they could be successfully internalized into glioblastoma cells. The most important thing is that synthesized nanocarrier was a more efficient tool in delivery ATN-RNA than routinely used Lipofectamine In consequence, the gene therapy employing ATN was improved resulting in stronger silencing of TN-C, followed by the further diminishing of migration of glioblastoma cells. Finally, since the magnetic core provided high contrast properties in MRI, therefore, synthesized nanocarrier system can be considered as the robust theranostic nanoplatforms for simultaneous gene therapy and imaging. The present approach is then the first demonstration of an effective and safe dsRNA delivery based on multifunctional nanoplatforms. The used technology is an evidence of a promising nanoparticles-based shuttle with a high potential for further clinical use in GBM treatment.

Supporting information

S1 File. (Figure A) Destabilization kinetic of Mag@PEI recorder by Turbiscan apparatus over 24 h, (Figure B) Representative high-content images of U-118 cells exposed to Mag@PEI nanoparticles at various concentrations. 10% DMSO was used as a positive control. Images were obtained using different filters to detect nuclei (DAPI), live cells (FITC), and dead cells (TexasRed). The scale bars denote 100 **μ**m. Cell viability of U118 cells exposed to Mag@PEI, (Figure C) Cytotoxicity SRB of Mag@PEI for various nanoparticles concertation, (Figure D) Schratch test.
(DOCX)

S1 Video. MNP@PEI_RNA_5well_3_3d.
(AVI)

Acknowledgments

Author Contributions

Conceptualization: Katarzyna Rolle, Radosław Mrówczyński.

Formal analysis: Dariusz Wawrzyniak.

Funding acquisition: Jan Barciszewski, Stefan Jurga.

Investigation: Małgorzata Grabowska, Bartosz F. Grześkowiak, Kosma Szutkowski, Paweł Głodowicz, Radosław Mrówczyński.

Methodology: Małgorzata Grabowska, Bartosz F. Grześkowiak, Katarzyna Rolle, Radosław Mrówczyński.

Project administration: Stefan Jurga, Radosław Mrówczyński.

Resources: Jan Barciszewski, Stefan Jurga, Katarzyna Rolle, Radosław Mrówczyński.

Supervision: Jan Barciszewski, Katarzyna Rolle, Radosław Mrówczyński.

Validation: Małgorzata Grabowska, Dariusz Wawrzyniak.

Visualization: Małgorzata Grabowska, Bartosz F. Grześkowiak, Dariusz Wawrzyniak, Katarzyna Rolle, Radosław Mrówczyński.

Writing – original draft: Małgorzata Grabowska, Bartosz F. Grześkowiak, Katarzyna Rolle, Radosław Mrówczyński.

Writing – review & editing: Bartosz F. Grześkowiak, Katarzyna Rolle, Radosław Mrówczyński.

References

1. Wen PY, Macdonald DR, Reardon DA, Cloughesy TF, Sorensen AG, Galanis E, et al. Updated Response Assessment Criteria for High-Grade Gliomas: Response Assessment in Neuro-Oncology Working Group. J. Clin. Oncol. 2010, 28, 1963–1972, https://doi.org/10.1200/JCO.2009.26.3541 PMID: 20231676

2. Stuplich M, Hadizadeh DR, Kuchelmeister K, Scorzin J, Filss C, Langen K J, et al. Late and prolonged pseudoprogression in glioblastoma after treatment with lomustine and temozolomide. J. Clin. Oncol. 2012, 30, https://doi.org/10.1200/JCO.2011.40.3188

3. Mrugala MM. Advances and challenges in the treatment of glioblastoma: a clinician's perspective. Discov. Med. 2013, 15, 221–30. PMID: 23636139

4. Kruser TJ, Mehta MP, Robins HI. Pseudoprogression after glioma therapy: A comprehensive review. Expert Rev. Neurother. 2013, 13, 389–403. https://doi.org/10.1586/ern.13.7 PMID: 23545054

5. Schonberg DL, Lubelski D, Miller TE, Rich JN. Brain tumor stem cells: Molecular characteristics and their impact on therapy. Mol. Aspects Med. 2013, 39, 82–101. https://doi.org/10.1016/j.mam.2013.06.004 PMID: 23831316

6. Lozada-Delgado EL, Grafals-Ruiz N, Vivas-Mejía PE. RNA interference for glioblastoma therapy: Innovation ladder from the bench to clinical trials. Life Sci. 2017, 188, 26–36, https://doi.org/10.1016/j.lfs.2017.08.027 PMID: 28864225

7. Aigner A, Kögel D. Nanoparticle/siRNA-based therapy strategies in glioma: which nanoparticles, which siRNAs? Nanomedicine 2017, 13, 89–103, https://doi.org/10.2217/nnm-2017-0230 PMID: 29199893

8. Mansoori B, Sandoghchian Shotorbani S, Baradaran B. RNA Interference and its Role in Cancer Therapy. Adv. Pharm. Bull. 2014, 4, 313–321, https://doi.org/10.5681/apb.2014.046 PMID: 25436185

9. Mathupala SP, Guthikonda M, Sloan AE RNAi Based Approaches to the Treatment of Malignant Glioma. Technol. Cancer Res. Treat. 2006, 5, 261–269, https://doi.org/10.1177/153303460600500313 PMID: 16700622

10. Rolle K, Nowak S, Wyszko E, Nowak M, Zukiel R, Piestrzeniewicz et al. Promising human brain tumors therapy with interference RNA intervention (iRNAi). Cancer Biol. Ther. 2010, 9, 396–406, https://doi.org/10.4161/cbt.9.5.10958 PMID: 20118657

11. Zukiel R, Nowak S, Wyszko E, Rolle K, Gawronska I, Barciszewskaet al. Suppression of human brain tumor with interference RNA specific for tenascin-C. Cancer Biol. Ther. 2006, 5, 1002–1007, https://doi.org/10.4161/cbt.5.8.2886 PMID: 16775434

12. Jin G, Zhao X, Xu F. Therapeutic nanomaterials for cancer therapy and tissue regeneration. Drug Discov. Today 2017, 22, 1285–1287, https://doi.org/10.1016/j.drudis.2017.08.002 PMID: 28803819

13. Flak D, Yate L, Nowaczyk G, Jurga S. Hybrid ZnPc@TiO2 nanostructures for targeted photodynamic therapy, bioimaging and doxorubicin delivery. Mater. Sci. Eng. C 2017, 78, 1072–1085, https://doi.org/10.1016/j.msec.2017.04.107 PMID: 28575942

14. Przysiecka L, Michalska M, Nowaczyk G, Peplinska B, Jesionowski T, Schneider R, et al. iRGD peptide as effective transporter of CuInZnxS2+x quantum dots into human cancer cells. Colloids Surfaces B Biointerfaces 2016, 146, 9–18, https://doi.org/10.1016/j.colsurfb.2016.05.041 PMID: 27244046

15. Woźniak-Budych MJ, Przysiecka Ł, Langer K, Peplińska B, Jarek M, Wiesner M, et al. Green synthesis of rifampicin-loaded copper nanoparticles with enhanced antimicrobial activity. J. Mater. Sci. Mater. Med. 2017, 28, https://doi.org/10.1007/s10856-016-5838-7

16. Wilczewska AZ, Niemirowicz K, Markiewicz KH, Car H. Nanoparticles as drug delivery systems. Pharmacol. Reports 2012, 64, 1020–1037, https://doi.org/10.1016/S1734-1140(12)70901-5.

17. Mrówczyński R, Jurga-Stopa J, Markiewicz R, Coy EL, Jurga S, Woźniak A. Assessment of polydopamine coated magnetic nanoparticles in doxorubicin delivery. RSC Adv. 2016, 6, https://doi.org/10.1039/c5ra24222c

18. Ulbrich K, Holá K, Šubr V, Bakandritsos A, Tuček J, Zbořil R. Targeted Drug Delivery with Polymers and Magnetic Nanoparticles: Covalent and Noncovalent Approaches, Release Control, and Clinical Studies. Chem. Rev. 2016, 116, 5338–5431, https://doi.org/10.1021/acs.chemrev.5b00589 PMID: 27109701

19. Tietze R, Zaloga J, Unterweger H, Lyer S, Friedrich RP, Janko C, et al. Magnetic nanoparticle-based drug delivery for cancer therapy. Biochem. Biophys. Res. Commun. 2015, 468, 463–470, https://doi.org/10.1016/j.bbrc.2015.08.022 PMID: 26271592

20. Grześkowiak BF, Sánchez-Antequera Y, Hammerschmid E, Döblinger M, Eberbeck D, Woźniak A, et al. Nanomagnetic activation as a way to control the efficacy of nucleic acid delivery. Pharm. Res. 2015, 32, 103–121, https://doi.org/10.1007/s11095-014-1448-6 PMID: 25033763

21. Lam T, Avti PK, Pouliot P, Maafi F, Tardif JC, Rhéaume É, et al. Fabricating Water Dispersible Superparamagnetic Iron Oxide Nanoparticles for Biomedical Applications through Ligand Exchange and Direct Conjugation. Nanomaterials 2016, 6, 100, https://doi.org/10.3390/nano6060100 PMID: 28335228

22. Mahmoudi K, Hadjipanayis CG. The application of magnetic nanoparticles for the treatment of brain tumors. Front. Chem. 2014, 2, 109, https://doi.org/10.3389/fchem.2014.00109 PMID: 25520952

23. Chertok B, David AE, Yang VC. Brain Tumor Targeting of Magnetic Nanoparticles for Potential Drug Delivery: Effect of Administration Route and Magnetic Field Topography. J. Control. Release 2011, 155, 393–399, https://doi.org/10.1016/j.jconrel.2011.06.033 PMID: 21763736

24. Wang X, Zhu L, Hou X, Wang L, Yin S. Polyethylenimine mediated magnetic nanoparticles for combined intracellular imaging, siRNA delivery and anti-tumor therapy. RSC Adv. 2015, 5, 101569–101581, https://doi.org/10.1039/C5RA18464A

25. Mykhaylyk O, Antequera YS, Vlaskou D, Plank C. Generation of magnetic nonviral gene transfer agents and magnetofection in vitro. Nat. Protoc. 2007, 2, 2391–2411, https://doi.org/10.1038/nprot.2007.352 PMID: 17947981

26. Mannell H, Pircher J, Räthel T, Schilberg K, Zimmermann K, Pfeifer A, et al. Targeted endothelial gene delivery by ultrasonic destruction of magnetic microbubbles carrying lentiviral vectors. Pharm. Res. 2012, 29, 1282–1294, https://doi.org/10.1007/s11095-012-0678-8 PMID: 22274557

27. Chomczyński P, Sacchi N. Single-step method of RNA isolation by acid guanidinum thiocyanate-phenol-chlotoform extraction. Anal. Biochem. 1987, 162, 156–159. https://doi.org/10.1006/abio.1987.9999 PMID: 2440339

28. Mrówczyński R, Jędrzak A, Szutkowski K, Grześkowiak BF, Coy E, Markiewicz R, et al. Cyclodextrin-based magnetic nanoparticles for cancer therapy. Nanomaterials 2018, 8, https://doi.org/10.3390/nano8030170 PMID: 29547559

29. Na H B, Song IC, Hyeon T. Inorganic nanoparticles for MRI contrast agents. Adv. Mater. 2009, 21, 2133–2148, https://doi.org/10.1002/adma.200802366

30. Mariano O, Dolores GM, Rafael S, Ana JR, Samanta DJ, Javier LF, et al. Polyethyleneimine-Coated Gold Nanoparticles: Straightforward Preparation of Efficient DNA Delivery Nanocarriers. Chem.–An Asian J. 2016, 11, 3365–3375, https://doi.org/10.1002/asia.201600951 PMID: 27685032

31. Aderem A, Ulevitch RJ. Toll-like receptors in the induction of the innate immune response. Nature 2000, 406, 782. https://doi.org/10.1038/35021228 PMID: 10963608

32. Karikó K, Bhuyan P, Capodici J, Ni H, Lubinski J, Friedman H, et al. Exogenous siRNA Mediates Sequence-Independent Gene Suppression by Signaling through Toll-Like Receptor 3. Cells Tissues Organs 2004, 177, 132–138. https://doi.org/10.1159/000079987 PMID: 15388987

33. Marques JT, Williams BRG. Activation of the mammalian immune system by siRNAs. Nat. Biotechnol. 2005, 23, 1399. https://doi.org/10.1038/nbt1161 PMID: 16273073

34. Xia S, Lal B, Tung B, Wang S, Goodwin CR, Laterra J. Tumor microenvironment tenascin-C promotes glioblastoma invasion and negatively regulates tumor proliferation. Neuro. Oncol. 2016, 18, 507–517, https://doi.org/10.1093/neuonc/nov171 PMID: 26320116

SUPPLEMENTARY MATERIALS
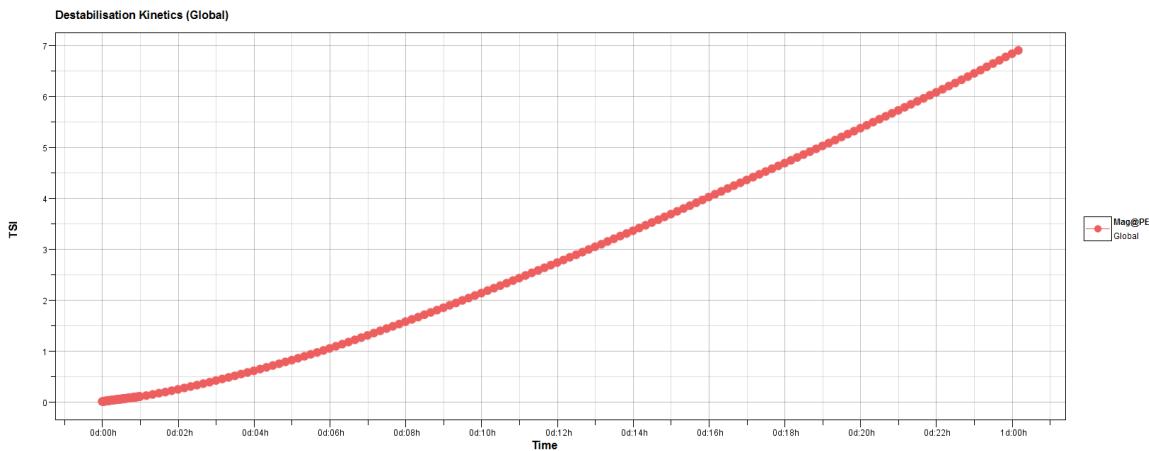
Figure A. Destabilization kinetic of Mag@PEI recorder by Turbiscan apparatus over 24 h.
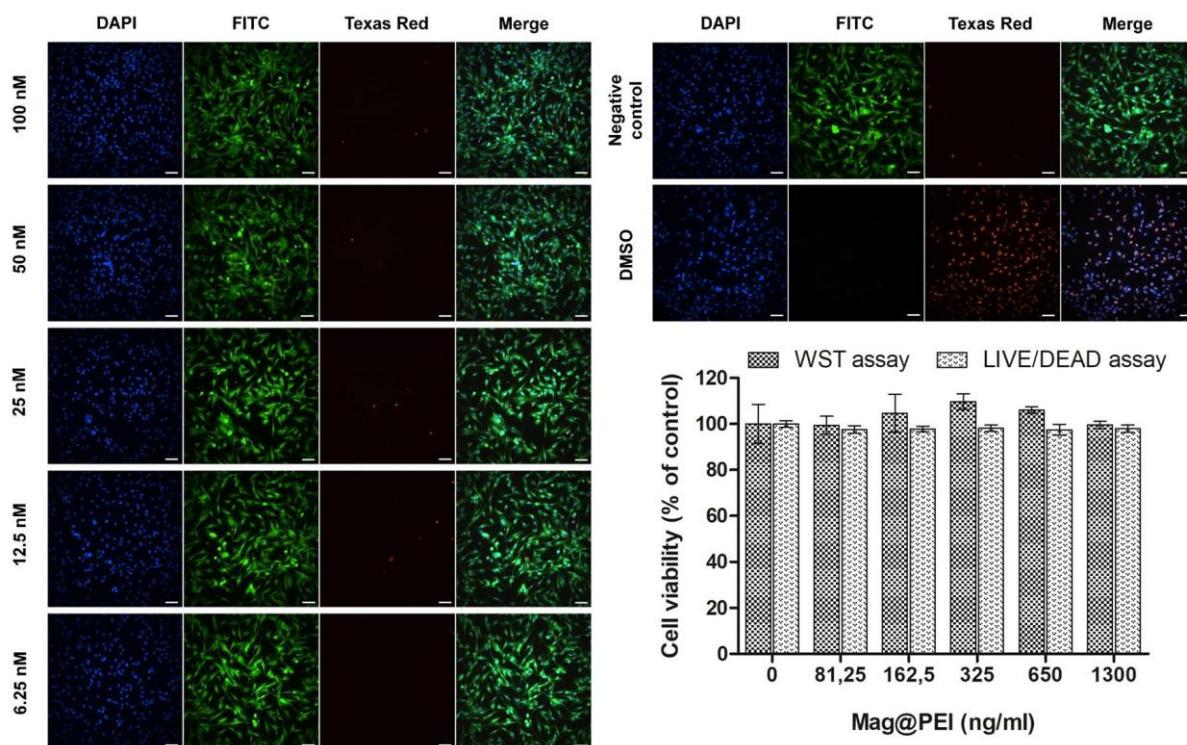
Figure B. Representative high-content images of U-118 cells exposed to Mag@PEI nanoparticles at various concentrations. 10% DMSO was used as a positive control. Images were obtained using different filters to detect nuclei (DAPI), live cells (FITC), and dead cells (TexasRed). The scale bars denote 100 μm. Cell viability of U118 cells exposed to Mag@PEI.

SRB assay

The protein-staining sulforhodamine B (SRB, Sigma–Aldrich) microculture colorimetric assay, developed by the National Cancer Institute (USA) for in vitro antitumor screening was used in this study, to estimate the cell number by providing a sensitive index of total cellular protein content, being linear to cell density. The monolayer cell culture was trypsinized and counted. To each well of the 96-well plate, 100 µL of the diluted cell suspension (5,000 and 10,000 cells) was added. After 24 hours, when a partial monolayer was formed, 100µl of fresh medium with different Mag@PEI concentrations (81.25, 162.5, 325, 650 and 1300 ng/mL) were added to the wells. The cells were exposed to compounds for 24 h at 37°C in a humidified atmosphere (90% RH) containing 5% CO_2. After that, 100 µL of 10% trichloroacetic acid was added to the wells and the plates were incubated for 1 h at 4°C. The plates were then washed out with the distilled water to remove traces of medium and next dried by the air. The air-dried plates were stained with 100 µL of 0.057% sulforhodamine B (prepared in 1% acetic acid) and kept for 30 min at room temperature. The unbound dye was removed by washing five times with 1% acetic acid and then the plates were air-dried overnight. The protein-bound dye was dissolved in 200 µL of 10 mM unbuffered Tris base (pH 10.5) for optical density determination at 510 nm. All experiments were performed in triplicates. Cell survival was measured as the percentage absorbance compared to the control (non-treated cells).
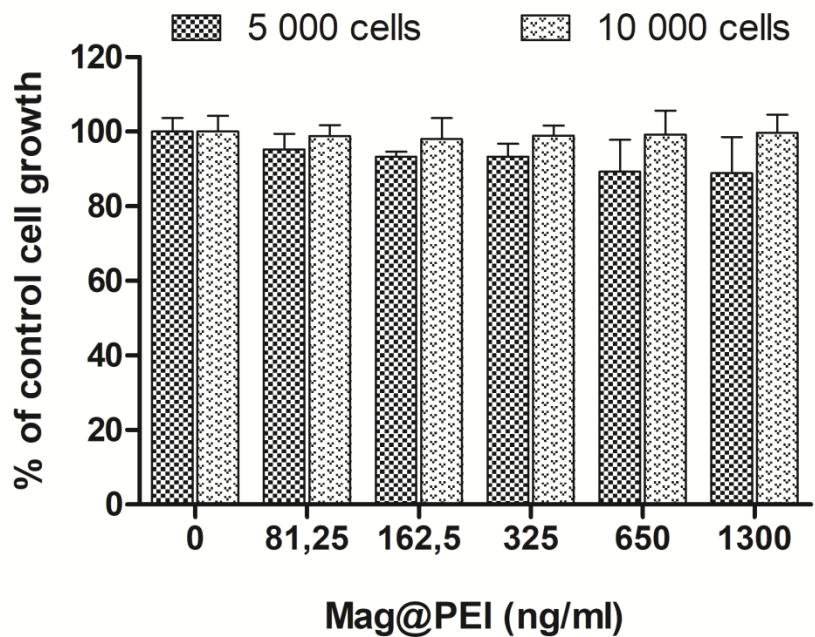
Figure C. Cytotoxicity SRB of Mag@PEI for various nanoparticles concentration.

Figure D. Scratch test